NEW INSIGHTS INTO CATCHMENT DYNAMICS USING NOVEL APPROACHES

NEW INSIGHTS INTO THE CONTROLS ON HYDROCHEMICAL BEHAVIOUR AND ECOHYDROLOGICAL DYNAMICS IN A COLD ALPINE CATCHMENT, SOUTHERN YUKON

By: NADINE J. SHATILLA, B.Sc., M.Sc.

A Thesis Submitted to the School of Graduate Studies in Partial Fulfillment of the Requirements for the Degree

Doctor of Philosophy

McMaster University © Copyright by Nadine Shatilla, February 2020

McMaster University Doctor of Philosophy (2020)

Hamilton, Ontario, Canada (School of Geography and Earth Sciences)

TITLE: New insights into the controls on hydrochemical behaviour and ecohydrological dynamics in a cold alpine catchment, Southern Yukon

AUTHOR: Nadine J. Shatilla

Master of Science and Bachelor of Science

McMaster, 2013

SUPERVISOR: Dr. Sean K. Carey, Professor

NUMBER OF PAGES: 244

ABSTRACT

Climate warming has been extensively documented over the last few decades, with northern environments experiencing greater increases in temperature than lower and mid-latitudes. Impacts of climate warming include: an increase in the rain to snow ratio, changes in precipitation magnitude and timing, increased soil warming, permafrost thaw, latitudinal and altitudinal expansion of tree-line, proliferation of tall shrubs into tundra, intensification of the freshwater cycle, and changes to stream volume and water quality. However, forecasting how these changes will affect northern, high latitude environments is difficult due to a lack of process-based research across scales. Wolf Creek Research Basin (WCRB) in Southern Yukon is a well-established mesoscale alpine catchment comprised of three ecozones and has hydrometric and meteorological records spanning 25 years. In this thesis, extensive field campaigns generated hydrochemical, stable isotope, and high-frequency in-situ datasets that were analyzed in conjunction with historical data from WCRB to refine and advance existing conceptual models. These distinct datasets were collected within a nested experimental design to more precisely describe relationships between catchment conditions, ecohydrological processes and stream water quantity and quality beginning at the headwater scale and with scaling to the outlet of WCRB. Optical data was combined with dissolved organic carbon (DOC) concentrations to assess source areas and in-stream dissolved organic matter (DOM) quality across landscape units. Headwater DOC concentrations and fluxes from 2015-2016 were compared to the previous decade to assess changing export. In situ sensors that record chromophoric DOM (CDOM) at high frequency were paired with discharge and conductivity measurements to assess concentration-

discharge relationships at event, seasonal and annual scales. Conceptual models of conductivity and major ion transport were confirmed while high-frequency CDOM-Q insights refined our understanding of DOC movement. As vegetation community composition and characteristics change, it is expected that components of the water balance will be altered at both the canopy level and within the critical zone. Compartmentalization of water within the critical zone is increasingly important to provide insights into how water cycles within catchments. Dual isotope and lc-excess approaches showed that bulk and xylem water were significantly different from the LMWL and stream water isotopes of δ^2H and $\delta^{18}O$. Meanwhile, an increasingly enriched xylem water isotope signal overlapped with bulk soil water values as the growing season continued, which suggests the opportunistic use of available mobile soil water.

ACKNOWLEDGEMENTS

This process involved more than I (naively) imagined, however, the people I met and places I visited along the way were well worth the effort. To start, I'd like to thank Sean Carey for his time, energy, patience, kindness, generosity and enthusiasm over the past few years. I would also like to thank the members of my PhD committee, Dr. Mike Waddington, and Dr. Altaf Arain, for their helpful advice over the last few years. A special thanks to Dr. Chris Spence, Dr. Jeff McKenzie and Dr. Max Lukenbach for insightful discussions, friendship and a mix of scientific and emotional support along the way.

My time in the field was greatly enriched by an initial camping trip with Sean and Mike Treberg, which introduced me to the best and worst parts of fieldwork in Southern Yukon. Subsequent seasons spent in the field were challenging, enlightening, entertaining and rewarding thanks to Erin Nicholls, Renée Lemmond and Heather Bonn. Drop offs and pick ups from Granger Basin by Delmar and Melvin at Capital Helicopters were always a highlight during spring, particularly when they graciously dropped off beer, a spatula and other assorted necessities.

I am grateful for the funding and opportunities given to me by the Changing Cold Regions Network (NSERC), VeWa (ERC) and Mountain Water Futures (NSERC) to build on a legacy of multidisciplinary research at Wolf Creek Research Basin. I am especially thankful for time spent with Ric Janowicz and his family (Leslie Gomm, Anna Janowicz). Ric was truly singular and his commitment to Wolf Creek research, saunas, adventure and having fun whenever possible was truly inspirational and he is greatly missed.

The Watershed Hydrology Group (both new and old) is a group of people that made courses, conferences, meetings, afternoons at Fairweather Brewing Company, long drives and fieldwork in miserable weather meaningful and fun. Thanks to Kelly Biagi, Victor Tang and Erin Nicholls for your help, friendship, and I am grateful for the experiences we've all had together. During my time in the Watershed Hydrology Group (pre- and post-branding efforts), Dr. Mike Treberg and Dr. Gord Drewitt provided key field, technical and coding support. Thanks for the life lessons Mike and thanks for taking care of the data Gord. Special thanks as well to Dr. Claire Oswald for introducing the Group to in-situ optical monitoring and the Aqualog, Supriya Singh and Sarah Irvine for Aqualog support, and to Krysha Dukacz for the initial geospatial analyses with follow up by Sean Leipe. Some heartfelt gratitude for Yukon views, camping, hikes, bike rides and breweries (Yukon Brewing Co, Winterlong Brewery).

Finally, thank you to my family and friends for putting up with me while I was consumed by this process. I'm sure we're all grateful that that I won't be talking about it anymore.

PREFACE

This Ph.D. dissertation is composed of five chapters. Chapters 2, 3, and 4 constitute the main body of the dissertation; each of these three chapters is written as a peer-viewed journal article. Chapter 2 explores how dissolved organic carbon (DOC) and related optical indices vary across a mesoscale alpine catchment underlain by discontinuous permafrost in Yukon Territory, Canada. Chapter 3 evaluates differences between high-frequency monitoring data and more traditional grab samples in a concentration-discharge (C-Q) framework. This chapter explores how headwater C-Q relationships can be assessed at a range of time scales to improve process understanding and update previous conceptual models of solute transport and export. Chapter 4 explores how stable isotopes of hydrogen and oxygen can be used to provide insights into the critical zone and vegetation water use across a growing season.

DECLARATION OF ACADEMIC ACHIEVEMENT

Chapter 2:

Shatilla, N. J. & Carey, S. K. (2019) Assessing inter-annual and seasonal patterns of DOC and DOM quality across a complex alpine watershed underlain by discontinuous permafrost in Yukon, Canada. *Hydrology and Earth System Sciences 23.9 (2019): 3571-3591.*

Nadine Shatilla (dissertation author) is the first author, main researcher, and the corresponding author for this paper. Nadine Shatilla collected and processed both the

fieldwork data and samples with help from Renee Lemmond. Optical indices samples were run by Nadine Shatilla. The data analysis and writing were executed by Nadine Shatilla with support and guidance from Dr. Carey.

Chapter 3:

Shatilla, N. J., Tang, W. & Carey, S. K. New insights into event-scale CDOM and conductivity dynamics from high-frequency in situ sensors at an alpine headwater catchment underlain by discontinuous permafrost in Yukon Territory, Canada.

Nadine Shatilla (dissertation author) is the main researcher, first and corresponding author of this paper. Nadine Shatilla collected the bulk of the field data with assistance from Crystal Beaudry, David Barrett, Tyler de Jong, Renée Lemmond and Heather Bonn. Data analysis was conducted by Nadine Shatilla and Weigang Tang. Dr. Carey and Dr. Lukenbach edited the manuscript and helped guide the discussion.

Chapter 4:

Shatilla, N. J. & Carey, S.K. A multi-year, seasonal evaluation of ecohydrological separation in an alpine discontinuous permafrost environment.

Nadine Shatilla (dissertation author) is the first author of this research paper and chose the sample locations and frequency of the isotope study. More recent field sampling was conducted by Nadine Shatilla, Renée Lemmond, Heather Bonn, Tyler Williams, Crystal Beaudry, David Barrett. Any samples dated prior to 2013 were collected by Dr.

Carey's research group at Carleton and other researchers located in Wolf Creek Research Basin. Vegetation surveys were conducted by Dr. Maxwell Lukenbach, Erin Nicholls, Renee Lemmond, and Nadine Shatilla. Liquid water isotope analyses were conducted by the Mitchell Research Group led by Dr. Carl Mitchell (University of Toronto Scarborough), bulk soil water analyses by the McDonnell Hillslope Hydrology Lab (K. Janzen, University of Saskatchewan) and xylem water by the Stable Isotope Lab (S. Evans, Boise State University). Data analysis was undertaken by Nadine Shatilla, and the manuscript was written by Nadine Shatilla with guidance from Dr. Carey.

Collaboration with the researchers at the Northern Rivers Institute (University of Aberdeen) resulted in two peer-reviewed journal articles published in tandem with this thesis:

Sprenger, M., Tetzlaff, D., Buttle, J., Carey, S.K., McNamara, J.P., Laudon, H., Shatilla, N.J., & Soulsby, C. (2018). Storage, mixing, and fluxes of water in the critical zone across northern environments inferred by stable isotopes of soil water. Hydrological processes 32 (12): 1720-37.

Piovano, T.I., Tetzlaff, D., Carey, S.K., Shatilla, N.J., Smith, A., & Soulsby, C. (2019). Spatially distributed tracer-aided runoff modelling and dynamics of storage and water ages in a permafrost-influenced catchment. Hydrology and Earth System Sciences 23: 2507–2523.

TABLE OF CONTENTS

LIST OF FIGURES

LIST OF TABLES

CHAPTER 1

INTRODUCTION

Climate warming has been extensively documented over the last few decades, with northern environments experiencing greater increases in temperature than lower and mid-latitudes. Impacts of climate warming include: An increase in the rain to snow ratio, changes in precipitation magnitude and timing, increased soil warming, permafrost thaw, latitudinal and altitudinal expansion of tree-line, proliferation of tall shrubs into tundra, intensification of the freshwater cycle, and changes to stream volume and water quality. However, changes to water balance partitioning and biogeochemical cycling is limited by a lack of process-based research across spatial scales. Traditionally, catchment hydrology has combined hydrometric data with stable isotopes of water to determine hydrograph composition while approaches assessing flow pathways, water cycling, and storage proliferated in later decades (e.g., Hooper and Shoemaker, 1986; Vitvar, Aggarwal and McDonnell, 2005; McGuire and McDonnell, 2006; Tetzlaff et a., 2014; Kirchner et al., 2016a,b; Penna et al., 2018). Solute concentrations and hydrochemistry are other staples to investigate flow pathways, assess the linkages between terrestrial and aquatic environments, and estimate solute fluxes at multiple catchment scales (e.g., Godsey et al., 2009; Shogren et al., 2019). A framework that incorporates novel technologies and analysis methods has enormous potential to provide new information on both the spatial and temporal processes that determine the movement of water and chemicals in watersheds and their susceptibility to change (Kircher et al., 2004). This thesis employed high-frequency

monitoring, and combined soil and vegetation isotopic tracers, coupled with traditional methods to gain new insights into catchment function and behaviour. The combination of In the past ten years, there has been limited application of new techniques and technologies in cold environments and it has been several decades since our ideas of runoff generation and water and chemical cycling in permafrost watersheds have been challenged.

1.1 Background

Climate warming at high latitudes has been extensively documented over the last few decades with northern environments experiencing greater increases in temperature than lower latitudes (Serreze et al., 2009, 2011; Screen et al., 2014; DeBeer et al., 2016). Alterations due to warming include: (i) an increase in the rain to snow ratio, (ii) changes in precipitation magnitude and timing (Prokushkin et al., 2005; Pumpanen et al., 2014; Spence et al., 2014; Dore, 2015; DeBeer et al., 2016; Duan et al., 2017), (iii) increased soil warming, (iv) permafrost thaw (O'Donnell et al., 2011; Natali et al., 2015; Loranty et al., 2017), (v) latitudinal and altitudinal expansion of tree-line and shrubification (Serreze et al., 2000; Jorgenson et al., 2001; Schuur et al., 2007; Bonfils et al., 2012; Teufel and Sushama, 2019), (vi) intensification of the freshwater cycle, (vii) and changes to stream volume and water quality (Frey and McClelland, 2009; Frey et al., 2015; Bring et al., 2016). Disturbances, including thermokarst and fire, are triggered by these changes; in turn, these disturbances often exacerbate the aforementioned changes leading to altered solute sources, fluxes and movement across terrestrial and aquatic environments (O'Donnell et al., 2012;

Malone et al., 2013; Kokelj et al., 2013; Nossov et al., 2013; Koch et al., 2014; Abbott et al., 2015; Burd et al., 2018).

Historically, our understanding of catchment hydrology in northern regions has been based predominantly on data and monitoring records from the MacKenzie, Yukon, Lena, Ob, and Yenisey River watersheds (Dittmar and Kattner, 2003; Raymond et al., 2007). These continental scale river basins have long been recognized for their disproportionately large contribution of water, solutes, and dissolved organic carbon (DOC) to the Arctic Ocean. Sporadic sampling and focus on the snowmelt period were common (Raymond et al., 2007; McClelland et al., 2007; Manizza et al., 2009). At this large scale, more recent studies have demonstrated uncertain trajectories of stream volume and solute sources under climate change, which will affect solute fluxes and export across catchment scales (Holmes et al., 2012; Hugelius et al., 2014; Toohey et al., 2016; Tank et al., 2016). This approach is limited due to a lack of integrated, process-based studies spanning a range of conditions. Inferences made from observations in complex landscapes are often mistranslated and there is a strong risk of drawing incorrect conclusions without datasets and analysis from nested catchment studies that incorporate altitudinal gradients with consequent landscape heterogeneity and vegetation gradients.

Headwaters contribute disproportionately large amounts of solute flux to downstream environments and are often considered to be a base unit of larger-scale catchments. Despite their relatively small area, headwater catchments typically include a large amount of diversity including functionally distinct parts of the landscape (Abbott et

al., 2018) such as riparian zones. In montane environments at larger scales, precipitation phase and magnitude, vegetation species and size, temperature and a whole host of additional hydroclimatic and ecological factors change rapidly with increasing elevation. The Wolf Creek Research Basin (WCRB) has a hydroclimatic dataset spanning more than two decades and existing monitoring infrastructure located at varying elevations and within distinct ecozones (Rasouli et al., 2019). The multitude of detailed process-based investigations on snow processes and the freshet period from previous research campaigns are the foundation of existing conceptual models of catchment behaviour. This thesis adds new information and uses novel approaches to assess catchment function in a nested catchment study design at a variety of temporal scales. Sample collection began in 2014 and new datasets assembled from fieldwork campaigns include: (1) Hundreds of major ion, dissolved organic carbon, and optical (including fluorescence) samples, (2) high-frequency records for multiple, consecutive years at 15-minute resolution, and (3) thousands of stable isotopes of water from plant xylems, soil layers and surrounding water bodies and sources. These new datasets were assessed in the context of the long-term hydrometric datasets and previous, detailed biogeochemical studies at WCRB to provide insights into processes.

1.1.1 Dissolved organic matter and optical methods

There is an emerging scientific consensus and growing societal concern over the arctic carbon bomb theory, which suggests that feedbacks from climate warming will accelerate atmospheric carbon dioxide (CO_2) concentrations through the massive release of organic carbon (OC) from permafrost soils (Treat and Frolking, 2015). At present, arctic permafrost soils contain an estimated 1700 Pg of OC, over twice the carbon stock of the atmospheric

CO_2 pool (Schuur et al., 2009; Tarnocai et al., 2009). This permafrost OC is increasingly vulnerable to change as the arctic freezer is thawing. Average annual temperatures in the Arctic have increased at almost twice the global average in recent decades (Serreze et al., 2009, 2011; Screen et al., 2014) with dramatic increases forecast under business-as-usual climate scenarios (Hinzman et al., 2005). It is projected that permafrost thaw resulting from arctic warming will release 41-288 Pg-C by 2100 and up to 616 Pg-C by 2300 (Schaefer et al., 2011; Schurr et al., 2013). These numbers are staggering when it is considered that the atmospheric CO_2 pool in 1750 contained 580 Pg-C and current climate change effects are occurring with an additional accumulation of ~250 Pg-C in the atmosphere. While the exact magnitude of increase is uncertain, increased methane emissions, ecosystem respiration, dissolved organic carbon export, and widespread thermokarst that may liberate ancient OC have been documented (Vonk et al., 2015).

With an enhanced focus on arctic carbon processes, particularly in the fluvial domain, optical techniques have become increasingly common as an approach to measure carbon quality and to partition carbon chemical character according to sources such as the relative contribution of soil, microbial and plant-derived sources and connectivity based on time of year as well as episodic wetness (Stedmon, Markager and Bro, 2003). Optical methods including spectral fluorescence rely on the capacity of organic matter molecules to absorb light and/or fluoresce. The wavelength(s) at which light is absorbed and fluoresced provides information as to the molecular structure, composition of the sample and origin (McKnight et al., 2001; Cory and McKnight, 2005; Murphy et al., 2008; Hansen et al., 2016). The extent of the absorption or fluorescence reaction and the calculated ratios are

an additional line of evidence that build on older studies that used concentrations to investigate sources and transformation pathways of dissolved OC (DOC) and organic matter (DOM) (Perdrial et al., 2014). In **Chapter 2**, a nested study design was used to explore the role and seasonal contribution of different landscape elements (headwater, wetland, lake) to variability in DOC concentrations, flux, and DOM quality with increasing contributing area. Water samples were collected from two headwater streams, a lake, wetland, and the outlet of a complex mesoscale catchment underlain by discontinuous permafrost for two consecutive years (2015-2016), along with metereological and hydrometric measurements. Samples were analyzed for DOC concentration, a suite of optical indices (e.g., biological index (BIX), fluorescence index (FI), freshness index (fresh), modified humification index (HIX)), and a combination of the two (e.g., SUVA254), to link DOC concentrations to DOM quality in both space and time across landscape elements. Over 200 samples from three years of data (including 2017) were placed in a principal component analysis (PCA) to determine how landscape elements and seasonal controls influenced DOC concentrations and optical indices.

1.1.2 Chemistry-flow interactions

One of the largest unknowns is how permafrost thaw will affect carbon and nutrient production and fluxes in northern catchments. Organic carbon plays a large role in the global carbon budget in the form of dissolved organic carbon (DOC) and particulate organic carbon (POC). Dissolved organic carbon (DOC) is important to numerous biogeochemical processes and acts as an energy source for stream ecosystems (Wetzel, 2003; Jansson et al.,

2007,). DOC is a complexing agent for metals (iron, copper, aluminum, zinc and mercury) and affects their solubility, transport and toxicity (Palmer et al., 2005). DOC also influences organic pollutant transport, pH buffering and contributes to the acidity of surface waters (Laudon et al., 2013; Birkel, Soulsby and Tetzlaff, 2014). Changes in the temperature and water flow pathways at high-latitudes will impact the production and mobilization of DOC and other dissolved and suspended materials in terrestrial and aquatic ecosystems (Frey & McClelland, 2009; Tetzlaff et al., 2013; Vonk et al., 2015). Processes of DOC production are strongly controlled by hydroclimate, soil characteristics, microbial and fungal biological activity and vegetation cover (Laudon et al., 2013; Tetzlaff et al., 2014; Vonk et al., 2015).

Permafrost environments are also characterized by high hydraulic conductivity, low mineral content and low DOC sorption capacity in the soil layer lying above permafrost (Striegl et al., 2005). These properties limit microbial transformation by facilitating rapid transport of DOC to streams and rivers. Increases in the temperature, seasonal duration and depth of the active layer due to climate warming will result in new sources of DOC from thawed permafrost and vegetation shifts (Sturm et al., 2005) and shifting flow pathways may transport this DOC to stream ecosystems. However, it is uncertain as to whether catchment processes will facilitate or mitigate the transport of newly mobilized DOC to streams and larger rivers. Permafrost thaw is expected to increase water transit times, which provides the opportunity for increased microbial mineralization as well as DOC respiration rather than increased transport from terrestrial to aquatic systems (Striegl et al., 2005). Uncertainties about DOC concentrations fluxes in northern river systems are mirrored in

predictions of altered annual and seasonal patterns in nitrogen, silica and other major ion concentrations (McClelland et al., 2007; Walvoord & Striegl, 2007; Frey & McClelland, 2009; Tank et al., 2012; Holmes et al., 2012, Koch et al., 2013).

The impacts of disturbances such as thermokarst and fire on major ion and DOC concentrations and export have been investigated in recent years. These abrupt changes occur in addition to climate change impacts with already uncertain trajectories and it can be difficult to disentangle these disturbance-based changes from climate change impacts. Climate change impacts are forecasted to affect processes occurring throughout the year while most conceptual models of solute sources, mobilization and transport are based on investigations during the freshet period. Major ions can provide important information about flow pathways and water-rock interactions through analysis of hysteresis loops. Hysteresis is almost ubiquitous in natural systems and occurs whenever timing of solute or stream discharge responses differ. These concentration-discharge patterns are typically referred to as "C-Q" hysteresis loops and there is an extensive collection of literature on the topic. Early analysis of in-stream C-Q hysteresis typically included qualitative characterization of C-Q loop direction to provide information about the source areas and their distance from the in-stream monitoring location (Evans and Davies, 1998; Godsey et al., 2009). Rotational pattern (clockwise, anti-clockwise), concavity/geometry (convex, concave), and slope/trend (positive, negative) were initially used to determine component source water mixing although interpretation of C-Q patterns was constrained by several assumptions (Evans and Davies, 1998).

Techniques developed in subsequent years include calculation of log-log regression slopes to provide more information about typical catchment behaviour responsible for solute movement from the terrestrial to aquatic environment (Godsey et al., 2009). Catchment behaviour can be described by three categories based on the value of the log-log regression slope: (i) dilution, (ii) chemostatic or (iii) mobilization. A slope value that is negative describes dilution while a neutral or positive slope described chemostatic or mobilization behaviour, respectively (Godsey et al., 2009; Saraceno et al., 2015). In recent years, the development of in situ sensors with the capacity to record concentrations at high-frequency has led to new approaches and insights into dynamics between hydroclimatic factors and in-stream hysteresis (e.g., Ruhala and Zarnetske, 2017). Using in-situ optical sensors to study dissolved organic carbon dynamics of streams and watersheds. In this thesis, major ions and DOC were the primary solutes of interest. For major ions, the often-used specific conductivity (SpC) in situ sensor record was assessed in tandem with a novel technology developed by Turner Designs. This high-frequency optical sensor is used for dye dilution discharge monitoring and to record wavelengths that describe chromophoric dissolved organic matter (CDOM) concentration. The in-stream dissolved organic matter measurements are typically highly correlated to DOC concentration (Stedmon et al., 2011).

New normalized C-Q hysteresis metrics have been developed to keep pace with high-frequency datasets (Lloyd et al., 2016). In **Chapter 3**, I explored this higher resolution monitoring data to traditional grab samples, and determine if our previously held views of catchment function and calculations of solute flux are supported or challenged.

1.1.3 Stable isotopes of water as tracers

Tracers, particularly $\delta^{18}O$ and $\delta^{2}H$, provide alternative insight into catchment hydrological processes, and when combined with hydrometric measurements allow a more nuanced understanding of how water is stored, mixed, and released. They provide information on water sources and ages (e.g. McGuire and McDonnell, 2006; Kirchner, 2016a, b), and are useful as they reflect water velocity (as opposed to celerity, which refers to the speed that precipitation is translated to runoff) and flow paths, which are often difficult to observe (Botter, Bertuzzo and Rinaldo, 2010; Birkel and Soulsby, 2015). Information on water storage and ages has become increasingly important as hydrological research has broadened its focus from quantifying water fluxes toward understanding which specific waters are in flux and which are less mobile in storage (Tetzlaff et al., 2015; Birkel, Soulsby and Tetzlaff, 2011, 2015; Smith, Tetzlaff and Soulsby, 2019). Much recent work suggests that there is considerable compartmentalization in the hydrological cycle and mixing is poorer than assumed (Tetzlaff et al., 2014). The hypothesis was initially introduced as "two water worlds" by McDonnell (2014) and theorized that two separate soil-water pools were sourced for plants and streams. An emerging body of research has focused on the exploration of this hypothesis along with the slightly more nuanced "ecohydrological separation" theory (Brooks, Barnard, Coulombe, & McDonnell, 2009; Goldsmith et al., 2012; McDonnell et al., 2014; Evaristo, Jasechko, & McDonnell, 2015; Bowling, Schulze, & Hall, 2017; Evaristo, Mcdonnell, Scholl, Bruijnzeel, & Chun, 2016; Hervé-Fernández et al., 2016; Berry et al., 2017). A global analysis confirms an absence of data with regards to soil, xylem and ground water isotopic investigations in permafrost

regions (Evaristo et al., 2015; Amin et al., 2019). Travel times and hydrological compartmentalization have been identified as grand challenges in hydrology (Bloschl et al., 2019) and are critical in bridging complex geochemistry issues with large-scale, integrative hydrological characterization. Many biogeochemical processes occur along hydrological flow paths (e.g., redox reactions, heterogeneous reaction kinetics, varying solubility equilibria).

As with much of the circumpolar North, vegetation is rapidly changing in the Southern Yukon. Vegetation influences spatiotemporal patterns in soil water moisture, groundwater recharge and flow paths through interception, stemflow, transpiration, hydraulic redistribution, and soil physical hydrological characteristics through root functions (Brantley et al., 2017). Interception and evapotranspiration influence travel times and volumes of percolating water in the unsaturated zone (Zwieback et al., 2019), which regulates streamflow generation and the time scales for transport of solutes (Snelgrove, Buttle and Tetzlaff, 2019). With rapid changes in vegetation, it is critical to understand the water sources and potential age distribution within the various compartments of the soil-plant-atmosphere continuum (Tetzlaff et al., 2015; Tetzlaff et al., 2015; Soulsby, Birkel and Tetzlaff, 2016; Penna et al., 2018; Dubbert and Werner, 2019). Quantifying water ages within evaporation, transpiration, recharge and soil storage compartments has been a recent focus of work in temperate zones, with an increasing number of studies assessing the impact of ecohydrological separation and water sources. Much of this work suggests transpired water is derived from deeper, older sources of water, and that soil evaporation is from younger, more surficial water with larger pores (McDonnell, 2014; Goldsmith et al., 2012;

Evaristo et al., 2015; Berry et al., 2017). Plants are also thought to preferentially sample bound, immobile water as opposed to more freely accessible mobile water. Despite some focus on global, aggregated datasets (Evaristo et al., 2015; Amin et al., 2019), there has been a gradual shift to meta-analysis and increased attention on inferring process understanding from spatially and temporally diverse isotope investigations within individual catchments. In permafrost environments, frozen ground typically provides a first-order control on flow pathways and water availability depending on time of year (Woo, 1990). The expectation in this environment is that perennially and seasonally frozen ground will also be a strong control on soil and transpired water, however, there has been no testing of this hypothesis in permafrost regions. In **Chapter 4**, new and historical datasets from Granger Creek headwater catchment and other locations in WCRB were combined with newly emerged techniques for determining bulk soil and xylem water isotope composition. Soil and vegetation samples collected from within the Granger Creek headwater catchment across two growing seasons were used to assess: (i) Whether the main tenets of the "two water world" hypothesis held true, (ii) if patterns in bulk soil water observed in other environments were consistent with our observations in a cold, montane environment in the discontinuous permafrost zone, and (iii) if landscape position significantly influenced soil and xylem water isotopic composition.

1.2 Objectives

The goal of this thesis is to employ new technologies and tracers to further our process understanding of conceptual models of water and solute transport in northern

environments. This research introduces new types of data, results of analytical innovations and applies novel approaches to explore how distinct streams of data can be used to refine existing conceptual models. The new datasets were generated from extensive field campaigns over multiple years using a nested study design in Wolf Creek Research Basin to explore both temporal and spatial scaling. The mesoscale research catchment, along with the headwater basin Granger Creek, are long-term study sites with hydrometric and climatic records spanning 25 years (Rasouli et al., 2019) along with sporadic hydrochemical and isotope datasets from previous research initiatives (Boucher and Carey, 2010, Carey, Boucher and Duarte, 2013). Traditional approaches and data collection were combined with novel measurement methods and analyses to question existing conceptual models, and whether new streams of data can be used to improve our understanding. Specifically, I asked:

1) How does dissolved organic carbon quantity and quality vary seasonally and spatially in a well-studied headwater environment?
2) Is concentration-discharge information revealed at finer temporal resolution meaningful, and does it challenge existing conceptual models?
3) What can patterns of xylem and bulk soil water isotopes tell us about vegetation water sources in a shrub taiga landscape and can we observe ecohydrological separation?

The results of this research are presented as three chapters that follow the format of peer-reviewed journal articles in Chapters 2, 3 and 4. Conclusions drawn from the three research chapters are summarized in Chapter 5, which also includes suggestions for future work.

References

Abbott, B. W., Gruau, G., Zarnetske, J. P., Moatar, F., Barbe, L., Thomas, Z., Fovet O, Kolbe T, Gu S, Pierson-Wickmann AC, & Davy, P. (2018). Unexpected spatial stability of water chemistry in headwater stream networks. Ecology letters, 21(2), 296-308.

Alexander, R. B., Boyer, E. W., Smith, R. A., Schwarz, G. E., and Moore, R. B.(2007). The role of headwater streams in downstream water quality. J. Am.Water Res. Assoc.43, 41–59. doi: 10.1111/j.1752-1688.2007.00005.x

Amin, A., Zuecco, G., Geris, J., Schwendenmann, L., McDonnell, J. J., Borga, M., & Penna, D. (2019). Depth distribution of soil water sourced by plants at the global scale: a new direct inference approach. Ecohydrology, e2177.

Berry, Z. C., Evaristo, J., Moore, G., Poca, M., Steppe, K., Verrot, L., Asbjornsen, H., Borma, L. S., Bretfeld, M., Herve-Fernandez, P., Seyfried, M., Schwendenmann, L., Sinacore, K., De Wispelaere, L., & McDonnell, J.J. (2017). The two water worlds hypothesis: Addressing multiple working hypotheses and proposing a way forward, Ecohydrology, e1843, 20. doi:10.1002/eco.1843.

Birkel, C., Soulsby, C., & Tetzlaff, D. (2011). Modelling catchment-scale water storage dynamics: Reconciling dynamic storage with tracer-inferred passive storage. Hydrological Processes, 25(25), 3924-3936.

Birkel, C., Soulsby, C., & Tetzlaff, D. (2014). Integrating parsimonious models of hydrological connectivity and soil biogeochemistry to simulate stream DOC dynamics. Journal of Geophysical Research: Biogeosciences, 119(5), 1030-1047.

Birkel, C., & Soulsby, C. (2015). Advancing tracer-aided rainfall–runoff modelling: a review of progress, problems and unrealised potential. Hydrological Processes, 29(25), 5227-5240.

Birkel, C., Soulsby, C., & Tetzlaff, D. (2015). Conceptual modelling to assess how the interplay of hydrological connectivity, catchment storage and tracer dynamics controls nonstationary water age estimates. Hydrological Processes, 29(13), 2956-2969.

Blöschl, G., Bierkens, M.F., Chambel, A., Cudennec, C., Destouni, G., Fiori, A., Kirchner, J.W., McDonnell, J.J., Savenije, H.H., Sivapalan, M. and Stumpp, C. (2019). Twenty-three unsolved problems in hydrology (UPH)–a community perspective. Hydrological Sciences Journal, 64(10), 1141-1158.

Burd, K., Tank, S. E., Dion, N., Quinton, W. L., Spence, C., Tanentzap, A. J., & Olefeldt, D. (2018). Seasonal shifts in export of DOC and nutrients from burned and unburned

peatland-rich catchments, Northwest Territories, Canada. Hydrology & Earth System Sciences, 22(8).

Bonfils, C. J. W., Phillips, T. J., Lawrence, D. M., Cameron-Smith, P., Riley, W. J., & Subin, Z. M. (2012). On the influence of shrub height and expansion on northern high latitude climate. Environmental Research Letters, 7(1), 015503.

Boucher, J. L., & Carey, S. K. (2010). Exploring runoff processes using chemical, isotopic and hydrometric data in a discontinuous permafrost catchment. Hydrology Research, 41(6), 508-519.

Botter, G., Bertuzzo, E., & Rinaldo, A. (2010). Transport in the hydrologic response: Travel time distributions, soil moisture dynamics, and the old water paradox. Water Resources Research, 46(3).

Brantley, S. L., Eissenstat, D. M., Marshall, J. A., Godsey, S. E., Balogh-Brunstad, Z., Karwan, D. L., & Chadwick, O. (2017). Reviews and syntheses: on the roles trees play in building and plumbing the critical zone. Biogeosciences (Online), 14(22).

Bring, A., Fedorova, I., Dibike, Y., Hinzman, L., Mård, J., Mernild, S.H., Prowse, T., Semenova, O., Stuefer, S.L. and Woo, M.K., 2016. Arctic terrestrial hydrology: A synthesis of processes, regional effects, and research challenges. Journal of Geophysical Research: Biogeosciences, 121(3), pp.621-649.

Carey, S. K., Boucher, J. L., & Duarte, C. M. (2013). Inferring groundwater contributions and pathways to streamflow during snowmelt over multiple years in a discontinuous permafrost subarctic environment (Yukon, Canada). Hydrogeology Journal, 21(1), 67-77.

Cory, R. M., & McKnight, D. M. (2005). Fluorescence spectroscopy reveals ubiquitous presence of oxidized and reduced quinones in dissolved organic matter. Environmental science & technology, 39(21), 8142-8149.

DeBeer, C. M., Wheater, H. S., Carey, S. K., & Chun, K. P. (2016). Recent climatic, cryospheric, and hydrological changes over the interior of western Canada: a review and synthesis. Hydrology and Earth System Sciences, 20(4), 1573.

Dittmar, T., & Kattner, G. (2003). The biogeochemistry of the river and shelf ecosystem of the Arctic Ocean: a review. Marine chemistry, 83(3-4), 103-120.

Dore, M. H. (2005). Climate change and changes in global precipitation patterns: what do we know?. Environment international, 31(8), 1167-1181.

Duan, L., Man, X., Kurylyk, B. L., & Cai, T. (2017). Increasing winter baseflow in response to permafrost thaw and precipitation regime shifts in Northeastern China. Water, 9(1), 25.

Dubbert, M., & Werner, C. (2019). Water fluxes mediated by vegetation: emerging isotopic insights at the soil and atmosphere interfaces. New Phytologist 221(4), 1754-1763.

Evaristo, J., Jasechko, S., & McDonnell, J.J. (2015). Global separation of plant transpiration from groundwater and streamflow. Nature 525:91–94. doi:10.1038/nature14983

Frey, K. E., & McClelland, J. W. (2009). Impacts of permafrost degradation on arctic river biogeochemistry. Hydrological Processes: An International Journal, 23(1), 169-182.

Frey, K. E., Sobczak, W. V., Mann, P. J., & Holmes, R. M. (2015). Optical properties and bioavailability of dissolved organic matter along a flow-path continuum from soil pore waters to the Kolyma River, Siberia. Biogeosciences Discussions, 12(15).

Holmes, R.M., McClelland, J.W., Peterson, B.J., Tank, S.E., Bulygina, E., Eglinton, T.I., Gordeev, V.V., Gurtovaya, T.Y., Raymond, P.A., Repeta, D.J. and Staples, R. (2012). Seasonal and annual fluxes of nutrients and organic matter from large rivers to the Arctic Ocean and surrounding seas. Estuaries and Coasts, 35(2), 369-382.

Godsey, S. E., Kirchner, J. W., & Clow, D. W. (2009). Concentration–discharge relationships reflect chemostatic characteristics of US catchments. Hydrological Processes: An International Journal, 23(13), 1844-1864.

Goldsmith, G.R., Muñoz-Villers, L.E., Holwerda, F., McDonnell, J.J., Asbjornsen, H., & Dawson, T.E. (2012). Stable isotopes reveal linkages among ecohydrological processes in a seasonally dry tropical montane cloudforest. Ecohydrology 5: 779–790.

Hansen, A. M., Kraus, T. E., Pellerin, B. A., Fleck, J. A., Downing, B. D., & Bergamaschi, B. A. (2016). Optical properties of dissolved organic matter (DOM): Effects of biological and photolytic degradation. Limnology and Oceanography, 61(3), 1015-1032.

Hinzman, L.D., Bettez, N.D., Bolton, W.R., Chapin, F.S., Dyurgerov, M.B., Fastie, C.L., Griffith, B., Hollister, R.D., Hope, A., Huntington, H.P. and Jensen, A.M. (2005). Evidence and implications of recent climate change in northern Alaska and other arctic regions. Climatic change, 72(3), 251-298.

Hooper, R. P., & Shoemaker, C. A. (1986). A comparison of chemical and isotopic hydrograph separation. Water Resources Research, 22(10), 1444-1454.

Hugelius, G., Strauss, J., Zubrzycki, S., Harden, J.W., Schuur, E.A.G., Ping, C.L., Schirrmeister, L., Grosse, G., Michaelson, G.J., Koven, C.D. and O'Donnell, J.A. (2014). Estimated stocks of circumpolar permafrost carbon with quantified uncertainty ranges and identified data gaps. Biogeosciences (Online), 11(23).

Jansson, M., Persson, L., De Roos, A. M., Jones, R. I., & Tranvik, L. J. (2007). Terrestrial carbon and intraspecific size-variation shape lake ecosystems. Trends in Ecology & Evolution, 22(6), 316-322.

Jorgenson, M. T., Racine, C. H., Walters, J. C., & Osterkamp, T. E. (2001). Permafrost degradation and ecological changes associated with a warmingclimate in central Alaska. Climatic change, 48(4), 551-579.

Kirchner, J. W., Feng, X., Neal, C., & Robson, A. J. (2004). The fine structure of water-quality dynamics: the (high-frequency) wave of the future. Hydrological processes, 18(7), 1353-1359.

Kirchner, J. W. (2016a). Aggregation in environmental systems-Part 1: Seasonal tracer cycles quantify young water fractions, but not mean transit times, in spatially heterogeneous catchments. Hydrology and Earth System Sciences, 20(1), 279-297.

Kirchner, J. W. (2016b). Aggregation in environmental systems-Part 2: Catchment mean transit times and young water fractions under hydrologic nonstationarity. Hydrology and Earth System Sciences, 20(1), 299-328.

Koch, J. C., Kikuchi, C. P., Wickland, K. P., & Schuster, P. (2014). Runoff sources and flow paths in a partially burned, upland boreal catchment underlain by permafrost. Water Resources Research, 50(10), 8141-8158.

Koch, J. C., Runkel, R. L., Striegl, R., & McKnight, D. M. (2013a). Hydrologic controls on the transport and cycling of carbon and nitrogen in a boreal catchment underlain by continuous permafrost. Journal of Geophysical Research: Biogeosciences, 118(2), 698-712.

Kokelj, S. V., Lacelle, D., Lantz, T. C., Tunnicliffe, J., Malone, L., Clark, I. D., & Chin, K. S. (2013). Thawing of massive ground ice in mega slumps drives increases in stream sediment and solute flux across a range of watershed scales. Journal of Geophysical Research: Earth Surface, 118(2), 681-692.

Laudon, H., Tetzlaff, D., Soulsby, C., Carey, S., Seibert, J., Buttle, J., Shanley, J., McDonnell, J.J. and McGuire, K. (2013). Change in winter climate will affect dissolved organic carbon and water fluxes in mid-to-high latitude catchments. Hydrological Processes, 27(5), 700-709.

Lloyd, C. E. M., Freer, J. E., Johnes, P. J., & Collins, A. L. (2016). Using hysteresis analysis of high-resolution water quality monitoring data, including uncertainty, to infer controls on nutrient and sediment transfer in catchments. Science of the Total Environment, 543, 388-404.

Loranty, M. M., Abbott, B. W., Blok, D., Douglas, T. A., Epstein, H. E., Forbes, B. C., Jones, B.M., Kholodov, A.L., Kropp, H., Malhotra, A., Mamet, S. D., Myers-Smith, I.H., Natali, S.M., O'Donnell, J.A., Phoenix, G.K., Rocha, A.V., Sonnentag, O., Tape, K.D. & Walker, D. (2018). Reviews and syntheses: Changing ecosystem influences on soil thermal regimes in northern high-latitude permafrost regions. Biogeosciences 15 (17): 5287-5313.

Malone, L., D. Lacelle, S. V. Kokelj, and I. D. Clark (2013), Impacts of hillslope thaw slumps on the geochemistry of permafrost catchments (Stony Creek watershed, NWT, Canada), Chem. Geol., 356, 38–49.

Manizza, M., Follows, M.J., Dutkiewicz, S., McClelland, J.W., Menemenlis, D., Hill, C.N., Townsend-Small, A. and Peterson, B.J. (2009). Modeling transport and fate of riverine dissolved organic carbon in the Arctic Ocean. Global Biogeochemical Cycles, 23(4).

McClelland, J. W., Stieglitz, M., Pan, F., Holmes, R. M., & Peterson, B. J. (2007). Recent changes in nitrate and dissolved organic carbon export from the upper Kuparuk River, North Slope, Alaska. Journal of Geophysical Research: Biogeosciences, 112(G4).

McDonnell, J. J. (2014). The two water worlds hypothesis: Ecohydrological separation of water between streams and trees?. Wiley Interdisciplinary Reviews: Water, 1(4), 323-329.

McGuire, K. J., & McDonnell, J. J. (2006). A review and evaluation of catchment transit time modeling. Journal of Hydrology, 330(3-4), 543-563.

McKnight, D. M., Boyer, E. W., Westerhoff, P. K., Doran, P. T., Kulbe, T., & Andersen, D. T. (2001). Spectrofluorometric characterization of dissolved organic matter for indication of precursor organic material and aromaticity. Limnology and Oceanography, 46(1), 38-48.

Murphy, K. R., Stedmon, C. A., Waite, T. D., & Ruiz, G. M. (2008). Distinguishing between terrestrial and autochthonous organic matter sources in marine environments using fluorescence spectroscopy. Marine Chemistry, 108(1-2), 40-58

Natali, S. M., Schuur, E. A., Mauritz, M., Schade, J. D., Celis, G., Crummer, K. G., Johnston, C., Krapek, J., Pegoraro, E., Salmon, V.G., & Webb, E. E. (2015). Permafrost thaw and soil moisture driving CO2 and CH4 release from upland tundra. Journal of Geophysical Research: Biogeosciences 120 (3): 525-537.

Nossov, D. R., Jorgenson, M. T., Kielland, K., & Kanevskiy, M. Z. (2013). Edaphic and microclimatic controls over permafrost response to fire in interior Alaska. Environmental Research Letters, 8(3), 035013.

O'Donnell, J. A., Harden, J. W., McGuire, A. D., & Romanovsky, V. E. (2011). Exploring the sensitivity of soil carbon dynamics to climate change, fire disturbance and permafrost thaw in a black spruce ecosystem. Biogeosciences. 8: 1367-1382, 8, 1367-1382.

O'Donnell, J. A., Aiken, G. R., Walvoord, M. A., & Butler, K. D. (2012). Dissolved organic matter composition of winter flow in the Yukon River basin: Implications of permafrost thaw and increased groundwater discharge. Global Biogeochemical Cycles, 26(4).

Palmer, S. M., Wellington, B. I., Johnson, C. E., & Driscoll, C. T. (2005). Landscape influences on aluminium and dissolved organic carbon in streams draining the Hubbard Brook valley, New Hampshire, USA. Hydrological Processes: An International Journal, 19(9), 1751-1769.

Penna, D., Hopp, L., Scandellari, F., Allen, S. T., Benettin, P., Beyer, M., Geris, J., Klaus, J., Marshall, J.D., Schwendenmann, L., Volkmann, T. H. M., Freiin von Freyberg, J., Amin, A., Ceperley, N., Engel, M., Frentress, J., Giambastiani, Y., McDonnell, J.J., Zuecco, G., Llorens, P., Siegwolf, R.T.W., Dawson, T.E., & Kirchner, J.W. (2018). Ideas and perspectives: Tracing terrestrial ecosystem water fluxes using hydrogen and oxygen stable isotopes-challenges and opportunities from an interdisciplinary perspective. Biogeosciences 15 (21): 6399-6415.

Perdrial, J.N., McIntosh, J., Harpold, A., Brooks, P.D., Zapata-Rios, X., Ray, J., Meixner, T., Kanduc, T., Litvak, M., Troch, P.A. and Chorover, J. (2014). Stream water carbon controls in seasonally snow-covered mountain catchments: impact of inter-annual variability of water fluxes, catchment aspect and seasonal processes. Biogeochemistry, 118(1-3), 273-290.

Prokushkin, A. S., Kajimoto, T., Prokushkin, S. G., McDowell, W. H., Abaimov, A. P., & Matsuura, Y. (2005). Climatic factors influencing fluxes of dissolved organic carbon from the forest floor in a continuous-permafrost Siberian watershed. Canadian journal of forest research, 35(9), 2130-2140.

Pumpanen, J., Lindén, A., Miettinen, H., Kolari, P., Ilvesniemi, H., Mammarella, I., Hari, P., Nikinmaa, E., Heinonsalo, J., Bäck, J. and Ojala, A. (2014). Precipitation and net ecosystem exchange are the most important drivers of DOC flux in upland boreal catchments. Journal of Geophysical Research: Biogeosciences, 119(9),1861-1878.

Rasouli, K., Pomeroy, J. W., Janowicz, J. R., Williams, T. J., & Carey, S. K. (2019). A long-term hydrometeorological dataset (1993–2014) of a northern mountain basin: Wolf Creek Research Basin, Yukon Territory, Canada. Earth System Science Data 11(1): 89-100.

Raymond, P.A., McClelland, J.W., Holmes, R.M., Zhulidov, A.V., Mull, K., Peterson, B.J., Striegl, R.G., Aiken, G.R. and Gurtovaya, T.Y. (2007). Flux and age of dissolved organic

carbon exported to the Arctic Ocean: A carbon isotopic study of the five largest arctic rivers. Global Biogeochemical Cycles, 21(4).

Ruhala, S. S., & Zarnetske, J. P. (2017). Using in-situ optical sensors to study dissolved organic carbon dynamics of streams and watersheds: A review. Science of the Total Environment, 575, 713-723.

Schaefer, K., Zhang, T., Bruhwiler, L., & Barrett, A. P. (2011). Amount and timing of permafrost carbon release in response to climate warming. Tellus B: Chemical and Physical Meteorology, 63(2), 168-180.

Schuur, E. A., Crummer, K. G., Vogel, J. G., & Mack, M. C. (2007). Plant species composition and productivity following permafrost thaw and thermokarst in Alaskan tundra. Ecosystems, 10(2), 280-292.

Schuur, E. A., Vogel, J. G., Crummer, K. G., Lee, H., Sickman, J. O., & Osterkamp, T. E. (2009). The effect of permafrost thaw on old carbon release and net carbon exchange from tundra. Nature, 459(7246), 556-559.

Schuur, E.A., Abbott, B.W., Bowden, W.B., Brovkin, V., Camill, P., Canadell, J.G., Chanton, J.P., Chapin, F.S., Christensen, T.R., Ciais, P. and Crosby, B.T. (2013). Expert assessment of vulnerability of permafrost carbon to climate change. Climatic Change, 119(2), 359-374.

Screen, J. A. (2014). Arctic amplification decreases temperature variance in northern mid- to high-latitudes. Nature Clim. Change 4, 577–582.
Serreze, M. C., Walsh, J. E., Chapin, F. S., Osterkamp, T., Dyurgerov, M., Romanovsky, V., Oechel, C., Morison, J., Zhang, T. & Barry, R. G. (2000). Observational evidence of recent change in the northern high-latitude environment. Climatic change, 46(1-2), 159-207.

Serreze, M. C., Barrett, A. P., Stroeve, J. C., Kindig, D. N. & Holland, M. M. (2009). The emergence of surface-based Arctic amplification. Cryosphere 3, 11–19.

Serreze, M. C. & Barry, R. G. (2011). Processing and impacts of Arctic amplification: A research synthesis. Global Planet. Change 77, 85–96.

Stedmon, C. A., Markager, S., & Bro, R. (2003). Tracing dissolved organic matter in aquatic environments using a new approach to fluorescence spectroscopy. Marine Chemistry, 82(3-4), 239-254.

Spence, C., Kokelj, S. V., Kokelj, S. A., McCluskie, M., & Hedstrom, N. (2015). Evidence of a change in water chemistry in Canada's subarctic associated with enhanced winter streamflow. Journal of Geophysical Research: Biogeosciences, 120(1), 113-127.

Sturm, M., Schimel, J., Michaelson, G., Welker, J.M., Oberbauer, S.F., Liston, G.E., Fahnestock, J. and Romanovsky, V.E. (2005). Winter biological processes could help convert arctic tundra to shrubland. Bioscience, 55(1), 17-26.

Striegl, R. G., Aiken, G. R., Dornblaser, M. M., Raymond, P. A., & Wickland, K. P. (2005). A decrease in discharge-normalized DOC export by the Yukon River during summer through autumn. Geophysical Research Letters, 32(21).

Smith, A. A., Tetzlaff, D., & Soulsby, C. (2019). Using StorAge Selection functions to quantify ecohydrological controls on the time-variant age of evapotranspiration, soil water, and recharge. Hydrology and Earth System Sciences 23: 3319-3334. doi: 10.5194/hess-23-3319-2019

Snelgrove, J. R., Buttle, J. M., & Tetzlaff, D. (2019). Importance of rainfall partitioning in a northern mixed forest canopy for soil water isotopic signatures in ecohydrological studies. Hydrological Processes.

Shogren, A. J., Zarnetske, J. P., Abbott, B. W., Iannucci, F., Frei, R. J., Griffin, N. A., & Bowden, W. B. (2019). Revealing biogeochemical signatures of Arctic landscapes with river chemistry. Scientific reports, 9(1), 1-11.

Stedmon, C. A., Amon, R. M. W., Rinehart, A. J., & Walker, S. A. (2011). The supply and characteristics of colored dissolved organic matter (CDOM) in the Arctic Ocean: Pan Arctic trends and differences. Marine Chemistry, 124(1-4), 108-118.

Soulsby, C., Birkel, C., & Tetzlaff, D. (2016). Modelling storage-driven connectivity between landscapes and riverscapes: towards a simple framework for long-term ecohydrological assessment. Hydrological Processes, 30(14), 2482-2497.

Tank, S. E., Frey, K. E., Striegl, R. G., Raymond, P. A., Holmes, R. M., McClelland, J. W., & Peterson, B. J. (2012). Landscape-level controls on dissolved carbon flux from diverse catchments of the circumboreal. Global Biogeochemical Cycles, 26(4).

Tank, S. E., Striegl, R. G., McClelland, J. W., & Kokelj, S. V. (2016). Multi-decadal increases in dissolved organic carbon and alkalinity flux from the Mackenzie drainage basin to the Arctic Ocean. Environmental Research Letters, 11(5), 054015.

Tarnocai, C., Canadell, J. G., Schuur, E. A., Kuhry, P., Mazhitova, G., & Zimov, S. (2009). Soil organic carbon pools in the northern circumpolar permafrost region. Global biogeochemical cycles, 23(2).

Tetzlaff, D., Soulsby, C., Buttle, J., Capell, R., Carey, S.K., Laudon, H., McDonnell, J., McGuire, K., Seibert, J. and Shanley, J. (2013). Catchments on the cusp? Structural and functional change in northern ecohydrology. Hydrological Processes, 27(5), 766-774.

Tetzlaff, D., Birkel, C., Dick, J., Geris, J., & Soulsby, C. (2014). Storage dynamics in hydropedological units control hillslope connectivity, runoff generation, and the evolution of catchment transit time distributions. Water resources research 50(2): 969-985.

Tetzlaff, D., Buttle, J., Carey, S. K., McGuire, K., Laudon, H., & Soulsby, C. (2015). Tracer-based assessment of flow paths, storage and runoff generation in northern catchments: A review. Hydrological Processes 29 (16), 3475–3490. doi: 10.1002/hyp.10412

Teufel, B., & Sushama, L. (2019). Abrupt changes across the Arctic permafrost region endanger northern development. Nature Climate Change, 9(11), 858-862.

Toohey, R. C., Herman-Mercer, N. M., Schuster, P. F., Mutter, E. A., & Koch, J. C. (2016). Multidecadal increases in the Yukon River Basin of chemical fluxes as indicators of changing flowpaths, groundwater, and permafrost. Geophysical Research Letters, 43(23), 12-120.

Vitvar, T., Aggarwal, P. K., & McDonnell, J. J. (2005). A review of isotope applications in catchment hydrology. In Isotopes in the water cycle (pp. 151-169). Springer, Dordrecht.

Vonk, J.E., Tank, S.E., Bowden, W.B., Laurion, I., Vincent, W.F., Alekseychik, P., Amyot, M., Billet, M.F., Canario, J., Cory, R.M. and Deshpande, B.N. (2015). Reviews and syntheses: Effects of permafrost thaw on Arctic aquatic ecosystems. Biogeosciences, 12(23), 7129-7167.

Walvoord, M. A., & Striegl, R. G. (2007). Increased groundwater to stream discharge from permafrost thawing in the Yukon River basin: Potential impacts on lateral export of carbon and nitrogen. Geophysical Research Letters 34(12).

Wetzel, R. G. (2003). Dissolved organic carbon: detrital energetics, metabolic regulators, and drivers of ecosystem stability of aquatic ecosystems. In Aquatic Ecosystems (pp. 455-477). Academic Press.

Woo, M. K. (1990). Consequences of climatic change for hydrology in permafrost zones. Journal of cold regions engineering 4 (1): 15-20.

Zwieback, S., Chang, Q., Marsh, P., & Berg, A. (2019). Shrub tundra ecohydrology: rainfall interception is a major component of the water balance. Environmental Research Letters, 14(5), 055005.

CHAPTER 2

ASSESSING INTER-ANNUAL AND SEASONAL PATTERNS OF DOC AND DOM QUALITY ACROSS A COMPLEX ALPINE WATERSHED UNDERLAIN BY DISCONTINUOUS PERMAFROST IN YUKON, CANADA

ABSTRACT

High latitude environments store approximately half of the global organic carbon pool in peatlands, organic soils and permafrost while large Arctic rivers convey an estimated 18-50 Tg C a-1 to the Arctic Ocean. Warming trends associated with climate change affect dissolved organic carbon (DOC) export from terrestrial to riverine environments. However, there is limited consensus as to whether exports will increase or decrease due to complex interactions between climate, soils, vegetation, and associated production, mobilization and transport processes. A large body of research has focused on large river system DOC and DOM lability and observed trends conserved across years, whereas investigations at smaller watershed scales show that thermokarst and fire have transient impacts on hydrologically-mediated solute transport. This study, located in the Wolf Creek Research Basin situated ~20 km south of Whitehorse, YT, Canada, utilises a nested design to assess seasonal and annual patterns of DOC and DOM composition across diverse landscape types (headwater, wetland, lake) and watershed scales. Peak DOC concentration and export occurred during freshet per most northern watersheds, however, peaks were lower than a decade ago at the headwater site Granger Creek. DOM composition was most variable during freshet with high A254, SUVA254 and low FI and BIX. DOM composition was

relatively insensitive to flow variation during summer and fall. The influence of increasing watershed scale and downstream mixing of landscape contributions was an overall dampening of DOC concentrations and optical indices with increasing groundwater contribution. Forecasted vegetation shifts, enhanced permafrost and seasonal thaw, earlier snowmelt, increased rainfall and other projected climate driven changes will alter DOM sources and transport pathways. Results here support a projected shift from predominantly organic soils (high aromaticity, less fresh) to decomposing vegetation (more fresh and lower aromaticity). These changes may also facilitate flow and transport through deeper flow pathways and enhance groundwater contributions to runoff.

2.1 INTRODUCTION

High latitudes, particularly north-western regions of North America, are experiencing some of the most rapid documented warming on the planet (Serreze and Francis, 2006; DeBeer et al., 2016). This warming has intensified the Arctic freshwater cycle (Bring et al., 2016) and resulted in landscape disturbance and change that alters biogeochemical cycles (Vonk et al., 2015; Wrona et al., 2016). Carbon storage and cycling have been the focus of considerable attention, as soils and sediments in the northern high latitudes are estimated to store approximately 1300 Pg (~40 %) of the global belowground organic carbon pool (Hugelius et al., 2014) and deliver ~10 % of the total freshwater input to global oceans (Gordeev et al., 1996; Opsahl et al., 1999; Shiklomanov, 2000). The mobilization and delivery of this terrestrial organic carbon has been identified as critical to the global carbon cycle given initial estimates that Arctic rivers convey 18-26 Tg C a^{-1} to the Arctic Ocean (Dixon et al., 1994; Dittmar and Kattner, 2003). More recent studies estimate between 25 and 50 Tg C a^{-1} are exported (Raymond et al., 2007; McGuire et al., 2009; Johnston et al., 2018).

Changes in DOC export associated with warming are largely associated with analysis of data from large rivers and links to altered catchment characteristics and processes vary across study areas (McClelland et al., 2007). Regionally, Tank et al., 2016 reported a 39% increase in DOC flux estimates between 1978 and 2012 while Striegl et al. (2005) documented an increase in flux along with a 40% decline in flow weighted DOC concentration between 1978-1980 and 2001-2003 for the Yukon River. In a more recent

analysis of the Yukon River, Toohey et al. (2016) suggest that from 2001-2014, there has been no trend in DOC export whereas Ca, Mg, Na and SO4 and P fluxes have increased significantly over the last thirty years. These increases are attributed to deeper flowpaths as permafrost degrades, increased weathering and increased sulphate oxidation (Toohey et al., 2016). Typically, DOC flux estimates are derived from limited spot water quality sampling and rely on a relationship between water yield and DOC concentration to calculate loads (Raymond et al., 2007; McClelland et al., 2007; Manizza et al., 2009; Holmes et al., 2012; Tank et al., 2016). While the influence of changing mean annual temperature on DOC production and transport across 49 northern watersheds was summarized by Laudon et al. (2012), northern landscapes are also susceptible to fire and thermokarst. These disturbances have a transient influence on hydrologically-mediated DOC transport that confounds spatial and temporal patterns of DOC flux from non-permafrost terrigenous sources to the river-ocean continuum (Larouche et al., 2015; Littlefair et al., 2017; Burd et al., 2018).

In northern and permafrost landscapes, the link between hydrological and biogeochemical cycles and the role of frozen ground and organic matter has been well documented in process-based studies (e.g. Maclean et al., 1999; Carey, 2003; O'Donnell and Jones, 2006; Petrone et al., 2006; Carey et al., 2013a; Koch et al., 2013; Olefeldt and Roulet, 2014; Burd et al., 2018). While wetlands have been highlighted as a source of DOC, particularly in Scandinavian catchments, in permafrost environments the presence of thermally-mediated flowpaths are critical. DOC export is often greatest during snowmelt freshet when DOC is mobilized from organic rich layers such that peak concentrations and high spring flows result in a large annual 'flush' (Boyer et al., 2000; Carey, 2003; Finlay

et al., 2006). This behaviour is often observed in Western Canada but is not ubiquitous (Li Yung Lung et al., 2018). Dependent on the soil profile, as flowpaths descend in response to soil thaw, DOC mobilization typically declines and flow in mineral layers provides more opportunity for immobilization and adsorption (MacLean et al., 1999; review by Kalbitz et al., 2000; Carey, 2003; Kawahigashi et al., 2004, 2006; Frey and Smith, 2005). In some environments, an increase in late fall DOC flux has been ascribed to freezing processes in the soil column (Johnson et al., 2018). How this temporal relationship varies across scales is less certain as few studies provide nested datasets yet analysis by Tiwari et al. (2014, 2017), and synthesis by Creed et al. (2015), suggest downstream mixing and deeper subsurface sources of DOC mask process drivers including in-stream transformation as scale increases. In addition, the role of photodegradation and oxidation of DOC to CO_2 in large Arctic rivers has received considerable attention (Cory et al., 2014; Ward and Cory, 2016).

The lability (i.e. biodegradability) of dissolved organic matter (DOM) is a key regulator of ecosystem function and primarily linked to molecular structure and environmental factors such as temperature, vegetation, oxygen availability and microbial activity (Schmidt et al., 2011). DOC is the mass of C in the DOM pool whose lability, aromaticity and origins can in part be characterized using optical techniques. DOM exported from large Arctic rivers during spring freshet has previously been reported as highly labile (Raymond et al., 2007; Holmes et al., 2008; Spencer et al., 2008) with more refractory DOM during recession periods (Holmes et al., 2008; Wickland et al., 2012). DOM quality is expected to shift in response to permafrost thaw, thermokarst, vegetation

shifts, wildfire and increasing precipitation during summer months associated with climate warming (Davidson and Janssens, 2006; Frey and McClelland, 2009; Schuur et al., 2015). Spectral indices and multi-dimensional analysis of large optical data sets from northern landscapes have resulted in important insights into how DOM quality varies seasonally (e.g. Striegl et al., 2005; Neff et al., 2006; Finlay et al., 2006; Spencer et al., 2008, 2009; Prokushkin et al., 2011; Mutschlecner et al., 2018), and is linked to source material, landscape characteristics (Kawahigashi et al., 2004; Harms et al., 2016) and disturbance (Balcarczyk et al 2009; Abbott et al., 2015; Littlefair et al., 2017; Burd et al., 2018).

While information from large rivers is critical for estimates of DOM loading to the Arctic Ocean, research at headwater scales that identifies controls on DOC production and transport is relatively scarce and often points to multiple process mechanisms (Maclean et al., 1999; Temnerud and Bishop, 2005; Larouche et al., 2015). Furthermore, much of our understanding of DOC is biased towards lowland ecosystems, with relatively scarce information from northern alpine systems (Laudon et al., 2012). The goal of this paper is to enhance our understanding of the coupled dynamics of hydrology and DOC export and composition (using optical properties of DOM) in a well-studied, discontinuous permafrost alpine catchment in subarctic Yukon, Canada. We collected samples over two consecutive years from freshet to late fall from two headwater catchments, a lake, wetland and the outlet of a mesoscale catchment in a nested design to explore seasonal and annual variability in DOC concentrations and DOM composition. Impacts of increasing catchment scale and differing landscape types on DOM optical indices were also assessed.

The specific questions addressed in this work were:

1) How do DOC concentration and DOM composition vary over multiple seasons across a diverse mountain watershed, and 2) what are the factors that drive this variability across scales?

This study provides important insights into how season and scale influence the sources and transport of DOM in a cold alpine setting.

2.2 METHODS

2.2.1 Study Area

Several headwater streams, a wetland and a high elevation lake outlet were studied within the Wolf Creek Research Basin (WCRB, 61°310 N, 135°310 W) located ~20 km south of Whitehorse in Yukon Territory, Canada (Fig. 2-1). WCRB is a long-term research watershed located at the edge of the Coast Mountains, spans an elevation ranging from 712 m a.s.l. to 2080 m a.s.l., and has a drainage area of ~179 km^2. WCRB straddles three ecological zones with boreal forest at lower elevations (predominantly White Spruce (*Picea glauca var. porsildii*)) covering ~28% of the watershed; at intermediate elevations shrub taiga comprises ~47 %, and at elevations above ~1500 m, alpine tundra and bare rock surfaces predominate. WCRB has a relatively dry Subarctic climate (Koppen classification *Dfc*) with 30-year climate normals (1981-2010) reported for Whitehorse Airport (706 m). Average airport air temperature is -0.1 ^{o}C and precipitation is 262.3 mm, with 161 mm falling as rain. However, considering that WCRB covers a large elevation gradient, colder temperatures and considerably larger volumes of precipitation have been reported for high-

elevation sub-watersheds (Pomeroy et al., 1999; Carey et al., 2013b; Rasouli et al., 2019). The geological setting of WCRB is sedimentary sandstone, siltstone, limestone and conglomerate. Atop bedrock, thick stony till and glacial drift covers most of the basin. Soils in the top metre are generally sandy to silty and at higher elevations (taiga and lower tundra ecozones), a veneer of surface organic soils with variable thickness predominates. Permafrost underlies much of the basin (~43 %), particularly at higher elevations and on north-facing slopes in the taiga and alpine ecozones (Lewkowicz and Ednie, 2004).

Much of this study focussed on the headwater catchment of Granger Creek (GC), which drains an area of 7.6 km^2 and ranges in elevation from 1355 to 2080 m a.s.l. (McCartney et al., 2006; Carey et al., 2013a) (Fig. 2-1). GC is above treeline (~1200 m) and is dominated by Willow (*Salix* Sp.) and Birch (*Betula* Sp.) shrubs at lower elevations with dwarf shrubs, lichen and bare rock above 1500 m. South facing slopes have a thin organic layer overtop sandy soils whereas north slopes have thicker organic layers (10-30 cm) and are underlain with discontinuous permafrost. A wide riparian zone (50 to 100 m) with a consistently high water table in the lower reaches of GC lies between the slopes. Buckbrush Creek (BB, 60°31'18.01" N, 135°12'17.27" W), another headwater catchment, drains an area of 5.75 km^2 and is located approximately 2 km west of GC (Fig. 2-1). BB ranges in elevation from 1324 to 2080 m a.s.l. with similar physiographic characteristics to GC. However, Buckbrush Creek is less incised than GC and the riparian zone shows evidence of multiple overbank channels during high flow events.

The site Wetland 1 (W1, 60°31'18.72" N, 135°11'34.71" W) is located at the edge of a wetland complex located downstream of BB with an indeterminate drainage area. The vegetation is dominantly sedges, with ponded water covering 200 m^2. Coal Lake (CL, 60°30'36.65" N, 135° 9'44.47" W) is a long-term hydrometric station located approximately at the mid-point in the watershed at the outlet of an ~1 km^2 lake (Rasouli et al., 2019). A large wetland complex is located upstream of CL, which is surrounded by steep slopes and vegetation that transitions from boreal forest at lake level to alpine tundra at the top of surrounding slopes.

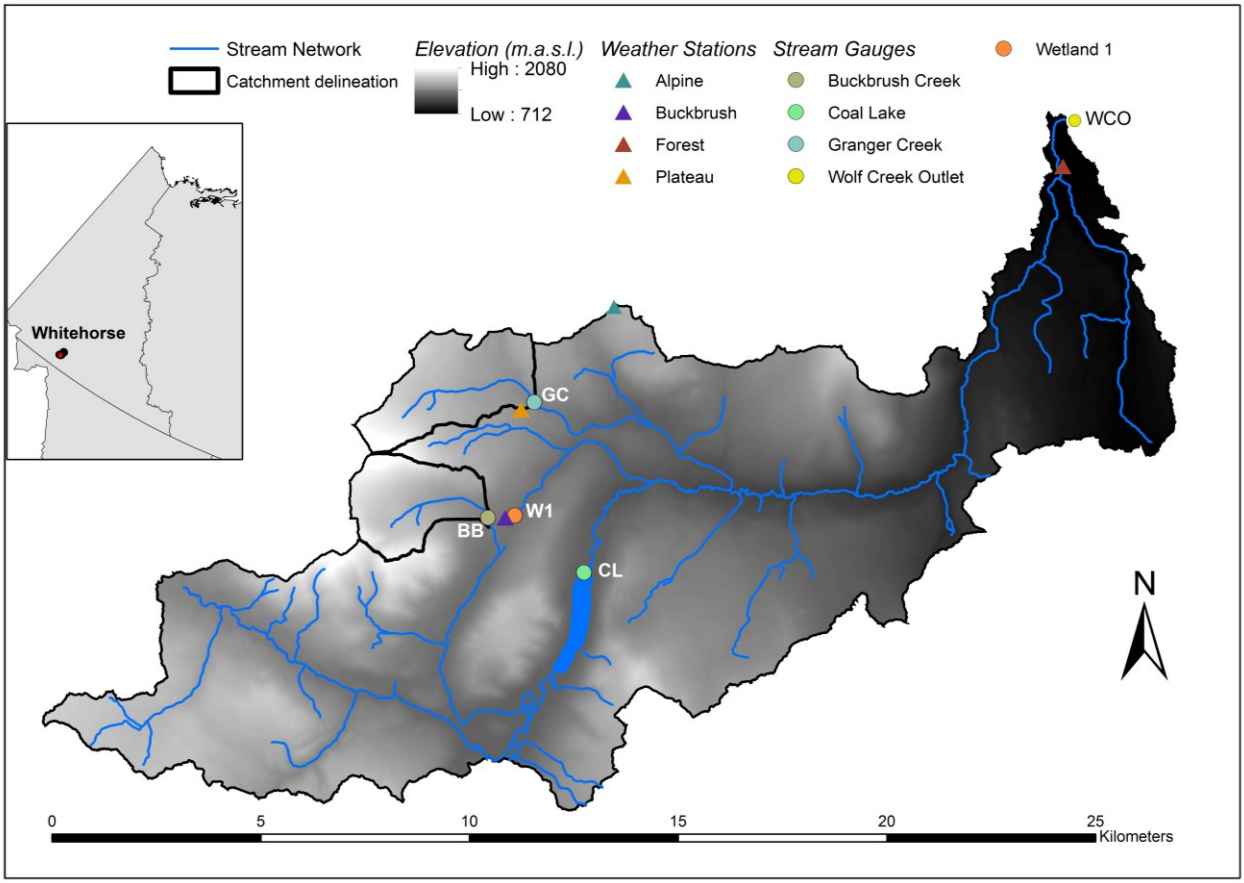

Figure 2-1. Map of Wolf Creek Research Basin (WCRB) with BB and GC catchments delineated. All stream gauges (BB, GC, CL, W1 and WCO) are indicated by circles; weather stations within WCRB are shown as triangles.

2.2.2 Field measurements

Discharge was measured using rating curves developed for each study season at all sites except the WCRB outlet (WCO) and CL, which has retained a stable curve for the past several years (discharge measurements at the WCRB outlet exist from 1992). Stilling wells at each site were instrumented with Solinst Leveloggers and compensated with adjacent Solinst Barologgers measuring stage/pressure every 15 minutes to provide continuous flow records. Manual flows were taken frequently using a SonTek Flowtracker

during high and low flows with salt-dilution gauging during periods when the channels were beneath ice. Bushnell game cameras and in-person observation were used to document when the headwater streams and outlet were ice-free in spring to validate the use of pressure transducer measurements.

WCRB has three long-term weather stations to characterize the climate in each ecozone (Alpine, Buckbrush, Forest). All radiation components, air temperature, wind speed, vapour pressure and total precipitation are measured at 30 minute resolution, year-round at each site with some gaps due to power loss (Rasouli et al., 2019). The rainfall data reported in this study is from a tipping bucket rain gauge located at the nearby Buckbrush weather station and have been compared with an Alter-shielded Geonor total precipitation gauge for accuracy. A fourth meteorological tower (Plateau) in GC watershed has been operating since 2015. Monthly snow courses are completed in each ecozone to determine snow water equivalent (SWE), and on-site continuous measurements from a SR50 sensor at Plateau along with snow pillow measurements from Buckbrush (Rasouli et al., 2019 provide instrumentation details) supplement these and provide information on melt rates.

2.2.3 Surface water sample collection and preparation

Surface water samples were collected from April 2015 to December 2016, with the bulk of collection between April and September of each year with most samples collected at GC and frequent sampling at BB and WCO. Only a few samples were taken at W1 from 2015 to 2016. For DOC, samples were field filtered with single use plastic syringes submersed in the sample water immediately prior to sampling. Water was displaced through

a 0.45 µm VWR polyethersulfone syringe filter and collected in a 60 ml opaque amber HDPE bottle. Duplicates were taken approximately every 10 samples. All samples were kept cool and out of direct light before being shipped for analysis. DOM water samples were filtered in situ and stored cool in 40 ml glass amber vials. In situ filtration with a syringe kept the time between sample collection and filtration to a minimum, particularly during freshet when logistical constraints meant that researchers remained in the catchment for up to two weeks at a time before returning to Whitehorse.

2.2.4 DOC and DOM fluorescence analysis

Water samples were sent to the Biogeochemical Analysis Service Laboratory (University of Alberta) for analysis on a Shimadzu 5000A Total Organic Carbon analyzer for DOC concentration following the US EPA protocol 415.1. The reportable detection limit provided by BASL for these samples was 0.1 mg/L In total, 330 surface water samples were collected from 2015 to 2016 as outlined in Table 1. Of the 330 DOC samples, ~215 were analysed for DOM quality using fluorescence spectroscopy. Seven additional samples from CL in 2017 were analysed for DOC concentration and DOM quality.

The fluorescence excitation emission matrices (EEMs) were obtained from 0.45 µm PES-filtered water samples using a Yvon Jobin Aqualog Benchtop Spectrofluorometer (HORIBA Scientific, Edison, NJ, USA). I ran the majority of water samples at McMaster University with support for samples from 2017-2018. Fluorescence spectra were recorded at an excitation range of 240-600 nm in steps of 5 nm with an emission range of 212-620 nm, in steps of 3 nm. The integrated Raman spectrum was checked before each run and

compared to prior values to ensure consistent lamp intensity. A sealed Quinone Sulfate sample and blank pair were also run prior to each batch of samples and compared to prior values to ensure consistency. Fluorescence spectra were normalized to the area under the Raman scatter peak (peak excitation wavelength 397 nm) of a sealed Milli-Q water sample prior to all sample runs. A lab blank of distilled water was also appended to each sample run and every 4 sample runs, a sample was repeated. Scatter from the sealed Raman Milli-Q sample was subtracted from each sample fluorescence spectrum. The correction and normalization of samples to the Raman standard resulted in normalized intensity spectra being expressed in Raman units (R.U., nm^{-1}).

Blank subtraction, Rayleigh scatter and inner filter effects were corrected using the Aqualog(R) software. Subsequent EEM corrections and smoothing were done with the DrEEM toolbox (Murphy et al., 2013) in Matlab (Mathworks Inc., Massachusetts, USA). Results were considered comparable to each other since all data were collected from a single instrument and the Raman standard emission intensity was verified for each data run.

Optical data obtained from the Aqualog(R) was used to calculate optical indices. $SUVA_{254}$ (L mg C^{-1} m^{-1}) is calculated as UV absorbance at 254 nm (m^{-1}) divided by DOC concentration (mg L^{-1}) (Weishaar et al., 2003) with a unit correction based on the cuvette path length. $SUVA_{254}$ is commonly reported along with DOC concentration and is positively related to aromaticity in bulk DOM (Weishaar et al., 2003) with higher values indicative of a strong terrestrial signal (Jaffé et al., 2008).Typically, SUVA values greater than 4.5 L mg C^{-1} m^{-1} denote high absorption at 254 nm due to colloids or iron (Weishaar

et al., 2003; Hudson et al., 2007). Research in northern peatlands associated peat soil leachates with relatively lower $SUVA_{254}$ values of 3.0 L mg C^{-1} m^{-1} (Olefeldt et al., 2013). Allochtonous, terrestrial DOM is associated with increased aromaticity and a higher $SUVA_{254}$ value while lower SUVA values are related to modified terrestrial DOM. The biological index (BIX) is the ratio of emission intensities at 380/430 nm at an excitation wavelength of 310 nm (Huguet et al., 2009). Higher BIX values indicate greater autotrophic productivity (Huguet et al., 2009) or greater relative freshness of bulk DOM (Wilson and Xenopoulos, 2009) while lower values indicate older, more terrestrial DOM. The fluorescence index (FI) is calculated as the ratio of fluorescence emission intensities at 470/520 nm at an excitation wavelength of 370 nm (Cory and McKnight, 2005). FI is used to differentiate between DOM derived from microbial sources (1.7-2.0) or higher terrestrial plant sources (1.3-1.4) with intermediary values indicative of mixing (McKnight et al., 2001; Jaffé et al., 2008; Fellman et al., 2010). Typical values reported for inland rivers are between 1.3-1.8 (Brooks and Lemon, 2007).

In addition to the DOM quality indices reported and discussed throughout this paper, absorbance at 254 nm (A254), the freshness index (Parlanti et al., 2000) and the modified humification index (HIX: Ohno, 2002) were also calculated and compared with the other indices. BIX and the freshness index were highly correlated (r^2 : 0.99, $p<0.001$) for all sites, years and seasons. A254 and DOC concentrations also showed high correlation (r^2 : 0.95-7, $p<0.001$). Due to similarity in temporal trends of DOM indices, HIX was not reported independently of the parameters mentioned above. HIX is calculated by summing the peak area under emission intensities from 435-480 nm divided by that of 300-345 nm

at an excitation of 254 nm (Zsolnay et al., 1999). Higher HIX values are related to an increased degree of humification (Huguet et al., 2009; Fellman et al., 2010).

2.2.5 DOC Load Calculations

DOC fluxes for GC were estimated using the R package RiverLoad (Nava et al., 2019). RiverLoad provided several methods to generate estimates of DOC flux and for this paper, Method1 (time- weighted Q and C) was chosen as most appropriate. Briefly, Method1 considers the mean concentration and mean flow of each sample to obtain a load value and is biased towards underestimating load in some situations (see Nava et al. 2019, Section 2.1.1 for full details and equation). Daily discharge data and DOC concentrations (maximum of 1 measurement per day) for 2002, 2003, 2006 and 2008 were obtained from the authors of Carey et al., 2013a. DOC concentrations (maximum of 2 per day) and discharge at 15 minute resolution for 2015 and 2016 are outlined in Sections 3.2 and 3.3). Any gaps in the discharge data were filled by time-weighted interpolation, however there were no gaps greater than 3 days during springs flows for any year (2002, 2003, 2006, 2008, 2015, 2016.

2.2.6 Statistical analysis

General descriptive statistics including the mean and standard deviation were calculated for DOC, $SUVA_{254}$ and the fluorescence indices and compiled in Table 1. To better assess differences between landscape units (e.g. headwaters, wetland, lake, catchment outlet), principal component analysis (PCA) was performed using DOC concentrations and optical indices (i.e. FI, BIX, Freshness, HI, $SUVA_{254}$). These variables

were scaled and then standardized into a covariance matrix to avoid larger magnitudes exerting greater influence than smaller magnitudes. The PCA was performed using R software version 3.4.0 (R Core Team 2017) in RStudio with R function princomp(), and packages ggplot2, GGally, ggpubr, lubridate, magrittr, grid, dplyr and tidyr for calculating descriptive statistics, correlations, data manipulation and visualization.

Year	*Sites*	DOC (mg/L)			$SUVA_{254}$			BIX			FI		
		Spring	Summer	F/W	Spring	Summer	F/W	Spring	Summer	F/W	Spring	Summer	F/W
2015													
	BB	1.77±0.66(5)^{A*}	1.25±0.31(11) ^{A*}	1.19±0.39(9)^{A*,B*}	3.30±0.58(3)	3.88±0.55 (4)	2.72±0.42 (2)	0.55±0.04	0.60±0.01	0.60±0.03	1.49±0.06	1.54±0.03	1.57±0.76
	CL	2.90(1)		2.60(1)									
	GC	2.89±2.29(52) ^{A**}	1.07±0.21(36) ^{A**}	1.75±0.76(17) ^{A**,B*}	3.21±0.84(22)	3.81±0.75 (14)	2.42±0.33 (3)	0.69±0.06	0.60±0.02	0.65±0.02	1.52±0.06	1.54±0.04	1.57±0.04
	W1	15.8(1)			3.94(1)			0.47 (1)			1.46(1)		
	WCO			1.79±0.90(14) ^{B*}			2.21±0.17 (10)			0.66±0.03			1.62±0.03
2016													
	BB	2.34±0.87(14) ^{A**,B**}	1.42±0.27(23) ^{A**,B**}	1.50±0.20(3)	3.56±0.48(10) ^{A**,B**}	2.81±0.59 (16) ^{A**,B**}	2.45±0.28 (3)	0.513±0.03 ^{A**,B**}	0.58±0.03 ^{A**,B**}	0.62±0.02	1.45±0.04 ^{A**}	1.52±0.06 ^{A**,B*}	1.52±0.00
	CL		3.15±0.35(2)										
	GC	4.32±2.56(43) ^{A**,B**}	1.71±0.34(32) ^{A**,B**}	2.00±0.57(20) ^{A**}	3.86±1.40(37) ^{A**,B**}	2.86±0.38 (17) ^{A**,B**}	3.14±0.32 (11) ^{A**}	0.513±0.06 ^{A**,B**}	0.58±0.03 ^{A**,B**}	0.60±0.04 ^{A**}	1.45±0.04 ^{A**,B**}	1.50±0.04 ^{A**,B*}	1.50±0.02 ^{A**}
	W1	6.70(1)	7.37±0.64(10)	6.95±0.21(2)	4.77(1)	4.04±0.60 (7)		0.58(1)	0.63±0.05		1.58(1)	1.54±0.04	
	WCO	2.69±0.80(18) ^{A**,B**}	2.58±0.44(22) ^{A**,B**}	2.35±0.35(3)	2.83±0.42(12) ^{A**,B**}	2.70±0.28 (19) ^{A**,B**}	2.69±0.11 (2)	0.582±0.04 ^{A*,B**}	0.60±0.02 ^{A*,B**}	0.66±0.03	1.53±0.02 ^{A*,B**}	1.54±0.03 ^{A*,B*}	1.55±0.01

Table 2-1. Summary statistics for DOC, SUVA, BIX and FI at all sites over 2015-6. Seasons are separated with spring (15 April - 15 June); Summer (16 June - 15 August); Fall/Winter (16 August - 14 April). Significant differences from non-parametric Kruskall-Wallis tests across seasons for the same site are indicated by A while significant differences across sites during the same season in the same year were indicated by B. $p<0.05$ (*) or $p<0.001$ (**). Notation = ± standard deviation (n: number of samples).

2.3 RESULTS

2.3.1 Climate

For 2015 and 2016, the average annual air temperature as recorded at the Whitehorse airport weather station was 1.4 and 2.4 °C respectively, which is warmer than the 30-year normal (1980-2010). May average monthly temperatures in both years were well above the normal, with an average air temperature of 11.8 °C in May 2015 compared with a normal of 7.3 °C. Average annual air temperatures measured at the Buckbrush weather station (mid-basin) were -0.6 and -0.0 °C respectively for the two years (Fig. 2-2). Persistent inversions in winter result in warmer temperatures at higher elevations from December through to February. Accurate measurements of total precipitation have not been recorded at Whitehorse airport for several years, limiting long-term context but rainfall values from a nearby (~ 3 km) station were used for 2015-6 as well as rainfall from the Buckbrush weather stations (Fig. 2-2).

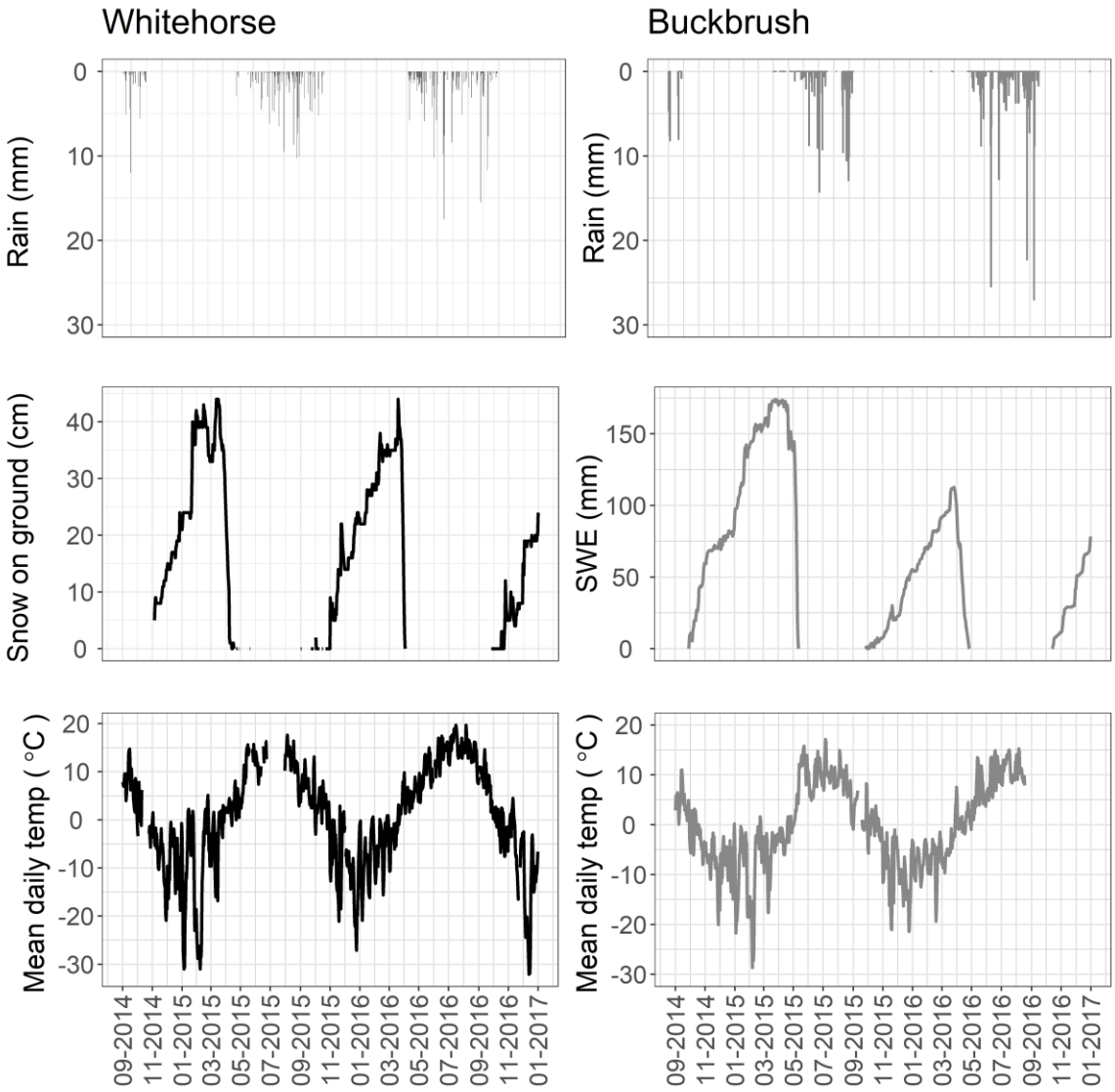

Figure 2-2. Climate variables from Whitehorse Auto (Rainfall; 60°43'59.000" N, 135°05'52.000" W135°05'52.000" W, 707 m a.s.l., Whitehorse Airport (Snow on ground, Mean daily temp; 60°42'34.200" N, 135°04'07.800" W) and Buckbrush weather stations. (Left) Rain (measured in mm) from Whitehorse Auto (Climate ID: 2101310) located 3 km from Whitehorse Airport, snow on ground (in cm) and mean daily air temperature (°C) from the Environment Canada Airport weather station (YXY, Climate ID: 2101300) located ~ 14 km NW of Forest at 706 m a.s.l. (Right) Rainfall daily totals in mm were derived from hourly measurements, snow water equivalent (SWE) in mm based on 3 hour measurements from a snow pillow beside Buckbrush weather station. Daily average air temperature (°C), derived from 30 min measurements.

2.3.2 Discharge

The 2015 and 2016 hydrographs for GC and the Wolf Creek outlet (WCO) exhibited patterns typical of northern watersheds but were distinct in that both years have a late-season increase (Fig. 2-3), which is rare in the GC and WCO historical record (Carey et al., 2013a,b; Rasouli et al., 2019).

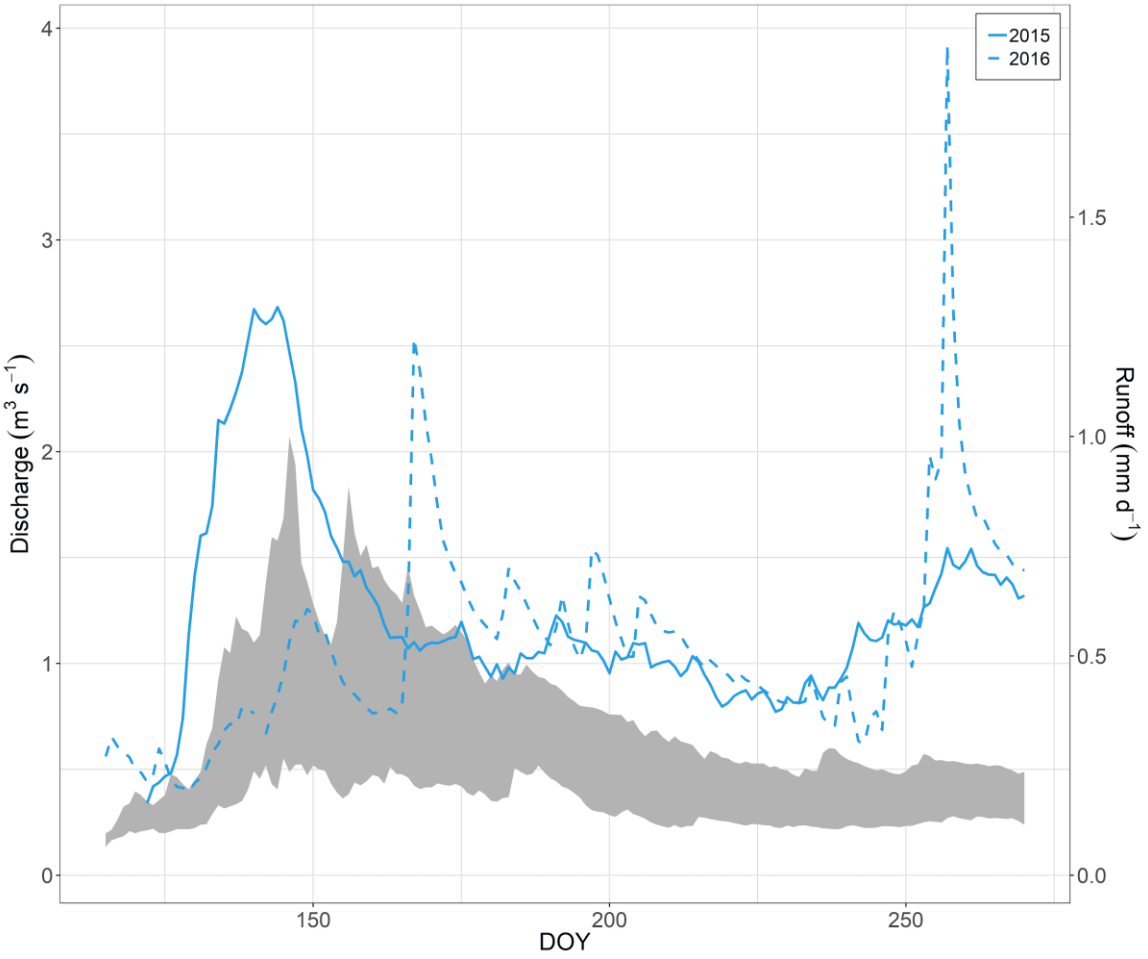

Figure 2-3. Historical flow at WCO with 2015-6 flows superimposed. Grey area represents inter-quartile range of 1993-2013 data. Solid line = 2015; dashed line = 2016. Day of year (DOY) along x-axis.

Summer flows were also greater than typically observed. For GC, in 2015 while there was an early measurable stream response on 9 May, freshet began on 14 May when flows increased from ~0.02 m^3s^{-1} to daily flows averaging ~0.5 m^3s^{-1} over 9 days. Peak 2015 daily discharge was 0.67 m^3s^{-1} on 22 May, thereafter flows began to decline to summer levels ~0.2 m^3s^{-1}. In response to ~125 mm of rain between 17 August and 11 September, flows increased to ~0.46 m^3s^{-1} on 14 September before gradually declining. Discharge at BB for 2015 and 2016 were slightly lower magnitude than GC with delayed flow response to both freshet and summer rainfall. Data loss resulted in incomplete discharge data for both years at BB. Manual measurements are shown in Fig. 2-3 to supplement continuous measurements. Discharge at WCO followed a similar pattern to GC, rising from a winter baseflow of ~0.4-0.5 m^3s^{-1} on 3 May to a peak freshet of 2.68 m^3s^{-1} on 24 May. As with GC, flows increased in September prior to the removal of the transducer on 1 October. Flows in 2016 were distinct at both GC and WCO when compared with 2015 and the historical record, exhibiting a more pronounced response to snowmelt than 2015 that occurred much earlier in the year in comparison to the 25 year record (Fig. 2-3). There was no distinct snowmelt freshet event in 2016, instead a gradual increase in flows was punctuated with hydrograph rises that corresponded with both snowmelt and summer rainfall events. Flows were of the same general magnitude to those in 2015, and once again large late season rainfalls (~115 mm between 17 August and 10 September) resulted in high September flows, with peak discharge at WCO recorded at 3.9 m^3s^{-1}on 13 September. Flows declined again until the transducers were removed on 17 October, yet were very high compared with mid-season flows.

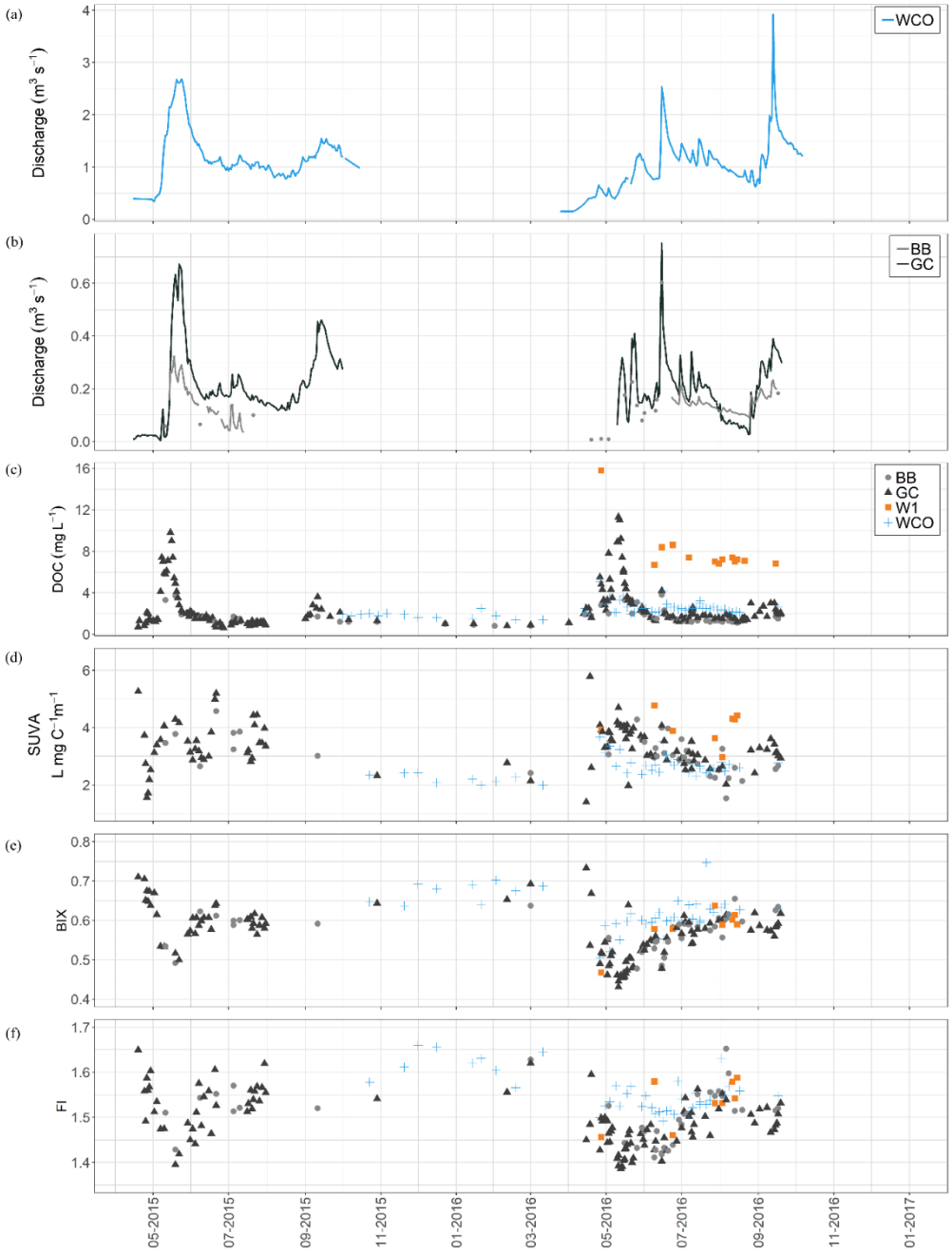

Figure 2-4. Flow, DOC and optical indices for WCRB study sites. (a) Daily discharge data from WCO shown from April 2015 to October 2016. (b) Daily discharge data from GC (dark grey) and BB (light grey). (c) DOC concentrations in mg/L from grab samples over the study period with BB (light grey, circle), GC (dark grey, triangle), Wetland 1 or W1 (orange, square), WCO (light blue, +).

2.3.3 Dissolved Organic Carbon (DOC) Concentrations

Sampling in 2015 was largely confined to GC and BB with more extensive sampling at other sites in 2016. For GC, similar patterns were observed in both years with over-winter and pre-freshet DOC concentrations below 1 mg L^{-1} and rising to ~10 mg L^{-1} on the rising limb of the first snowmelt flush followed by a rapid decline to levels between 1 and 2 mg L^{-1} throughout the summer and with a slight rise in the fall. Seasonal statistics for DOC are presented in Table 2-1. In 2015, the single freshet event corresponded with the rise in DOC, yet the rise and fall in DOC concentration occurred fully on the rising limb of the freshet hydrograph between 7 May and 29 May. The maximum DOC concentration of 9.8 mg L^{-1} on 15 May corresponded to a 13.8 mm rain event atop a sporadic snowpack with largely frozen soils. After June, DOC concentrations continued to decline with slight increases corresponding to rainfall events. Towards the end of the measurement period in 2015, DOC concentrations rose to a maximum of 3.6 mg L^{-1} with increasing discharge in response to sustained precipitation. Over-winter values in December and January declined to ~1 mg L^{-1}. This pattern of DOC behaviour was remarkably similar at the adjacent BB catchment which had more limited sampling. In 2016, the spring rise in DOC at GC and BB corresponded to the period immediately after the first small snowmelt pulse but prior to the bulk of the freshet signal (Fig. 2-3). Concentrations again rose to ~11 mg L^{-1} with a steep recession to summer levels where rainstorms would occasionally increase concentrations above 2 mg L^{-1}. As in 2015, a wet late season with a large hydrograph increase resulted in increased DOC concentrations near 3 mg L^{-1} but concentrations were much less than for corresponding freshet flows.

Sampling at WCO began in late fall 2015 with DOC concentrations of ~2 mg L^{-1} and remained near this level through April 2016. Concentrations increased during the early phases of open water freshet, yet only rose to ~5 mg L^{-1} on 26 April and then declined to summer levels between 2 and 3 mg L^{-1}, with some variability related to rainfall events. While sampling was limited, there did not appear to be a notable increase at WCO during the wet fall in 2016. At W1, DOC was ~16 mg L^{-1} on the first sampling date of 27 April, and then post-freshet samples in June through September had concentrations between 7 and 9 mg L^{-1}. Concurrent DOC and fluorescence samples were only collected from CL post-freshet during summer and fall of 2017.

2.3.4 DOC Loads

Export estimates for the six years of available data from GC range from 0.29 to 1.48 g C m^{-2} during spring (15 April to 14 June); between 0.08 to 0.31 g C m^{-2} in summer (15 June to 14 August); 0.28 and 0.20 g C m^{-2} during fall in 2015 and 2016, respectively (Table 2-2). No estimates were made for fall in 2002, 2003, 2006 and 2008 due to a lack of concentration data. Spring DOC export was lowest during 2003 (0.42 g C m^{-2}) and 2016 (0.29 g C m^{-2}), two years characterized by a staggered snowmelt leading to relatively low discharge during peak DOC concentrations (Fig. 2-4abc; Fig 4 in Carey et al., 2013a). Total export during summer was relatively consistent across 2002, 2003, 2006 and 2015 at 0.12, 0.19, 0.14 and 0.08 g C m^{-2} while it was appreciably higher in 2008 and 2016 at 0.31 and 0.28 g C m^{-2}, respectively. Fall DOC export estimates for 2015 and 2016 were 0.28 g C m^{-2} and 0.20 g C m^{-2}. DOC export estimates for WCO in 2016 were 0.06 g C m^{-2} in spring, 0.09 g C m^{-2} in summer and 0.09 g C m^{-2} for fall (Table 2-2).

2.3.5 Optical Indices

While there exists a large number of optical indices in the literature (see Hansen et al. 2016), in this work we report the widely utilized $SUVA_{254}$, biological index (BIX) and fluorescence index (FI) to help infer the source and composition of DOM (Table 2-1). For GC, $SUVA_{254}$ exhibited considerable variability compared with DOC concentrations. In 2015, $SUVA_{254}$ declined from > 5 to ~ 1 L mg C^{-1} m^{-1} rapidly between 19 and 26 April in response to loss of channel ice, and then rose to reach a local maximum of ~4.1 L mg C^{-1} m^{-1} on 10 May that corresponds to the annual peak in stream discharge. $SUVA_{254}$ then declined on the receding freshet limb yet increased markedly in June in response to 18 mm of rain (11 to 18 June), whereupon it ranged between 2.8 and 4.5 L mg C^{-1} m^{-1}.

Limited under-ice sampling suggests $SUVA_{254}$ remained relatively consistent between 2 and 3 L mg C^{-1} m^{-1} before falling to 1 L mg C^{-1} m^{-1}, prior to the onset of freshet when values rose dramatically to 5.2 L mg C^{-1} m^{-1} before gradually declining through August with considerable variability. Following the wet fall in 2016, $SUVA_{254}$ began to rise to values > 3 L mg C^{-1} m^{-1}. Patterns of $SUVA_{254}$ for BB were similar to GC in both years. $SUVA_{254}$ started low in spring 2015 at the headwater catchments before rising slightly in summer whereas the opposite occurred in 2016. For WCO, samples over the 2015-16 winter declined slightly from 2.5 to 2 L mg C^{-1} m^{-1}, and then during freshet increased to ~3.7 L mg C^{-1} m^{-1} and then gradually declined to ~2.5 L mg C^{-1} m^{-1} with some increases associated with rising discharge. $SUVA_{254}$ at W1 was on average higher compared with other sites, although limited sampling makes it uncertain as to any temporal pattern.

BIX tended to be inversely related to discharge (and DOC concentration) during freshet at the headwater sites (GC, BB) (Fig. 2-4). For GC in 2015, BIX fell from just above 0.7 to 0.49 during peak freshet and then increased to between 0.55 and 0.65 during summer. Values increased over winter to a maximum of 0.71 prior to 2016 freshet where a steep decline to values < 0.45 occurred during the early phase of runoff in May and then gradually returned to values between 0.55 and 0.65 with declines associated with rainfall-driven spikes in the hydrograph. The late season increase in discharge did not strongly influence BIX at GC. BIX exhibited similar patterns between 2015 and 2016 at the headwater sites with minimum values during spring in both years followed by an increase, which plateaued in summer 2015 but continue to rise slightly during the 2016 summer. BIX for WCO increased over winter before also declining during early melt in 2016 and then rose to values ~0.65 with some large increases (as opposed to decreases at GC) during storm events. Timing of declines to rainfall events was slightly offset between the headwater sites and the outlet WCO. At W1, BIX values increased slightly throughout the sampling period in 2016 (Fig. 2-4).

FI at GC and BB exhibited patterns similar to BIX but inverse to $SUVA_{254}$ (Fig. 2-4). In 2015, FI declined from 1.65 to 1.4 as DOC rose on the rising freshet limb, and then declined to values between 1.5 and 1.6 during summer. In 2016, FI values again declined from 1.6 to 1. during freshet yet were on average lower than 2015 but also gradually increased throughout summer with a small decline during the wet late summer. For WCO, winter FI ranged between 1.55 and 1.65 and more gradually declined during freshet to ~ 1.5 and then increased slightly with more limited variability throughout the

summer. A small decline during the wet period in late September was observed. Over the two study years at GC, BB and WCO, mean FI was lowest during spring, and higher in summer (2015, 2016) than in fall 2016. For W1, FI was low at 1.45 on the first sampling date in spring 2016 when DOC was high, and then increased with some variability but values were on average greater than those at GC and BB.

2.3.6 Principal Component Analysis

A principal component analysis (PCA) using 216 samples from across WCRB over three years was completed to explore landscape and seasonal climate controls on DOC concentration and quality (Fig. 2-4). DOC concentrations and fluorescence indices at BB (2015-7), CL (2017), GC (2015-7), W1 (2016-7) and WCO (2015-7) were introduced into the PCA for insight into how landscape type influences DOM quality at WCO (Table 2-S1). The first principal component (PC1) explained 56.8 % of the variance in the data and was selected based on screeplot analysis, a drop in the proportion of variance explained and the Kaiser criterion (Kaiser and Rice, 1974). The remaining principal components (PCs) explained much less of the variance than PC1 (Table 2-S3). PC1 predominantly represents the relationship among DOM quality and concentration and is positively and negatively correlated with all DOM fluorescence indices except for HIX. PC2 explained 15.8% of the variance and was most closely related to a single variable (HIX) with little relationship to the other analytes (Fig. 2-4). Further PCs were not explored (See Supplemental Materials for more details).

BB and GC plotted similarly and are shown together (Fig. 2-5) to highlight differences between the landscape types rather than between the two headwater sites. DOC concentrations and $SUVA_{254}$, BIX/Freshness and HIX most strongly distinguish the samples in the PCA. Spring samples from the headwaters and wetland plot mostly to the right along PC1 due to high DOC concentrations and $SUVA_{254}$ measured during that time period. Headwater samples span almost the entire PC1 axis due to the high variability in spring-time DOC and streamflow. Fall/winter samples are predominantly located left of the zero-line (Fig. 2-5) for all sites. All CL samples cluster together. Some separation of DOC concentrations and DOM indices is shown due to high DOC, BIX and/or $SUVA_{254}$ values (Fig. 2-6).

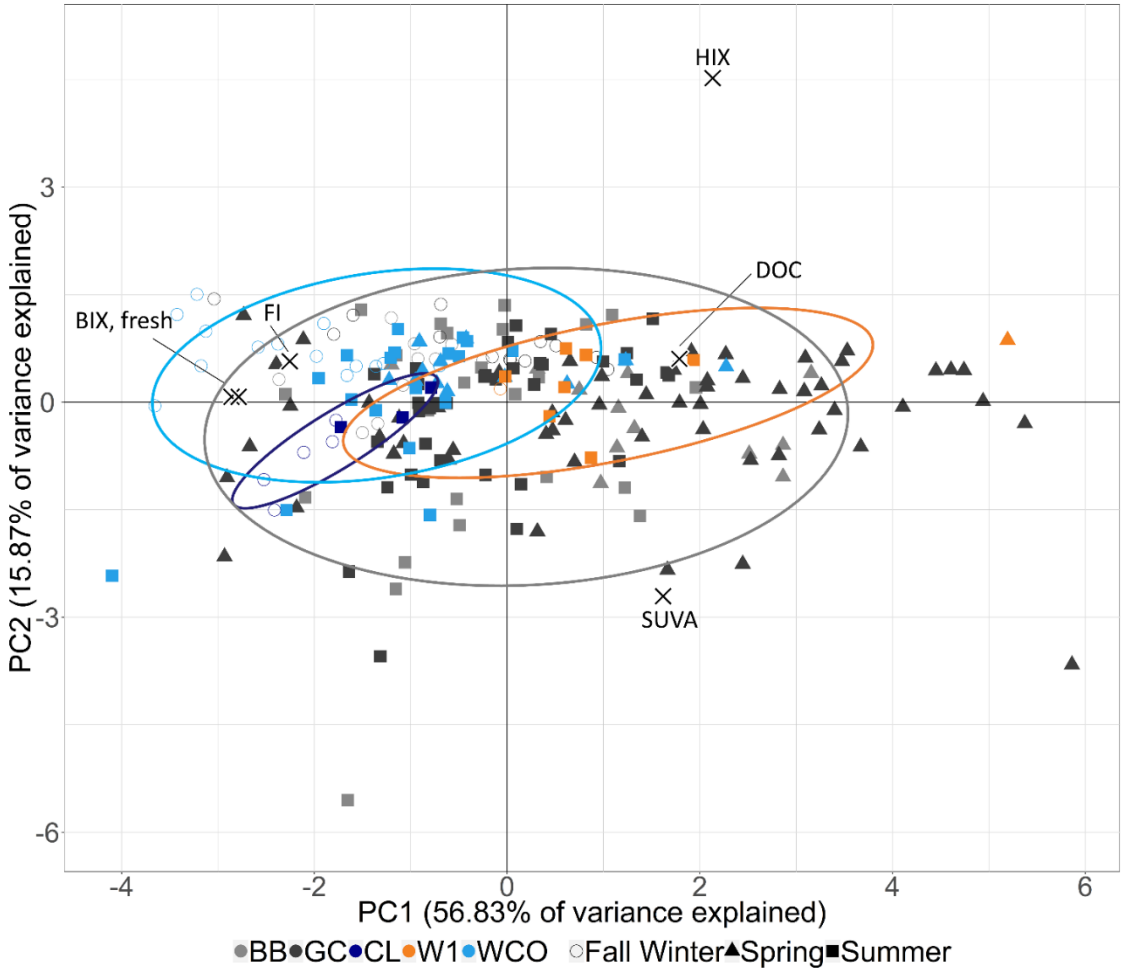

Figure 2-5. Biplot from PCA. PC1 on the x-axis and PC2 along the y-axis. X indicates where the point of the loadings with the applicable index written nearby. Samples are grouped by season: Triangles = Spring (15 April-15 June); Squares = Summer (16 June-15 August); Circles = Fall/Winter (16 August-14 April). Samples are also grouped by landscape type: Bright blue = Mesoscale outlet (WCO); Dark blue = Lake (CL); Orange = Wetland (W1); Grey = Headwaters (light grey – BB, dark grey – GC).

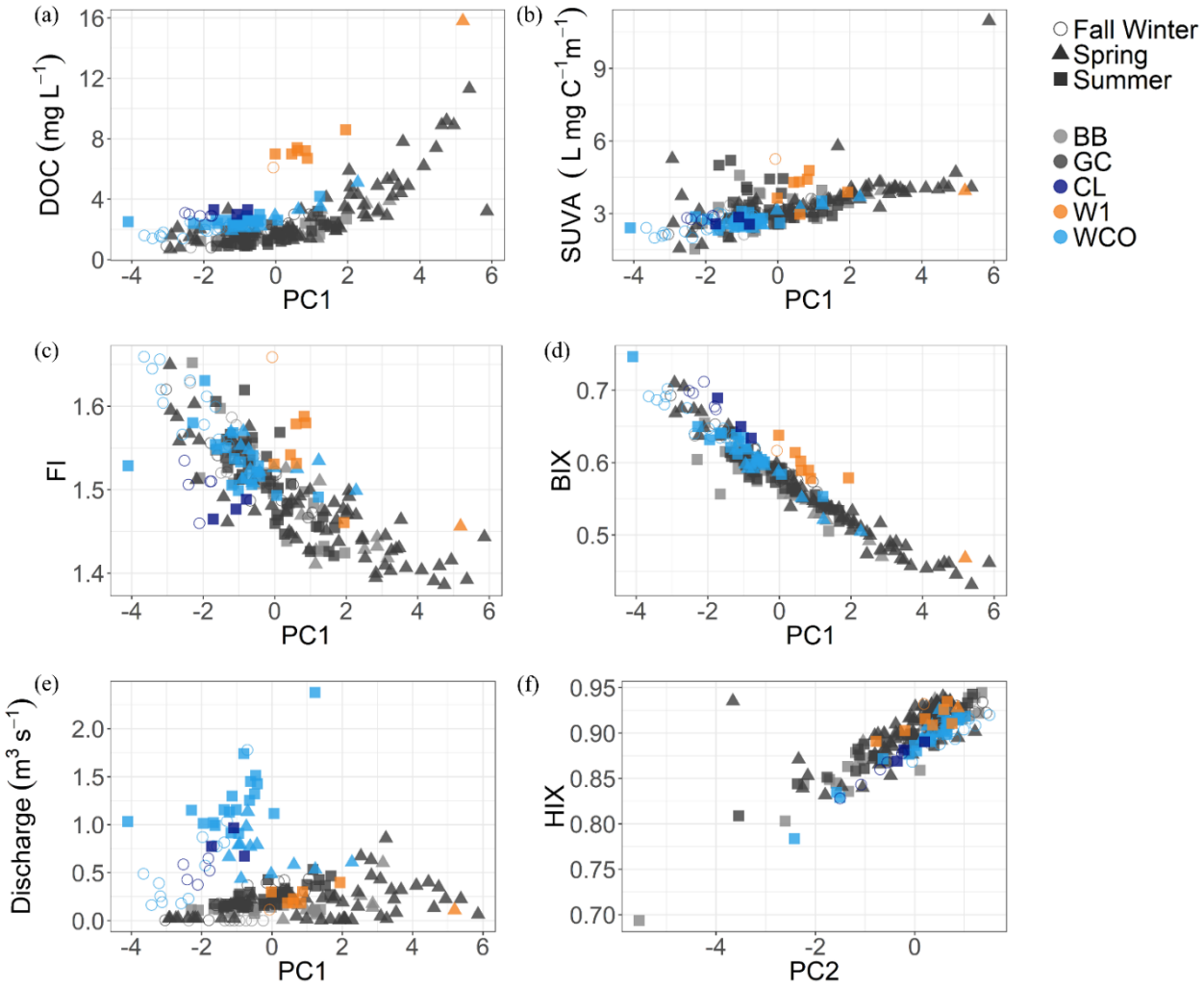

Figure 2-6. Regressions of principal components to DOC concentrations and DOM indices. Regression of PC1 to DOC concentrations implies some non-linear behaviour. Samples are grouped by season: Triangles = Spring (15 April-15 June); Squares = Summer (16 June-15 August); Circles = Fall/Winter (16 August-14 April). Samples are also grouped by landscape type: Bright blue = Mesoscale outlet (WCO); Dark blue = Lake (CL); Orange = Wetland (W1); Grey = Headwaters (light grey – BB, dark grey – GC).

2.4 DISCUSSION

2.4.1 DOC quantity and timing in streams

The most distinct feature of OC export in some northern watersheds is the sudden increase in DOC concentration on the rising limb of the freshet hydrograph as the baseflow-driven system switches to near-surface flowpaths in organic-rich soils (Striegl et al., 2005; Raymond et al., 2007; Holmes et al., 2012). This is particularly well resolved in headwater catchments where there is limited mixing of signals and sources (Ågren et al., 2007). For GC, DOC concentrations have now been observed over freshet for six years (Fig. 2-7).

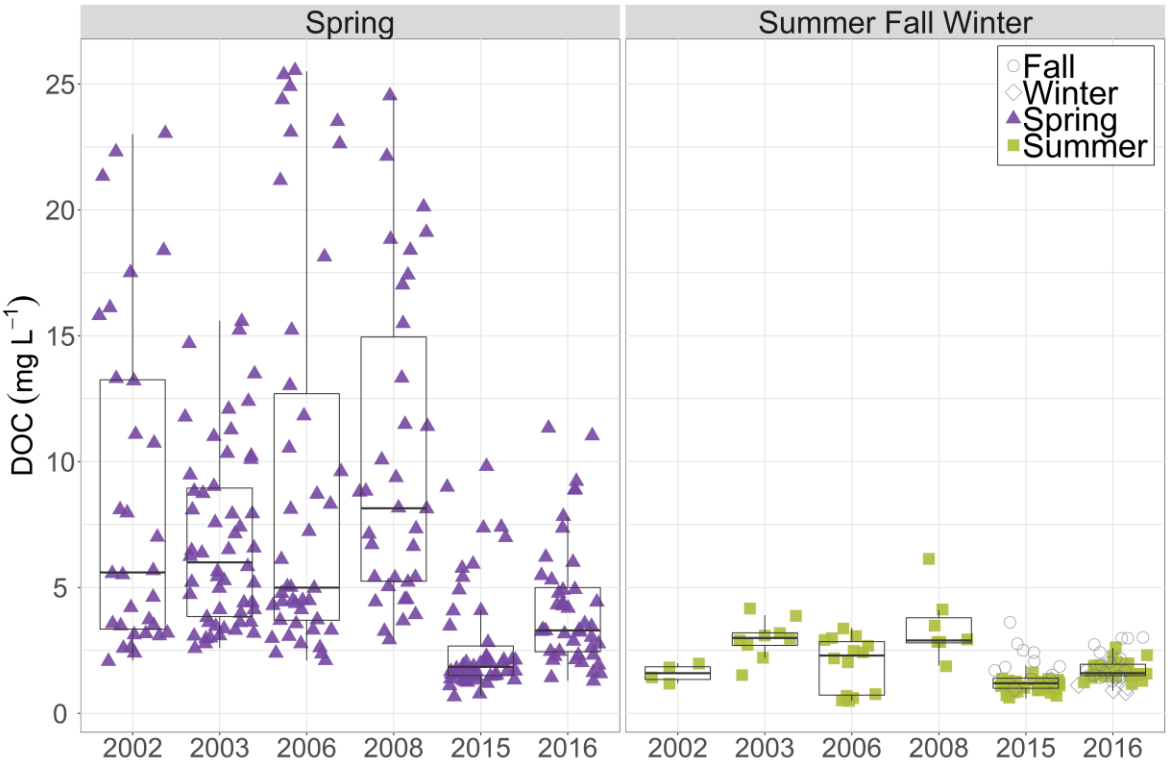

Figure 2-7. DOC concentration in mg/L is displayed on the y-axis with the left panel showing DOC concentrations measured in 2002, 2003, 2006, 2008, 2015 and 2016 during spring (April 15 to June 14). The right panel displays DOC concentrations for the same years during summer, fall and winter (prior to April 15; June 15 to Dec 31). Season is additionally indicated by shape and color (purple/filled triangle - Spring; light green/filled square - Summer; open circle - Fall; open diamond - Winter).

There is a considerable variability in freshet timing and volume as some years show a single, rapid event (e.g. 2015) while others have a staggered response in relation to multiple spring warming events (e.g. 2003, 2016). Regardless of freshet timing and volume, DOC concentrations always rise in response to the first onset of flows and are insensitive to the volume of water exported during freshet. While there are notable contrasts in both 2015 and 2016 freshets, in both cases, the initial DOC response to flows is similar (Fig. 2-4), and corresponds with those reported in earlier years (Carey et al, 2013a). The implication of these historical and recent observations is that while DOC exported during spring is hydrologically mediated via the transport pathways, DOC concentrations are not

related to flow volumes at the headwater scale. Although investigation into headwaters is relatively rare (Bishop et al., 2008), studies have reported greater variation in DOC at the headwater scale than in large rivers (Sedell and Dahm, 1990; Wolock et al., 1997; Temnerud and Bishop, 2005; Temnerud et al., 2010; Creed et al., 2015). Relatively small amounts of water are sufficient to extinguish the available pool of OM responsible for DOC peak concentration in the spring at this headwater catchment. For GC, estimates of DOC export between 15 April-14 June over the six years range between 0.29 and 1.48 g C m^{-2} with 2015 and 2016 on the lower end (Table 2-2).

Year	*Site*	Spring (g C m^{-2})	Summer (g C m^{-2})	Fall (g C m^{-2})	Spring & Summer (g C m^{-2})	Spring, Summer & Fall (g C m^{-2})
2002	*GC*	0.83	0.12		0.95	
2003	*GC*	0.42	0.19		0.61	
2006	*GC*	1.48	0.14		1.61	
2008	*GC*	0.97	0.31		1.28	
2015	*GC*	0.55	0.08	0.28	0.63	0.90
2016	*GC*	0.29	0.28	0.20	0.57	0.77
2016	*WCO*	0.06	0.09	0.09	0.15	0.24

Table 2-2. Load estimates for GC and WCO for 6 years by individual season, spring and summer, all relevant seasons together (spring, summer, fall) in g C m^{-2}.

In the years that had multiple spring warming events (2003, 2016), loads were typically smaller as DOC concentrations had declined ahead of larger runoff volumes. For WCO, the pattern of DOC concentrations during freshet was similar to GC, yet dampened with lower values during freshet over a longer period from mixing of various landscapes that integrate three distinct ecosystems and a small lake over a large elevation range. From an export perspective, springtime area-normalized loads were much smaller at WCO, suggesting that headwater ecosystems such as GC is where the bulk of DOC is sourced during freshet.

Following freshet, DOC concentrations were remarkably consistent across the

sampling sites. The headwater GC and BB values were ~1.5 mg L^{-1} whereas those at WCO were typically 2-3 mg L^{-1}, suggesting that additional sources such as wetlands and Coal Lake contributed slightly to downstream increases in DOC concentration during summer months. There were small increases in DOC concentrations associated with rainfall events in summer. A notable feature of both 2015 and 2016 were the substantial late season rains that generated flows outside the typical range at both GC and WCO (Fig. 2-3). Despite these large flows, DOC concentrations did not rise to the levels observed during freshet, and the effect on DOC export varied between years (Table 2-2). In 2015, freshet was typical of prior observations with a large increase in both discharge and DOC concentrations with 1.9 times the DOC exported compared to fall. While DOC concentrations peaked in spring at both GC and WCO in 2016, export remained similar across all seasons. In both years, DOC export was consistent or approached half of spring export suggesting either alternate runoff pathways/flow generation mechanisms or a reduced source of soluble OM in soils available for transport. Considering water tables were very high during this period, we presume that the available pool of OM in shallow organic layers was more depleted than in spring yielding less terrestrially-derived, aromatic DOM (Mutschlecner et al., 2018).

Unlike results elsewhere (Petrone et al., 2006, 2007; Raymond et al., 2007; Striegl et al., 2007; Balcarczyk et al 2009; Prokushkin et al., 2011; Holmes et al., 2012), there is no robust relationship between discharge and DOC over multiple years or within single years, suggesting that for this environment and at the headwater scale, discharge is a poor predictor of DOC export on an annual basis at the GC catchment (Table 2-S2). However, on a seasonal basis, the relationship between DOC and discharge was at times stronger

during summer, fall and winter when concentrations and discharge were relatively low (Table 2-S2, Fig. 2-8).

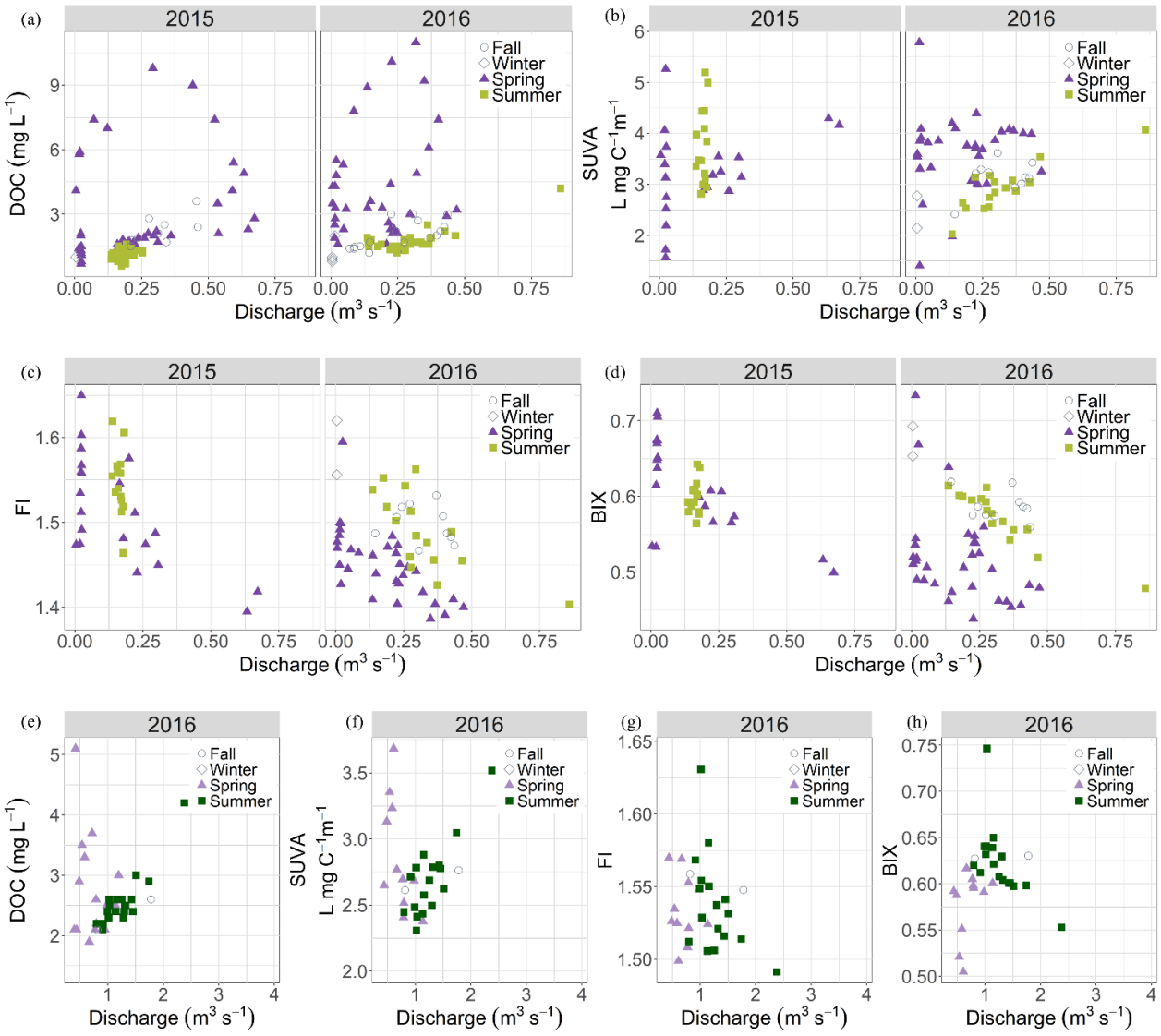

Figure 2-8. Concentration-discharge (C-Q) plots of DOC concentration, SUVA, FI and HIX for GC (2015-6) and WCO (2016). Panels a, b, c, d show DOC concentration, SUVA254, FI and HIX optical indices in relation to discharge for 2015 and 2016 at Granger Creek (GC). The bottom four panels (e, f, g, h) show the same sets of concentration-discharge relationships for 2016 at Wolf Creek Outlet (WCO). Season is indicated by shape and color (purple/filled triangle - Spring; green/filled square - Summer; open circle - Fall; open diamond - Winter). Y-axis values differ for each plot.

The lack of robust relationships between flow and DOC concentration over time is not surprising given the complex interaction of transport pathways and available organic carbon as the season progresses (Table 2-S2). The highly dynamic nature of freshet complicates C-Q patterns when concentration and export is greatest, whereas later in the

year as thaw increases and subsurface pathways contribute more, weaker (yet more significant) relations exist. We caution the use of regression equations relating DOC and flow to predict DOC loads, at least on an annual basis. However, for larger streams such as WCO, this approach may be more tractable due to mixing of sources and process integration (Buffam et al., 2007; Creed et al., 2015; Peralta-Tapia et al., 2015a).

A curious result was a notable decline in freshet DOC concentrations between the four years in the 2000s (Carey et al., 2013a) and the 2015-2016 study years (Fig. 2-7). In each of the early years, peak DOC concentrations ranged between 17 and 27 mg L^{-1} (0.42 to 1.48 g C m^{-2} exported) with overall higher concentrations during freshet, whereas the maximum DOC values for GC were 9.5 and 11.3 mg L^{-1} (0.55 and 0.29 g C m^{-2} exported) in 2015 and 2016, respectively. The reason for this decline is uncertain, yet is not related to freshet conditions as flows and climate during freshet were similar among certain years. We have also largely ruled out instrumentation or sampling as a source of this difference as mid-season values were unchanged. Tiwari et al. (2018), using 23 years of data from the Krycklan research catchment in central Sweden, suggest that peak DOC concentrations are most closely related to warm fall temperatures, cold winter conditions and shallow snowpacks. In addition, Ågren et al. (2010a) used 15 years of data from boreal catchments also located in the Krycklan research catchment to show that high export of DOC in the snow-free season led to decreased export in the subsequent year. For six years of data at GC catchment, winter (Nov-Mar) temperatures show a weak correspondence with DOC export, in that warmer winters tend to have lower DOC export during the following spring, which is supported by Scandinavian research (Ågren et al., 2010a,b; Haei et al., 2010).

However, there was no relation between snow depth and peak DOC concentration for the six years (data not shown, snow data available in Rasouli et al., 2019). A final possibility may be that increased summer and fall wetness that has occurred in recent years is reducing decomposition as outlined by Balcarcyzk et al. (2009).

2.4.2 DOM indices in streams

Optical indices are closely aligned with seasonal hydrological patterns in northern rivers across scales (Neff et al., 2006; Striegl et al., 2007; Spencer et al., 2008; Holmes et al., 2012). An expanding knowledge base linking optical indices with OM sources and biodegradability (Balcarczyk et al., 2009; Kellerman et al., 2018) and catchment processes exists with observations from both temperate and northern study sites. A number of widely-used indices (reviewed in Hansen et al. 2016) facilitate comparison among sites, and chemometric components through the ever-expanding library OpenFluor (http://www.openfluor.org). We applied the widely used drEEM toolkit (Murphy et al., 2013) to our dataset, yet we were unable to validate the model using a split-half approach to the dataset. However, the overall relationship between CDOM and DOC is robust in WCRB (Fig. 2-S1) as observed in other rivers (Stedmon et al., 2011; Spencer et al., 2012; Frey et al., 2015), with a strong relationship between A254 and DOC (r^2: 0.97, $p<0.001$).

The predominant signals in DOM indices observed in WCRB streams correspond well with those reported in the literature for northern and permafrost basins (Walker et al., 2013; Cory et al., 2014), and support conceptual models of coupled runoff generation and DOM transport (Mu et al., 2017). At the onset of freshet and the rise in DOC, $SUVA_{254}$ rises while

both BIX and FI decline to annual minima. This freshet response is attributed to the mobilization of DOM derived from leaf litter and older terrestrial precursor material with high molecular weight and aromatic DOM (Wickland et al., 2012). This pattern is particularly clear at GC, where BIX and FI are closely correlated with each other and negatively correlated with $SUVA_{254}$. At this time, near-surface pathways across frozen ground are the only mechanism to rapidly transport OM and water to the stream. Once DOC declines, $SUVA_{254}$ decreases and FI and BIX begin to increase. A number of mechanisms can be attributed to these changes: an increase in more microbial DOM as thaw depths increase and soil temperatures warm, and an increased ability of mineral soils to adsorb DOM with high organic weight and large aromatic structures along flow pathways (Ussiri and Johnson, 2004). The gradual change in the three fluorescence indices as summer progresses suggests a continual decline in high molecular weight, older DOM (lower $SUVA_{254}$) and a greater proportion of recently produced DOM. During the unusually wet fall periods, rising water tables and activation of near-surface and overland flow pathways resulted in increases in SUVA and declines in BIX and FI, yet not to the same magnitude as spring when flows were of similar volume. The smaller influence of wet fall periods on changing DOM composition can be explained in part by a much wider range of flow pathways across deeply thawed soils and also considerable adsorption sites for DOM. In addition, sources of leaf decomposition compounds located in upper soil horizons leached in spring have had less time to replenish prior to leaf-fall. As with DOC concentration, the important implication is that seasonality as opposed to flow magnitude has a greater influence on the quality of DOM. By early November, temperatures throughout WCRB are

below freezing and a long winter recession occurs. Limited over-winter sampling at WCO and GC show $SUVA_{254}$ values declining to their lowest values prior to freshet with a corresponding maximum in BIX and FI. This pattern corresponds to those reported elsewhere in the Yukon River Basin and other watersheds in Alaska (Striegl et al., 2007; O'Donnell et al., 2010; Mutschlecner et al., 2018).

2.4.3 Patterns across space and time

Understanding the integration of biogeochemical signals across temporal and spatial scales is a fundamental challenge in diverse catchments such as WCRB. The link between catchment processes and spatial scale to control coupled hydrological-biogeochemical processes has garnered considerable attention (Ågren et al., 2007; Buffam et al., 2007; Creed et al., 2015; Tiwari et al., 2017). Whereas flowpaths at the headwater catchments (GC, BB) are well documented (Quinton and Carey, 2008; Carey et al., 2013a), the dominant hydrological pathways at the scale of WCRB shift from the supra- and intra-permafrost pathways to one that is more groundwater driven. In addition, a ~1 km^2 lake in the centre of the basin has an important storage and mixing effect. The impact of these changes on the pattern of DOM indices at WCO is complex and not easily resolved back to component landscape types.

From the PCA, a host of controls act to influence DOC and fluorescence indices throughout WCRB (Fig. 2-5, Fig. 2-6). As scale increases, DOC concentrations increase during summer and low flows yet are more muted during freshet at the outlet compared with headwater streams in accordance with the river continuum concept (Creed et al., 2015).

WCO had lower $SUVA_{254}$, greater BIX and FI compared with both headwater and wetland systems. The lower $SUVA_{254}$ at WCO corresponds to an increasing dominance of groundwater or greater baseflow along with deeper subsurface pathways due to a lesser extent of frozen ground (Walvoord and Striegl, 2007; O'Donnell et al., 2010). In contrast, higher FI and BIX likely reflect the influence of these deeper flow pathways and any processes and production that occur in Coal Lake, which sits in the approximate mid-point of WCRB. Most FI values at the headwater catchments are between 1.4 and 1.6, reflecting terrestrial plants as the dominant source of DOM. By contrast, values in excess of 1.6 at WCO, particularly during winter and low flow periods, suggest some microbial DOM sources. The high values of BIX in winter at WCO supports some moderate autotrophic production, yet certainly not at the levels of many aquatic ecosystems (Kellerman et al., 2018).

Changes in DOC export as a result of climate change in permafrost regions are uncertain for aquatic ecosystems and in the overall carbon balance of northern regions (Striegl et al., 2005, 2007; Raymond et al., 2007; Frey and McClelland, 2009; Guo et al., 2012; Laudon et al., 2013; Kicklighter et al., 2013; Abbott et al., 2015; Johnston et al., 2018). DOC concentration, optical properties and associated biodegradability change with source, residence time and processing, all of which vary with thaw depth (review by Kalbitz et al., 2000; Wickland et al., 2007). At the scale of WCRB and its sub-catchments, results from other research in permafrost regions not experiencing rapid thermokarst that suggest a gradual increase in biodegradability (Spencer et al., 2008; Mann et al., 2015) are not necessarily discernable. However, changes in DOC concentrations and export are likely

due to mineralization and adsorption within the soil profile as thaw increases and active layers expand (Striegl et al., 2007; Mu et al., 2017) with a warming climate. Whereas most conceptual models have focussed on the implications of thaw and thermokarst on DOM (Mu et al., 2017), in this study we had the opportunity to evaluate the influence of increased late summer and fall precipitation, which is a notable feature in fall across much of subarctic Canada (Spence and Rausch, 2005; Spence et al., 2015; DeBeer et al., 2016). Despite late-season wetness and flow conditions similar to freshet in both years, which is anomalous in the WCRB record (Fig. 2-5), the change in DOC concentration and DOM indices were small compared to changes observed during snowmelt. Large late-season rain events on deeply thawed soils did not transport the same volume of DOM as freshet despite high water tables due to a depleted DOM source and increased adsorption potential. FI and BIX were typically higher at the outlet than the headwater and wetland sites, which is attributed to lake influences and greater autotrophic production with increasing stream order.

While there was an increase in concentrations and a shift to heavier, more aromatic DOM during fall, values were still closer to those experienced during summer baseflow.

The implication is that changes in precipitation, particularly in summer, will have a limited influence on changing DOC export and quality compared to changes that result from emergent flow pathways, thermokarst or factors that influence values during freshet. From DOC concentrations that have been measured intermittently over the course of 15 years, we report a recent decline in freshet DOC concentrations at a headwater catchment, which is difficult to reconcile with permafrost thaw (which has not been observed or documented).

Possible explanations are warmer winters and winter soils (Haei et al., 2010; Tiwari et al., 2017), or that the increase in fall wetness results in a decline in spring DOC concentrations through a second, albeit smaller, flushing event (similar to Ågren et al., 2010b).

2.5 CONCLUSIONS

This study reports patterns of DOC concentration and DOM quality derived from optical indices over several years in a subarctic alpine watershed where hydrological processes have been studied for approximately two decades. We show that DOC concentration and optical indices have a strong temporal variability associated with seasonality, and that A254 and CDOM were reliable proxies for DOC concentrations. Observations from nested watersheds with drainage areas of ~6 to 179 km^2 indicate that mixing and complex process interactions dampen variability in downstream responses and result in a gradual shift in DOM characteristics. Despite considerable fluctuations among years, DOC concentrations and export are consistently highest during freshet despite differences in timing and magnitude of hydrological response during six years of coupled DOC and discharge measurements. Optical indices also showed the largest variation during freshet and were relatively insensitive to flow volumes despite large differences in freshet between 2015 and 2016. At the headwater scale, DOM is less responsive to rainfall events in summer when the water table descends into deeper mineral soil layers.

Mobilization and transport mechanisms operating at the headwater scale are linked to stream hydrochemistry while material inputs from different landscape types causes mixing and dilutes DOM signals at increasing watershed scales. Recent years have shown

an increase in late fall streamflow that is uncommon in the long-term hydrometric record that is more often observed across northern watersheds. DOC flux in recent years falls on the low end of the range reported a decade ago.

Other factors that have the capacity to influence the availability, movement and export of DOC and DOM are forecasted to change with rapid warming in this environment (DeBeer et al., 2016). Factors at play are a longer growing season, a shift in vegetation community composition and spatial extent, warmer winters, increased baseflow with greater groundwater input, earlier freshet or disruption of the typical northern hydrograph and an altered precipitation regime. Ultimately, watershed scale and the arrangement of landscape types will play important roles in determining how DOC flux and DOM lability change under a warming climate, and altered precipitation, disturbance and vegetation regimes.

Acknowledgements

Financial support for this project was provided by the Changing Cold Regions Network (CCRN) through the Natural Sciences and Engineering Research Council of Canada (NSERC). The authors would like to thank Renée Lemmond, Heather Bonn, Dave Barrett, Mike Treberg, Tyler Williams and Crystal Beaudry for help in the field from 2013-2017. We also thank Claire Oswald for help with preliminary Aqualog sample runs and analysis, and Sean Leipe for verifying WCRB geospatial data to create an updated site map; and Supriya Singh for providing Spencer Creek DOC and optical data for filter method validation. Comments from two anonymous reviewers greatly improved the clarity and quality of the manuscript.

References

Abbott, B. W., Jones, J. B., Godsey, S. E., Larouche, J. R., and Bowden, W. B.: Patterns and persistence of hydrologic carbon and nutrient export from collapsing upland permafrost, J. Geophys. Res. Biogeosci., 12, 12, 3725-3740, 2015.

Ågren, A., Buffam, I., Jansson, M., and Laudon, H.: Importance of seasonality and small streams for the landscape regulation of dissolved organic carbon export. J. Geophys. Res. Biogeosci., 112, G3, 2007.

Ågren, A., Haei, M., Köhler, S., Bishop, K., and Laudon, H.: Long cold winters give higher stream water dissolved organic carbon (DOC) concentrations during snowmelt, Biogeosci. Discuss., 7, 3, 4857, 2010a.

Ågren, A., Haei, M., Kohler, S. J., Bishop, K., and Laudon, H.: Regulation of stream water dissolved organic carbon (DOC) concentrations during snowmelt: The role of discharge, winter climate and memory effects, J. Geophys. Res. Biogeosci., 7, 9, 2901-2913, 2010b.

Bache, S. M. and Wickham, H.: magrittr: A Forward-Pipe Operator for R. R package version 1.5, https://CRAN.R-project.org/package=magrittr, 2014.

Balcarczyk, K. L., Jones, J. B., Jaffé, R., and Maie, N.: Stream dissolved organic matter bioavailability and composition in watersheds underlain with discontinuous permafrost, Biogeochemistry, 94, 3, 255-270, 2009.

Bishop, K., Buffam, I., Erlandsson, M., Fölster, J., Laudon, H., Seibert, J., and Temnerud, J.: Aqua Incognita: the unknown headwaters, Hydrol. Process., 22, 8, 1239-1242, 2008.

Boyer, E. W., Hornberger, G. M., Bencala, K. E., and McKnight, D. M.: Effects of asynchronous snowmelt on flushing of dissolved organic carbon: a mixing model approach, Hydrol. Process., 14, 18, 3291-3308, 2000.

Bring, A., Fedorova, I., Dibike, Y., Hinzman, L., Mård, J., Mernild, S. H., Prowse, T., Semenova, O., and Woo, M. K.: Arctic terrestrial hydrology: A synthesis of processes, regional effects, and research challenges, J. Geophys. Res. Biogeosci., 121, 3, 621-649, 2016.

Brooks, P. D., and Lemon, M. M.: Spatial variability in dissolved organic matter and inorganic nitrogen concentrations in a semiarid stream, San Pedro River, Arizona, J. Geophys. Res. Biogeosci., 112, G3, 2007.

Buffam, I., Laudon, H., Temnerud, J., Mörth, C. M., and Bishop, K.: Landscape-scale variability of acidity and dissolved organic carbon during spring flood in a boreal stream network, J. Geophys. Res. Biogeosci., 112, G1, 2007.

Burd, K., Tank, S. E., Dion, N., Quinton, W. L., Spence, C., Tanentzap, A. J., and Olefeldt, D.: Seasonal shifts in export of DOC and nutrients from burned and unburned peatland-rich catchments, Northwest Territories, Canada, Hydrol. Earth Syst. Sci., 22, 4455–4472, doi: 10.5194/hess-22-4455-2018, 2018.

Carey, S. K.: Dissolved organic carbon fluxes in a discontinuous permafrost subarctic alpine catchment, Permafrost Periglacial Processes, 14, 2, 161-171, 2003.

Carey, S. K., Boucher, J. L., and Duarte, C. M.: Inferring groundwater contributions and pathways to streamflow during snowmelt over multiple years in a discontinuous permafrost subarctic environment (Yukon, Canada), Hydrogeol. J., 21, 1, 67-77, 2013a.

Carey, S. K., Tetzlaff, D., Buttle, J., Laudon, H., McDonnell, J., McGuire, K., Seibert, J., Soulsby, C., and Shanley, J.: Use of color maps and wavelet coherence to discern seasonal and interannual climate influences on streamflow variability in northern catchments, Water Resour. Res., 49, 10, 6194-6207, 2013b.

Coch, C., Juhls, B., Lamoureux, S.F., Lafrenière, M., Fritz, M., Heim, B., and Lantuit, H.: Characterizing organic matter composition in small Low and High Arctic catchments using terrestrial colored dissolved organic matter (cDOM), Biogeosci. Discuss., 2019 (In review).

Cory, R. M., and McKnight, D. M.: Fluorescence spectroscopy reveals ubiquitous presence of oxidized and reduced quinones in dissolved organic matter, Environ. Sci. Technol., 39, 21, 8142-8149, 2005.

Cory, R. M., Ward, C. P., Crump, B. C., and Kling, G. W.: Sunlight controls water column processing of carbon in arctic fresh waters, Science, 345, 6199, 925-928, 2014.

Creed, I. F., McKnight, D. M., Pellerin, B. A., Green, M. B., Bergamaschi, B. A., Aiken, G. R., Burns, D. A., Findlay, S. E. G., Shanley, J. B., Striegl, R. G., Aulenbach, B. T., Clow, D. W., Laudon, H., McGlynn, B. L., McGuire, K. J., Smith, R. A., and Stackpoole, S. M.: The river as a chemostat: fresh perspectives on dissolved organic matter flowing down the river continuum, Can. J. Fish. Aquat. Sci., 72, 8, 1272-1285, 2015.

Davidson, E. A., and Janssens, I. A.: Temperature sensitivity of soil carbon decomposition and feedbacks to climate change, Nature, 440, 7081, 165, 2006.

DeBeer, C. M., Wheater, H. S., Carey, S. K., and Chun, K. P.: Recent climatic, cryospheric, and hydrological changes over the interior of western Canada: a review and synthesis, Hydrol. Earth Syst. Sci., 20, 4, 1573, 2016.

Dittmar, T., and Kattner, G.: The biogeochemistry of the river and shelf ecosystem of the Arctic Ocean: a review, Mar. Chem., 83, 3-4, 103-120, 2003.

Dixon, R. K., Solomon, A. M., Brown, S., Houghton, R. A., Trexier, M. C., and Wisniewski, J.: Carbon pools and flux of global forest ecosystems, Science, 263, 5144, 185-190, 1994.

Fellman, J. B., Hood, E., and Spencer, R. G.: Fluorescence spectroscopy opens new windows into dissolved organic matter dynamics in freshwater ecosystems: A review, Limnol. Oceanogr., 55, 6, 2452-2462, 2010.

Finlay, J., Neff, J., Zimov, S., Davydova, A., and Davydov, S.: Snowmelt dominance of dissolved organic carbon in high-latitude watersheds: Implications for characterization and flux of river DOC, Geophys. Res. Lett., 33, 10, 2006.

Finlay, J. C., Hood, J. M., Limm, M. P., Power, M. E., Schade, J. D., and Welter, J. R.: Light-mediated thresholds in stream-water nutrient composition in a river network, Ecology, 92, 1, 140-150, 2011.

Frey, K. E., and Smith, L. C.: Amplified carbon release from vast West Siberian peatlands by 2100. Geophys. Res. Lett., 32(9), 2005.

Frey, K. E., and McClelland, J. W.: Impacts of permafrost degradation on arctic river biogeochemistry. Hydrol. Process., 23 (1), 169-182, doi: 10.1002/hyp.7196, 2009.

Frey, K. E., Sobczak, W. V., Mann, P. J., and Holmes, R. M.: Optical properties and bioavailability of dissolved organic matter along a flow-path continuum from soil pore waters to the Kolyma River, Siberia. Biogeosci. Discuss., 12 (15), 2015.

Gordeev, V. V., Martin, J. M., Sidorov, I. S., and Sidorova, M. V.: A reassessment of the Eurasian river input of water, sediment, major elements, and nutrients to the Arctic Ocean, Am. J. Sci., 296, 6, 664-691, 1996.

Grolemund, G., and Wickham, H.: Dates and Times Made Easy with lubridate, J. Stat. Soft., 40, 3, 1-25, http://www.jstatsoft.org/v40/i03/, 2011.

Guo, L., Cai, Y., Belzile, C., and Macdonald, R. W.: Sources and export fluxes of inorganic and organic carbon and nutrient species from the seasonally ice-covered Yukon River, Biogeochemistry, 107, 1–3, 187–206, https://doi.org/10.1007/s10533-010-9545-z, 2012.

Haei, M., Öquist, M. G., Buffam, I., Ågren, A., Blomkvist, P., Bishop, K., Ottosson Löfvenius, M., and Laudon, H.: Cold winter soils enhance dissolved organic carbon concentrations in soil and stream water, Geophys. Res. Lett., 37, 8, 2010.

Hansen, A. M., Kraus, T. E., Pellerin, B. A., Fleck, J. A., Downing, B. D., and Bergamaschi, B. A.: Optical properties of dissolved organic matter (DOM): Effects of biological and photolytic degradation. Limnol. Oceanogr., 61, 3, 1015-1032, 2016.

Harms, T. K., Edmonds, J. W., Genet, H., Creed, I. F., Aldred, D., Balser, A., and Jones, J. B.: Catchment influence on nitrate and dissolved organic matter in Alaskan streams across a latitudinal gradient. J. Geophys. Res. Biogeosci., 121, 2, 350-369, 2016.

Herod, M. N., Li, T., Pellerin, A., Kieser, W. E., and Clark, I. D.: The seasonal fluctuations and accumulation of iodine-129 in relation to the hydrogeochemistry of the Wolf Creek Research Basin, a discontinuous permafrost watershed, Science of the Total Environment, 569, 1212-1223, 2016.

Holmes, R. M., McClelland, J. W., Raymond, P. A., Frazer, B. B., Peterson, B. J., and Stieglitz, M.: Lability of DOC transported by Alaskan rivers to the Arctic Ocean, Geophys. Res. Lett., 35, L03402, doi: 10.1029/2007GL032837, 2008.

Holmes, R. M., McClelland, J. W., Peterson, B. J., Tank, S. E., Bulygina, E., Eglinton, T. I., Gordeev, V. V., Gurtovaya, T. Y., Raymond, P. A., Repeta, D. J., Staples, R., Striegl, R. G., Zhulidov, . V., and Zimov, S. A.: Seasonal and annual fluxes of nutrients and organic matter from large rivers to the Arctic Ocean and surrounding seas, Estuaries Coasts, 35, 2, 369–382, doi:10.1007/ s12237-011-9386-6, 2012.

Hugelius, G., Strauss, J., Zubryzck, S., Schirrmeister, L., Grosse, G., Michaelson, G.J., Koven, C.D., O'Donnell, J.A., Elberling, B., Mishra, U., Camill, P., Yu, Z., Palmtag, J., and Kuhry, P.: Estimated stocks of circumpolar permafrost carbon with quantifieduncertainty ranges and identified data gaps, Biogeosci., 11, 6573–6593, 2014.

Huguet, A., Roux-De Balmann, H., and Parlanti, E.: Fluorescence spectroscopy applied to the optimisation of a desalting step by electrodialysis for the characterisation of marine organic matter, J. Membr. Sci., 326, 1, 186-196, 2009.

Jaffé, R., McKnight, D., Maie, N., Cory, R., McDowell, W. H., and Campbell, J. L.: Spatial and temporal variations in DOM composition in ecosystems: The importance of long-term monitoring of optical properties. J. Geophys. Res. Biogeosci., 113(G4), 2008.

Johnston, S. E., Shorina, N., Bulygina, E., Vorobjeva, T., Chupakova, A., Klimov, S. I., Kellerman, A. M., Guillemette, F., Shiklomanov, A., Podgorski, D. C., and Spencer, R. G.: Flux and seasonality of dissolved organic matter from the Northern Dvina (Severnaya Dvina) River, Russia, J. Geophys. Res. Biogeosci., 123, 3, 1041-1056, 2018.

Kaiser, H. F., and Rice, J.: Little jiffy, mark IV, SAGE J. Education. Psychol. Measur., 34, 1, 111-117, 1974.

Kalbitz, K., Solinger, S., Park, J. H., Michalzik, B., and Mtzner, E.: Controls on the dynamics of dissolved organic matter in soils: a review, Soil Sci., 165, 4, 277-304, 2000.

Kassambara, A. (2018).: ggpubr: 'ggplot2' Based Publication Ready Plots, R package version 0.1.7, https://CRAN.R-project.org/package=ggpubr, 2018.

Kawahigashi, M., Kaiser, K., Kalbitz, K., Rodionov, A., and Guggenberger, G.: Dissolved organic matter in small streams along a gradient from discontinuous to continuous permafrost, Global Change Biol., 10, 9, 1576-1586, 2004.

Kawahigashi, M., Kaiser, K., Rodionov, A., and Guggenberger, G.: Sorption of dissolved organic matter by mineral soils of the Siberian forest tundra, Global Change Biol., 12, 10, 1868-1877, 2006.

Kellerman, A. M., Guillemette, F., Podgorski, D. C., Aiken, G. R., Butler, K. D., and Spencer, R. G.: Unifying concepts linking dissolved organic matter composition to persistence in aquatic ecosystems, Environ. Sci. Technol., 52, 5, 2538-2548, 2018.

Kicklighter, D. W., Hayes, D. J., McClelland, J. W., Peterson, B. J., McGuire, A. D., and Melillo, J. M.: Insights and issues with simulating terrestrial DOC loading of Arctic river networks, Ecol. Appl., 23, 8, 1817–1836, doi:10.1890/11-1050.1, 2013.

Koch, J. C., Runkel, R. L., Striegl, R., and McKnight, D. M.: Hydrologic controls on the transport and cycling of carbon and nitrogen in a boreal catchment underlain by continuous permafrost, J. Geophys. Res. Biogeosci., 118, 2, 698-712, 2013.

Kokelj, S. V., Lacelle, D., Lantz, T. C., Tunnicliffe, J., Malone, L., Clark, I. D., and Chin, K. S.: Thawing of massive ground ice in mega slumps drives increases in stream sediment and solute flux across a range of watershed scales, J. Geophys. Res. Earth Surf., 118, 2, 681-692, 2013.

Meteorological Service of Canada (MSC): National climate data archive of Canada.Environment Canada, Dorval, QB, 202017.

Larouche, J. R., Abbott, B. W., Bowden, W. B., and Jones, J. B.: The role of watershed characteristics, permafrost thaw, and wildfire on dissolved organic carbon biodegradability and water chemistry in Arctic headwater streams, J. Geophys. Res. Biogeosci., 12, 14, 4221-4233, 2015.

Laudon, H., Buttle, J., Carey, S. K., McDonnell, J., McGuire, K., Seibert, J., Shanley, J., Soulsby, C., and Tetzlaff, D.: Cross-regional prediction of long-term trajectory of stream water DOC response to climate change. Geophys. Res. Lett., 39 (18), 2012.

Laudon, H., Tetzlaff, D., Soulsby, C., Carey, S., Seibert, J., Buttle, J., Shanley, J., McDonnell, J. J., and McGuire, K.: Change in winter climate will affect dissolved organic carbon and water fluxes in mid-to-high latitude catchments, Hydrol. Process., 27, 5, 700-709, 2013.

Lewkowicz, A. G., and Ednie, M.: Probability mapping of mountain permafrost using the BTS method, Wolf Creek, Yukon Territory, Canada, Permafrost Periglacial Processes, 15, 1, 67-80, 2004.

Li Yung Lung, J.Y.S., Tank, S.E., Spence, C., Yang, D., Bonsal, B., McClelland, J.W., and Holmes, R.: Seasonal and Geographic Variation in Dissolved Organic Biogeochemistry of Rivers Draining to the Arctic Ocean and Hudson Bay, J. Geophys. Res. Biogeosci., 123 (10), 3371-3386, 2018.

Littlefair, C. A., Tank, S. E., and Kokelj, S. V.: Retrogressive thaw slumps temper dissolved organic carbon delivery to streams of the Peel Plateau, NWT, Canada. J. Geophys. Res. Biogeosci., 14(23), 5487-5505, 2017.

MacLean R., Oswood, M. W., Irons, J. G., and McDowell, W. H.: The effect of permafrost on stream biogeochemistry: a case study of two streams in the Alaskan (USA) taiga. Biogeochemistry, 47 (3), 239-267, 1999.

Manizza, M., Follows, M. J., Dutkiewicz, S., McClelland, J. W., Menemenlis, D., Hill, C. N., Townsend-Small, A., and Peterson, B. J.: Modeling transport and fate of riverine dissolved organic carbon in the Arctic Ocean. Global Biogeochem. Cycles, 23 (4), 2009.

McClelland, J. W., Stieglitz, M., Pan, F., Holmes, R. M., and Peterson, B. J.: Recent changes in nitrate and dissolved organic carbon export from the upper Kuparuk River, North Slope, Alaska. J. Geophys. Res. Biogeosci., 112 (G4), 2007.

McGuire, A. D., Anderson, L. G., Christensen, T. R., Dallimore, S., Guo, L., Hayes, D. J., Heimann, M., Loreenson, T. D., MacDonald, R. W., and Roulet, N.: Sensitivity of the carbon cycle in the Arctic to climate change, Ecol. Monogr., 79 (4), 523-555, 2009.

McKnight, D. M., Boyer, E. W., Westerhoff, P. K., Doran, P. T., Kulbe, T., and Andersen, D. T.: Spectrofluorometric characterization of dissolved organic matter for indication of precursor organic material and aromaticity, Limnol. Oceanogr., 46 (1), 38–48, doi: 10.4319/lo.2001.46.1.0038, 2001.

Mu, C. C., Abbott, B. W., Zhao, Q., Su, H., Wang, S. F., Wu, Q. B., Zhang, T. J., and Wu, X. D.: Permafrost collapse shifts alpine tundra to a carbon source but reduces N2O and CH4 release on the northern Qinghai-Tibetan Plateau, Geophys. Res. Lett., 44 (17), 8945-8952, 2017.

Murphy, K. R., Stedmon, C. A., Graeber, D., and Bro, R.: Fluorescence spectroscopy and multi-way techniques PARAFAC, Anal. Methods, 5 (23), 6557-6566, 2013.

Mutschlecner, A. E., Guerard, J. J., Jones, J. B., and Harms, T. K.: Regional and intra-annual stability of dissolved organic matter composition and biolability in high-latitude Alaskan rivers, Limnol. Oceanogr., 63, 4, 1605-1621, doi: 10.1002/lno.10795, 2018.

Neff, J. C., Finlay, J. C., Zimov, S. A., Davydov, S. P., Carrasco, J. J., Schuur, E. A. G., and Davydova, A. I.: Seasonal changes in the age and structure of dissolved organic carbon in Siberian rivers and streams, Geophys. Res. Lett., 33(23), 2006.

O'Donnell, J. A., and Jones, J. B.: Nitrogen retention in the riparian zone of catchments underlain by discontinuous permafrost, Freshwater Biol., 51 (5), 854-864, 2006.

O'Donnell, J. A., Aiken, G. R., Kane, E. S., and Jones, J. B.: Source water controls on the character and origin of dissolved organic matter in streams of the Yukon River basin, Alaska, J. Geophys. Res. Biogeosci., 115 (G3), 2010.

Ohno, T.: Fluorescence inner-filtering correction for determining the humification index of dissolved organic matter, Environ. Sci. Technol., 36 (4), 742-746, 2002.

Olefeldt, D., Roulet, N., Giesler, R., and Persson, A.: Total waterborne carbon export and DOC composition from ten nested subarctic peatland catchments—importance of peatland cover, groundwater influence, and inter-annual variability of precipitation patterns, Hydrol. Process., 27 (16), 2280-2294, 2013.

Olefeldt, D., and Roulet, N. T.: Permafrost conditions in peatlands regulate magnitude, timing, and chemical composition of catchment dissolved organic carbon export, Global Change Biol., 20 (10), 3122-3136, 2014.

Opsahl, S., Benner, R., and Amon, R. W.: Major flux of terrigenous dissolved organic matter through the Artic Ocean, Limnol. Oceanogr., 44, 2017–2023, 1999.

Parlanti, E., Wörz, K., Geoffroy, L., and Lamotte, M.: Dissolved organic matter fluorescence spectroscopy as a tool to estimate biological activity in a coastal zone submitted to anthropogenic inputs, Org. Geochem., 31(12), 1765-1781, 2000.

Peralta-Tapia, A., Sponseller, R. A., Ågren, A., Tetzlaff, D., Soulsby, C., and Laudon, H.: Scale-dependent groundwater contributions influence patterns of winter baseflow stream chemistry in boreal catchments, J. Geophys. Res. Biogeosci., 120 (5), 847-858, 2015.

Petrone, K. C., J. B. Jones, L. D. Hinzman, and R. D. Boone.: Seasonal export of carbon, nitrogen, and major solutes from Alaskan catchments with discontinuous permafrost, J. Geophys. Res., 111, G02020, doi:10.1029/2005JG000055, 2006.

Petrone, K., Buffam, I., and Laudon, H.: Hydrologic and biotic control of nitrogen export during snowmelt: a combined conservative and reactive tracer approach, Water Resour. Res., 43(6), 2007.

Pomeroy, J. W., Hedstrom, N., and Parviainen, J.: The snow mass balance of Wolf Creek, Yukon: effects of snow sublimation and redistribution, Wolf Creek, Research Basin: Hydrology, Ecology, Environment, edited by: Pomeroy, JW and Granger RJ, 15-30, 1999.

Prokushkin, A. S., Pokrovsky, O. S., Shirokova, L. S., Korets, M. A., Viers, J., Prokushkin, S. G., Amon, R. M. W., Guggenberger, G., and McDowell, W. H.: Sources and the flux pattern of dissolved carbon in rivers of the Yenisey basin draining the Central Siberian Plateau, Environ. Res. Lett., 6 (4), 045212, 2011.

Quinton, W. L., and Carey, S. K.: Towards an energy-based runoff generation theory for tundra landscapes, Hydrol. Process., 22 (23), 4649-4653, 2008.

Rasouli, K., Pomeroy, J. W., Janowicz, J. R., Williams, T. J., and Carey, S. K.: A long-term hydrometeorological dataset (1993–2014) of a northern mountain basin: Wolf Creek Research Basin, Yukon Territory, Canada, Earth Sys. Sci. Data 11, 89-100, https://doi.org/10.5194/essd-11-89-2019, 2019.

Raymond, P. A., McClelland, J. W., Holmes, R. M., Zhulidov, A. V., Mull, K., Peterson, B. J., Striegl, R. G., Aiken, G. R., and Gurtovaya, T. Y.: Flux and age of dissolved organic carbon exported to the Arctic Ocean: A carbon isotopic study of the five largest arctic rivers, Global Biogeochem. Cycles, 21(4), 2007.

R Core Team. R: A language and environment for statistical computing. R Foundation for Statistical Computing, Vienna, Austria. https://www.R-project.org/, 2017.

Schloerke, B., Crowley, J., Cook, D., Briatte, F., Marbach, M., Thoen, E., Elberg, A., and Larmarange, J.: GGally: Extension to 'ggplot2', R package version 1.4.0, https://CRAN.R-project.org/package=GGally, 2018.

Schmidt, B. H., Kalbitz, K., Braun, S., Fuß, R., McDowell, W. H., and Matzner, E.: Microbial immobilization and mineralization of dissolved organic nitrogen from forest floors, Soil Biol. Biochem., 43(8), 1742-1745, 2011.

Schuur, E. A. G., McGuire, A. D., Schädel, C., Grosse, G., Harden, J. W., Hayes, D. J., Hugelius, G., Koven, C. D., Kuhry, P., Lawrence, D. M., Natali, S. M., Olefeldt, D., Romanovsky, V. E., Schaefer, K., Turetsky, M. R., Treat, C. C., and Vonk, J. E.: Climate change and the permafrost carbon feedback, Nature, 520 (7546), 171–179, https://doi.org/10.1038/nature14338, 2015.

Sedell, J. R., and Dahm, C. N.: Spatial and temporal scales of dissolved organic carbon in streams and rivers, Organic acids in aquatic ecosystems, edited by: Perdue, E. M., and Gjessing, E. T., John Wiley & Sons Ltd, Berlin, Germany, 261-279, 1990.

Serreze, M. C., and Francis, J. A.: The Arctic amplification debate, Clim. Change, 76 (3-4), 241-264, 2006.

Shiklomanov, I. A.: Appraisal and assessment of world water resources, Water Int., 25 (1), 11-32, https://doi.org/10.1080/02508060008686794, 2000.

Spence, C., and Rausch, J.: Autumn synoptic conditions and rainfall in the subarctic Canadian Shield of the Northwest Territories, Canada, Int. J. Climatol., 25 (11), 1493-1506, 2005.

Spence, C., Kokelj, S. V., Kokelj, S. A., McCluskie, M., and Hedstrom, N. Evidence of a change in water chemistry in Canada's subarctic associated with enhanced winter streamflow, J. Geophys. Res. Biogeosci., 120 (1), 113-127, 2015.

Spencer, R. G. M., Aiken, G. R., Wickland, K. P., Striegl, R. G., and Hernes, P. J.: Seasonal and spatial variability in dissolved organic matter quantity and composition from the Yukon River basin, Alaska: Yukon River basin DOM dynamics, Global Biogeochem. Cycles, 22, GB4002, https://doi.org/10.1029/2008GB003231, 2008.

Spencer, R. G., Aiken, G. R., Butler, K. D., Dornblaser, M. M., Striegl, R. G., and Hernes, P. J.: Utilizing chromophoric dissolved organic matter measurements to derive export and reactivity of dissolved organic carbon exported to the Arctic Ocean: A case study of the Yukon River, Alaska, Geophys. Res. Lett., 36(6), 2009.

Spencer, R. G., Butler, K. D., and Aiken, G. R. Dissolved organic carbon and chromophoric dissolved organic matter properties of rivers in the USA, J. Geophys. Res. Biogeosci., 117(G3), 2012.

Stedmon, C. A., Amon, R. M. W., Rinehart, A. J., and Walker, S. A. The supply and characteristics of colored dissolved organic matter (CDOM) in the Arctic Ocean: Pan Arctic trends and differences, Mar. Chem., 124 (1-4), 108-118, 2011.

Striegl, R. G., Aiken, G. R., Dornblaser, M. M., Raymond, P. A., and Wickland, K. P.: A decrease in discharge-normalized DOC export by the Yukon River during summer through autumn, Geophys. Res. Lett., 32(21), 2005.

Striegl, R. G., Dornblaser, M. M., Aiken, G. R., Wickland, K. P., and Raymond, P. A.: Carbon export and cycling by the Yukon, Tanana, and Porcupine Rivers, Alaska, 2001–2005, Water Resour. Res., 43, W02411, https://doi.org/10.1029/2006WR005201, 2007.

Tang, Y., Horikoshi, M., and Li, W.: ggfortify: Unified Interface to Visualize Statistical Result of Popular R Packages, The R Journal 8.2, 478-489, https://CRAN.R-project.org/package=ggfortify, 2016.

Tank, S. E., Striegl, R. G., McClelland, J. W., and Kokelj, S. V.: Multi-decadal increases in dissolved organic carbon and alkalinity flux from the Mackenzie drainage basin to the Arctic Ocean, Environ. Res. Lett., 11(5), 054015, 2016.

Tarnocai, C., Canadell, J. G., Schuur, E. A. G., Kuhry, P., Mazhitova, G., and Zimov, S.: Soil organic carbon pools in the northern circumpolar permafrost region., Global Biogeochem. Cycles, 23 (2), 2009.

Temnerud, J., and Bishop, K.: Spatial variation of streamwater chemistry in two Swedish boreal catchments: Implications for environmental assessment, Environ. Sci. Technol., 39 (6), 1463-1469, 2005.

Temnerud, J., Fölster, J., Buffam, I., Laudon, H., Erlandsson, M., and Bishop, K.: Can the distribution of headwater stream chemistry be predicted from downstream observations? Hydrol. Process., 24 (16), 2269-2276, 2010.

Tiwari, T., Laudon, H., Beven, K., and Ågren, A. M.: Downstream changes in DOC: Inferring contributions in the face of model uncertainties, Water Resour. Res., 50 (1), 514-525, 2014.

Tiwari, T., Buffam, I., Sponseller, R. A., and Laudon, H.: Inferring scale-dependent processes influencing stream water biogeochemistry from headwater to sea, Limnol. Oceanogr., 62 (S1), S58-S70. doi: 10.1002/lno.10738, 2017.

Tiwari, T., Sponseller, R. A., and Laudon, H.: Extreme Climate Effects on Dissolved Organic Carbon Concentrations During Snowmelt, J. Geophys. Res. Biogeosci., 123 (4), 1277-1288, 2018.

Toohey, R. C., Herman-Mercer, N. M., Schuster, P. F., Mutter, E. A., and Koch, J. C.: Multidecadal increases in the Yukon River Basin of chemical fluxes as indicators of changing flowpaths, groundwater, and permafrost, Geophys. Res. Lett., 43 (23), 2016.

Ussiri, D. A., and Johnson, C. E.: Sorption of organic carbon fractions by Spodosol mineral horizons, Soil Sci. Soc. Am. J., 68 (1), 253-262, 2004.

Vonk, J. E., Tank, S. E., Bowden, W. B., Laurion, I., Vincent, W. F., Alekseychik, P., Amyot, M., Billet, M. F., Canario, J., Cory, R. M., Deshpande, B. N., Helbig, M., Jammet, M., Karlsson, J., Larouche, MacMillan, G., Rautio, M., Walther Anthony, K. M., and Wickland, K. P.: Reviews and syntheses: Effects of permafrost thaw on Arctic aquatic

ecosystems, J. Geophys. Res. Biogeosci., 12(23): 7129-7167. doi: 10.5194/bg-12-7129-2015, 2015.

Walker, S. A., Amon, R. M., and Stedmon, C. A.: Variations in high-latitude riverine fluorescent dissolved organic matter: A comparison of large Arctic rivers, J. Geophys. Res. Biogeosci., 118 (4), 1689-1702, 2013.

Walvoord, M. A., and Striegl, R. G.: Increased groundwater to stream discharge from permafrost thawing in the Yukon River basin: Potential impacts on lateral export of carbon and nitrogen, Geophys. Res. Lett., 34 (12), 2007.

Ward, C. P., and Cory, R. M.: Complete and partial photo-oxidation of dissolved organic matter draining permafrost soils, Environ. Sci. Technol., 50 (7), 3545-3553, 2016.

Weishaar, J. L., Aiken, G. R., Bergamaschi, B. A., Fram, M. S., Fujii, R., and Mopper, K.: Evaluation of specific ultraviolet absorbance as an indicator of the chemical composition and reactivity of dissolved organic carbon, Environ. Sci. Technol., 37 (20), 4702–4708, doi: 10.1021/es030360x, 2003.

Wickham, H.: ggplot2: Elegant Graphics for Data Analysis, R package version 3.1.0.9000, http://ggplot2.org, 2016.

Wickham, H., François, R., Henry, L., and Müller, K. dplyr: A Grammar of Data Manipulation, R package version 0.7.6, https://CRAN.R-project.org/package=dplyr, 2018.

Wickham, H. and Henry, L.: tidyr: Easily Tidy Data with 'spread()' and 'gather()' Functions, R package version 0.8.1, https://CRAN.R-project.org/package=tidyr, 2018.

Wickland, K. P., Neff, J. C., and Aiken, G. R.: Dissolved organic carbon in Alaskan boreal forest: sources, chemical characteristics, and biodegradability, Ecosystems, 10 (8), 1323–1340, doi: 10.1007/s10021-007-9101-4, 2007.

Wickland, K. P., Aiken, G. R., Butler, K., Dornblaser, M. M., Spencer, R. G. M., and Striegl, R. G.: Biodegradability of dissolved organic carbon in the Yukon River and its tributaries: Seasonality and importance of inorganic nitrogen, Global Biogeochem. Cycles, 26(4), 2012.

Wilson, H. F., and Xenopoulos, M. A.: Effects of agricultural land use on the composition of fluvial dissolved organic matter, Nat. Geosci., 2 (1), 37, 2009.

Wolock, D. M., Fan, J., and Lawrence, G. B.: Effects of basin size on low-flow stream chemistry and subsurface contact time in the Neversink River watershed, New York, Hydrol. Process., 11 (9), 1273-1286, 1997.

Wrona, F. J., Johansson, M., Culp, J. M., Jenkins, A., Mård, J., Myers-Smith, I. H., Prowse, D. T., Vincent, W.F., and Wookey, P. A.: Transitions in Arctic ecosystems: Ecological implications of a changing hydrological regime, J. Geophys. Res. Biogeosci., 121 (3), 650-674, 2016.

Zsolnay, A., Baigar, E., Jimenez, M., Steinweg, B., and Saccomandi, F.: Differentiating with fluorescence spectroscopy the sources of dissolved organic matter in soils subjected to drying, Chemosphere, 38 (1), 45-50, 1999.

Supplemental Information

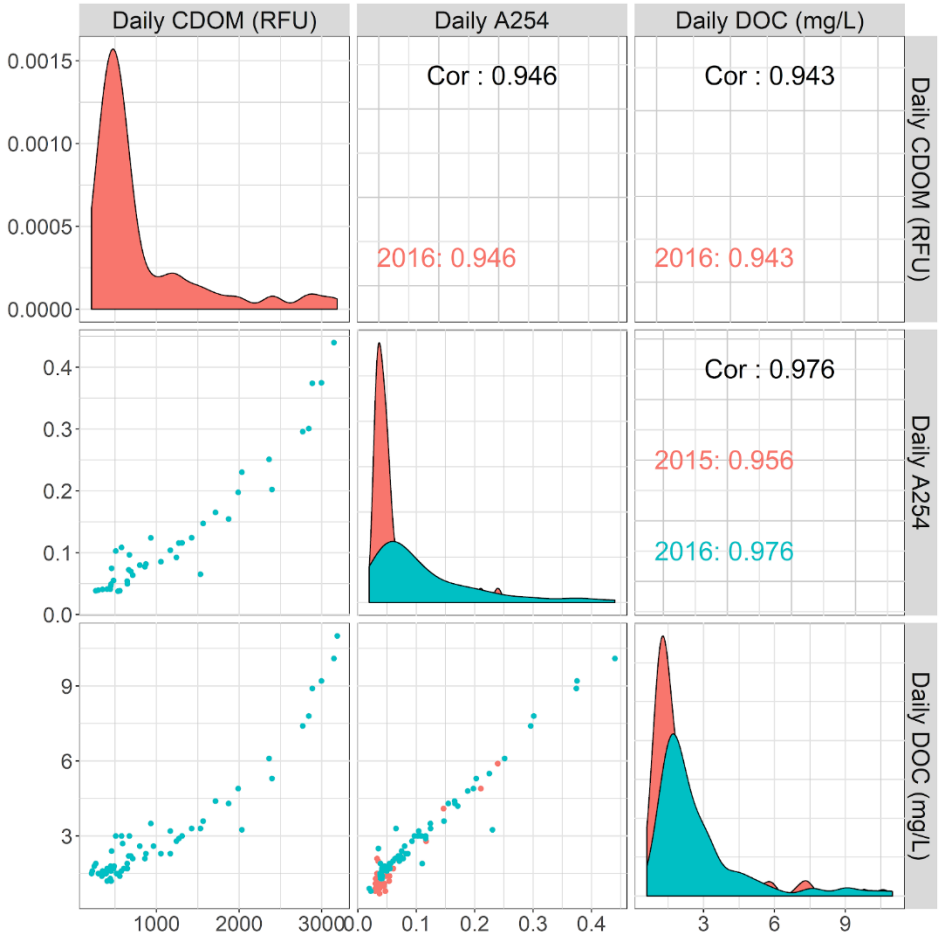

Figure 2-S1. Correlation matrices of average daily CDOM (RFU), A254 (nm-1) and DOC concentration (mg L-1). No CDOM was measured in 2015 so it was not possible to separate out that year. Correlations were calculated using Pearson correlation tests at 95 % significance level ($p<0.001$ in all cases).

Year	Sites	DOC (mg/L)			$SUVA_{254}$			BIX			FI		
		Spring	Summer	F/W	Spring	Summer	F/W	Spring	Summer	F/W	Spring	Summer	F/W
2015													
	BB	1.77±0.66(5)	1.25±0.31(11)	1.19±0.39(9)	3.30±0.58(3)	3.88±0.55(4)	2.72±0.42(2)	0.55±0.04	0.60±0.01	0.60±0.03	1.49±0.06	1.54±0.03	1.57±0.76
	CL	2.90(1)		2.60(1)									
	GC	2.89±2.29(52)	1.07±0.21(36)	1.75±0.76(17)	3.21±0.84(22)	3.81±0.75(14)	2.42±0.33(3)	0.69±0.06	0.60±0.02	0.65±0.02	1.52±0.06	1.54±0.04	1.57±0.04
	W1	15.8(1)			3.94(1)			0.47 (1)			1.46(1)		
	WCO			1.79±0.90(14)			2.21±0.17(10)			0.66±0.03			1.62±0.03
2016													
	BB	2.34±0.87(14)	1.42±0.27(23)	1.50±0.20(3)	3.56±0.48(10)	2.81±0.59(16)	2.45±0.28(3)	0.513±0.03	0.58±0.03	0.62±0.02	1.45±0.04	1.52±0.06	1.52±0.00
	CL		3.15±0.35(2)										
	GC	4.32±2.56(43)	1.71±0.34(32)	2.00±0.57(20)	3.86±1.40(37)	2.86±0.38(17)	3.14±0.32(11)	0.513±0.06	0.58±0.03	0.60±0.04	1.45±0.04	1.50±0.04	1.50±0.02
	W1	6.70(1)	7.37±0.64(10)	6.95±0.21(2)	4.77(1)	4.04±0.60(7)		0.58(1)	0.63±0.05		1.58(1)	1.54±0.04	
	WCO	2.69±0.80(18)	2.58±0.44(22)	2.35±0.35(3)	2.83±0.42(12)	2.70±0.28(19)	2.69±0.11(2)	0.582±0.04	0.60±0.02	0.66±0.03	1.53±0.02	1.54±0.03	1.55±0.01
2017	BB	2.70(1)	2.17±0.45(7)	1.15±0.14(6)		3.02±0.38(6)	3.15±0.17(6)		0.55±0.03	0.61±0.02		1.48±0.03	1.55±0.02
	CL		3.23±0.15(4)	2.96±0.09(5)		2.66±0.15(3)	2.82±0.08(5)		0.66±0.03	0.69±0.02		1.48±0.01	1.50±0.03
	GC	3.15±0.64(2)	2.33±0.71(7)	1.28±0.18(6)		3.14±0.23(5)			0.55±0.03			1.45±0.03	
	W1			6.10(1)			5.26(1)			0.62(1)			1.66(1)
	WCO	4.42±1.84(6)	2.72±0.37(5)	2.14±0.11(5)		2.83±0.25(3)	2.94±0.10(3)		0.61±0.03	0.64±0.01		1.51±0.02	1.57±0.02

Table 2-S1**.** This table is similar to Table 1 in the manuscript but incorporates all samples used for principal component analysis (PCA). Additional sites (CL, W1) and additional years of data for sites BB, GC and WCO were used in the analysis to investigate influence of landscape type. Notation: Mean ± standard deviation (number of samples).

Year	*Site*	Spring (R^2)	Summer (R^2)	Fall (R^2)	Spring & Summer (R^2)	Spring, Summer & Fall (R^2)
2002	*GC*	0.047	0.180		0.063	
2003	*GC*	0.041	0.001		0.034	
2006	*GC*	0.021	0.175		0.029	
2008	*GC*	0.024	0.215		0.005	
2015	*GC*	0.263	0.004	0.547	0.316	0.314
2016	*GC*	0.115	0.536	0.551	0.039	0.048
2016	*WCO*	0.066	0.783		0.010	0.011

Table 2-S2. Regressions between discharge (Q) and DOC concentrations (DOC) were performed using the CQ regression function in the RiverLoad package (Nava et al., 2019) for GC in 2002, 2003, 2006, 2008, 2015 and 2016. A statistically significant correlation between C and Q was necessary to perform the regression.

Kaiser-Meyer-Olkin factor

Overall MSA = 0.77

MSA for each item:

FI = 0.98

Fresh = 0.68

HIX = 0.86

BIX = 0.69

SUVA = 0.91

DOC = 0.94

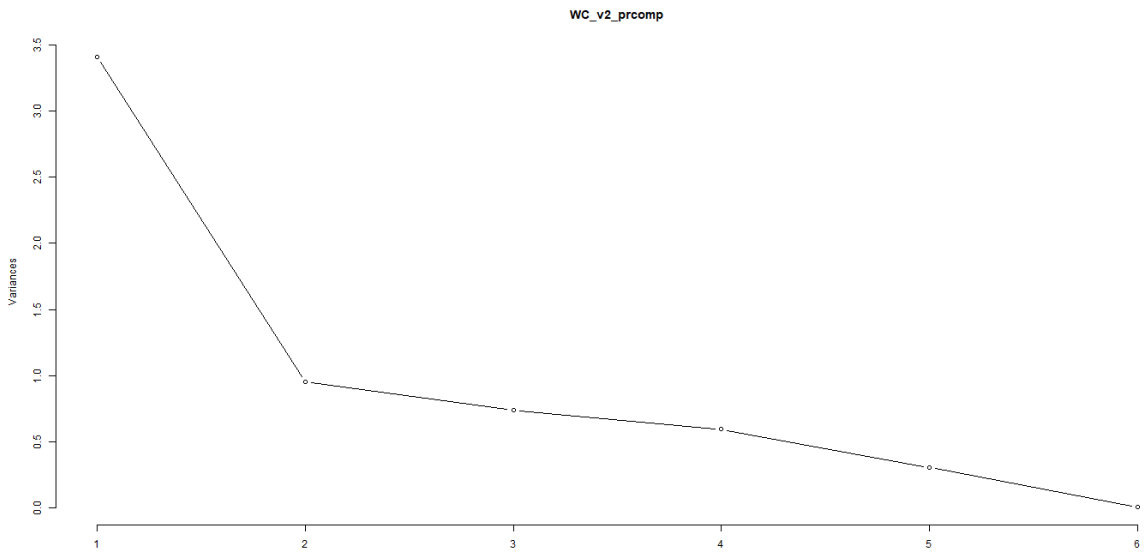

Figure 2-S2. Scree plot for PCA.

	PC1	**PC2**	**PC3**	**PC4**
Standard dev	1.8472	0.9747	0.8577	0.7702
Proportion of variance	0.5687	0.1583	0.1226	0.09887
Cumulative proportion	0.5687	0.7270	0.8496	0.9485

Table 2-S3. Standard deviation, proportion of variance explained by each PC (x100 for %) and cumulative proportion explained.

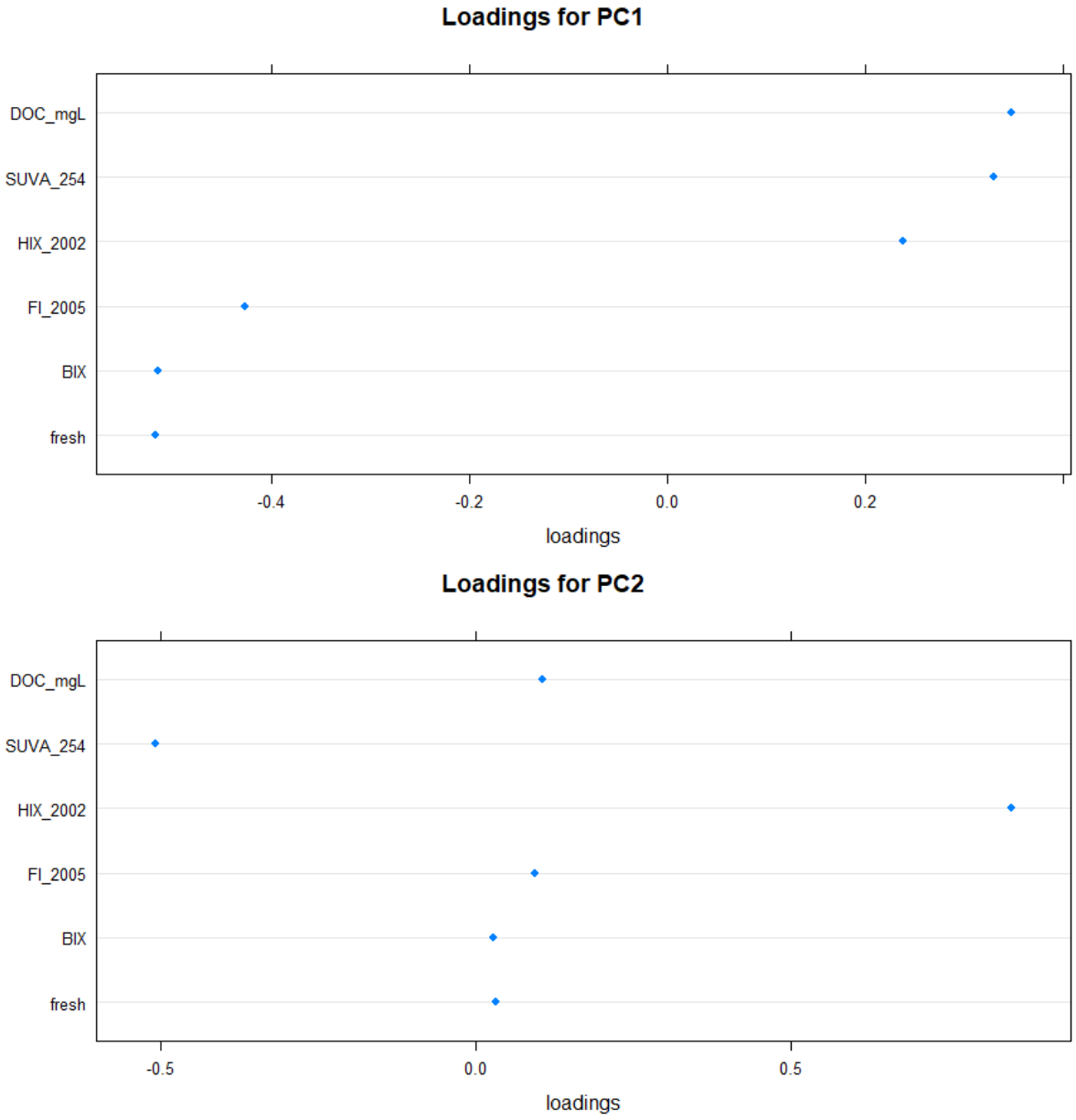

Figure 2-S3. Dot plots of loadings per PC in PCA.

CHAPTER 3

NEW INSIGHTS INTO EVENT-SCALE CDOM AND CONDUCTIVITY C-Q DYNAMICS FROM HIGH-FREQUENCY IN SITU SENSORS AT AN ALPINE HEADWATER CATCHMENT UNDERLAIN BY DISCONTINUOUS PERMAFROST IN YUKON TERRITORY, CANADA

ABSTRACT

Permafrost-underlain watersheds in the Subarctic are extremely sensitive to warming, as small changes in ground thermal status will alter all components of the hydrological cycle. At continental and large river basin scales, observed increases in winter flows and hydrochemical changes have typically been ascribed to permafrost thaw and deepening runoff pathways. Few studies in northern headwater environments investigate interactions between catchment conditions, and coupled concentration-discharge (C-Q) relationships. C-Q approaches have historically been used to determine solute source location and catchment behavior during key seasons and more recently, during flow events of differing magnitudes. High-frequency monitoring of SpC and CDOM was compared to discrete grab samples of major ions and DOC were assessed on the event to annual scale at a headwater site situated in the Wolf Creek Research Basin situated ~20 km south of Whitehorse, YT, Canada. Normalized C-Q hysteresis plots were calculated from high-frequency measurements on an event basis and correlations with meteorological, eventflow and catchment variables were overridden by seasonal patterns caused by thermally-mediated flowpaths controlled by frozen ground. CDOM was highly correlated to DOC

concentrations and flux estimates from continuous monitoring were 26% less than grab sample estimates over the measurement period. The freshet flux was 3% greater than previous estimates while summer and fall were 44% less. This comparison showed how resolution loss due to infrequent sampling influences loading estimates to the downstream environment. This has important implications for assessing carbon balances in northern catchments and demonstrates the potential for more accurate flux calculations as well as greater capture of hydrochemical dynamics to better understand catchment function.

3.1 INTRODUCTION

From a global perspective, permafrost-underlain watersheds in the Subarctic are extremely sensitive to warming, as small changes in ground thermal status will alter all components of the hydrological cycle. At continental and large river basin scales, observed increases in winter flows and hydrochemical changes have typically been ascribed to permafrost thaw and altered runoff pathways (Spencer et al., 2015; Vonk et al., 2015; Toohey et al., 2016). However, at small scales, fewer long-term records exist to be used as baselines (Laudon et al., 2017) and this results in less frequent reporting of signals of change. The lack of process-based information across all scales means that it is unclear to what extent thawing permafrost drives hydrological and chemical change (Shogren et al., 2019). Often, permafrost thaw occurs in response to a combination of climate warming and disturbance, such as thermokarst (O'Donnell et al., 2012; Malone et al., 2013; Kokelj et al., 2013; Anthony et al., 2014; Littlefair et al., 2017) and fire (Nossov et al., 2013; Koch et al., 2014). For example, increased rainfall (Prokushkin et al., 2005; Pumpanen et al., 2014), changing amount and seasonality of precipitation (Spence et al., 2014; Dore, 2015; DeBeer et al., 2016; Duan et al., 2017), vegetation change (Serreze et al., 2000; Schuur et al., 2007; Bonfils et al., 2012; Krogh, Pomeroy and Marsh, 2017; Krogh and Pomeroy, 2018) and over-winter thaw events (DeBeer et al., 2016) can act to alter streamflow volume and timing. The response of permafrost-underlain catchments to climate change is governed by complex interactions. When these complex interactions are poorly understood at small and intermediate scales, there is a risk that this process understanding will be inappropriately applied, or oversimplified, at larger scales (Finlay et al., 2006). Additionally, there has been

limited application of novel hydrological approaches due to limits in scientific capacity in remote environments due to logistical issues (e.g., site access and increased cost).

Discussion of water quality at any scale is often tied to upstream source areas, mobilization mechanisms, and transport processes operating in both time and space (Bishop et al., 2004). Upstream catchments, headwaters in particular, are important sources and conduits of solutes to downstream surface waters despite their relatively small drainage areas (Finlay et al., 2006; Alexander et al., 2007; Bishop et al., 2008; Temnerud et al., 2016; Creed et al., 2015; Ameli and Creed, 2017; Bol et al., 2018; Wollheim et al., 2018; Abbott et al., 2018). Conceptual models of runoff developed for cold, montane ecosystems show a strong seasonal control on flow pathways driven by a combination of frozen ground status, the soil profile, and connectivity driven by snowmelt and the timing of precipitation (Carey and Woo, 2001; Carey et al., 2013; Koch et al., 2013a,b). During spring freshet, a large fraction of the annual water input to the catchment is delivered via snowmelt over several weeks, yet frozen ground limits flow pathways to near-surface, organic-rich horizons (Carey and Woo, 2001; Quinton and Carey, 2004; Ågren et al., 2010; Laudon et al., 2011). This results in a large pulse of dissolved organic carbon (DOC), yet relatively low concentration of dissolved solutes (Carey et al., 2013). As seasonal thaw continues, deeper flow pathways become active, DOC declines rapidly (Carey, 2003; Quinton and Carey, 2004; Chapter 2 (Shatilla and Carey, 2019)), and the concentration of weathering solutes increases (Carey et al., 2013a). The nature and extent of groundwater (supra-, intra- and sub-permafrost in sources) varies broadly, and there remains limited exploration and data on groundwater's relative contribution geographically (Walvoord and Kurylyk, 2016;

Lamontagne-Hallé et al., 2018) and how this influences solute load and flow (Grosse et al., 2016; Fovet et al., 2018). There has been considerable interest on the role of disturbance, such as thermokarst and fire, on interactions between flow and DOC (Larouche et al., 2015; Tank et al., 2018; Burd et al., 2018) or major ions (Petrone et al., 2007). Most often, this focus is limited to shorter measurement scales although, increasingly, attention has shifted to assess flow-chemistry interactions across multiple years to better account for seasonal factors that strongly control most processes in northern, high latitude environments (Townsend-Small, 2011; Burd et al., 2018)

There has been a transformation in our understanding of catchment functioning through the utilization of new, high-frequency stream chemistry data available from new low- and moderate-cost sensors (Bieroza and Heathwaite, 2015; Kämäri et al., 2018). While not widely utilized, particularly in cold regions, the ability to combine water balance and discharge data with concomitant water quality measures, such as salinity, turbidity, temperature, specific ions, and fluorescence indices, can be used to open new avenues to understanding the links between hydrological, biogeochemical, and transport processes in cold environments (e.g., Coch et al., 2019). Already these novel measurements have revealed complex temporal dynamics that can be obscured by traditional sampling frequencies (Halliday et al., 2013; Bieroza et al., 2014; Chappell, Jones and Tych, 2017; Dupas et al., 2019), and have enabled new insights into the inner working of catchments (Bende-Michl, Verburg and Cresswell, 2013; Sherson et al., 2015; Lloyd et al., 2016b; Vaughn et al., 2017; Fovet et al., 2018; Burn et al., 2019; Knapp et al., 2020). In cold environments, high-frequency data may be particularly relevant because of the strong

vertical and spatial gradients in soil properties and time-variant flow pathways (Quinton and Gray, 2001; Carey and Quinton, 2004; Carey and Woo, 2005), which confound our understanding of transport processes and catchment connectivity (Ali et al., 2015).

Coupled flow-hydrochemical responses are often investigated to calculate solute flux and gain a greater understanding of sources, mobilization, and transport processes (e.g., Evans and Davies, 1998; Godsey et al., 2009; Musolff et al., 2015). The power-law slopes generated in C-Q space provide insights into hydrochemical dynamics that lead to observed downstream C-Q patterns and hysteresis. The C-Q hysteresis pattern occurs when stream solute concentrations and flow are out of phase, resulting in clockwise, anticlockwise or more complex loops. The overall direction, shape, and width of these loops have been used to define the relative proximity of source areas to surface waters as well as the relative proportions of contributing water sources (Evans & Davies, 1998; Lloyd et al., 2016a). For a single storm-response event, clockwise hysteresis indicates a greater concentration on the rising hydrograph limb than the falling and a positive hysteresis index (HI). When the concentration is greater on the hydrograph falling limb, C-Q hysteresis is anticlockwise (negative HI). Clockwise hysteresis is typically associated with sources of solutes located near the stream and most often dilution whereas anticlockwise suggests a combined contribution of near and distal sources (Evans and Davies, 1998). A second component of the C-Q behaviour is the event slope, known as the flushing index (FI). A positive FI indicates increasing concentrations throughout an event whereas negative FI indicates decreasing concentrations with increased flows (Lloyd et al., 2016a,b; Minaudo et al., 2019).

Similar to the FI, C-Q slopes are also calculated in log-log space to minimize dispersion effects and summarize longer-term hydrochemical behaviour as chemodynamic or chemostatic (Godsey et al., 2009). This type of C-Q analysis commonly used to relate log-log slopes to catchment characteristics such as geology, soil type, vegetation cover, and other common descriptors (Godsey et al., 2009; Saraceno et al., 2015). However, Minaudo et al., (2019) highlighted how high dispersion in C-Q patterns can render power-law slope less appropriate to summarise hydrochemical behaviour. This high dispersion can be introduced by multiple factors including: (1) source and transport limitations (Benettin et al., 2017); (2) in-stream biogeochemical transformations disconnected from hydrological changes (Bieroza and Heathwaite, 2015; Moatar et al., 2017); and (3) long-term and seasonal variations (Hirsch, 2014; Zhang et al., 2016).

Monitoring of C-Q patterns over seasons and a range of flow conditions has been explored using high-frequency methods across temperate to snow-dominated catchments (Butturini et al., 2006; Bende-Mischl, Verburg and Cresswell, 2013; Blaen et al., 2017; Vaughn et al., 2017; Burn et al., 2019; Knapp et al., 2020), although implementation in northern environments is less common. Recent assessments of C-Q patterns made possible through high-frequency measurements have introduced normalized metrics including a flushing index (slope of normalized loop) and a hysteresis index (distance between rising and falling limb) to facilitate event comparison across temporal and spatial scales (Butturini et al., 2006; Lloyd et al., 2016a; Feinson et al., 2016). The improved temporal resolution of C-Q can provide novel and nuanced information on solute sources, mechanisms of mobilization, and the time sensitivity of processes that determine the measured stream C-

Q response (Kirchner et al., 2004; Bieroza and Heathwaite, 2015; Coch et al., 2019; Knapp et al., 2020).

Higher resolution monitoring is particularly important in high latitude environments where seasonality exerts considerable control over stream solutes and flow volume (Whitfield and Schreier, 1981; Finlay et al., 2006; Townsend-Small et al., 2011). The combination of this high-frequency monitoring and more traditional water quality sampling has the potential to advance conceptual models of catchment response based on grab samples or more limited study periods (Kirchner et al., 2004). The objective of this chapter is to identify how information emerging from high-frequency monitoring of water quality variables: Specific conductance (SpC) and coloured dissolved organic matter (CDOM), can be linked to traditional water quality sampling and flow data to advance our understanding of runoff sources and transport processes in a cold, alpine watershed. We pair discrete measurements of DOC and major ions with a high-resolution data set of CDOM and SpC to evaluate the impact of resolution loss on annual and seasonal C-Q patterns over multiple years in a well-studied discontinuous permafrost watershed. Then, we assess how these differences in temporal resolution influence our understanding of catchment processes. Finally, by coupling this new information with more spatially extensive findings from Chapter 2, we help refine conceptual models of the processes that govern flow-chemical processes at the headwater catchment scale.

3.2 METHODS

3.2.1 Study Site

Granger Basin is an alpine headwater catchment with a watershed area of ~ 7.59 km^2 located above the treeline (~1200 m a.s.l.) within Wolf Creek Research Basin (WCRB) (Figure 3-1). WCRB, a long-term research watershed situated ~20 km south of Whitehorse in Yukon Territory, Canada. The climate is classified as continental subarctic and the 30-year climate normal (1981-2010) obtained from Whitehorse Airport (706 m) has a mean annual precipitation of 262.3 mm, with approximately 45% falling as snow (Carey et al., 2010). However, WCRB has some orographic influence on precipitation, with high elevation areas receiving greater than 400 mm in many years (Rasouli et al., 2019).

Granger Basin spans elevations of 1310 to 2080 m a.s.l., with vegetation ranging from shrub taiga to alpine tundra, dependent primarily on elevation and aspect. Below 1500 m.a.s.l., willow (Salix sp.) and birch (Betula sp.) are common as dwarf shrubs with a gradual increase in height downslope towards the riparian zone. White spruce (Picea glauca) occur sporadically along the south-facing slope. Above 1500 m a.s.l., lichen and bare rock predominate (Quinton and Carey, 2004; McCartney et al., 2006; Carey et al., 2013).

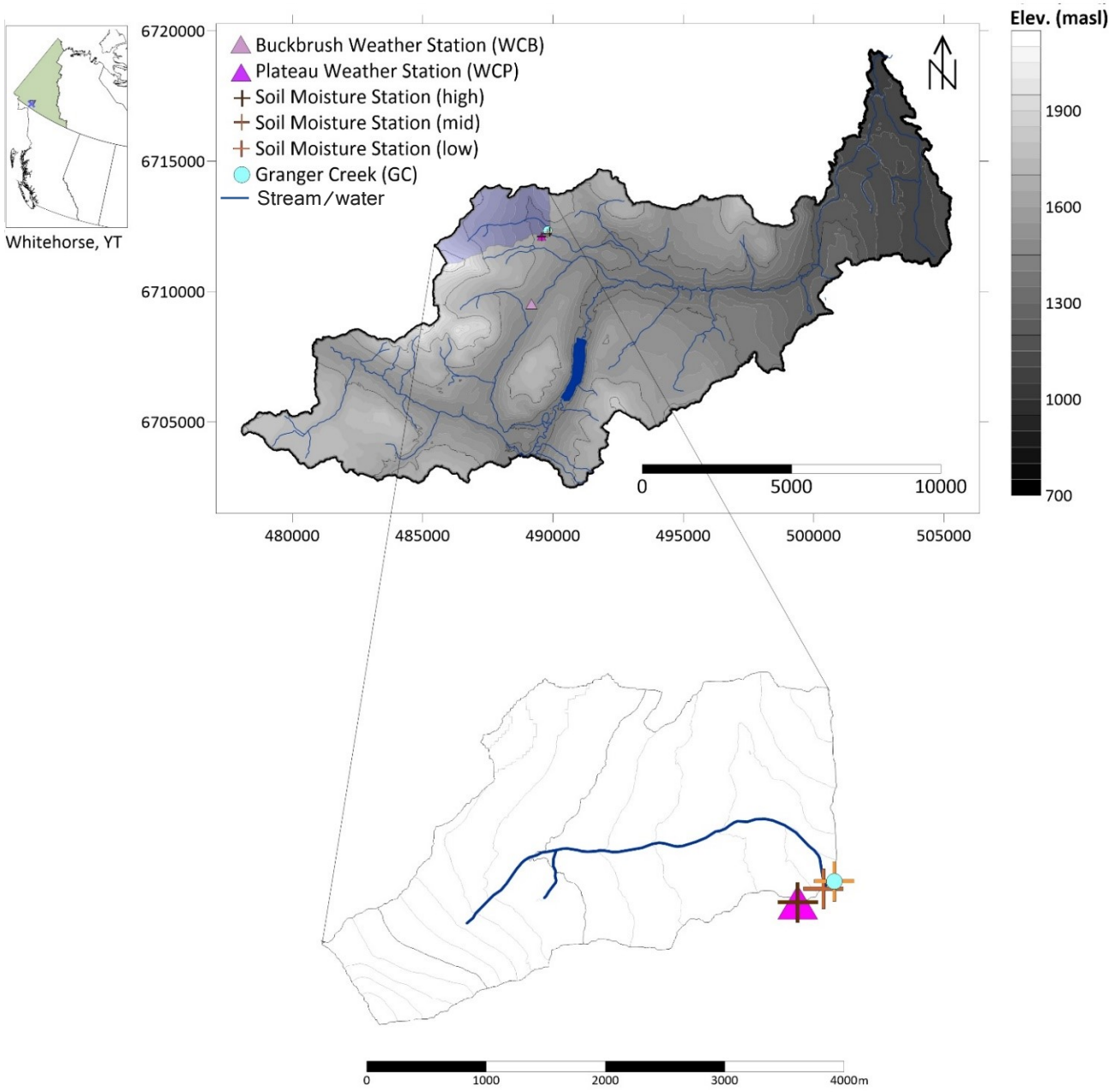

Figure 3-1. Map of Wolf Creek Research Basin (WCRB) with BB and GC catchments delineated. All stream gauges (BB, GC, CL, W1 and WCO) are indicated by circles; weather stations within WCRB are shown as triangles. Blue lines and polygons indicate streams and water bodies, respectively.

The geological setting is defined by sedimentary sandstone, siltstone, limestone and conglomerate. Atop bedrock, thick stony till and glacial drift cover most of the basin. Below 1650 m a.s.l., soils in the top metre are generally comprised of silts and sands, while higher elevations (taiga and lower tundra ecozones) have a veneer of surface organic soils with variable thickness (0.1-0.4 m). South facing slopes have a thin organic layer overlying sandy soils, whereas north slopes have thicker organic layers (10-30 cm) and are underlain with discontinuous permafrost. Between the slopes in the lower portion of Granger Basin, a wide riparian zone (50 to 100 m) exists with a consistently raised water table.

Elevation and aspect are the main controls of permafrost distribution and it is assumed that >50 % of the catchment is underlain by permafrost (Lewkowicz & Ednie, 2004). South-facing slopes are dominated by seasonal frost, while north-facing slopes and higher elevations are historically considered to have permafrost, yet the exact distribution remains uncertain (Carey, 2003).

3.2.2 Meteorological and soil moisture records

A long-term weather station (WCB) is located approximately 2 km south of Granger Basin and records all radiation components, air temperature, wind speed, vapour pressure, and total precipitation year-round, with some gaps due to power loss (Rasouli et al., 2019). Rainfall data reported in this study were obtained from a tipping bucket rain gauge at Buckbrush weather station and verified against an Alter-shielded Pluvio total precipitation gauge.

Three automated soil stations instrumented with Stevens Hydra Probe II soil moisture sensors (Frondriest Environmental, Fairfield, Ohio, USA) in GC were installed in the riparian zone, at the mid-point of the north-facing slope and upslope in the plateau area at the low, mid and high Soil Moisture Station locations, respectively (Figure 3-1). In the riparian zone, sensors were installed at depths of 5, 15, 30, 45 cm, while the mid-slope station also had an additional sensor at 60 cm depth. Soil sensors were also installed at 5, 15, 30 cm but not deeper due to the rocky soil at the Plateau site

3.2.3 Hydrometric measurements and continuous monitoring of SpC and CDOM

The long-term rating curve at Granger Basin outlet (Granger Creek, GC) was updated by frequent measurements in 2015-2016 and less frequently in 2017-2018 using a SonTek FlowTracker across a range of flow conditions each year once the channel was ice free. A stilling well containing a pressure transducer (Solinst Levelogger) was compensated with an adjacent, above-water Solinst Barologger to generate water pressure/stage at 15-minute intervals. Loggers were in place once channels were no longer ice-covered and removed in September or October to prevent freezing. When snow and ice covered the stream, discharge was manually measured with salt-dilution gauging.

Electrical conductivity was measured every 15 minutes with in-situ Onset HOBO U24-002-C conductivity loggers (Onset, Cape Cod, Massachusetts, USA) which have the capacity to measure low conductivity values. Sensors were lab-calibrated for water temperature and for conductivity using 413 uS/cm and 1413 uS/cm calibration solutions obtained from Hoskin Scientific prior to deployment.

A Turner C3 submersible fluorometer (Turner Designs, San Jose, California, USA) was attached to the outside of the stilling well in 2016 to measure CDOM at [350 nm excitation/430 ± 30 nm emission] (Figure 3-2). The C3 sensor remained in the stream throughout the study period, but some gaps in measurements occurred in 2016 due to access issues and a faulty battery. The fluorometer was moved to a slightly less turbulent part of the stream channel in 2017-2018 to diminish noise initially present in the 2016 record. CDOM was recorded in relative fluorescence units (RFU) and was not converted to Raman or Quinone Sulfate units.

Figure 3-2. Photo of CDOM sensor deployed near Granger Creek stilling well.

3.2.4 Sample collection and analysis

Stream samples were collected from 2015-2018 with 258 samples analysed for major ions and 236 for DOC. Water samples were collected at a sub-daily to sub-weekly intervals from April to late August in 2015 and 2016, while winter sampling was limited to opportunistic grab samples. Sample collection from 2017 to 2018 was less frequent with no freshet samples collected due to difficulties accessing the catchment. For major ions and DOC, samples were field filtered with single use plastic syringes submersed in the sample water immediately prior to sampling. Water was displaced through a 0.45 µm VWR

polyethersulfone syringe filter and collected in a 60 ml opaque amber HDPE bottle for DOC and a separate 60 ml HDPE bottle for major ions. Duplicates were taken approximately every 10 samples. All samples were kept cool and out of direct light before being shipped for analysis. In-situ filtration with a syringe kept the time between sample collection and filtration to a minimum, particularly during freshet, when researchers remained in the catchment for up to two weeks at a time before returning to Whitehorse.

DOC was analysed by the Biogeochemical Analysis Service Laboratory (University of Alberta) on a Shimadzu 5000A Total Organic Carbon analyzer for DOC concentration. The method detection limit (MDL) for DOC was 0.1 mg/L and reportable results were within 0.1 mg/L accuracy. Details for historical DOC in Carey, Boucher and Duarte (2013a). Cations and anions (Na^+, K^+, Mg^{2+}, Ca^{2+}, Cl^-, NO_3^-, SO_4^{2-}) were analyzed at the Biogeochemistry Laboratory (University of Waterloo) using a Dionex ICS 3000 with results reported in mg/L. The MDL for Na^+, K^+, Mg^{2+}, Ca^{2+}, Cl^-, NO_3^- as N and SO_4^{2-} as S were 0.13, 0.1, 0.3, 0.67, 0.12, and 0.1 in mg/L, respectively. Standards from Thermofisher were used to build correction curves and 5% of samples were re-run for QA/QC procedures.

3.2.5 Event data processing

3.2.5.1 Event delineation

The HydRun tool kit (Tang and Carey, 2017) was used to pre-process discharge, SpC, and CDOM records as well as obtain metrics describing initial discharge values, and SpC and CDOM concentrations for each event as well as event response metrics. Pre-

processing steps included application of a recursive filter to the discharge time series and subtraction of baseflow from the hydrograph. Events were subsequently identified from the baseflow-free time series. HydRun identified 38, 29, and 45 events in 2016, 2017, and 2018, respectively.

Continuous SpC and CDOM were filtered to remove noise from these datasets while maintaining appropriate responsiveness. Filtering for SpC in 2016, 2017 and 2018, consisted of applying a moving median filter (window size = 5, nPass = 1) to smooth the time series. Subsequently, a moving average filter (window size = 3, nPass = 1) was applied to remove remaining artefacts and introduce smoother transitions between values. Only a moving average filter was applied to CDOM measurements. The application of the moving average filter differed between 2016 and 2017/2018 due to the change in sensor location (2016: window size = 3, nPass = 10, 2017/2018: window size = 3, nPass = 1), since the Turner C3 fluorometer was located in a relatively turbulent location during moderate to high flows in 2016. Segments of the SpC and CDOM time series that matched the start and end time of runoff events were clipped from the filtered time series.

3.2.5.2 Concentration-Discharge (C-Q) analysis

Discharge, SpC and CDOM were normalized in HydRun to values ranging from 0 to 1 by min-max normalization for each individual event (Equation 1) following procedures outlined in Lloyd et al., (2016a).

$$x' = \frac{x - x_{min}}{x_{max} - x_{min}} \qquad \text{(Equation 1)}$$

Where x_{min} is the minimum value of x,

x_{max} is the maximum value of x, and
x is any value of x.

If each time series (discharge, CDOM, SpC) was intact throughout the event period, filtered CDOM and SpC time series were matched to the discharge data. HydRun identified an event using the abrupt increase from baseflow, while the end of each event was the return to baseflow. Manual intervention was required to separate events based on the inflection point prior to a subsequent increase. Additionally, event start and end points were adjusted manually in some cases.

A new functionality added to HydRun enabled the transformation of dual time series (i.e. SpC-Q, CDOM-Q) into normalized hysteresis loops and generated descriptive hysteresis and flushing metrics based on recent C-Q investigations (Lloyd et al., 2016a, b). For each event, normalized CDOM or SpC was plotted against normalized discharge. Discharge at intervals (i.e. 25, 50, 75, 90 percentiles) specific to each event were paired to the corresponding SpC or CDOM values of each rising and falling limb. For each specific percentile, the hysteresis index (HI) was calculated as the distance between the rising and falling limbs of normalized SpC (or CDOM) throughout each event. The slope of the normalized hysteresis loop (flushing index per Lloyd et al., 2016a) began at the first corresponding discharge and SpC (or CDOM) measurements of each delineated event and ended at peak event discharge, which was the right-most point of the hysteresis loop within the normalized x and y axes. Events where the normalized hysteresis metrics were well-described were retained for further analysis (see Figure 3-S1) while other were not retained further as their complex geometry was not well represented by either the flushing or

hysteresis index (see Figure 3-S2). Further work is required to integrate these hysteresis events into the analysis.

In addition to event variables defined using HydRun, variables reflecting antecedent conditions were calculated for meteorological variables to assess their relationship to event variables and hysteresis metrics. The pre-event window ranged from the start of a given runoff event (at the ridge edge) to *n* days prior the start of the runoff event (at the left edge). For the analyses, *n* was examined at the following levels: 1, 4, 10, 21 days, based on previous research examining C-Q hysteresis in relation to precursor conditions. Antecedent temperature was calculated as the mean of the pre-event window, while antecedent precipitation was calculated as the sum of this same period. Total event precipitation was also calculated by taking the sum of measured precipitation from 6 hours before the hydrograph rise until the event peak. Individual events were numbered (Table 3-S1) and each event ID represented the same time period/event for corresponding SpC and CDOM time series.

3.3 RESULTS

3.3.1 Meteorology

Mean air temperature at Buckbrush weather station from 1 April to 31 October was 7.0 ℃, 8.3 ℃, 6.9 ℃ and 7.2 ℃ in 2015, 2016, 2017 and 2018, respectively (Figure 2). Total precipitation for the same period was greatest in 2016 (250 mm), followed by 2018 (235 mm) and 2015 (201 mm). Summer and fall months in 2015 and 2016 were

characterized by atypical large magnitudes of rainfall totalling 107 mm (170 mm including fall) and 110 mm (203 mm including fall), respectively (Figure 3-3).

Snow accumulation and melt varied among years with 174 mm SWE snowpack in 2015 by mid-March and a rapid melt with Buckbrush beginning on 11 April before an additional 30 mm of snowfall caused an increase in the snowpack. Accumulated SWE reached ~ 144 mm by 3 May before rapid melt occurred with snow-free conditions reported on 12 May 2015. The maximum SWE in 2016 ranged between 111-113 mm SWE by March and had an earlier but more prolonged melt than the previous year. Snowmelt began on 27 March with the first recorded snow-free day on 27 April 2016. In both years, snowpacks persisted past these dates at GC due to differences in elevation, aspect, and the presence of shaded depressions. The subsequent year was characterized as snow-free on 7 May 2017 after the melt of 140 mm SWE. For 2018, 175 mm SWE had melted at Buckbrush by 11 May.

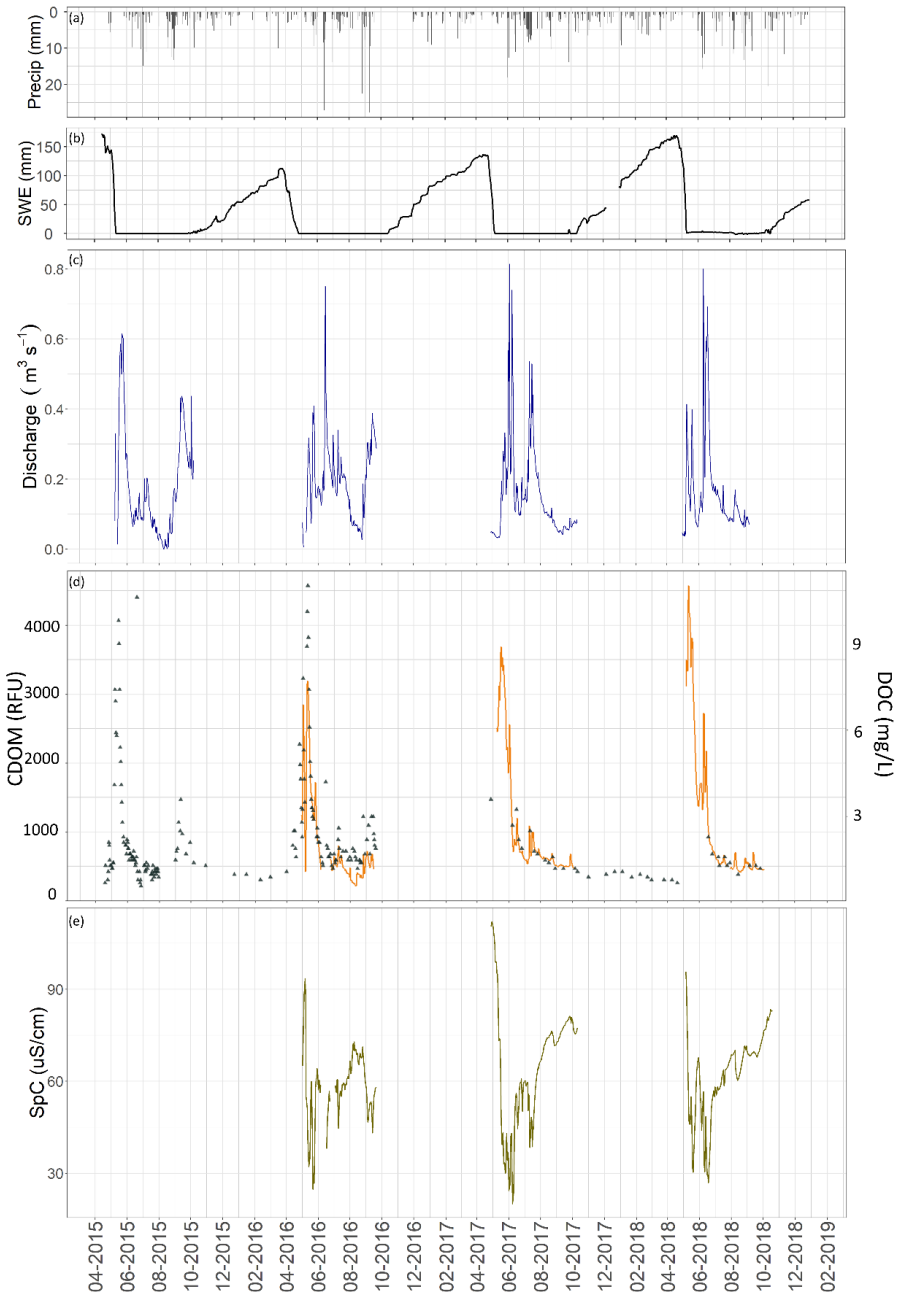

Figure 3-3. (a) Precipitation from 30-minute tipping bucket rain gauge and (b) accumulated SWE from snow pillow data at Buckbrush Weather Station. (c) Daily average discharge data from Granger Creek outlet. (d) Daily chromophoric dissolved organic matter (CDOM), shown as a continuous orange line, averaged from 15-minute measurements and dissolved organic carbon (DOC) concentrations, shown as dark grey triangles, from Granger Creek. (e) Daily average specific conductivity (SpC) concentrations from Granger Creek.

3.3.2 Discharge

Discharge from 2015 to 2018 at GC varied due to snowpack accumulation (i.e. SWE), snowmelt onset, and the timing of large magnitude rainfall events (Figure 3-3). Peak discharge in 2015 coincided with freshet, following the rapid melt of a large snowpack (and corresponding SWE volume) in spring (Figure 3-3). Similarly, peak discharge in 2016, 2017, and 2018 occurred in early June, coinciding with large magnitude rainfall events. During 2016, the gradual increase prior to peak discharge was related to a staggered freshet and freeze-thaw cycles between April and mid-June (Figure 3-3). In all years, summer rainfall events resulted in increases in discharge. During 2015 and 2016, appreciable increases in discharge occurred in fall, corresponding to late-season rainfall events. Comparatively, no large magnitude rainfall events and consequent streamflow increases were observed late in the open-water seasons of 2017 and 2018.

3.3.3 Discrete measurements of DOC and major ions

DOC concentrations typically reached an annual maxima near 10 mg/L during freshet or immediately preceding the first discharge peak in all years (Figure 3-3). Subsequent to peak DOC concentrations in spring, DOC declined throughout the rest of the open-water season to values between 1 and 3 mg/L, with intermittent increases related to summer precipitation events (and resultant increases in discharge). In particular, large magnitude rainfall events in fall of 2015 and 2016 led to DOC concentrations increasing to approximately half of their peak freshet concentrations (Figure 3-3). Although winter data were sparse (note that no samples were collected in winter 2016 to 2017), DOC concentrations appeared to consistently reach their minima over winter.

Concentrations of Ca^{2+}, Mg^{2+}, and to a lesser extent SO_4^{2-} and Na^+, exhibited similar patterns in 2015 and 2016 (Figure 3-4), while K^+ followed a temporal pattern coincident with DOC. Notable correlations, with r^2 values greater than 0.50, were observed for K^+ and DOC (r^2 = 0.74), and Ca^{2+} and Mg^{2+} (r^2 = 0.91). Ca^{2+}, Mg^{2+}, Na^+, and SO_4^{2-} reached their annual minima during freshet in 2015 and 2016, subsequently increasing throughout the summer and fall and eventually reaching their highest concentrations in the winter. Comparatively, K^+ concentrations peaked in 2015 and 2016 during or shortly after spring freshet and also exhibited slight increases in concentration in response to rainfall events. NO_3^- had a temporal pattern that was distinct from other anions and cations, where it decreased during peak discharge in spring for both 2015 and 2016, but subsequently increased throughout the summer. NO_3^- concentrations fell below summer levels in fall 2015, then rose above summer concentrations in 2016 and were once again low in fall/winter 2017-2018. The decline in grab sampling resolution for discrete data in 2017

and 2018 obfuscated temporal relationships for cations and anions that were readily apparent in 2015 and 2016 (Figure 3-4).

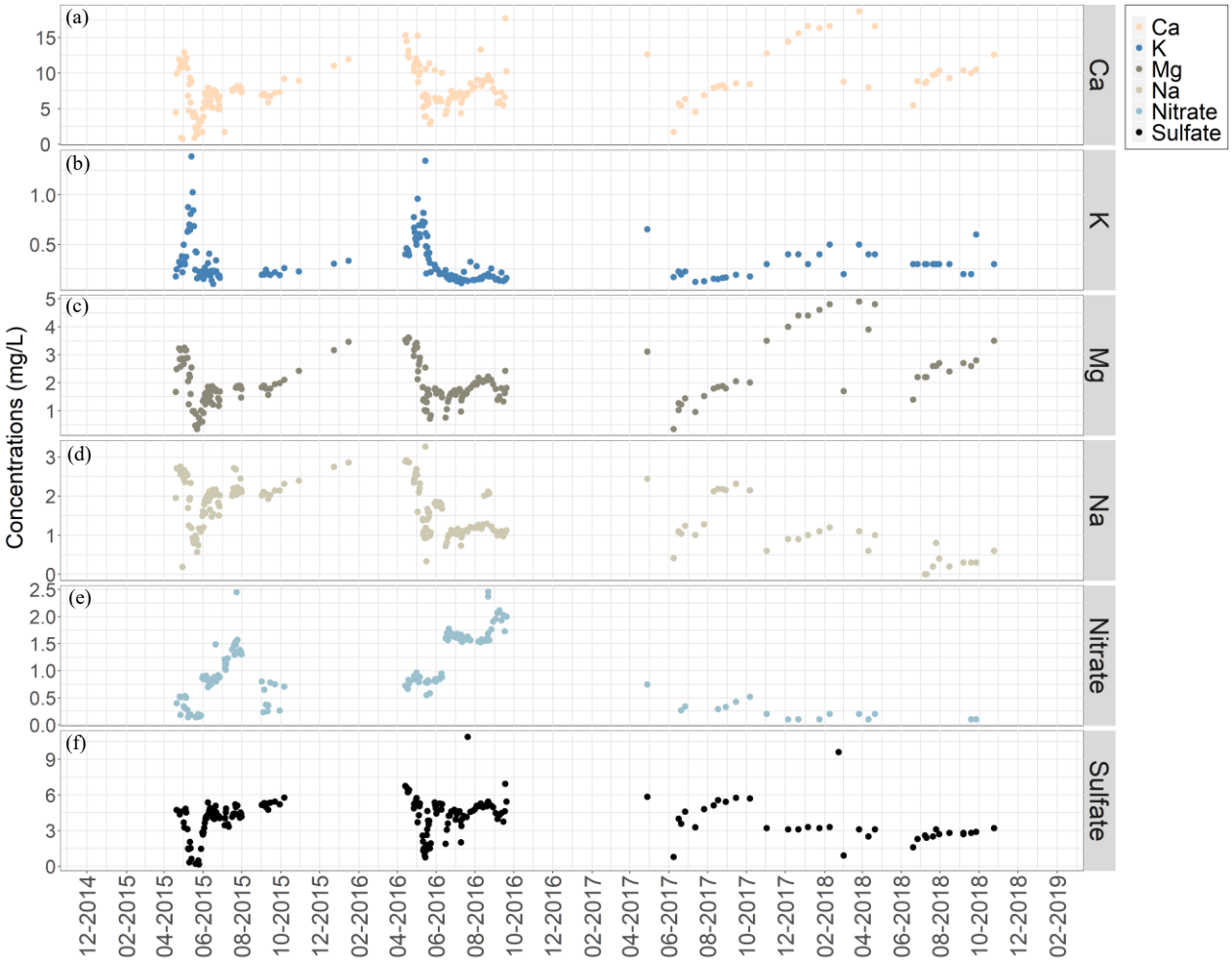

Figure 3-4. Concentrations of major ions in mg/L from 2015 to 2018. (a) Calcium ion denoted with pale beige filled-in circle. (b) Potassium ion in dark blue. (c) Magnesium ion in dark brown. (d) Sodium ion in light taupe. (e) Nitrate as N in light blue. (f) Sulfate ion as S in black.

3.3.4 Continuous measurements of CDOM and SpC

3.3.4.1. General Trends

CDOM peaked during spring freshet at GC in all years (Figure 3-3), with RFU maxima ranging from ~3200 RFU (2016) to 4500 RFU (2018), while minimum values

typically occurred during late summer or fall and ranged from ~ 500 RFU (2016) to ~ 1000 RFU (2017). CDOM generally increased in response to rainfall events throughout the summer, although the magnitude of these increases was small relative to increases observed during freshet. Rainfall in 2017 and 2018 was less than in the previous two study years, and no late summer/fall increase in CDOM was observed. SpC displayed an inverse relationship to CDOM and discharge, where SpC consistently decreased with increasing discharge and CDOM. The largest observable decreases in SpC occurred in response to snowmelt water inputs in spring, with annual minima concurrent with annual peaks in discharge in early June (Figure 3-3).

3.3.4.2 Inter-annual and intra-annual hysteresis

Inter-annual CDOM-Q hysteresis generally followed a clockwise pattern and was consistent across years (Figure 3-5). Nested within the intra-annual pattern were shorter-duration event-response anticlockwise loops and, less frequently, clockwise loops (Figure 3-5). Shorter-duration loops within the overall annual pattern were predominantly clockwise during late May/early June and anticlockwise events occurred during spring, summer and fall. The overall pattern (i.e. clockwise-dominant) was consistent across years, with the primary difference between 2016 and 2017/2018 being the presence of larger magnitude discharge events in 2017/2018, as evidenced by lower and less variable CDOM values despite large concomitant discharge variability after mid-July (~ day of year 200; Figure 3-3 and Figure 3-5).

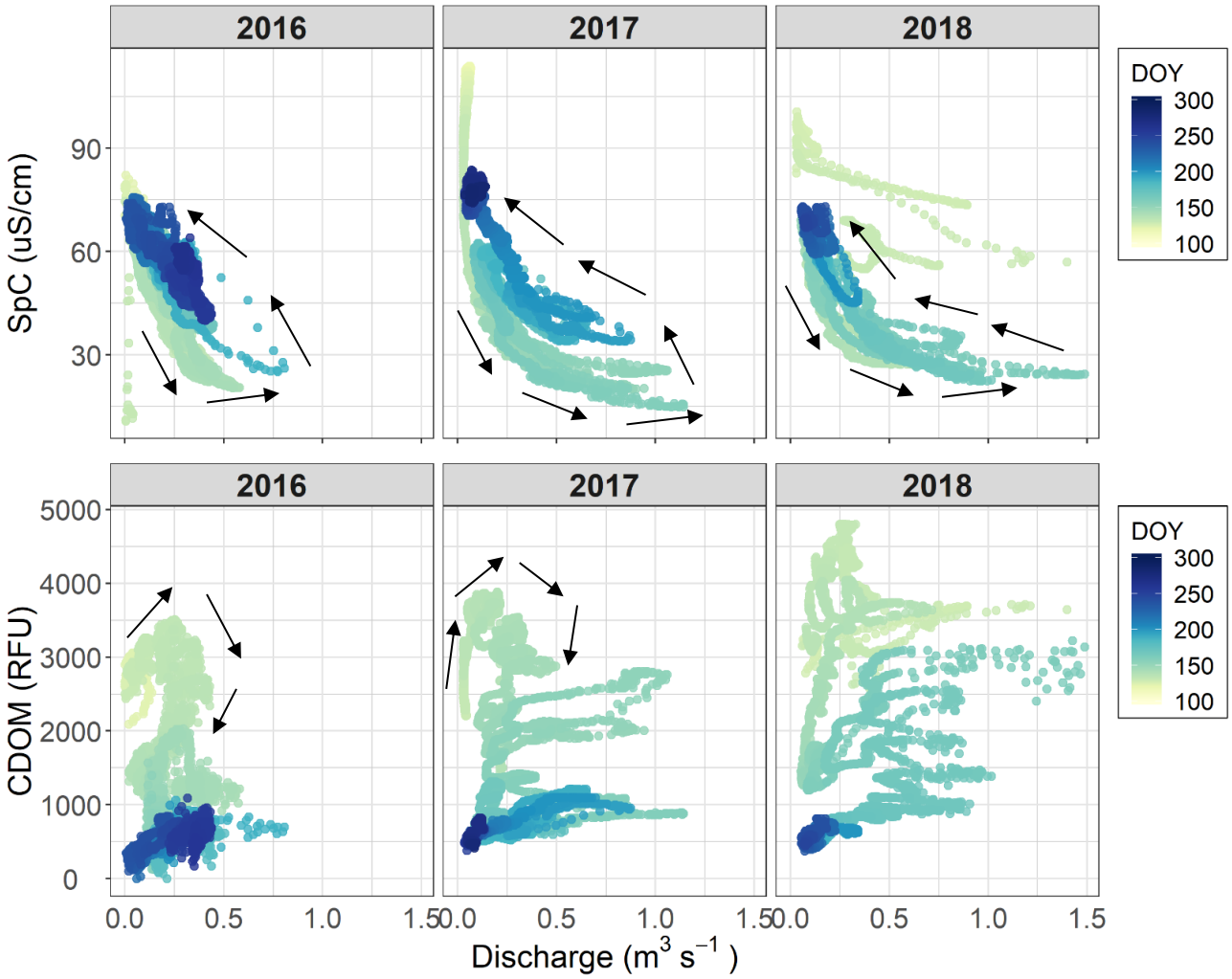

Figure 3-5. Annual concentration-discharge (C-Q) for Granger Creek in 2016, 2017 and 2018 for (a) specific conductivity (SpC) in µS/cm and (b) chromophoric dissolved organic matter (CDOM) in RFU. The color ramp shows day of year 100 (light yellow) to day of year 200 (dark blue).

Anticlockwise patterns dominated the annual SpC-Q pattern, while smaller loops that were primarily clockwise occurred during events as well as diel variation. Hysteresis response and patterns were more consistent for SpC than for CDOM, where a similar magnitude change in discharge led to approximately the same magnitude of response in SpC. This consistency in C-Q hysteresis has been reported for other northern river basins

(Whitfield and Schreier, 1981). Similar to CDOM-Q hysteresis, the overall pattern (i.e. anticlockwise dominant) was consistent among years.

3.3.4.3 Event hysteresis and relationships to antecedent conditions

Sixty events with sufficient CDOM, SpC and Q records were extracted using HydRun, while 52 events were discarded due to: (1) gaps in the SpC or CDOM records; or (2) avoid false equivalencies due to atypical loop geometry. Analysis of event hysteresis loops was often confounded by complex patterns in sub-daily data, including diurnal variability that obscured or exceeded event-based stream response. Events with hysteresis characteristics inaccurately quantified using the loop analysis approach were discarded, while well-characterized events were used for further analysis (Table 3-S1). Many snowmelt-driven events were retracted from the analysis due to complex loop geometry that could not be adequately characterized using the normalized hysteresis index (HI) and flushing index (FI). Examples of discarded CDOM and SpC events (Figure 3-S1: events 5 and 11) and retained (Figure 3-S2: events 30 and 38) from the 2017 dataset are provided in Supplemental Information (SI). Initial conditions and event changes were calculated (Table 3-1) in addition to normalized event hysteresis metrics (Table 3-2) based on hysteresis metric calculations introduced in (Lloyd et al., 2016a). Summary statistics for antecedent meteorological conditions and soil moisture are presented in SI (Table 3-S2).

Season		Initial Q_i (m^3s^{-1})	$CDOM_i$ (RFU)	SpC_i (uS/cm)	P_{event} (mm)	Q_{peak}	Event ΔQ	T r (hrs)	$\Delta CDOM$	Event mean CDOM	ΔSpC	Event mean SpC
Spring	**Mean**	**0.158**	**1988.9**	**50.4**	**0.6**	**0.433**	**0.277**	**12.0**	**632.4**	**2171.1**	**16.1**	**43.8**
	Std Dev	0.089	877.2	15.7	1.3	0.391	0.362	8.5	920.8	922.7	12.2	12.5
	Min	0.001	528.6	15.5	0	0.065	0.047	4.0	106.8	568.2	1.0	24.8
	Max	0.389	3555.2	87.7	5.4	1.485	1.401	48.25	2020.0	3657.5	55.0	68.5
	IQR	0.099	1554	24.3	0.7	0.256	0.145	4.25	467.9	1565.0	8.6	21.0
	n	34	33	34	34	34	34	34	34	34	34	34
Summer	**Mean**	**0.216**	**834.1**	**50.5**	**8.0**	**0.488**	**0.272**	**10.2**	**270.9**	**863.4**	**13.1**	**45.8**
	Std Dev	0.112	444.3	10.9	5.0	0.255	0.195	4.5	342.2	326.4	7.4	10.3
	Min	0.095	445.4	33.6	0.6	0.185	0.064	4.75	61.6	447.1	3.7	28.4
	Max	0.422	2217.2	70.2	19.6	1.015	0.634	22.75	648.4	1926.3	33.3	65.5
	IQR	0.184	294.3	16.8	5.1	0.409	0.319	5.88	346.4	227.6	8.7	12.0
	n	22	20	20	12	22	22	22	21	21	20	20
Fall	**Mean**	**0.111**	**523.4**	**70.6**	**9.7**	**0.204**	**0.093**	**27.0**	**314.6**	**602.3**	**5.5**	**69.7**
	Std Dev	0.088	61.2	13.0	5.4	0.110	0.035	3.25			2.1	11.3
	Min	0.059	476.4	52.2	3.6	0.133	0.055	23.75			3.0	52.8
	Max	0.241	608.8	82.1	13.9	0.364	0.124	31.5			7.7	79.7
	IQR	0.061	66.4	10.8	5.2	0.092	0.056	4.0			2.9	10.5
	n	4	4	4	3	4	4	4	1	1	4	4
All seasons	**Mean**	0.161	1115.5	57.2	6.1	0.375	0.214	16.39	415.0	1212.3	11.5	53.1

Table 3-1. Summary table of initial conditions and event response spanning 2016-2018 for events separated by season.

		CDOM							SpC						
Season		HI_{25}	HI_{75}	HI_{90}	HI_{avg}	FI slope	Loop Area	Loop Area (+/-)	HI_{25}	HI_{75}	HI_{90}	HI_{avg}	FI slope	Loop Area	Loop Area (+/-)
Spring	**Mean**	-0.292	-0.258	-0.101	-0.299	0.443	0.295	-0.260	0.451	0.263	0.115	0.367	-0.780	0.357	0.332
	Std Dev	0.322	0.299	0.191	0.286	0.402	0.187	0.234	0.315	0.206	0.091	0.267	0.235	0.192	0.232
	Min	-0.980	-0.86	-0.620	-0.850	-0.520	0.058	-0.746	-0.440	-0.120	0.010	-0.320	-1.10	0.107	-0.309
	Max	0.410	0.360	0.420	0.410	1.092	0.746	0.338	0.880	0.660	0.330	0.780	-0.162	0.697	0.697
	IQR	0.360	0.413	0.213	0.310	0.590	0.181	0.202	0.505	0.345	0.145	0.445	0.348	0.347	0.363
	n	31	31	31	31	31	29	29	27	27	27	27	29	26	26
Summer	**Mean**	-0.170	-0.141	-0.101	-0.168	-0.013	0.301	-0.131	0.363	0.365	0.206	0.386	-0.801	0.352	0.332
	Std Dev	0.436	0.286	0.187	0.312	0.785	0.156	0.314	0.240	0.274	0.181	0.223	0.205	0.153	0.194
	Min	-0.730	-0.940	-0.680	-0.810	-1.278	0.073	-0.662	-0.140	-0.280	-0.060	-0.200	-1.032	0.128	-0.197
	Max	0.560	0.260	0.160	0.340	1.005	0.662	0.329	0.780	0.990	0.710	0.810	-0.186	0.687	0.687
	IQR	0.650	0.340	0.155	0.480	1.523	0.160	0.483	0.260	0.318	0.253	0.228	0.263	0.215	0.215
	n	18	18	18	18	17	18	18	20	20	20	20	20	20	20
Fall	**Mean**	-0.333	-0.128	-0.125	-0.350	0.612	0.360	-0.360	0.060	0.880	0.960	0.400	-0.479	0.356	0.356
	Std Dev	0.132	0.296	0.334	0.135	0.078	0.085	0.085					0.344		
	Min	-0.440	-0.480	-0.470	-0.480	0.496	0.308	-0.458					-0.805		
	Max	-0.140	0.200	0.300	-0.210	0.660	0.458	-0.308					-0.118		
	IQR	0.083	0.358	0.328	0.135	0.045	0.075	0.075					0.343		
	n	3	3	3	3	4	3	3	1	1	1	1	3	1	1
All seasons	**Mean**	-0.264	-0.176	-0.072	-0.278	0.347	0.319	-0.250	0.291	0.503	0.427	0.384	-0.687	0.355	0.340

Table 3-2. Summary of hysteresis metrics for CDOM and SpC separated by season.

Smaller, intra-annual hysteresis patterns (Figure 3-5) represented event and diel CDOM-discharge and SpC-discharge dynamics. Diel amplitude was greatest in spring and decreased during summer and fall. For CDOM-Q events, 42 of 60 events exhibited negative HI (i.e. anticlockwise hysteresis), with a mean HI of -0.278 for all events (Table 3-2). Additionally, 41 of 60 CDOM-Q events had a positive FI (i.e. increasing concentration during event; Table 3-S1), with a mean FI of 0.347 (Table 3-2). Comparatively, SpC-Q event hysteresis was characterized by positive HI indices (i.e. clockwise hysteresis), as indicated by 46 of 60 events having positive HI indices (Table 3-S1) with a mean HI index of 0.384 (Table 3-2). The flushing index for SpC-Q events was negative for 52 of the 60 events (i.e. decreasing concentrations during event), with a mean FI of -0.687 (Table 3-2). SpC-Q events categorized using hysteresis metrics were more tightly clustered than CDOM-Q events, but neither showed seasonal separation.

Pearson r correlations between descriptive variables are provided in SI (Table 3-S3). Significance was set to 95% and only significant correlations are reported in this section. Total event precipitation, runoff ratio, and other metrics related to precipitation during the melt period were removed from the correlation analysis. Initial and event SpC concentrations were clearly linked to stream discharge, hydrograph characteristics and SpC-Q hysteresis metrics, whereas relationships with CDOM concentration were limited. Specifically, SpC mean concentration was inversely correlated to Q start, peak and end, and the time to recession. Similar relationships were not significant for CDOM concentrations. Initial CDOM concentration was significantly and negatively correlated to antecedent air temperature, soil moisture at 15 cm depth (mineral soil) and positively to

antecedent rainfall, soil moisture at 5 cm (typically organic soil). Initial CDOM concentration and CDOM-Q HI values were negatively correlated to near-surface soil moisture and negatively correlated to deeper soil moisture values, while SpC-Q HI values were negatively correlated to soil moisture at all depths. Both CDOM-Q (absolute value) and SpC-Q loop area were positively correlated to total event precipitation while CDOM-Q was also positively correlated to soil moisture. SpC-Q loop area was also negatively correlated to storm discharge (peak, end, range), the runoff ratio and time to rise. CDOM-Q slopes had a strong positive correlation to the runoff ratio, and weaker positive correlations to antecedent air temperature. SpC-Q slopes were weakly negatively correlated to SpC-Q loop area, and positively to SpC event concentration (minimum, maximum, mean). Both hysteresis slopes were negatively correlated with 21-day antecedent rainfall and discharge (initial, end), with SpC-Q slopes also negatively correlated to peak event and the range in discharge.

3.4 DISCUSSION

In catchments with permafrost, shallow, active-layer soils are typically affected by distinct soil boundaries, including the frozen boundary and the organic-mineral boundary where highly porous and hydraulically conductive organic material overlies fine-grained mineral soils (Koch et al., 2017). In two dimensions, the position of the water table controls the rate of water movement from the catchment to the stream (Quinton et al., 2005). The soil layers where flow is being generated also affects subsequent water quality parameters. During freshet, the near-surface organic layer is typically flushed of dissolved organic

carbon that is often produced the previous year and only transported once annually during freshet (Boyer et al., 2000; Carey, 2003; Finlay et al., 2006). This behaviour is often observed in cold northern and alpine catchments but is not ubiquitous (Li Yung Lung et al., 2018). As thaw progresses, the thickening active layer deepens flow pathways into mineral soils that have longer flow pathways and increases the frequency of DOC sorption while increasing the load of dissolved solutes. In areas with discontinuous permafrost, unfrozen taliks and areas without permafrost can elongate flow pathways and integrate a complex mixture of DOC that includes inputs from vegetation, the active layer, and deeper microbial composition.

While the above conceptual model has been developed and refined over several decades, there remains limited longer-term multi-year data sets that combine flows with water quality and DOC. In addition, how catchment spatial structure influences these flow-chemistry patterns is less clear, as riparian and hillslope contributions in cold environments have not been clearly defined. Finally, high-frequency water quality data has had limited application in cold environments and provides avenues for discovery. In this work, we utilize a novel, multi-year data set from a well-studied headwater catchment to advance our understanding of runoff sources and transport processes and develop new research directions.

3.4.1 Intra-annual and seasonal solute concentration patterns

Intra-annual patterns of major ions and DOC concentrations observed over four years are largely consistent with those previously reported at GC (Carey and Quinton, 2004;

Boucher and Carey, 2010; Carey et al., 2013a) and in other northern basins (Petrone et al., 2006; Koch et al., 2013) for the snowmelt period. Both SpC and CDOM show distinct and inverse patterns with discharge over multiple years (Figure 3-3). SpC consistently decreased with increasing discharge, most notably during snowmelt in spring and during rainfall events, which is a consistent pattern among permafrost watersheds (Koch et al., 2013; Miller et al., 2014). SpC was highest just prior to freshet, reflecting deeper groundwater-driven baseflow connections to the stream over winter.

Snowmelt provided a considerable volume of water and activated near-surface flow pathways through organic soils containing limited dissolved solutes. Routing of water through these pathways diminished the importance of deeper flow pathways, resulting in a rapid decline in SpC and the concentration of weathering ions (Ca^{2+}, Mg^{2+}, and Na^{+}) and sulfate (SO_4^{2-}). Following freshet and as thaw progressed, deeper flow pathways became more active as water took increasingly longer and deeper subsurface pathways to the stream, increasing SpC and weathering ion concentrations as spring transitioned into summer and fall. During rainfall events, declines in SpC were observed suggesting newer water contributions that can be explained by the activation of near-surface pathways (Carey and Quinton, 2004).

The inverse pattern was observed for CDOM and DOC compared with discharge, although there were notable exceptions. In Granger Basin, CDOM is a reliable proxy for DOC (r^2=0.93; Chapter 2 (Shatilla and Carey, 2019)) and is considered equivalent to DOC concentration due to the consistent relationship between high-frequency CDOM and DOC grab samples (Figure 3-3). Peak CDOM and DOC concentrations occur during freshet

immediately preceding the first discharge rise when soils were largely frozen and freshet-driven flow pathways were restricted to surface and organic layers. Peak DOC concentrations on the rising limb of the freshet hydrograph have previously been reported at GC and in other northern catchments. In addition, the more biologically active ions (NO_3^-, K^+) rose (Figure 3-4), suggesting a shift to more shallow organic layers (Langmuir, 1997). Following freshet, DOC concentrations and CDOM rapidly declined and were low throughout most of summer with some increases in fall, during wet years (2015, 2016), indicating wetter conditions favouring the reactivation of near-surface flow pathways and an increase in DOC transport.

3.4.2 New insights on C-Q and solute flux from high resolution data

3.4.2.1 Temporal resolution and information loss

While the 15-minute and discrete sampling data agree well, there is considerably more information and dynamic behaviour captured with the higher frequency CDOM and SpC records (Figure 3-5). This challenges our understanding of catchment behaviour from infrequent water quality samples at large and intermediate time scales, which neglect the dynamic nature of flow-chemistry interactions. The first step in quantifying the information gathered from continuous monitoring and grab samples was to calculate linear regressions in log-log space. Seasonal and annual regressions of SpC-Q and C-Q of major ions (Figure 3-6) were evaluated as were CDOM-Q and DOC-Q (Figure 3-7) The relation between flow, SpC, and major ions in log-log space suggest that there is a chemostasis during low flows and a dilution signal at higher flows, particularly with respect to weathering ions which all showed similar dilution slopes (Figure 3-6). The SpC signal is comprised of differing relative contributions from major ions, meaning that high-frequency SpC data could not be directly compared to the ion data. However, similar patterns were apparent overall, and the divergent patterns noted during 2018 high-flow conditions resulted from a staggered early and late season snowmelt peak (Figure 3-6). The later and larger peak had similar conductivity, despite higher flows. This pattern can largely be explained by water pathways; when flow is in lower mineral layers it has a distinct composition that mixes with less saline, near-surface organic layers at higher flow conditions.

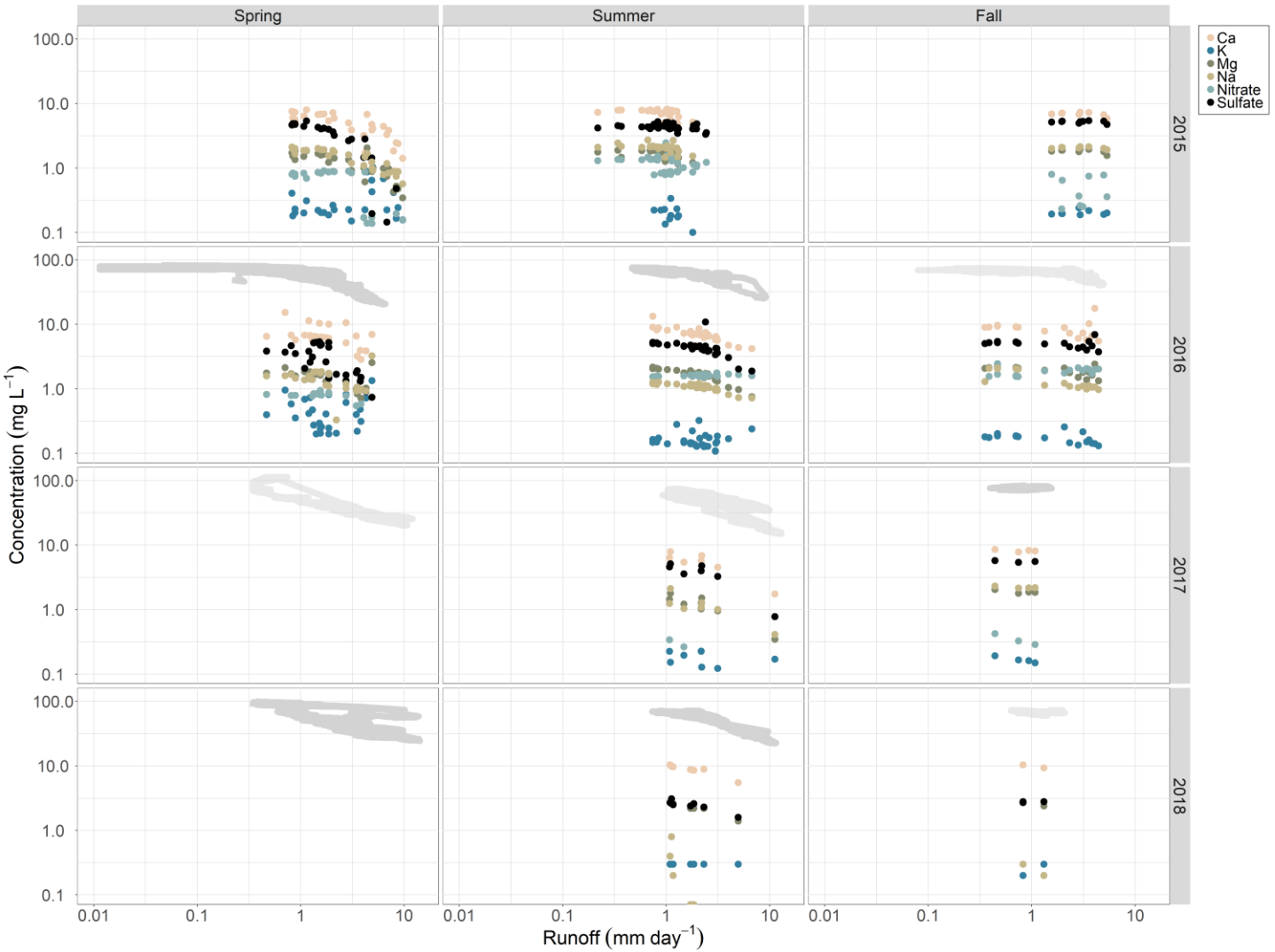

Figure 3-6. Concentrations of major ions in mg L^{-1} shown on y-axis by year (indicated by panel labels) and runoff in mm day^{-1} per season (indicated by panel labels). Axes are log_{10}. Each ion is presented by a distinct color (shown in legend and conserved from previous figure).

To allow direct comparison, CDOM was converted to DOC concentration (regression provided in Chapter 2 (Shatilla and Carey, 2019)). The slope of the DOC-Q slope was predominantly positive yet varied among years, suggesting a general trend of mobilization (accretion) of DOC with increasing flows. However, the dispersion evident in the C-Q relationship also implies that a linear regression is perhaps inadequate to summarize C-Q behaviour as a whole (Minaudo et al., 2019). Spring hysteresis showed reduced slopes on an annual basis with slopes computed using data from sparse grab samples during freshet in 2017 and 2018. Freshet slopes indicated a greater mobilization signal compared to 2016 yet a more limited range of conditions was observed (Figure 3-7).

To further explore the influence of temporal resolution on models of catchment C-Q behavior, we focussed on 2016 when both CDOM and DOC measurements were most complete. Depending upon the temporal selection (i.e. the inclusion of freshet), and the season, the log-log slopes differed between CDOM-Q and DOC-Q (Figure 3-7). A positive log-log slope supported the assertion of DOC flushing during freshet, however the higher CDOM temporal resolution record captured between 2016-2018 suggests much more complex dynamics not observed at daily or weekly sampling time scales (Figure 3-7). The disconnect between C-Q slopes computed at smaller timescales compared to seasonal or annual time scales has been reported in the literature in more temperate environments (Duncan et al., 2017; Dupas et al., 2017; Li et al., 2019; Minaudo et al., 2019). In fact, mobilization, dilution, and chemostatic C-Q frameworks (Musolff et al., 2017) were all represented within GC during freshet by CDOM-Q with more limited representation from

SpC-Q. The changing dynamic between CDOM/DOC and discharge patterns during freshet has not been previously reported and suggests complex interplay between catchment processes related to both sources and transport during this key period. For summer and fall, log-log slopes were more constrained and showed a general mobilization pattern, although flows and concentrations were lower.

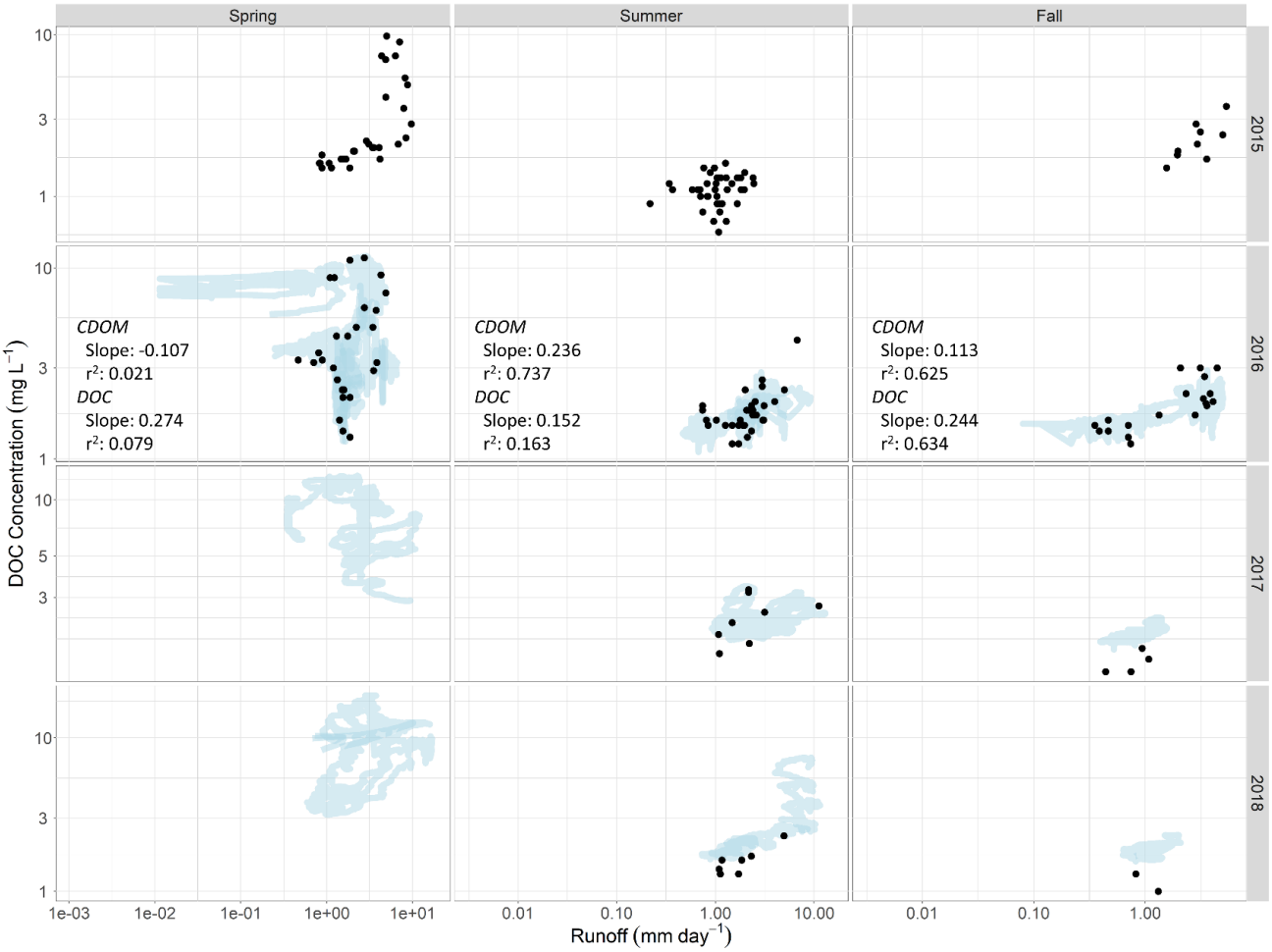

Figure 3-7. Concentration-runoff (C-Q) plots for Granger Creek in 2015 through 2018 for spring, summer and fall seasons. Continuous CDOM record is shown using light blue and grab samples of DOC are indicated with filled-in, black circles. The within-plot text indicates the log-log slope and associated r-squared for CDOM-runoff and DOC-runoff.

The effect of increased sampling frequency on load estimates has been explored in previous research (Johnson et al., 1969; Harmel et al., 2009; Yanai et al., 2014; Chappell, Jones and Tych, 2017) and was assessed for GC by applying the methodology used in Chapter 2 based on the RiverLoad software (Nava et al., 2019). For 2016, the load calculated for the entire study period using DOC grab samples was 26% or 0.20 g C m-2 higher than loads calculated from DOC-inferred CDOM. Seasonally, CDOM-based load calculations were 0.30 g C m^{-2}, 0.16 g C m^{-2} and 0.11 g C m^{-2} for spring, summer and fall, respectively. Relative to Chapter 2 (Shatilla and Carey, 2019) the CDOM based load was 3% greater in the spring and 44% less in the summer and fall. This discrepancy between estimates from grab samples and calculated DOC load from CDOM highlights how resolution loss due to infrequent sampling can influence loading estimates to the downstream environment. This has important implications for assessing carbon balances in northern catchments.

3.4.2.2 Event-scale analyses

High-resolution measurements enable a more holistic assessment of integrated catchment behaviour by sampling many (if not all) storm-response events over a sampling period of interest. Here, using the approach of Lloyd et al., (2016a, b) we evaluated the fine-scale controls on CDOM and SpC and by extension the behaviour of DOM and major ions. Event loops were assessed and excluded from analysis if normalized event metrics did not accurately summarize the C-Q hysteresis as summarized in Section 3.2.5. Normalized SpC event slopes were predominantly negative indicating dilution; however, slope reversals did occur. These reversals were not clearly linked to antecedent conditions.

Rather, for both SpC-Q (and CDOM-Q), reversals in slope (from positive to negative or vice versa) were observed when events had a secondary peak or occurred within 24 hours of a previous event, similar to observations of days between discharge peaks indicating enhanced mobilization (negative to positive) or source limitation (positive to negative) (Feinson et al., 2016).

As with the annual SpC-Q and C-Q for weathering ions that exhibited dilution behaviour, event-scale responses exhibited clockwise behaviour (positive HI) with higher concentrations on the rising limb of the hydrograph and a negative flushing index, indicating dilution during input events (Figure 3-8). SpC-Q hysteresis was relatively consistent among conditions and years, with only two events in 2017 having anticlockwise hysteresis. In contrast, anticlockwise (negative) loops dominated the CDOM-Q events, with a generally positive flushing index, with CDOM peak following peak event discharge (Figure 3-9). However, there was much greater variability within and among years, and 2018 had a large number of events with CDOM dilution signatures (negative FI). These CDOM dilution events occurred primarily in the late spring and early fall. Unlike SpC-Q, during individual storm events there was most often a mobilization CDOM signature superimposed on the longer-term dilution signature.

Presumably there are distinct and complementary mechanisms driving annual, seasonal, and event responses for SpC and DOC (as CDOM). While larger scale patterns can be explained by existing conceptual models, event-scale responses provide information on catchment connectivity and runoff processes. Using the HydRun toolbox (Tang and Carey, 2017), we compared dozens of precipitation, flow, and hysteresis metrics (Table 3-

S1) in a correlation matrix to evaluate possible factors that control loop behaviour in an exploratory framework (Table 3-S3). We hypothesized that a number of distinct and seasonal-dependent factors controlled the dominant source and transport processes driving SpC-Q and CDOM-Q.

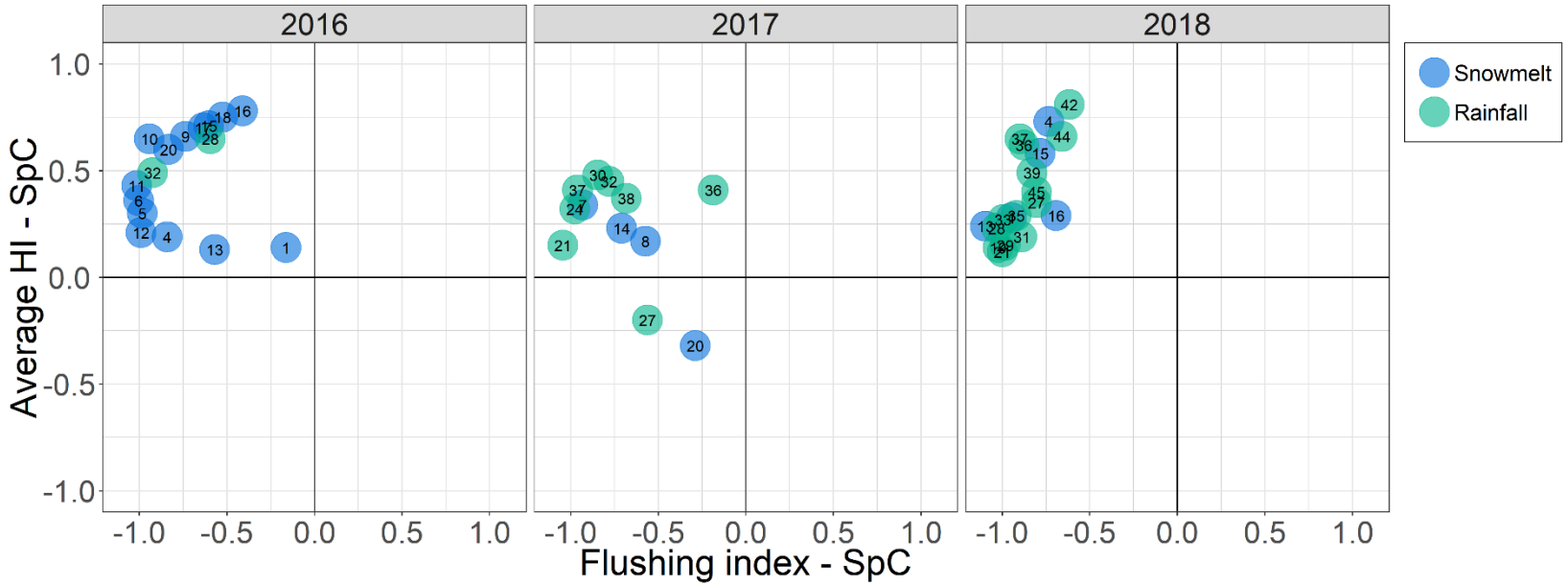

Figure 3-8. Quadrant plots of flushing index (x-axis) and hysteresis index (y-axis) for 2016, 2017 and 2018 for individual events captures from high-frequency specific conductivity (SpC) record.

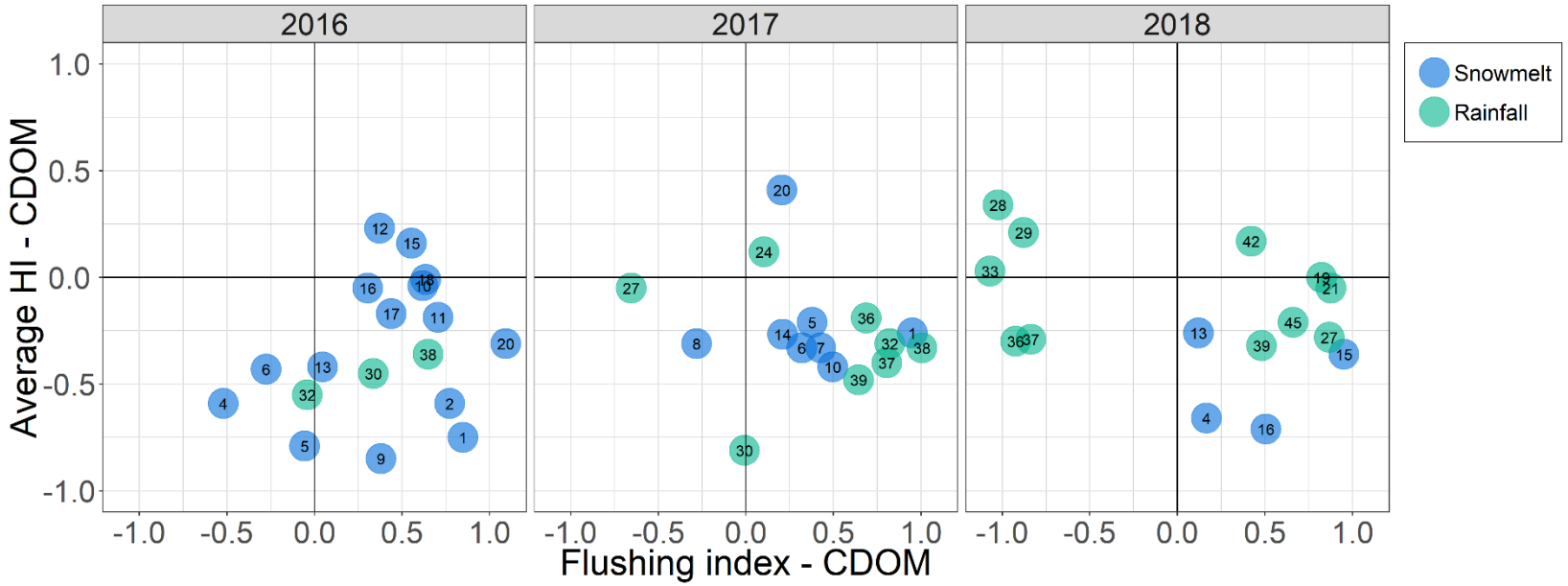

Figure 3-9. Quadrant plots of flushing index (x-axis) and hysteresis index (y-axis) for 2016, 2017 and 2018 for individual events captures from high-frequency chromophoric dissolved organic matter (CDOM) record.

SpC-Q and CDOM HI and FI for individual events were typically opposite to one another, indicating the source and transport processes between these two constituents are distinct. SpC-Q loops were explained well through existing conceptual models of permafrost runoff processes. As flow pathways became deeper as the season progressed, salinity increased, as did hysteresis and loop area, whereas the flushing index became less negative (the slope between Q and SpC declined). The increase in hysteresis can be explained by mixing of progressively more saline groundwater with less dilute precipitation and potential near-surface or riparian waters, although the overall decline in runoff ratios suggests less total water is mixing. The predominance of "old" water previously stored in the catchment and large mixing volumes through the utilization of stable isotopes has been previously reported for Granger Basin (Boucher and Care, 2010; Piovano et al., 2019).

CDOM-Q patterns were driven by a series of more variable, complex interactions that control catchment connectivity, water table position, and DOM production. Some seasonal influence was accounted for through weak but significant positive correlations with antecedent 10- and 21-day air temperature and loop area, HI average, and negative correlation between slope and 1-10 day antecedent air temperature. This effect is assumed to be a combination of seasonal characteristics and increased air temperature linked with increased production of DOM and in-stream processing. Time series observations showed increasing CDOM during events, reflected by strong positive correlations with total event rainfall. CDOM concentrations during events did not always have strong positive correlations with the previous 1-10 days of rainfall during drier periods, suggesting that the event rainfall could sometimes overcome priming effects or that rainfall accumulated over a longer period had an effect (Ali et al., 2015). The time required for transport along flowpaths is important as shown by the strong positive correlation between increased event CDOM concentrations and 21-day antecedent rainfall. With regards to FI, there was a negative correlation between antecedent rainfall and slope, indicating that mobilization was greatest for events during wetter periods. 3.4.3 Integration of high-resolution data into a conceptual model

The conceptual models of flow, dissolved ion, and DOC transport discussed above were developed without the utilization of high-frequency data, which provides additional insight, particularly at shorter time scales. For CDOM-Q, anticlockwise loops dominated the event hysteresis, yet followed a general clockwise loop on a seasonal basis. Anticlockwise loops occurring in spring were associated with the system being “primed”

with abundant organic carbon accumulated over winter, which coincided the flushing of both proximal sources (i.e. riparian zone) and up-slope organic soils, primarily through the near-surface due to a shallow frost table.

During spring, in-stream DOC was comprised of organic material from the previous year collected from near-stream as well as more distant, upslope areas (Chapter 2 (Shatilla and Carey, 2019)). Contributions of snowmelt water on top of mostly frozen soils connected distant, typically disconnected areas to the stream during this time. The diel variation in streamflow and solutes is exaggerated during the freshet period and confounds the event response signal (Figure S3-3). In summer and fall, anticlockwise hysteresis occurred on an event basis as periods of high rainfall and wetter antecedent conditions facilitated hydrologically-mediated transport pathways. Clockwise CDOM-Q loops (i.e., higher DOC concentration on the rising slope) occurred much less frequently and occurred primarily in late spring and fall (Figure 3-9). Clockwise loops suggest the importance of near-stream riparian contributions (Laudon et al., 2011). The interplay between anticlockwise and clockwise hysteresis during the latter part of the snowmelt period may be attributed to the depletion of the previous year's accumulated organic carbon source. Previous research at GC showed that depleted freshness and fluorescence indices coincided with peak DOC in response to freshet (Shatilla & Carey, 2019). During summer and fall, active layer thickening presumably led to a disconnect between DOC sources and the stream (Striegl et al., 2006; Petrone et al., 2006).

Thus, as most areas of the catchment showed decreased soil moisture and low water tables, the riparian zone maintained near-surface water tables and was responsible for the

DOC dynamics in the stream and newly produced organic material (Chapter 2 (Shatilla and Carey, 2019)). High-frequency salinity and discharge data largely support our understanding of flow pathways. In GC, the soil profile and the water and frost table positions control the rate, timing, and magnitude of runoff. High-frequency data suggests that there is considerable complexity in runoff responses, yet the well-documented seasonal shift in runoff pathways from near-surface organic layers to deeper groundwater-driven flow is observed at temporalities exceeding the event scale.

3.4.4 Implications for Change

Changes in water chemistry in large arctic rivers have almost been exclusively attributed to thawing permafrost and shifting flow pathways, with much less emphasis on alternate explanations such as changes in precipitation, vegetation, and other biogeochemical processes. While this research occurs in only one well-studied headwater catchment, multi-year, high-frequency data suggests that different processes drive the response of weathering solutes and dissolved organic matter. SpC patterns in GC reflect the seasonal interplay of near-surface and deeper groundwater pathways in a relatively predictable matter. It is presumed that as frozen ground declines, deeper flow pathways will increase their influence, resulting in greater dissolved loads and shifts in flow regimes. However, CDOM and DOC show a much more complex response that links both production and transport mechanisms.

Historical and recent studies have shown that the initial pulse of DOC at the landscape-scale is largely mobilized during freshet when seasonal frost is widespread under

current conditions (Carey, Boucher and Duarte, 2013). We suggest that a large freshet DOC pulse will still occur in a warmer and wetter environment with less permafrost, but the magnitude of this pulse may be controlled by a combination of precipitation and temperature across multiple seasons prior to spring (Tiwari, Sponseller, and Laudon, 2019). Summer DOM in this headwater stream is likely controlled by the riparian zone and near-surface saturated areas with more limited permafrost; perhaps that change will be limited. However, as shown in Chapter 2 (Shatilla and Carey, 2019), there has been an apparent decline in DOC since the mid-2000s at GC, which cannot be explained. Wet falls and a secondary seasonal flush were used to explain this decline, yet the lack of freshet sampling in 2017 and 2018 was not able to confirm this hypothesis following dry years. Regardless, more attention should be paid to in-stream biogeochemical transformations as well as other late-season conditions and processes as drivers for change as stated in Shogren et al. (2019). In addition, more information on spatial variability and the mobilization of DOM in pore water to the stream is necessary (Vonk et al., 2019).

3.5 CONCLUSIONS

New insights into runoff production and associated chemical transport were obtained through the use of high-frequency data at a well-studied subarctic alpine catchment. On annual and seasonal time scales, conductivity and CDOM were largely controlled by the predominant runoff pathways that shift throughout the year in response to wetness and ground thermal status. At event scales, high-frequency data suggests that conductivity from dissolved solutes becomes diluted, whereas organic material is

mobilized. There is considerable complexity in these responses, which are controlled by a host of interrelated factors that defy simple explanation. High-frequency data has provided considerable information that suggests greater complexity in sources and pathways of water and chemicals that are not captured by traditional sampling methods.

Estimates of chemical loading and their dilution and mobilization patterns are all poorly represented by traditional sampling methods. While this multi-year study is limited in its spatial representation, it is important to highlight that there are different hydrological processes that drive the response of dissolved solutes and organic matter. The snowmelt period is still a dominant driver of intra-annual hydrochemical patterns, but important information on catchment processes have also been revealed in the summer and fall seasons. The inclusion of snowmelt-driven events was constrained due to the superposition of diel variability atop event signals. A better understanding of this phenomenon, which was predominant during the snowmelt period at the headwater site, and its underlying drivers will help with CQ analysis during this important period. Recent literature has focussed almost exclusively on permafrost thaw as a means to explain hydrochemical changes in large watersheds, but results here suggest that there are alternate mechanisms that may act to partially explain chemical response.

References

Abbott, B. W., Gruau, G., Zarnetske, J. P., Moatar, F., Barbe, L., Thomas, Z., Fovet O, Kolbe T, Gu S, Pierson-Wickmann AC, & Davy, P. (2018). Unexpected spatial stability of water chemistry in headwater stream networks. Ecology letters, 21(2), 296-308.

Ågren, A., Buffam, I., Bishop, K., & Laudon, H. (2010). Modeling stream dissolved organic carbon concentrations during spring flood in the boreal forest: A simple empirical approach for regional predictions. Journal of Geophysical Research: Biogeosciences, 115(G1).

Alexander, R. B., Boyer, E. W., Smith, R. A., Schwarz, G. E., and Moore, R. B.(2007). The role of headwater streams in downstream water quality. J. Am.Water Res. Assoc.43, 41–59. doi: 10.1111/j.1752-1688.2007.00005.x

Ali, G., Tetzlaff, D., McDonnell, J.J., Soulsby, C., Carey, S., Laudon, H., McGuire, K., Buttle, J., Seibert, J. and Shanley, J., 2015. Comparison of threshold hydrologic response across northern catchments. Hydrological Processes, 29(16), pp.3575-3591.

Bende-Michl, U., Verburg, K., & Cresswell, H. P. (2013). High-frequency nutrient monitoring to infer seasonal patterns in catchment source availability, mobilisation and delivery. Environmental monitoring and assessment, 185(11), 9191-9219.

Bieroza, M. Z., Heathwaite, A. L., Mullinger, N. J., & Keenan, P. O. (2014). Understanding nutrient biogeochemistry in agricultural catchments: the challenge of appropriate monitoring frequencies. Environmental Science: Processes & Impacts, 16(7), 1676-1691.

Bieroza, M. Z., & Heathwaite, A. L. (2015). Seasonal variation in phosphorus concentration–discharge hysteresis inferred from high-frequency in situ monitoring. *Journal of Hydrology 524*: 333-347.

Bishop, K., Seibert, J., Köhler, S., & Laudon, H. (2004). Resolving the double paradox of rapidly mobilized old water with highly variable responses in runoff chemistry. Hydrological processes 18(1): 185-189.

Bishop, K., Buffam, I., Erlandsson, M., Fölster, J., Laudon, H., Seibert, J., & Temnerud, J. (2008). Aqua Incognita: the unknown headwaters. Hydrological Processes: An International Journal, 22(8), 1239-1242.

Bol, R., Gruau, G., Mellander, P. E., Dupas, R., Bechmann, M., Skarbøvik, E.,et al. (2018). Challenges of reducing phosphorus based water eutrophication in the agricultural landscapes of northwest Europe.Front. Mar. Sci.5:276.doi: 10.3389/fmars.2018.00276

Bonfils, C. J. W., Phillips, T. J., Lawrence, D. M., Cameron-Smith, P., Riley, W. J., & Subin, Z. M. (2012). On the influence of shrub height and expansion on northern high latitude climate. Environmental Research Letters, 7(1), 015503.

Boucher, J. L., & Carey, S. K. (2010). Exploring runoff processes using chemical, isotopic and hydrometric data in a discontinuous permafrost catchment. Hydrology Research, 41(6), 508-519.

Burd, K., Tank, S. E., Dion, N., Quinton, W. L., Spence, C., Tanentzap, A. J., & Olefeldt, D. (2018). Seasonal shifts in export of DOC and nutrients from burned and unburned peatland-rich catchments, Northwest Territories, Canada. Hydrology & Earth System Sciences, 22(8).

Burns, D. A., Pellerin, B. A., Miller, M. P., Capel, P. D., Tesoriero, A. J., & Duncan, J. M. (2019). Monitoring the riverine pulse: Applying high-frequency nitrate data to advance integrative understanding of biogeochemical and hydrological processes. Wiley Interdisciplinary Reviews: Water, 6(4), e1348.

Carey, S. K., & Woo, M. K. (2001). Slope runoff processes and flow generation in a subarctic, subalpine catchment. Journal of Hydrology 253 (1-4): 110-129.

Carey, S. K. (2003). Dissolved organic carbon fluxes in a discontinuous permafrost subarctic alpine catchment. Permafrost and Periglacial Processes 14 (2): 161-171.

Carey, S. K., & Quinton, W. L. (2004). Evaluating snowmelt runoff generation in a discontinuous permafrost catchment using stable isotope, hydrochemical and hydrometric data. *Hydrology Research*, *35*(4-5), 309-324.

Carey, S. K., Tetzlaff, D., Seibert, J., Soulsby, C., Buttle, J., Laudon, H., McDonnell, J.J., McGuire, K., Caissie, D., Shanley, J., Kennedy, M., Devito, K., & Pomeroy, J.W. (2010). Inter-comparison of hydro-climatic regimes across northern catchments: Synchronicity, resistance and resilience. Hydrological Processes 24(24): 3591-3602.

Carey, S. K., Boucher, J. L., & Duarte, C. M. (2013a). Inferring groundwater contributions and pathways to streamflow during snowmelt over multiple years in a discontinuous permafrost subarctic environment (Yukon, Canada). *Hydrogeology Journal*, *21*(1), 67-77.

Chappell, N. A., Jones, T. D., & Tych, W. (2017). Sampling frequency for water quality variables in streams: systems analysis to quantify minimum monitoring rates. Water research, 123, 49-57.

Creed, I. F., Mcknight, D. M., Pellerin, B. A., Green, M. B., Bergamaschi, B. A.,Aiken, G. R., et al. (2015). The river as a chemostat: fresh perspectives on dissolved organic matter flowing down the river continuum. Can. J. Fish. Aquat.Sci.72, 1272–1285. doi: 10.1139/cjfas-2014-0400.

DeBeer, C. M., Wheater, H. S., Carey, S. K., & Chun, K. P. (2016). Recent climatic, cryospheric, and hydrological changes over the interior of western Canada: a review and synthesis. Hydrology and Earth System Sciences, 20(4), 1573.

Dore, M. H. (2005). Climate change and changes in global precipitation patterns: what do we know?. Environment international, 31(8), 1167-1181.

Duan, L., Man, X., Kurylyk, B. L., & Cai, T. (2017). Increasing winter baseflow in response to permafrost thaw and precipitation regime shifts in Northeastern China. *Water*, *9*(1), 25.

Dupas, R., Musolff, A., Jawitz, J. W., Rao, P. S. C., Jaeger, C. G., Fleckenstein,J. H., et al. (2017). Carbon and nutrient export regimes from headwater catchments to downstream reaches. Biogeosciences14, 4391–4407.doi: 10.5194/bg-14-4391-2017.

Evans, C., & Davies, T. D. (1998). Causes of concentration/discharge hysteresis and its potential as a tool for analysis of episode hydrochemistry. Water Resources Research, 34(1), 129-137.

Feinson, L. S., Gibs, J., Imbrigiotta, T. E., & Garrett, J. D. (2016). Effects of land use and sample location on nitrate-stream flow hysteresis descriptors during storm events. JAWRA Journal of the American Water Resources Association, 52(6), 1493-1508.

Finlay, J., Neff, J., Zimov, S., Davydova, A., & Davydov, S. (2006). Snowmelt dominance of dissolved organic carbon in high-latitude watersheds: Implications for characterization and flux of river DOC. Geophysical Research Letters, 33(10).

Fovet, O., Humbert, G., Dupas, R., Gascuel-Odoux, C., Gruau, G., Jaffrézic, A., Thelusmaa, G., Faucheuxa, M., Gillieta, N., Hamona, Y. & Grimaldi, C. (2018). Seasonal variability of stream water quality response to storm events captured using high-frequency and multi-parameter data. Journal of Hydrology, 559, 282-293.

Godsey, S. E., Kirchner, J. W., & Clow, D. W. (2009). Concentration–discharge relationships reflect chemostatic characteristics of US catchments. Hydrological Processes: An International Journal, 23(13), 1844-1864.

Grosse, G., Goetz, S., McGuire, A. D., Romanovsky, V. E., & Schuur, E. A. (2016). Changing permafrost in a warming world and feedbacks to the Earth system. Environmental Research Letters, 11(4), 040201.

Halliday, S. J., Skeffington, R. A., Wade, A. J., Neal, C., Reynolds, B., Norris, D., and Kirchner, J. W.: Upland streamwater nitrate dynamics across decadal to sub-daily timescales: a case study of Plynlimon, Wales, Biogeosciences, 10, 8013–8038, https://doi.org/10.5194/bg-10-8013-2013, 2013.

Harmel, R. D., Smith, D. R., King, K. W., & Slade, R. M. (2009). Estimating storm discharge and water quality data uncertainty: A software tool for monitoring and modeling applications. Environmental Modelling & Software, 24(7), 832-842.

Hirsch, R. M. (2014). Large biases in regression-based constituent flux estimates: Causes and diagnostic tools. JAWRA Journal of the American Water Resources Association, 50(6), 1401-1424.

Johnson NM, Likens GE, Bormann FH, Fisher DW, Pierce RS. 1969. A working model for the variation in stream water chemistry at the Hubbard Brook Experimental Forest, New Hampshire.Water Re-sources Research5: 1353–1363. DOI: 10.1029/WR005i006p01353.

Kämäri, M., Tattari, S., Lotsari, E., Koskiaho, J., & Lloyd, C. E. M. (2018). High-frequency monitoring reveals seasonal and event-scale water quality variation in a temporally frozen river. Journal of Hydrology, 564, 619-639.

Kirchner, J. W., Feng, X., Neal, C., & Robson, A. J. (2004). The fine structure of water-quality dynamics: the (high-frequency) wave of the future. *Hydrological processes*, *18*(7), 1353-1359.

Knapp, J. L., Freyberg, J. V., Studer, B., Kiewiet, L., & Kirchner, J. W. (2020). Concentration-discharge relationships vary among hydrological events, reflecting differences in event characteristics. Hydrology and Earth System Sciences Discussions, 1-27.

Koch, J. C., Runkel, R. L., Striegl, R., & McKnight, D. M. (2013a). Hydrologic controls on the transport and cycling of carbon and nitrogen in a boreal catchment underlain by continuous permafrost. *Journal of Geophysical Research: Biogeosciences*, *118*(2), 698-712.

Koch, J. C., Ewing, S. A., Striegl, R., & McKnight, D. M. (2013b). Rapid runoff via shallow throughflow and deeper preferential flow in a boreal catchment underlain by frozen silt (Alaska, USA). *Hydrogeology Journal*, *21*(1), 93-106.

Koch, J. C., Kikuchi, C. P., Wickland, K. P., & Schuster, P. (2014). Runoff sources and flow paths in a partially burned, upland boreal catchment underlain by permafrost. *Water Resources Research*, *50*(10), 8141-8158.

Kokelj, S. V., Lacelle, D., Lantz, T. C., Tunnicliffe, J., Malone, L., Clark, I. D., & Chin, K. S. (2013). Thawing of massive ground ice in mega slumps drives increases in stream sediment and solute flux across a range of watershed scales. Journal of Geophysical Research: Earth Surface, 118(2), 681-692.

Lamontagne-Hallé, P., McKenzie, J. M., Kurylyk, B. L., & Zipper, S. C. (2018). Changing groundwater discharge dynamics in permafrost regions. *Environmental Research Letters*, *13*(8), 084017.

Laudon, H., Spence, C., Buttle, J., Carey, S.K., McDonnell, J.J., McNamara, J.P., Soulsby, C. and Tetzlaff, D., 2017. Save northern high-latitude catchments. Nature Geoscience, 10(5), pp.324-325.

Li, W., Liu, H., Zhai, L., Yen, H., Hu, W., Lei, Q., Stewart, R.J., Guo, S. & Ren, T. (2019). Evaluation of concentration-discharge dynamics and nitrogen export on anthropogenic inputs and stormflow across alternative time-scales. Ecological indicators, 98, 879-887.

Littlefair, C. A., Tank, S. E., & Kokelj, S. V. (2017). Retrogressive thaw slumps temper dissolved organic carbon delivery to streams of the Peel Plateau, NWT, Canada. Biogeosciences, 14(23), 5487-5505.

Li Yung Lung, J.Y.S., Tank, S.E., Spence, C., Yang, D., Bonsal, B., McClelland, J.W., & Holmes, R. (2018). Seasonal and Geographic Variation in Dissolved Organic Biogeochemistry of Rivers Draining to the Arctic Ocean and Hudson Bay, J. Geophys. Res. Biogeosci., 123 (10), 3371-3386.

Lloyd, C. E. M., Freer, J. E., Johnes, P. J., Coxon, G., & Collins, A. L. (2015). Discharge and nutrient uncertainty: implications for nutrient flux estimation in small streams. Hydrological Processes, 30(1), 135-152.

Lloyd, C. E. M., Freer, J. E., Johnes, P. J., & Collins, A. L. (2016a). Using hysteresis analysis of high-resolution water quality monitoring data, including uncertainty, to infer controls on nutrient and sediment transfer in catchments. Science of the Total Environment, 543, 388-404.

Lloyd, C. E. M., Freer, J. E., Johnes, P. J., & Collins, A. L. (2016b). Testing an improved index for analysing storm nutrient hysteresis. Hydrology and Earth System Sciences Discussions, 12(8), 7875-7892.

Lung, J. Y. L. Y., Tank, S. E., Spence, C., Yang, D., Bonsal, B., McClelland, J. W., & Holmes, R. M. (2018). Seasonal and geographic variation in dissolved carbon biogeochemistry of rivers draining to the Canadian Arctic Ocean and Hudson Bay. Journal of Geophysical Research: Biogeosciences, 123(10), 33

Malone, L., D. Lacelle, S. V. Kokelj, and I. D. Clark (2013), Impacts of hillslope thaw slumps on the geochemistry of permafrost catchments (Stony Creek watershed, NWT, Canada), Chem. Geol., 356, 38–49.

McCartney, S. E., Carey, S. K., & Pomeroy, J. W. (2006). Intra-basin variability of snowmelt water balance calculations in a subarctic catchment. Hydrological Processes: An International Journal 20 (4): 1001-1016.

Musolff, A., Schmidt, C., Selle, B., & Fleckenstein, J. H. (2015). Catchment controls on solute export. Advances in Water Resources, 86, 133-146.

Nava, V., Patelli, M., Rotiroti, M., & Leoni, B. (2019). An R package for estimating river compound load using different methods. Environ. Model. Softw., 117: 108. doi: 10.1016/j.envsoft.2019.03.012.

Nimick, D. A., Gammons, C. H., & Parker, S. R. (2011). Diel biogeochemical processes and their effect on the aqueous chemistry of streams: A review. Chemical Geology, 283(1-2), 3-17.

Nossov, D. R., Jorgenson, M. T., Kielland, K., & Kanevskiy, M. Z. (2013). Edaphic and microclimatic controls over permafrost response to fire in interior Alaska. *Environmental Research Letters*, *8*(3), 035013.

Quinton, W. L., Carey, S. K., & Goeller, N. T. (2004). Snowmelt runoff from northern alpine tundra hillslopes: major processes and methods of simulation. Geography and Environmental Studies Faculty Publications, 20. https://scholars.wlu.ca/geog_faculty/20

Quinton, W. L., Shirazi, T., Carey, S. K., & Pomeroy, J. W. (2005). Soil water storage and active-layer development in a sub-alpine tundra hillslope, southern Yukon Territory, Canada. *Permafrost and Periglacial Processes*, *16*(4), 369-382.

Rasouli, K., Pomeroy, J. W., Janowicz, J. R., Williams, T. J., & Carey, S. K. (2019). A long-term hydrometeorological dataset (1993–2014) of a northern mountain basin: Wolf Creek Research Basin, Yukon Territory, Canada. Earth System Science Data 11(1): 89-100.

Serreze, M. C., Walsh, J. E., Chapin, F. S., Osterkamp, T., Dyurgerov, M., Romanovsky, V., Oechel, C., Morison, J., Zhang, T. & Barry, R. G. (2000). Observational evidence of recent change in the northern high-latitude environment. Climatic change, 46(1-2), 159-207.

Shatilla, N. J., & Carey, S. K. (2019). Assessing inter-annual and seasonal patterns of DOC and DOM quality across a complex alpine watershed underlain by discontinuous permafrost in Yukon, Canada. Hydrology & Earth System Sciences 23 (9).

Sherson, L. R., Van Horn, D. J., Gomez-Velez, J. D., Crossey, L. J., & Dahm, C. N. (2015). Nutrient dynamics in an alpine headwater stream: use of continuous water quality sensors to examine responses to wildfire and precipitation events. Hydrological Processes, 29(14), 3193-3207.

Shogren, A. J., Zarnetske, J. P., Abbott, B. W., Iannucci, F., Frei, R. J., Griffin, N. A., & Bowden, W. B. (2019). Revealing biogeochemical signatures of Arctic landscapes with river chemistry. *Scientific reports*, *9*(1), 1-11.

Spencer, R. G., Mann, P. J., Dittmar, T., Eglinton, T. I., McIntyre, C., Holmes, R. M., Zimov, N. & Stubbins, A. (2015). Detecting the signature of permafrost thaw in Arctic rivers. Geophysical Research Letters, 42(8), 2830-2835.

Tank ,S.E., Fellman, J.B., Hood, E. and Kritzberg, E.S. (2018). Beyond Respiration: controls on lateral carbon fluxes across the terrestrial-aquatic interface. Limnology and Oceanography Letters 3, 76–88.

Temnerud, J., von Brömssen, C., Fölster, J., Buffam, I., Anders-son, J.-O., Nyberg, L., and Bishop, K. (2016). Map-based prediction of organic carbon in headwater streams improved by downstream observations from the river outlet. Biogeosciences, 13, 399–413. doi:10.5194/bg-13-399-2016

Toohey, R. C., Herman-Mercer, N. M., Schuster, P. F., Mutter, E. A., & Koch, J. C. (2016). Multidecadal increases in the Yukon River Basin of chemical fluxes as indicators of changing flowpaths, groundwater, and permafrost. Geophysical Research Letters, 43(23), 12-120.

Vaughan, M.C., Bowden, W.B., Shanley, J.B., Vermilyea, A., Sleeper, R., Gold, A.J., Pradhanang, S.M., Inamdar, S.P., Levia, D.F., Andres, A.S. and Birgand, F. (2017). High-frequency dissolved organic carbon and nitrate measurements reveal differences in storm hysteresis and loading in relation to land cover and seasonality. Water Resources Research, 53(7), 5345-5363.

Vonk, J.E., Tank, S.E., Bowden, W.B., Laurion, I., Vincent, W.F., Alekseychik, P., Amyot, M., Billet, M.F., Canario, J., Cory, R.M., & Deshpande, B.N. (2015). Reviews and syntheses: Effects of permafrost thaw on Arctic aquatic ecosystems. Biogeosciences, 12(23), 7129-7167.

Walvoord, M. A., & Striegl, R. G. (2007). Increased groundwater to stream discharge from permafrost thawing in the Yukon River basin: Potential impacts on lateral export of carbon and nitrogen. Geophysical Research Letters 34(12).

Wollheim, W. M., Bernal, S., Burns, D. A., Czuba, J. A., Driscoll, C.T., Hansen, A. T., et al. (2018). River network saturation concept: Factors influencing the balance of biogeochemical supply and demand of river networks. Biogeochemistry. 141:503. doi: 10.1007/s10533-018-0488-0

Yanai, R. D., Tokuchi, N., Campbell, J. L., Green, M. B., Matsuzaki, E., Laseter, S. N., Brown, C.L., Bailey, A.S., Lyons, P., Levine, C.R., Buso, D.C., Likens, G.E., Knoepp, J.D. & Fukushima, K. (2015). Sources of uncertainty in estimating stream solute export from headwater catchments at three sites. Hydrological processes, 29(7), 1793-1805.

Supplemental Information

							CDOM														SpC											
			Event Identifiers				Concentrations				HI					FI	Loop area				Concentration				HI					FI	Loop area			
Year	Season	Main Water Input	Start_Time	Peak_Time	End_Time	ID	Initial	Mean	Max	Min	HI25	HI50	HI75	HI90	HI_avg		Typical	Incl. Dir	Direction	Rep. Geometry	Initial	Mean	Max	Min	HI25	HI50	HI75	HI90	HI_avg		Typical	Incl. Dir	Direction	Rep. Geometry
2016	Spring	Snowmelt	09-May 14:45	09-May 22:45	10-May 08:45	1	2500.8	2788.0	2933.2	2488.4	-0.81	-0.81	-0.62	-0.29	-0.75	0.66	-0.66	acw	maybe	74.7	64.4	73.8	20.8	0.23	0.13	0.07	0.03	0.14	-0.16			cw	yes
2016	Spring	Snowmelt	10-May 09:15	10-May 22:15	11-May 09:30	2	2812.4	3008.4	3266.4	2675.6	-0.70	-0.67	-0.41	-0.32	-0.59	0.77			acw	maybe	15.5	51.2	67.9	12.9									cw	no
2016	Spring	Snowmelt	12-May 12:00	12-May 20:00	13-May 08:45	4	3154.4	3090.1	3419.6	2161.2	-0.31	-0.77	-0.69	-0.33	-0.59	-0.52	0.45	-0.45	acw	yes	44.8	39.0	45.5	34.8	0.24	0.20	0.13	0.10	0.19	-0.84	0.22	0.22	cw	yes
2016	Spring	Snowmelt	13-May 13:00	13-May 20:30	14-May 09:45	5	2706.4	2974.7	3370.0	2473.6	-0.63	-0.87	-0.86	-0.62	-0.79	-0.06	0.65	-0.65	acw	yes	43.1	33.3	43.1	31.0	0.66	0.20	0.05	0.08	0.30	-0.98	0.31	0.31	cw	yes
2016	Spring	Snowmelt	14-May 12:15	14-May 19:45	15-May 10:00	6	2338.4	2552.9	3013.2	2090.8	-0.26	-0.51	-0.52	-0.24	-0.43	-0.28	0.35	-0.35	acw	yes	36.6	30.5	36.6	26.8	0.48	0.36	0.25	0.12	0.36	-1.00	0.32	0.32	cw	yes
2016	Spring	Snowmelt	18-May 15:45	18-May 20:30	19-May 09:15	9	1375.2	1560.4	1712.4	1296.8	-0.98	-0.87	-0.69	-0.30	-0.85	0.38	0.75	-0.75	acw	yes	62.8	58.1	62.8	55.0	0.82	0.72	0.45	0.19	0.66	-0.74	0.56	0.56	cw	yes
2016	Spring	Snowmelt	19-May 16:15		20-May 12:45	10	1405.2	1474.2	1650.0	1184.8	-0.02	-0.14	0.03	0.13	-0.04	0.62	0.10	-0.10	acw	yes	65.9	53.9	65.9	48.3	0.77	0.73	0.45	0.21	0.65	-0.94	0.56	0.56	cw	yes
2016	Spring	Snowmelt	20-May 16:00	20-May 22:30	21-May 10:00	11	1228.8	1421.8	1597.2	1172.8	0.01	-0.35	-0.22	-0.06	-0.19	0.71	0.17	-0.17	acw	yes	59.6	47.9	59.6	42.6	0.60	0.40	0.28	0.10	0.43	-1.02	0.38	0.38	cw	yes
2016	Spring	Snowmelt	21-May 15:00	22-May 01:00	22-May 11:15	12	1201.2	1216.1	1353.2	846.8									cw	no	44.7	26.6	44.7	22.4	0.31	0.21	0.11	0.02	0.21	-0.99	0.20	0.20	cw	maybe
2016	Spring	Snowmelt	22-May 11:15	22-May 22:45	23-May 12:45	13	1176	1199.1	1795.6	739.2	-0.45	-0.31	-0.49	-0.15	-0.42	0.05	0.40	-0.40	acw	yes	28.1	25.6	35.3	20.6	0.12	0.15	0.13	0.06	0.13	-0.57	0.11	0.11	cw	yes
2016	Spring	Snowmelt	28-May 16:15	29-May 01:45	29-May 12:30	15	992.8	1113.4	1254.0	765.2	0.41	0.03	0.03	-0.06	0.16	0.55	0.17	0.17	cw	yes	66.1	60.5	67.2	54.1	0.84	0.80	0.48	0.17	0.71	-0.60	0.62	0.62	cw	yes
2016	Spring	Snowmelt	30-May 17:00	30-May 23:45	31-May 10:15	16	886	979.2	1064.4	397.9	-0.06	-0.07	-0.03	-0.07	-0.05	0.30	0.06	-0.06	acw	yes	70.0	61.9	70.1	55.0	0.87	0.85	0.62	0.33	0.78	-0.41	0.70	0.70	cw	yes
2016	Spring	Snowmelt	31-May 18:00	31-May 22:45	01-Jun 11:30	17	885.2	915.4	1000.8	447.2	-0.15	-0.17	-0.20	-0.17	-0.17	0.44	0.17	-0.17	acw	yes	69.9	56.2	69.9	50.7	0.86	0.72	0.51	0.21	0.70	-0.64	0.60	0.60	cw	yes
2016	Spring	Snowmelt	01-Jun 14:30	01-Jun 23:15	02-Jun 13:00	18	551.2	814.8	953.6	261.6	0.16	-0.09	-0.10	0.06	-0.01	0.64	0.13	-0.13	acw	yes	63.5	57.1	64.8	50.8	0.74	0.85	0.66	0.22	0.75	-0.52	0.61	0.61	cw	yes
2016	Spring	Snowmelt	04-Jun 15:30	04-Jun 23:30	05-Jun 13:30	20	528.6	568.2	752.4	227.6	-0.27	-0.45	-0.21	-0.01	-0.31	1.09	0.27	-0.27	acw	yes	63.9	54.0	63.8	48.8	0.73	0.58	0.49	0.14	0.60	-0.83	0.54	0.54	cw	yes
2016	Summer	Rainfall	19-Jun 16:15	19-Jun 23:15	20-Jun 13:00	28													acw	yes	41.7	49.3	55.5	45.9	0.76	0.75	0.43	0.09	0.65	-0.59	0.55	0.55	cw	yes
2016	Summer	Rainfall	27-Jun 17:45	28-Jun 05:00	28-Jun 15:30	29	445.36	447.1	535.0	84.6	0.49	0.06	0.01	0.00	0.19		0.19	0.19	cw	maybe													cw	
2016	Summer	Rainfall	30-Jun 02:15	30-Jun 20:45	01-Jul 14:15	30	478.64	573.8	730.0	170.5	-0.73	-0.73	0.11	0.01	-0.45	0.34	0.47		acw	yes													cw	
2016	Summer	Rainfall	09-Jul 13:30	09-Jul 18:30	10-Jul 16:30	32	672.4	771.8	1063.6	428.0	-0.67	-0.64	-0.34	-0.17	-0.55	-0.04	0.56	-0.56	acw	yes	56.9	41.3	58.8	25.5	0.50	0.61	0.36	0.17	0.49	-0.92	0.44	0.44	cw	yes
2016	Fall	Rainfall	09-Sep 04:30	10-Sep 05:30	10-Sep 17:15	38	476.4				-0.38	-0.55	-0.24	-0.03	-0.38	0.65	0.31	-0.31	acw	yes	52.2	52.8	55.3	50.8									cw	complex
2017	Spring	Snowmelt	16-May 14:30	17-May 04:30	17-May 12:00	1	3024.8	3464.3	3752.8	3023.6	-0.46	-0.21	-0.12	-0.06	-0.26	0.95	0.27	-0.27	acw	yes	63.1	55.4	63.1	52.7						-0.85			acw	yes
2017	Spring	Snowmelt	21-May 13:15	23-May 04:00	23-May 13:30	5	3188.8	3369.1	3541.2	3139.2	-0.28	-0.49	0.13	0.42	-0.21	0.38	0.33	-0.33	acw	complex	46.4	34.6	46.4	31.4						-0.89			acw	no
2017	Spring	Snowmelt	23-May 13:15	23-May 23:00	24-May 08:00	6	3232.8	3223.7	3277.6	3124.0	-0.40	-0.40	-0.19	-0.14	-0.33	0.32	0.26	-0.26	acw	yes	33.9	33.8	34.5	33.5									acw	no
2017	Spring	Snowmelt	24-May 13:30	24-May 20:30	25-May 11:15	7	2977.2	3042.0	3124.0	2918.4	-0.32	-0.33	-0.34	-0.11	-0.33	0.43			acw	yes	34.7	31.6	34.7	29.9	0.39	0.42	0.21	0.09	0.34	-0.93	0.31	0.31	cw	yes
2017	Spring	Snowmelt	25-May 10:00	25-May 21:15	27-May 00:15	8	2979.2	2802.9	2979.2	2611.6	-0.28	-0.36	-0.30	-0.02	-0.31	-0.28	0.22	-0.22	acw	yes	31.9	30.0	35.5	26.7	0.16	0.20	0.14	0.02	0.17	-0.57	0.13	0.13	cw	yes
2017	Spring	Snowmelt	27-May 13:30	27-May 23:30	28-May 07:30	10	2278.8	2287.1	2332.4	2225.6	-0.47	-0.43	-0.37	-0.04	-0.42	0.50	0.31	-0.31	acw	yes	40.1	42.0	44.6	40.1									acw	yes
2017	Spring	Snowmelt	28-May 13:15	29-May 02:00	29-May 10:30	12	2083.6	2229.3	2384.4	2051.2	-0.27	-0.10	-0.11	-0.01	-0.16	0.93	0.14	-0.14	acw	yes	45.5	37.7	45.5	32.7										no
2017	Spring	Snowmelt	29-May 11:15	29-May 23:15	30-May 10:30	13	2189.4	2142.9	2238.0	1937.6	-0.08	-0.09	-0.05	0.03	-0.07	0.25	0.07	-0.07	acw	yes	34.3	35.4	38.2	33.9									acw	no
2017	Spring	Snowmelt	30-May 11:30	30-May 22:30	31-May 11:30	14	1896.8	1924.7	2034.4	1776.0	0.02	-0.08	-0.43	-0.33	-0.27	0.21	0.20	-0.20	acw	yes	38.8	37.0	39.8	34.0	0.21	0.30	0.17	0.16	0.23	-0.71	0.18	0.18	cw	yes
2017	Spring	Snowmelt	05-Jun 13:00	05-Jun 21:45	06-Jun 07:45	20	1679.2	1651.1	1708.0	1539.4	0.38	0.48	0.36	0.11	0.41	0.21	0.34	0.34	cw	yes	43.5	44.2	47.6	42.3	-0.44	-0.39	-0.12	0.01	-0.32	-0.29	0.31	-0.31	acw	yes
2017	Spring	Rainfall	06-Jun 18:00	08-Jun 15:45	11-Jun 09:15	21	1421.6	935.3	1421.6	649.0									cw	no	38.7	24.8	38.7	14.9	0.23	0.16	0.05	0.03	0.15	-1.05	0.14	0.14	cw	complex
2017	Summer	Rainfall	17-Jun 17:00	17-Jun 21:30	18-Jun 12:45	24	1102	1069.0	1129.2	922.6	0.13	0.10	0.12	0.08	0.12	0.10	0.13	0.13	cw	yes	51.6	47.9	51.6	45.0	0.43	0.35	0.19	0.09	0.32	-0.98	0.30	0.30	cw	yes
2017	Summer	Rainfall	18-Jun 11:15	18-Jun 17:00	19-Jun 12:00	25	948.8	883.3	948.8	844.8									cw	no	49.9	44.3	50.0	36.8	0.10	0.23	0.38	0.29	0.24	-0.93	0.21	0.21	cw	yes
2017	Summer	Rainfall	19-Jun 12:15	19-Jun 22:30	20-Jun 14:15	27	843.2	812.2	848.8	787.2	0.56	-0.27	-0.44	-0.14	-0.05	-0.66	0.41	-0.41	acw	yes	50.0	49.2	53.2	45.8	-0.14	-0.19	-0.28	-0.06	-0.20	-0.56	0.20	-0.20	acw	yes
2017	Summer	Rainfall	26-Jun 15:15	26-Jun 20:00	27-Jun 18:15	30	653.6	729.7	784.0	600.4	-0.67	-0.82	-0.94	-0.68	-0.81	-0.01	0.66	-0.66	acw	yes	60.0	48.4	60.1	35.1	0.38	0.57	0.50	0.33	0.48	-0.85	0.42	0.42	cw	yes
2017	Summer	Rainfall	07-Jul 17:00	08-Jul 09:00	09-Jul 01:30	32	520	583.8	622.8	516.4	-0.59	-0.19	-0.14	-0.11	-0.31	0.82	0.31	-0.31	acw	yes	58.9	52.5	60.1	43.2	0.65	0.40	0.29	0.22	0.45	-0.78	0.42	0.42	cw	yes
2017	Summer	Rainfall	10-Jul 08:30	11-Jul 07:15	13-Jul 15:00	34	596.8	883.5	1216.8	568.4	-0.48	-0.48	-0.26	-0.11	-0.41	0.89	0.33	-0.33	acw	composite	56.0	43.6	56.0	34.0	0.27	0.36	0.42	0.18	0.35	-0.76	0.30	0.30	cw	composite
2017	Summer	Rainfall	13-Jul 14:00	13-Jul 22:00	14-Jul 09:15	36	650.4	679.3	722.0	638.0	-0.17	-0.16	-0.23	-0.17	-0.19	0.69	0.14	-0.14	acw	yes	46.8	47.0	48.3	44.7	0.01	0.50	0.73	0.45	0.41	-0.19	0.41	0.41	cw	maybe
2017	Summer	Rainfall	15-Jul 11:15	15-Jul 20:45	17-Jul 12:45	37	599	906.9	1036.8	588.4	-0.53	-0.44	-0.24	-0.11	-0.40	0.80	0.38	-0.38	acw	yes	50.3	41.7	50.4	34.0	0.57	0.35	0.30	0.20	0.41	-0.96	0.35	0.35	cw	yes
2017	Summer	Rainfall	17-Jul 17:30	17-Jul 23:45	19-Jul 10:30	38	836.8	969.3	1104.4	836.8	-0.42	-0.45	-0.13	-0.01	-0.33	1.01	0.29	-0.29	acw	yes	46.9	45.6	49.1	40.8	0.22	0.42	0.48	0.18	0.37	-0.68	0.29	0.29	cw	yes
2017	Fall	Rainfall	22-Aug 18:30	23-Aug 02:15	24-Aug 15:15	39	608.8				-0.37	-0.60	-0.48	-0.47	-0.48	0.64	0.46	-0.46	acw	complex	76.3	75.6	77.2	74.2						-0.12			acw	complex
2017	Fall	Rainfall	27-Sep 04:15	28-Sep 07:45	28-Sep 19:45	42	526.4				-0.14	-0.18	0.01	0.15		0.50			acw	complex	82.1	79.7	82.2	75.4						-0.51				complex
2018	Spring	Snowmelt	09-May 07:45	09-May 17:30	10-May 08:45	1		3279.1	3711.6	3049.6									acw	no	87.7	68.5	88.6	55.8	0.48	0.24	0.12	0.01	0.28	-0.95	0.26	0.26	cw	yes
2018	Spring	Snowmelt	10-May 08:45	10-May 15:30	11-May 03:45	4	3176	3625.6	4337.6	2481.2	-0.69	-0.72	-0.57	-0.13	-0.66	0.17	0.55	-0.55	acw	yes	69.0	60.4	69.2	55.1	0.88	0.85	0.47	0.08	0.73	-0.73	0.64	0.64	cw	yes
2018	Spring	Snowmelt	17-May 19:00	19-May 19:15	21-May 08:30	13	3555.2	3657.5	4044.4	3222.4	-0.37	-0.24	-0.16	-0.08	-0.26	0.12	0.19	-0.19	acw	yes	44.7	34.5	44.7	27.1	0.42	0.19	0.10	0.04	0.24	-1.10	0.21	0.21	cw	complex
2018	Spring	Snowmelt	04-Jun 14:45	04-Jun 23:30	05-Jun 12:15	15	1614	1722.5	1808.0	1609.6	-0.42	-0.42	-0.24	-0.07	-0.36	0.95	0.31	-0.31	acw	yes	52.9	46.1	53.0	41.8	0.61	0.67	0.45	0.30	0.58	-0.78	0.53	0.53	cw	yes
2018	Spring	Snowmelt	05-Jun 13:00	05-Jun 21:00	06-Jun 07:30	16	1623.6	1671.8	1747.6	1590.0	-0.69	-0.74	-0.69	-0.29	-0.71	0.51	0.55	-0.55	acw	yes	46.3	44.6	47.6	42.0	0.21	0.29	0.37	0.17	0.29	-0.69	0.22	0.22	cw	yes
2018	Spring	Rainfall	09-Jun 10:30	10-Jun 17:15	12-Jun 19:30	21	1258.4	2331.3	3222.0	1202.0	-0.16	-0.05	0.06	0.06	-0.05	0.88	0.08	-0.08	acw	complex	58.9	37.5	58.9	24.1	0.18	0.12	0.05	0.02	0.12	-1.00	0.15	0.15	cw	maybe
2018	Spring	Rainfall	09-Jun 22:30	10-Jun 17:15	11-Jun 23:30	19	2173.2	2706.1	3222.0	2173.2	-0.22	-0.05	0.26	0.06	0.00	0.82	0.14	-0.14	acw	complex	47.5	32.2	47.5	24.1	0.23	0.12	0.07	0.01	0.14	-1.02	0.14	0.14	cw	yes
2018	Spring	Rainfall	13-Jun 22:30	14-Jun 18:45	15-Jun 10:15	27	1537.2	2075.5	2568.0	1535.6					-0.28	0.87	0.29	-0.29	acw	yes	46.4	37.8	46.5	32.5	0.35	0.37	0.33	0.18	0.35	-0.80	0.31	0.31	cw	yes
2018	Summer	Rainfall	15-Jun 10:15	15-Jun 20:15	16-Jun 07:45	28	2217.2	1926.3	2218.0	1695.6	0.46	0.31	0.25	0.03	0.34	-1.02	0.33	0.33	cw	maybe	37.4	31.2	37.7	26.5	0.29	0.21	0.18	0.01	0.23	-1.03	0.21	0.21	cw	yes
2018	Summer	Rainfall	16-Jun 07:45	16-Jun 20:15	17-Jun 14:00	29	1822.8	1499.7	1828.0	1266.0	0.25	0.23	0.14	0.03	0.21	-0.88	0.23	0.23	cw	maybe	33.6	28.4	33.7	22.4	0.14	0.16	0.14	0.04	0.15	-0.98	0.13	0.13	cw	yes
2018	Summer	Rainfall	19-Jun 08:30	19-Jun 18:45	20-Jun 08:45	31		954.0	998.8	908.8									cw	no	34.4	31.7	42.0	27.5	0.29	0.19	0.08	0.03	0.19	-0.89	0.17	0.17	cw	yes
2018	Summer	Rainfall	20-Jun 12:45	20-Jun 18:30	21-Jun 04:30	33	908.8	877.4	913.2	837.2	0.13	0.06	-0.10	-0.10	0.03	-1.07	0.10	0.10	cw	maybe	36.2	33.9	37.4	31.4	0.27	0.34	0.19	0.03	0.27	-1.00	0.21	0.21	cw	yes
2018	Summer	Rainfall	21-Jun 12:30	21-Jun 18:45	22-Jun 05:45	35	874	831.5	874.0	799.2	0.09	0.07	-0.09	-0.01	0.02	-1.28	0.07	0.07	cw	maybe	39.7	37.6	40.4	35.1	0.35	0.36	0.16	0.13	0.29	-0.92	0.24	0.24	cw	yes
2018	Summer	Rainfall	29-Jun 10:15	29-Jun 20:15	30-Jun 12:45	37	710	699.5	730.0	597.6	-0.39	-0.28	-0.19	-0.15	-0.29	-0.84	0.27		acw	yes	57.7	53.8	57.8	47.2	0.50	0.75	0.69	0.34	0.65	-0.90	0.51	0.51	cw	yes
2018	Summer	Rainfall	18-Jul 03:00	18-Jul 17:30	20-Jul 04:00	39	558.4	646.2	719.2	555.2	-0.49	-0.13	-0.33	-0.37	-0.32	0.48	0.31	-0.31	acw	yes	65.1	59.1	65.4	45.1	0.31	0.65	0.52	0.33	0.49	-0.83	0.40	0.40	cw	yes
2018	Summer	Rainfall	08-Aug 14:00	08-Aug 23:45	09-Aug 14:15	42	563.4	677.0	762.8	563.4	-0.03	0.29	0.26	0.16	0.17	0.42	0.23	0.23	cw	yes	70.2	65.5	71.6	59.7	0.58	0.87	0.99	0.71	0.81	-0.62	0.69	0.69	cw	yes
2018	Summer	Rainfall	09-Aug 14:15	10-Aug 03:45	10-Aug 16:45	44	680.4	710.0	762.4	650.4									cw	maybe	66.0	63.7	68.1	60.1	0.78	0.66	0.55	0.35	0.66	-0.66	0.59	0.59	cw	yes
2018	Fall	Rainfall	27-Aug 20:00	28-Aug 19:45	30-Aug 04:30	45	482	602.3	817.2	475.6	-0.44	-0.38	0.20	0.30	-0.21	0.66	0.31	-0.31	acw	yes	71.9	70.6	73.1	65.4	0.06	0.25	0.88	0.96	0.40	-0.80	0.36	0.36	cw	yes

				HydRun Output					Discharge					Air Temperature					Precipitation (Rainfall)						Soil Moisture															
														Antedecent Period							Antedecent Period				Plateau (high) Station						Mid-slope (mid) Station						Riparian (low) Station				
Year	Season	Main Water Input	ID	T_LP	T_LC	T_c	Runoff Ratio	Event start	Event end	ΔQ	Event Peak	Volume	HBP	1 d	4 d	10 d	21 d	Event total	Cumulative	1 d	4 d	10 d	21 d	5 cm depth, 1 d	5 cm depth, 4 d	5 cm depth, 10 d	15 cm depth, 1 d	15 cm depth, 4 d	15 cm depth, 10 d	5 cm depth, 1 d	5 cm depth, 4 d	5 cm depth, 10 d	15 cm depth, 1 d	15 cm depth, 4 d	15 cm depth, 10 d	5 cm depth, 1 d	5 cm depth, 4 d	15 cm depth, 1 d	15 cm depth, 4 d	15 cm depth, 10 d
2016	Spring	Snowmelt	1	3.25	5.84	15.25	0.40	0.001	0.010	0.064	0.065	0.386		4.9	2.3	1.1	1.0	0.8	9.3	0.0	1.9	2.2	4.6	0.485	0.489	0.489	0.279	0.193	0.161	0.363	0.336	0.288	0.160	0.150	0.135	0.322	0.339	0.220	0.214	0.204
2016	Spring	Snowmelt	2	14.25	14.66	23.50	0.49	0.016	0.068	0.114	0.130	1.014	23.50	2.8	2.6	1.4	1.1	1.4	11.4	2.0	3.9	4.2	6.6	0.483	0.487	0.489	0.393	0.245	0.183	0.377	0.349	0.301	0.161	0.154	0.138	0.288	0.324	0.223	0.217	0.207
2016	Spring	Snowmelt	4					0.167	0.182	0.172	0.339	2.432	45.75	8.2	5.0	2.5	1.6		11.5	0.0	2.2	4.1	6.8	0.466	0.481	0.489	0.451	0.400	0.251	0.447	0.399	0.342	0.173	0.165	0.149	0.239	0.277	0.232	0.226	0.214
2016	Spring	Snowmelt	5					0.207	0.234	0.178	0.385	3.126	24.50	10.2	6.4	3.4	2.1		11.5	0.0	2.2	4.1	6.3	0.413	0.463	0.480	0.427	0.440	0.281	0.440	0.419	0.360	0.179	0.170	0.155	0.225	0.251	0.238	0.230	0.218
2016	Spring	Snowmelt	6					0.247	0.216	0.181	0.428	3.500	23.25	12.4	8.9	4.6	2.6		11.5	0.0	0.0	4.1	6.3	0.383	0.438	0.469	0.419	0.441	0.308	0.431	0.432	0.374	0.184	0.176	0.160	0.217	0.235	0.244	0.235	0.223
2016	Spring	Snowmelt	9					0.056	0.041	0.049	0.105	0.647	96.75	3.6	6.7	7.1	3.6		11.6	0.0	0.1	2.3	4.5	0.346	0.355	0.412	0.398	0.405	0.410	0.423	0.427	0.418	0.215	0.202	0.184	0.191	0.200	0.422	0.354	0.280
2016	Spring	Snowmelt	10	9.00	8.58	19.75	0.35	0.050	0.065	0.123	0.173	1.144		6.3	5.4	7.2	4.0	2.1	13.7	0.6	0.7	2.8	5.1	0.339	0.348	0.398	0.392	0.400	0.420	0.420	0.424	0.424	0.225	0.211	0.190	0.186	0.194	0.442	0.399	0.303
2016	Spring	Snowmelt	11					0.099	0.093	0.114	0.213	1.365		8.2	5.4	7.9	4.4		13.7	1.6	2.2	2.2	6.6	0.337	0.343	0.383	0.389	0.396	0.416	0.419	0.422	0.428	0.235	0.220	0.198	0.180	0.188	0.450	0.426	0.325
2016	Spring	Snowmelt	12					0.228	0.284	0.206	0.434	3.464	26.50	8.9	6.7	8.2	4.9		13.7	0.0	2.1	2.2	6.6	0.334	0.339	0.368	0.386	0.391	0.408	0.418	0.420	0.428	0.246	0.230	0.205	0.181	0.185	0.448	0.440	0.346
2016	Spring	Snowmelt	13	7.75	6.71	18.75	1.33	0.284	0.253	0.295	0.579	4.863	21.75	12.4	8.6	8.5	5.4	1.3	13.7	0.0	2.1	2.2	6.6	0.331	0.336	0.357	0.382	0.388	0.402	0.417	0.419	0.425	0.254	0.239	0.212	0.187	0.184	0.447	0.446	0.365
2016	Spring	Snowmelt	15			23.50	0.45	0.117	0.139	0.080	0.197	1.545	147.00	3.7	3.7	6.5	6.6	0.8	34.4	1.7	14.2	22.8	27.0	0.328	0.331	0.333	0.378	0.381	0.383	0.417	0.420	0.420	0.377	0.346	0.290	0.205	0.215	0.448	0.463	0.454
2016	Spring	Snowmelt	16	15.25	12.02	15.75	0.08	0.133	0.139	0.077	0.210	1.434	46.00	2.4	3.4	5.7	6.6	5.4	39.6	5.2	7.0	25.9	29.7	0.324	0.327	0.330	0.370	0.376	0.380	0.409	0.415	0.418	0.452	0.400	0.330	0.198	0.205	0.439	0.448	0.453
2016	Spring	Snowmelt	17					0.127	0.148	0.101	0.228	1.604	23.00	4.7	3.8	5.1	6.7		39.8	0.1	7.1	26.1	28.3	0.323	0.325	0.329	0.369	0.373	0.378	0.407	0.411	0.417	0.585	0.457	0.365	0.202	0.202	0.441	0.443	0.452
2016	Spring	Snowmelt	18	11.50	10.98	21.00	0.76	0.136	0.133	0.089	0.225	1.989	24.50	6.0	4.2	4.7	6.7	0.7	40.2	0.4	5.8	26.5	28.7	0.321	0.324	0.328	0.367	0.370	0.377	0.404	0.409	0.416	0.598	0.504	0.394	0.198	0.200	0.438	0.441	0.452
2016	Spring	Snowmelt	20					0.142	0.136	0.086	0.228	1.941	72.25	6.4	5.9	4.5	6.0		40.6	0.1	0.8	10.2	29.1	0.313	0.317	0.323	0.357	0.362	0.370	0.393	0.399	0.408	0.576	0.587	0.485	0.191	0.195	0.431	0.434	0.445
2016	Summer	Rainfall	28					0.256	0.265	0.068	0.324	2.939	359.75	13.8	12.5	9.9	7.6		81.3	0.0	4.0	40.7	46.9	0.302	0.304	0.302	0.344	0.345	0.339	0.341	0.347	0.346	0.510	0.523	0.510	0.209	0.208	0.436	0.441	0.436
2016	Summer	Rainfall	29					0.170	0.170	0.064	0.234	2.068	197.75	9.5	9.8	10.4	9.4		81.6	0.0	0.0	0.7	41.0	0.288	0.291	0.298	0.324	0.329	0.337	0.295	0.313	0.330	0.422	0.438	0.477	0.192	0.195	0.421	0.424	0.430
2016	Summer	Rainfall	30	17.25	10.24	19.25	0.17	0.182	0.222	0.323	0.505	5.502	63.75	11.4	10.0	9.9	10.0	12.4	83.4	1.8	1.8	2.1	42.8	0.279	0.285	0.292	0.311	0.319	0.330	0.245	0.277	0.310	0.402	0.414	0.452	0.193	0.193	0.411	0.417	0.424
2016	Summer	Rainfall	32	10.00	-2.91	4.50	0.48	0.173	0.250	0.634	0.807	4.619	213.75	11.8	10.7	9.5	9.9	4.1	100.8	1.8	2.3	19.2	19.5	0.291	0.280	0.287	0.319	0.310	0.320	0.205	0.196	0.236	0.383	0.384	0.395	0.216	0.205	0.423	0.416	0.421
2016	Fall	Rainfall	38					0.241	0.281	0.123	0.364	5.380	1499.00	4.6	5.3	4.6	6.7		194.0	0.0	0.0	0.0	0.0	0.272	0.275	0.282	0.304	0.309	0.318	0.141	0.137	0.111	0.366	0.367	0.368	0.227	0.228	0.436	0.436	0.440
2017	Spring	Snowmelt	1					0.042	0.060	0.063	0.104	0.705	5975.00	5.1	3.1	2.5	1.1		9.4	0.3	5.8	7.4	8.5	0.449	0.493	0.462	0.446	0.374	0.225	0.233	0.225	0.138	0.136	0.127	0.101	0.483	0.353	0.192	0.188	0.181
2017	Spring	Snowmelt	5	-0.25	10.17	38.00	9.19	0.106	0.203	0.228	0.334	6.048	143.50	2.0	3.1	3.5	1.9	0.2	10.7	1.3	1.3	8.6	9.8	0.352	0.363	0.433	0.402	0.408	0.367	0.244	0.242	0.230	0.163	0.155	0.138	0.213	0.271	0.209	0.202	0.194
2017	Spring	Snowmelt	6	5.00	4.00	12.50	0.67	0.203	0.182	0.066	0.269	2.141	19.00	3.7	3.1	3.6	2.4	0.5	10.9	0.0	1.5	1.8	10.0	0.340	0.349	0.400	0.390	0.398	0.416	0.248	0.245	0.238	0.175	0.166	0.149	0.192	0.209	0.218	0.211	0.200
2017	Spring	Snowmelt	7					0.206	0.255	0.174	0.380	2.947	21.50	6.3	4.1	4.0	2.7		11.4	0.5	2.0	2.3	9.9	0.335	0.343	0.383	0.384	0.393	0.415	0.247	0.247	0.241	0.182	0.172	0.155	0.196	0.201	0.226	0.217	0.204
2017	Spring	Snowmelt	8					0.218	0.245	0.279	0.497	5.887	24.75	6.1	5.0	4.3	3.0		11.4	0.0	0.7	2.3	9.9	0.331	0.338	0.368	0.378	0.388	0.407	0.249	0.248	0.243	0.192	0.179	0.161	0.207	0.199	0.254	0.227	0.210
2017	Spring	Snowmelt	10					0.133	0.123	0.047	0.179	1.379	50.25	3.1	4.8	3.9	3.4		11.4	0.0	0.5	2.0	9.4	0.324	0.329	0.345	0.368	0.376	0.392	0.247	0.248	0.246	0.240	0.207	0.179	0.197	0.202	0.444	0.329	0.256
2017	Spring	Snowmelt	12					0.119	0.194	0.187	0.306	2.195	26.50	7.0	5.0	4.2	3.6		11.4	0.0	0.0	2.0	9.4	0.321	0.326	0.340	0.365	0.371	0.387	0.243	0.247	0.246	0.265	0.228	0.191	0.186	0.200	0.474	0.391	0.283
2017	Spring	Snowmelt	13					0.200	0.142	0.066	0.266	2.358	21.25	10.3	6.0	4.8	4.0		11.4	0.0	0.0	2.0	9.4	0.318	0.323	0.335	0.362	0.367	0.383	0.241	0.245	0.246	0.307	0.255	0.205	0.177	0.193	0.471	0.439	0.308
2017	Spring	Snowmelt	14					0.145	0.147	0.117	0.262	2.256	23.25	6.9	6.7	5.3	4.3		11.4	0.0	0.0	2.0	9.4	0.317	0.320	0.331	0.359	0.364	0.378	0.243	0.244	0.246	0.316	0.281	0.221	0.175	0.184	0.469	0.463	0.335
2017	Spring	Snowmelt	20					0.168	0.150	0.070	0.238	1.817	143.25	5.1	5.0	6.1	5.2		42.0	0.0	23.8	30.6	32.9	0.310	0.317	0.318	0.352	0.359	0.360	0.256	0.260	0.250	0.481	0.457	0.371	0.216	0.221	0.477	0.503	0.482
2017	Spring	Rainfall	21	-46.00	-19.56	38.25	3.19	0.303	0.241	0.839	1.141	27.237	66.00	6.0	5.1	6.3	5.2	1.8	42.0	0.0	12.1	30.6	32.6	0.307	0.313	0.316	0.346	0.355	0.358	0.251	0.257	0.251	0.474	0.470	0.399	0.208	0.222	0.467	0.489	0.484
2017	Summer	Rainfall	24					0.113	0.117	0.093	0.206	1.516	221.75	3.3	3.4	8.2	7.4		62.4	0.2	16.4	20.4	51.0	0.299	0.295	0.293	0.341	0.331	0.329	0.261	0.254	0.251	0.508	0.478	0.474	0.198	0.192	0.451	0.446	0.450
2017	Summer	Rainfall	25					0.108	0.115	0.157	0.266	2.117	19.50	7.2	4.3	7.6	7.5		62.4	0.0	15.2	20.4	51.0	0.293	0.295	0.292	0.332	0.333	0.329	0.255	0.255	0.251	0.484	0.483	0.475	0.193	0.193	0.444	0.447	0.449
2017	Summer	Rainfall	27	9.00	11.14	23.75	0.88	0.108	0.113	0.077	0.185	1.854	29.50	11.1	6.1	6.9	7.5	0.6	62.4	0.0	15.1	20.4	51.0	0.287	0.295	0.291	0.323	0.333	0.328	0.249	0.256	0.251	0.467	0.487	0.474	0.190	0.194	0.439	0.446	0.447
2017	Summer	Rainfall	30	5.00	7.55	21.75	0.39	0.095	0.152	0.444	0.538	3.308	165.50	10.0	7.8	7.2	8.0	3.3	65.7	0.1	2.7	3.5	23.7	0.275	0.277	0.283	0.309	0.311	0.319	0.245	0.245	0.249	0.447	0.447	0.461	0.159	0.175	0.432	0.432	0.437
2017	Summer	Rainfall	32	14.50	7.48	18.00	0.09	0.130	0.197	0.246	0.376	3.558	277.00	12.5	9.9	8.4	7.9	10.3	75.2	0.0	5.2	7.4	14.2	0.267	0.273	0.275	0.299	0.305	0.308	0.223	0.236	0.242	0.398	0.415	0.430	0.167	0.166	0.427	0.428	0.429
2017	Summer	Rainfall	34	-8.25	-43.83	-2.50	0.44	0.176	0.258	0.472	0.648	13.851	70.25	6.0	9.5	8.4	8.0	5.8	89.9	4.4	14.7	22.0	28.7	0.280	0.276	0.276	0.316	0.309	0.308	0.247	0.237	0.240	0.392	0.397	0.417	0.187	0.179	0.435	0.432	0.429
2017	Summer	Rainfall	36	8.00	8.33	15.75	0.05	0.248	0.262	0.128	0.376	2.823	62.75	10.5	6.0	8.0	7.9	5.5	101.4	0.0	12.4	31.4	39.6	0.284	0.288	0.281	0.323	0.326	0.315	0.236	0.249	0.242	0.387	0.392	0.403	0.188	0.193	0.436	0.441	0.434
2017	Summer	Rainfall	37	9.25	10.09	9.25	0.18	0.258	0.322	0.615	0.873	11.289	46.75	9.1	8.3	8.5	8.0	9.8	113.1	6.2	12.0	37.9	50.7	0.284	0.287	0.282	0.322	0.326	0.317	0.243	0.244	0.242	0.387	0.389	0.395	0.191	0.192	0.437	0.440	0.436
2017	Summer	Rainfall	38	9.25	14.47	37.00	0.20	0.310	0.310	0.385	0.695	8.268	51.00	10.8	9.4	7.9	8.2	5.2	124.5	1.9	17.6	49.3	57.7	0.286	0.288	0.287	0.328	0.327	0.324	0.245	0.250	0.248	0.386	0.388	0.391	0.195	0.195	0.439	0.440	0.439
2017	Fall	Rainfall	39	29.00	12.32	44.75	0.06	0.082	0.082	0.055	0.137	2.345	866.50	8.3	6.8	6.5	10.4	13.9	146.6	1.7	7.3	9.8	14.0	0.144	0.141	0.143	0.166	0.163	0.166	0.033	0.033	0.032	0.369	0.369	0.370	0.166	0.162	0.403	0.401	0.396
2017	Fall	Rainfall	42	28.50	15.59	39.50	0.22	0.061	0.070	0.071	0.133	1.748	869.50	1.7	5.9	4.3	4.2	3.6	184.4	11.4	11.4	15.3	22.5	0.195	0.196	0.190	0.212	0.212	0.207	0.041	0.042	0.040	0.342	0.342	0.344	0.177	0.177	0.413	0.413	0.412
2018	Spring	Snowmelt	1					0.035	0.274	1.363	1.398	5.552	5361.75	7.2	5.0	2.3	0.4		0.8	0.0	0.2	0.3	0.4	0.122	0.112	0.084	0.127	0.119	0.100	0.211	0.192	0.135	0.112	0.085	0.067	0.345	0.319	0.203	0.197	0.188
2018	Spring	Snowmelt	4					0.274	0.255	0.201	0.474	3.090	22.00	10.6	6.6	3.4	1.0		0.8	0.0	0.2	0.3	0.4	0.134	0.122	0.092	0.131	0.125	0.105	0.225	0.205	0.157	0.120	0.101	0.074	0.378	0.339	0.208	0.201	0.191
2018	Spring	Snowmelt	13			21.00	44.96	0.200	0.194	0.514	0.714	12.121	219.75	7.8	4.5	5.5	3.2	0.1	0.8	0.0	0.0	0.0	0.3	0.369	0.399	0.351	0.427	0.440	0.323	0.236	0.237	0.230	0.173	0.161	0.139	0.334	0.367	0.251	0.239	0.223
2018	Spring	Snowmelt	15					0.111	0.125	0.097	0.207	1.658	388.25	8.3	5.6	4.2	5.0		9.6	0.0	7.2	7.5	8.8	0.305	0.306	0.309	0.366	0.367	0.372	0.255	0.255	0.253	0.435	0.406	0.352	0.213	0.212	0.460	0.460	0.464
2018	Spring	Snowmelt	16					0.127	0.126	0.075	0.202	1.416	21.50	6.8	6.0	4.6	5.2		9.9	0.3	4.9	7.8	9.1	0.304	0.306	0.308	0.366	0.367	0.370	0.254	0.256	0.253	0.462	0.426	0.370	0.210	0.213	0.457	0.461	0.462
2018	Spring	Rainfall	21	2.75	4.94	49.00	2.07	0.085	0.201	1.401	1.486	18.264	116.25	5.5	6.0	5.9	4.9	5.0	15.5	5.6	5.6	13.1	14.7	0.302	0.301	0.304	0.360	0.361	0.365	0.252	0.250	0.253	0.495	0.482	0.435	0.173	0.189	0.453	0.452	0.456
2018	Spring	Rainfall	19					0.388	0.420	1.097	1.486	14.991	116.25	4.9	5.6	5.8	4.7		29.2	12.9	18.4	25.9	27.5	0.302	0.301	0.304	0.360	0.361	0.365	0.252	0.250	0.253	0.495	0.482	0.435	0.173	0.189	0.453	0.452	0.456
2018	Spring	Rainfall	27					0.269	0.381	0.593	0.861	8.608	97.50	7.4	6.6	6.3	5.0		46.0	0.7	16.4	36.0	43.5	0.297	0.307	0.304	0.355	0.365	0.364	0.263	0.262	0.256	0.570	0.574	0.517	0.169	0.192	0.451	0.489	0.469
2018	Summer	Rainfall	28					0.381	0.422	0.486	0.867	5.852	25.50	5.9	6.7	6.1	5.2		58.8	5.2	13.9	48.9	56.7	0.311	0.303	0.305	0.368	0.361	0.364	0.266	0.264	0.258	0.601	0.580	0.539	0.198	0.182	0.511	0.476	0.475
2018	Summer	Rainfall	29					0.422	0.460	0.593	1.015	9.236	24.00	11.2	7.8	6.5	5.6		58.8	0.0	13.9	48.9	56.7	0.298	0.302	0.305	0.357	0.360	0.363	0.264	0.264	0.259	0.592	0.585	0.549	0.177	0.180	0.451	0.471	0.474
2018	Summer	Rainfall	31					0.400	0.381	0.356	0.755	6.084	70.50	14.3	12.2	8.5	7.0		58.8	0.0	0.0	43.4	56.4	0.286	0.292	0.302	0.341	0.349	0.359	0.263	0.265	0.264	0.579	0.594	0.582	0.166	0.171	0.450	0.448	0.473
2018	Summer	Rainfall	33					0.391	0.352	0.150	0.541	3.469	23.75	16.8	13.9	13.4	10.1		58.8	8.7	7.8	18.9	56.4	0.278	0.287	0.297	0.332	0.343	0.354	0.260	0.264	0.264	0.555	0.583	0.582	0.161	0.167	0.446	0.447	0.466
2018	Summer	Rainfall	35					0.346	0.314	0.115	0.461	3.224	24.25	17.7	15.5	11.2	8.3		58.8	0.0	0.0	13.9	56.4		0.284	0.295		0.340	0.352	0.257	0.261	0.263	0.536	0.566	0.578	0.160	0.164	0.444	0.447	0.458
2018	Summer	Rainfall	37					0.163	0.159	0.136	0.300	2.456	193.50	9.7	9.1	11.5	9.8		58.8	0.0	0.0	0.0	48.9			0.279			0.332	0.232	0.240	0.248	0.447	0.463	0.495	0.165	0.166	0.429	0.432	0.438
2018	Summer	Rainfall	39	19.50	10.60	32.00	0.14	0.096	0.102	0.245	0.342	3.669	453.25	8.1	7.1	8.3	9.7	9.5	76.3	0.9	3.4	7.2	17.5	0.221	0.224	0.228	0.258	0.261	0.266	0.152	0.159	0.169	0.381	0.384	0.390	0.176	0.176	0.429	0.430	0.429
2018	Summer	Rainfall	42	16.75	-5.56	-13.75	0.03	0.110	0.116	0.096	0.206	1.752	510.25	8.9	12.4	14.3	15.0	19.6	98.3	2.9	7.1	13.0	15.7	0.108	0.109	0.117	0.141	0.142	0.151	0.027	0.024	0.025	0.359	0.356	0.355	0.166	0.161	0.406	0.402	0.402
2018	Summer	Rainfall	44	21.00	7.50	6.25	0.06	0.116	0.148	0.108	0.224	2.106	28.00	7.5	10.7	13.3	14.9	9.9	104.7	7.8	15.2	21.2	21.2	0.203	0.132	0.125	0.213	0.159	0.156	0.063	0.034	0.029	0.372	0.360	0.357	0.192	0.169	0.430	0.409	0.405
2018	Fall	Rainfall	45	16.75	10.12	28.50	0.07	0.059	0.058	0.124	0.183	2.474	448.00	12.2	8.6	10.0	9.4	11.7	124.2	0.0	5.2	6.0	34.7	0.182	0.180	0.185	0.216	0.213	0.221	0.060	0.047	0.050	0.367	0.368	0.369	0.172	0.169	0.411	0.408	0.408

Table 3-S1. Events extracted from Hydrun and included in analysis.

Season		P_{24h} (mm)	$P_{4\ day}$ (mm)	P_{10d} (mm)	$Temp_{24h}$ (°C)	$Temp_{4d}$ (°C)	$Temp_{10d}$ (°C)	$SM_{rp\ 1d}$ 5cm	$SM_{rp\ 4d}$ 5cm	$SM_{rp\ 24h}$ 15cm	$SM_{rp\ 4d}$ 15cm	$SM_{mid\ 24h}$ 5cm	$SM_{mid\ 4d}$ 5cm	$SM_{mid\ 24h}$ 15 cm	SMmid-slope $_{4d}$ 15 cm
Spring	**Mean**	**1.0**	**4.5**	**9.5**	**6.5**	**5.2**	**4.9**	**0.223**	**0.232**	**0.365**	**0.354**	**0.319**	**0.315**	**0.306**	**0.283**
	Std Dev	2.5	5.9	11.0	2.7	1.6	1.8	0.070	0.056	0.113	0.115	0.086	0.086	0.157	0.148
	Min	0	0	0	2.0	2.3	1.1	0.169	0.183	0.192	0.188	0.211	0.192	0.112	0.085
	Max	12.9	23.8	36	12.4	8.9	8.5	0.483	0.367	0.477	0.503	0.447	0.432	0.598	0.587
	IQR	0.6	5.3	10.2	3.2	1.9	2.3	0.030	0.053	0.219	0.225	0.168	0.167	0.284	0.254
	n	34	34	34	34	34	34	34	34	34	34	34	34	34	34
Summer	**Mean**	**1.9**	**8.2**	**22.3**	**10.3**	**9.2**	**9.3**	**0.184**	**0.183**	**0.438**	**0.437**	**0.231**	**0.233**	**0.454**	**0.459**
	Std Dev	2.8	6.4	16.4	3.4	3.0	2.3	0.016	0.014	0.020	0.018	0.069	0.075	0.079	0.080
	Min	0	0	0	3.3	3.4	6.1	0.159	0.161	0.406	0.402	0.027	0.024	0.359	0.356
	Max	8.7	17.6	49.3	17.7	15.5	14.3	0.216	0.208	0.511	0.476	0.341	0.347	0.601	0.594
	IQR	2.7	12.1	27.5	3.4	3.4	2.3	0.026	0.023	0.015	0.018	0.028	0.026	0.123	0.124
	n	22	22	22	22	22	22	22	22	22	22	22	22	22	22
Fall	**Mean**	**3.3**	**6.0**	**7.8**	**6.7**	**6.7**	**6.3**	**0.185**	**0.184**	**0.416**	**0.415**	**0.069**	**0.065**	**0.361**	**0.362**
	Std Dev	5.5	4.7	6.4	4.6	1.4	2.6	0.028	0.030	0.014	0.015	0.050	0.048	0.013	0.012
	Min	0	0	0	1.7	5.3	5.2	0.165	0.162	0.403	0.401	0.033	0.033	0.342	0.342
	Max	11.4	11.4	15.3	12.2	8.6	10.0	0.226	0.228	0.436	0.436	0.141	0.137	0.369	0.369
	IQR	4.1	4.4	6.7	5.4	1.5	2.9	0.019	0.023	0.010	0.013	0.041	0.030	0.007	0.008
	n	4	4	4	4	4	4	4	4	4	4	4	4	4	4

Table 3-S2. Table summarizing event antecedent conditions for precipitation, air temperature, and soil moisture.

Indep.	Dep.	Cor. Coeff.	p-value	Indep.	Dep.	Cor. Coeff.	p-value	Indep.	Dep.	Cor. Coeff.	p-value	Indep.	Dep.	Cor. Coeff.	p-value
cdom_start	cdom_range	0.31	0.0228	HI50_cdom	HI_avg_cdom	0.95	0.0000	spc_start	cdom_min	-0.27	0.0457	HI50_spc	spc_mean	0.53	0.0001
cdom_start	HI_avg_spc	-0.32	0.0336	HI50_cdom	HI75_cdom	0.77	0.0000	spc_start	cdom_start	-0.47	0.0003	HI50_spc	spc_min	0.56	0.0000
cdom_start	HI50_spc	-0.31	0.0368	HI50_cdom	HI90_cdom	0.54	0.0000	spc_start	HBP	0.41	0.0022	HI50_spc	Temp_21_day	0.32	0.0262
cdom_start	HI75_spc	-0.48	0.0008	HI50_cdom	LoopArea_cdom	-0.75	0.0000	spc_start	HI_avg_spc	0.54	0.0001	HI50_spc	Tot_Q	-0.33	0.0224
cdom_start	HI90_spc	-0.49	0.0007	HI50_cdom	LoopArea_num_cdom	0.95	0.0000	spc_start	HI25_spc	0.47	0.0007	HI75_spc	cdom_max	-0.44	0.0021
cdom_start	LoopArea_spc	-0.34	0.0255	HI50_cdom	Q_start	0.29	0.0386	spc_start	HI50_spc	0.48	0.0005	HI75_spc	cdom_mean	-0.44	0.0020
cdom_start	P_accum	-0.70	0.0000	HI50_cdom	SM_L15_1_day	0.47	0.0005	spc_start	HI75_spc	0.50	0.0003	HI75_spc	cdom_min	-0.46	0.0010
cdom_start	Rain_10_day	0.70	0.0001	HI50_cdom	SM_L15_10_day	0.45	0.0008	spc_start	HI90_spc	0.43	0.0022	HI75_spc	dQ	-0.32	0.0247
cdom_start	Rain_21_day	0.56	0.0042	HI50_cdom	SM_L15_4_day	0.49	0.0002	spc_start	LoopArea_num_spc	0.60	0.0000	HI75_spc	HI_avg_spc	0.83	0.0000
cdom_start	Rain_4_day	0.44	0.0303	HI50_cdom	SM_L5_4_day	-0.35	0.0100	spc_start	LoopArea_spc	0.68	0.0000	HI75_spc	HI90_spc	0.85	0.0000
cdom_start	Runoff_Ratio	0.56	0.0291	HI50_cdom	SM_M15_1_day	0.51	0.0001	spc_start	P_accum	0.30	0.0232	HI75_spc	LoopArea_num_spc	0.81	0.0000
cdom_start	SM_H15_1_day	0.46	0.0004	HI50_cdom	SM_M15_10_day	0.42	0.0020	spc_start	Q_end	-0.45	0.0004	HI75_spc	LoopArea_spc	0.74	0.0000
cdom_start	SM_H15_4_day	0.33	0.0118	HI50_cdom	SM_M15_4_day	0.48	0.0003	spc_start	Q_start	-0.57	0.0000	HI75_spc	P_accum	0.45	0.0014
cdom_start	SM_H5_1_day	0.56	0.0000	HI50_cdom	Temp_10_day	0.37	0.0075	spc_start	Rain_10_day	-0.63	0.0009	HI75_spc	Q_end	-0.32	0.0277
cdom_start	SM_H5_10_day	0.57	0.0000	HI50_cdom	Temp_21_day	0.30	0.0298	spc_start	Rain_21_day	-0.73	0.0001	HI75_spc	Q_peak	-0.37	0.0088
cdom_start	SM_H5_4_day	0.57	0.0000	HI75_cdom	HI_avg_cdom	0.86	0.0000	spc_start	Slope_cdom	0.37	0.0081	HI75_spc	Rain_21_day	-0.51	0.0171
cdom_start	SM_L15_1_day	-0.73	0.0000	HI75_cdom	HI90_cdom	0.85	0.0000	spc_start	Slope_spc	0.32	0.0216	HI75_spc	Runoff_Ratio	-0.80	0.0019
cdom_start	SM_L15_10_day	-0.80	0.0000	HI75_cdom	LoopArea_cdom	-0.68	0.0000	spc_start	SM_H15_1_day	-0.60	0.0000	HI75_spc	SM_H15_1_day	-0.38	0.0097
cdom_start	SM_L15_4_day	-0.77	0.0000	HI75_cdom	LoopArea_num_cdom	0.83	0.0000	spc_start	SM_H15_10_day	-0.49	0.0001	HI75_spc	SM_H15_4_day	-0.34	0.0177
cdom_start	SM_L5_1_day	0.57	0.0000	HI75_cdom	SM_H5_10_day	-0.29	0.0398	spc_start	SM_H15_4_day	-0.56	0.0000	LoopArea_num_spc	dQ	-0.29	0.0482
cdom_start	SM_L5_4_day	0.70	0.0000	HI75_cdom	SM_H5_4_day	-0.29	0.0380	spc_start	SM_H5_1_day	-0.48	0.0002	LoopArea_num_spc	Q_end	-0.32	0.0260
cdom_start	SM_M15_1_day	-0.63	0.0000	HI_avg_cdom	SM_L15_4_day	0.47	0.0004	spc_start	SM_H5_10_day	-0.50	0.0001	LoopArea_num_spc	Q_peak	-0.36	0.0140
cdom_start	SM_M15_10_day	-0.71	0.0000	HI_avg_cdom	SM_L5_4_day	-0.33	0.0153	spc_start	SM_H5_4_day	-0.47	0.0002	LoopArea_num_spc	Q_start	-0.32	0.0267
cdom_start	SM_M15_4_day	-0.66	0.0000	HI_avg_cdom	SM_M15_1_day	0.51	0.0001	spc_start	SM_M5_1_day	-0.26	0.0459	LoopArea_num_spc	Rain_21_day	-0.61	0.0033
cdom_start	spc_max	-0.42	0.0012	HI_avg_cdom	SM_M15_10_day	0.43	0.0013	spc_start	SM_M5_10_day	-0.27	0.0380	LoopArea_num_spc	Runoff_Ratio	-0.79	0.0020
cdom_start	spc_mean	-0.44	0.0008	HI_avg_cdom	SM_M15_4_day	0.49	0.0002	spc_start	SM_M5_4_day	-0.27	0.0390	LoopArea_num_spc	spc_max	0.60	0.0000
cdom_start	spc_min	-0.45	0.0005	HI_avg_cdom	Temp_10_day	0.35	0.0105	spc_start	spc_max	0.88	0.0000	LoopArea_num_spc	spc_mean	0.61	0.0000
cdom_start	Temp_1_day	-0.27	0.0458	HI_avg_cdom	Temp_21_day	0.30	0.0281	spc_start	spc_mean	0.85	0.0000	LoopArea_num_spc	spc_min	0.58	0.0000
cdom_start	Temp_10_day	-0.67	0.0000	LoopArea_cdom	LoopArea_num_cdom	-0.75	0.0000	spc_start	spc_min	0.75	0.0000	LoopArea_num_spc	Tot_P	0.70	0.0114
cdom_start	Temp_21_day	-0.81	0.0000	LoopArea_cdom	SM_H15_10_day	-0.39	0.0047	spc_start	T_LP	0.43	0.0356	LoopArea_num_spc	Tot_Q	-0.33	0.0227
cdom_start	Temp_4_day	-0.50	0.0001	LoopArea_cdom	SM_L15_1_day	-0.33	0.0208	HI25_spc	HI_avg_spc	0.87	0.0000	LoopArea_spc	cdom_max	-0.30	0.0447
cdom_start	Tot_P	-0.56	0.0290	LoopArea_cdom	SM_L15_4_day	-0.33	0.0208	HI25_spc	HI50_spc	0.83	0.0000	LoopArea_spc	cdom_mean	-0.28	0.0627
cdom_max	HBP	0.31	0.0232	LoopArea_cdom	SM_M15_1_day	-0.32	0.0219	HI25_spc	HI75_spc	0.46	0.0009	LoopArea_spc	cdom_min	-0.34	0.0203
cdom_max	spc_min	-0.32	0.0190	LoopArea_cdom	SM_M15_4_day	-0.28	0.0479	HI25_spc	LoopArea_num_spc	0.88	0.0000	LoopArea_spc	dQ	-0.45	0.0016
cdom_mean	HBP	0.32	0.0212	LoopArea_num_cdom	Q_start	0.33	0.0226	HI25_spc	LoopArea_spc	0.75	0.0000	LoopArea_spc	LoopArea_num_spc	0.87	0.0000
cdom_mean	spc_min	-0.29	0.0342	LoopArea_num_cdom	Rain_21_day	0.48	0.0356	HI25_spc	SM_M5_1_day	0.29	0.0486	LoopArea_spc	Q_end	-0.49	0.0004
cdom_min	HBP	0.33	0.0146	LoopArea_num_cdom	SM_L15_1_day	0.40	0.0045	HI25_spc	spc_max	0.47	0.0007	LoopArea_spc	Q_peak	-0.54	0.0001
cdom_min	spc_min	-0.29	0.0357	LoopArea_num_cdom	SM_L15_10_day	0.42	0.0031	HI25_spc	spc_mean	0.42	0.0032	LoopArea_spc	Q_start	-0.45	0.0013
cdom_range	spc_range	0.35	0.0091	LoopArea_num_cdom	SM_L15_4_day	0.43	0.0023	HI25_spc	spc_min	0.44	0.0018	LoopArea_spc	Rain_21_day	-0.69	0.0005
HI25_cdom	HI_avg_cdom	0.89	0.0000	LoopArea_num_cdom	SM_L5_4_day	-0.30	0.0363	HI25_spc	HI_avg_spc	0.87	0.0000	LoopArea_spc	Runoff_Ratio	-0.61	0.0356
HI25_cdom	HI_avg_cdom	0.89	0.0000	LoopArea_num_cdom	SM_M15_1_day	0.47	0.0007	HI25_spc	HI50_spc	0.83	0.0000	LoopArea_spc	SM_H15_4_day	-0.29	0.0467
HI25_cdom	HI50_cdom	0.81	0.0000	LoopArea_num_cdom	SM_M15_10_day	0.42	0.0033	HI25_spc	HI75_spc	0.46	0.0009	LoopArea_spc	spc_max	0.70	0.0000
HI25_cdom	HI75_cdom	0.56	0.0000	LoopArea_num_cdom	SM_M15_4_day	0.46	0.0012	HI25_spc	LoopArea_num_spc	0.88	0.0000	LoopArea_spc	spc_mean	0.76	0.0000
HI25_cdom	HI90_cdom	0.42	0.0020	LoopArea_num_cdom	Temp_10_day	0.38	0.0082	HI25_spc	LoopArea_spc	0.75	0.0000	LoopArea_spc	spc_min	0.76	0.0000
HI25_cdom	LoopArea_cdom	-0.63	0.0000	LoopArea_num_cdom	Temp_21_day	0.30	0.0382	HI25_spc	SM_M5_1_day	0.29	0.0486	LoopArea_spc	T_c	-0.50	0.0253
HI25_cdom	LoopArea_num_cdom	0.84	0.0000	LoopArea_num_cdom	Tot_P	0.65	0.0234	HI25_spc	spc_max	0.47	0.0007	LoopArea_spc	T_LP	0.53	0.0249
HI25_cdom	LoopArea_num_spc	-0.32	0.0437					HI25_spc	spc_mean	0.42	0.0032	LoopArea_spc	T_r	-0.31	0.0316
HI25_cdom	Rain_21_day	0.50	0.0176					HI25_spc	spc_min	0.44	0.0018	LoopArea_spc	Temp_21_day	0.31	0.0324
HI25_cdom	Slope_cdom	-0.39	0.0050					HI50_spc	cdom_min	-0.33	0.0216	LoopArea_spc	Tot_P	0.73	0.0072
HI25_cdom	SM_H15_10_day	0.30	0.0303					HI50_spc	dQ	-0.31	0.0333	LoopArea_spc	Tot_Q	-0.48	0.0006
HI25_cdom	SM_L15_1_day	0.39	0.0040					HI50_spc	HI_avg_spc	0.98	0.0000		Tot_P	0.65	0.0234
HI25_cdom	SM_L15_10_day	0.41	0.0029					HI50_spc	HI75_spc	0.80	0.0000				
HI25_cdom	SM_L15_4_day	0.43	0.0013					HI50_spc	HI90_spc	0.46	0.0010				
HI25_cdom	SM_L5_1_day	-0.28	0.0420					HI50_spc	LoopArea_num_spc	0.97	0.0000				
HI25_cdom	SM_L5_4_day	-0.31	0.0242					HI50_spc	LoopArea_spc	0.86	0.0000				
HI25_cdom	SM_M15_1_day	0.49	0.0003					HI50_spc	Q_peak	-0.34	0.0164				
HI25_cdom	SM_M15_10_day	0.40	0.0036					HI50_spc	Rain_21_day	-0.55	0.0099				
HI25_cdom	SM_M15_4_day	0.46	0.0005					HI50_spc	Runoff_Ratio	-0.65	0.0229				
HI25_cdom	spc_range	-0.34	0.0142					HI50_spc	spc_max	0.49	0.0004				

Table 3-S3. Table of significant correlations across event hysteresis metrics, catchment conditions and meteorological parameters.

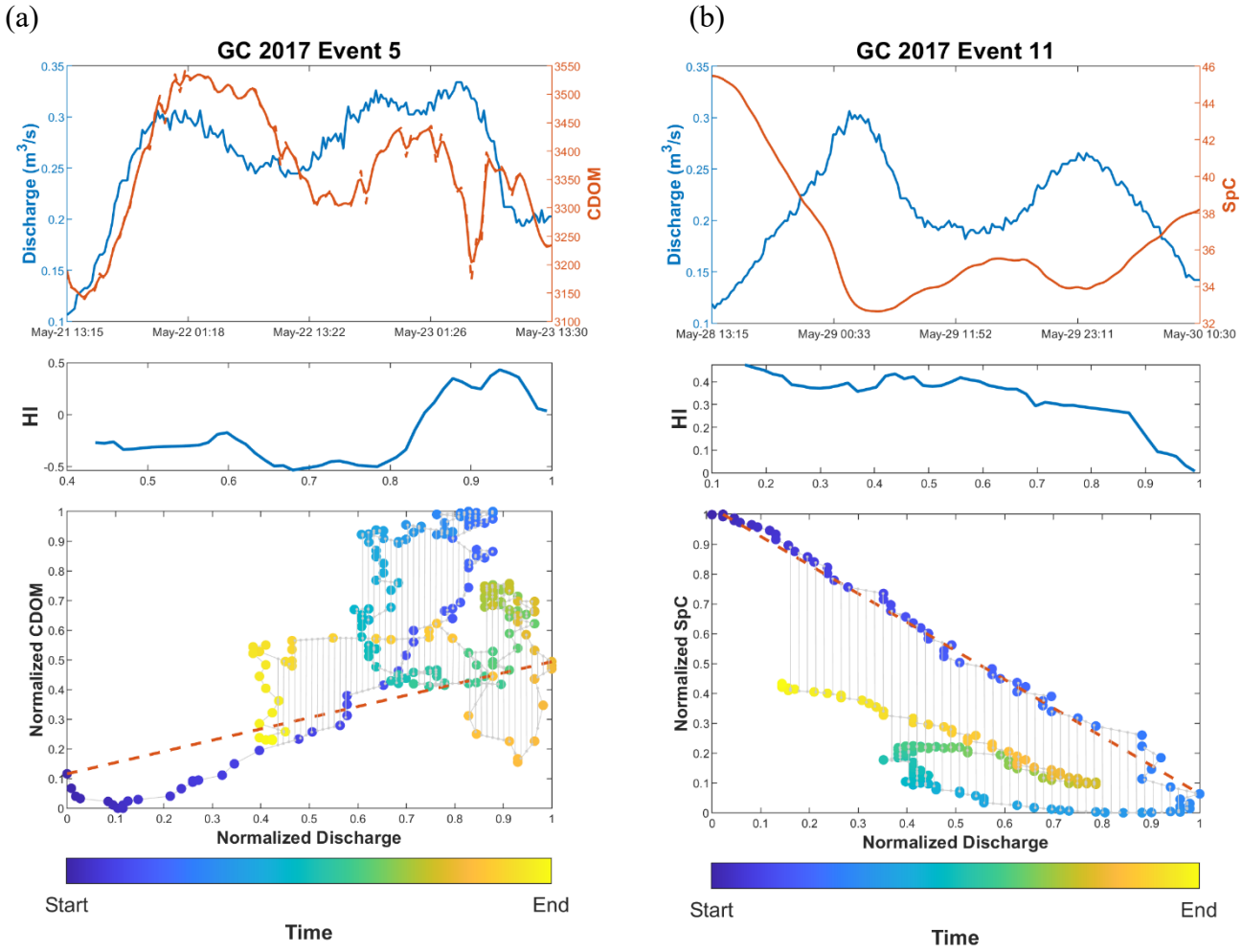

Figure 3-S1. (a) CDOM-Q and (b) SpC-Q events from 2017 not retained for further analysis.

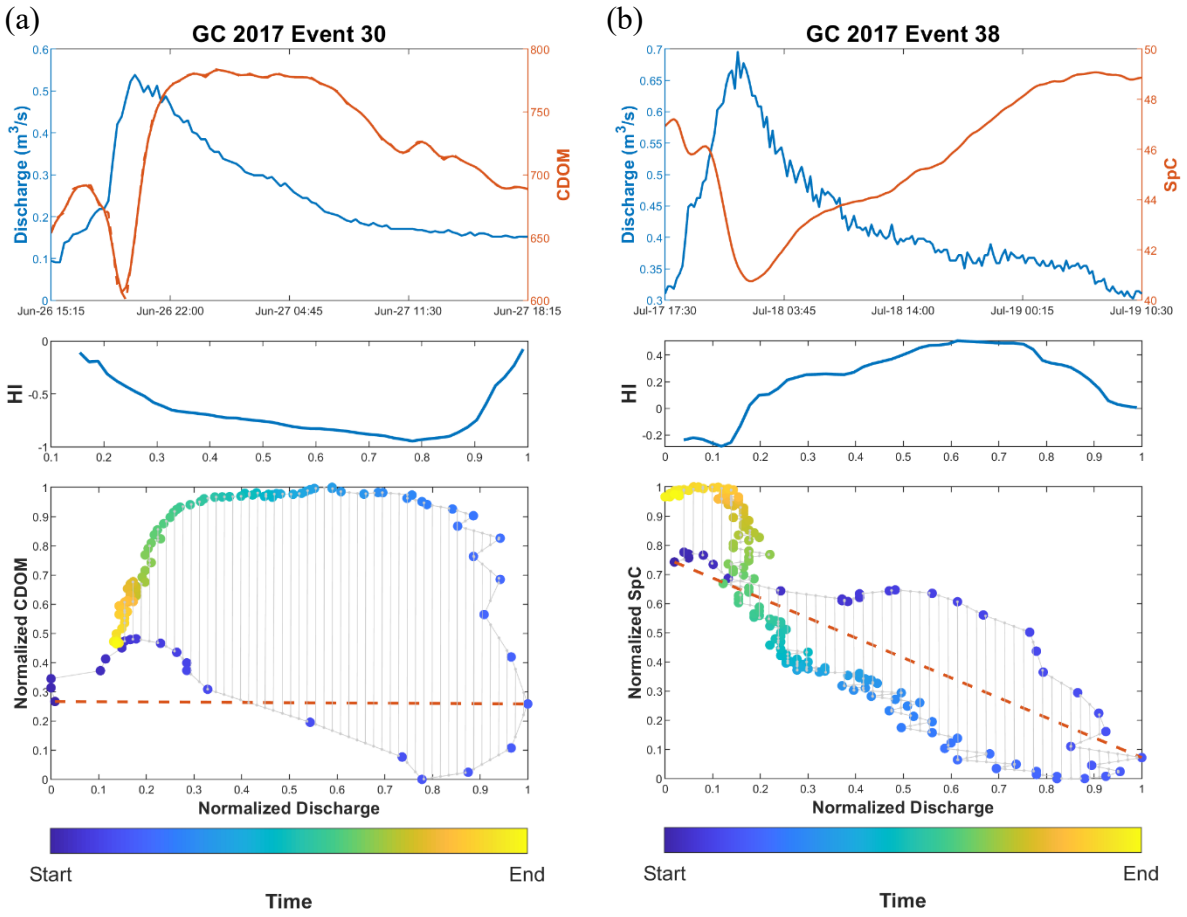

Figure 3-S2. (a) CDOM-Q and (b) SpC-Q events from 2017 not retained for further analysis.

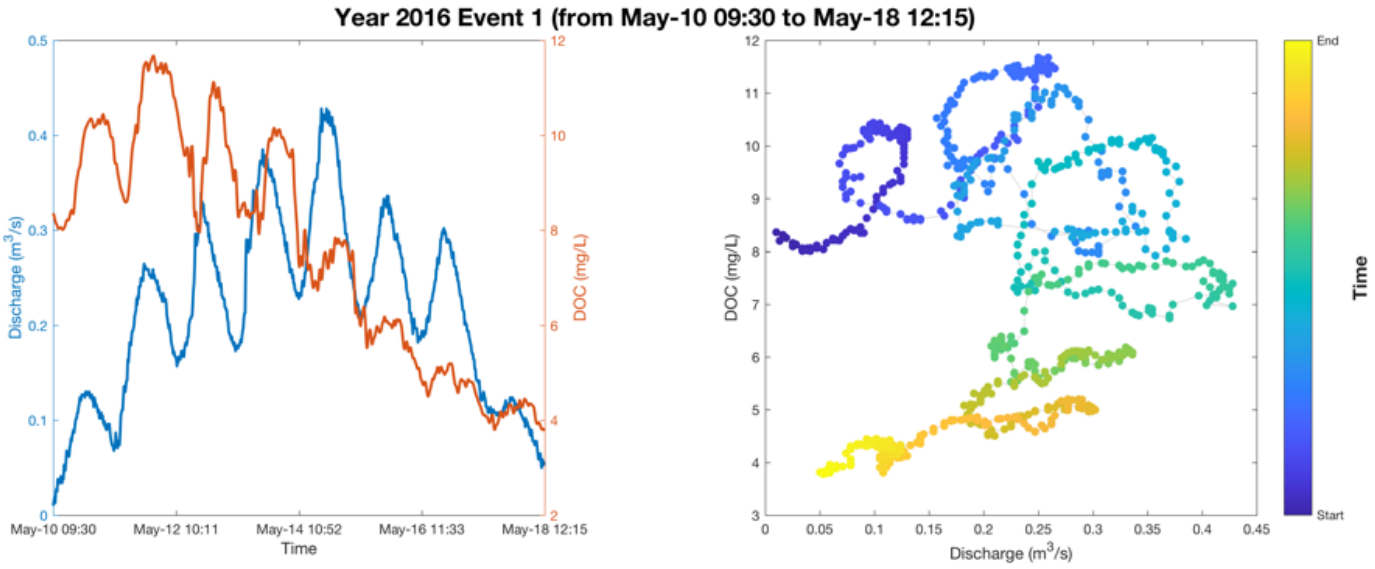

Figure S3-3. Example of diel variation in stream discharge (m^3 s^{-1}) and DOC (mg L^{-1}) captured during the snowmelt period at Granger Creek.

CHAPTER 4

A MULTI-YEAR, SEASONAL EVALUATION OF ECOHYDROLOGICAL SEPARATION IN A MONTANE HEADWATER CATCHMENT UNDERLAIN BY DISCONTINUOUS PERMAFROST.

ABSTRACT

Climate warming is expected to intensify the freshwater cycle and solute fluxes in northern environments. The compartmentalization of water within the critical zone is increasingly important to provide insights into how water cycles within catchments under current and changing conditions. However, the influence of changing vegetation communities and shrub height on interception, evapotranspiration and soil moisture is unresolved. Stable isotopes of water ($\delta^2H/\delta^{18}O$) were collected from the headwater site Granger Creek situated in the Wolf Creek Research Basin in YT, Canada to assess vegetation water sources and evaporative effects in the soil. The concurrent, multi-year record of stable isotopes of xylem, bulk soil, stream and meteoric waters were used to explore the "two water words" hypothesis or ecohydrological separation (TWW/ES). Dual isotope and lc-excess approaches showed that bulk and xylem water were significantly different from the LMWL and stream water isotopes. The bulk soil water isotope signal became more depleted over time along a defined soil evaporation line at progressively deeper depths in response to enhanced evaporation. Meanwhile, an increasingly enriched xylem water isotope signal overlapped with bulk soil water values as the growing season continued, which suggests the opportunistic use of available mobile soil water and refutes TWW/ES. Samples of the

mobile and nonmobile soil waters that comprise the bulk soil water signal are likely necessary to confirm the absence of TWW/ES at this site and resolve greatly depleted xylem water signature source.

4.1 INTRODUCTION

While there has been an enhanced interest in groundwater processes in permafrost environments (Walvoord and Kurylyk, 2016), there has been less focus on processes that occur in the seasonally frozen unsaturated zone, which provides water for vegetation growth (Green water), groundwater recharge (Blue water), and is susceptible to abrupt change (Chapin et al., 2005; Teufel & Sushama, 2019; Teufel et al., 2019). This is startling as projected changes in rain and snow, enhanced thaw of seasonally frozen soils, and changes in vegetation cover will all have large impacts on mediating evapotranspiration (ET) and recharge dynamics (Loranty et al., 2018). There has been considerable research documenting rapid vegetation change, particularly the advance of tree-dominated communities into shrub-taiga and tundra ecosystems, and the proliferation of tall shrubs into low tundra (Serreze et al., 2000; Schuur et al., 2007; Yang et al., 2010; Myers-Smith et al., 2011; Bonfils et al., 2012; Pearson et al., 2013; Wallace and Baltzer, 2019). Feedbacks from shrub expansion include enhanced snow trapping or redistribution (Sturm et al., 2001, 2005; Essery and Pomeroy, 2004; Pomeroy et al., 2006; Marsh et al., 2010; Myers-Smith and Hik, 2013; Domine et al., 2015; Krogh and Pomeroy, 2018; Vowles and Björk, 2019), changes in melt timing (Pomeroy et al., 2003), warming soils (O'Donnell et al., 2011; Bonfils et al., 2012; Guo et al., 2018), and the potential to alter nutrient availability (Cornelisson et al., 2007; Myers-Smith and Hik, 2013; Natali et al., 2015), most of which enhance further shrub growth and potential for tree establishment (Jorgenson et al., 2010).

The influence of changing vegetation communities on hydrological storage and flux remains uncertain (Lafleur and Humphreys, 2018), as modest changes in ET have been observed based on shrub abundance (McFadden et al., 2003; Chapin et al., 2005; Krogh, Pomeroy and Marsh, 2017). Yet vegetation characteristics (including height) and species effects on transpiration, interception, and energy partitioning can be considerable (Bonfils et al., 2012; van den Bergh et al., 2018; Zwieback et al., 2019).

Ecological responses to warming and other environment changes are often complex and nonlinear (Brown et al., 2001; Wookey et al., 2009; Leuzinger et al., 2011; Lavergne et al., 2019) with uncertain response timelines. Trajectories of future ecological change rely on the assumption that the results of short-term experiments are projections of long-term changes (Leuzinger et al. 2011; Wolkovich et al. 2012). This assumption is complicated by responses affected by lag times, species interactions, or effects diluted over time due to genetic adaptation (Brown et al. 2001; Leuzinger et al. 2011; Phoenix et al. 2012). How vegetation changes and feedbacks affect soil recharge processes in specific locations (Pomeroy et al., 2006; Loranty et al., 2018) and in the long term (Blume-Werry et al., 2016) is highly uncertain, yet this is a first-order control on both gains and losses of water.

Tracers, particularly $\delta^2H/\delta^{18}O$, provide alternative insight into catchment hydrological processes, and when combined with hydrometric measurements allow a more nuanced understanding of how water is stored, mixed, and released in northern catchments (Tezlaff et al., 2015). Information on water storage and ages has become increasingly important as hydrological research has broadened its focus from quantifying water fluxes toward understanding which specific waters are in flux and which are less mobile in storage

(Birkel et al., 2011; Sprenger et al., 2018; Smith et al., 2019). Stable isotope analysis of plant xylem water and various potential source waters have proved important to answering questions of plant water use (Penna et al., 2018; Dubbert et al., 2019), and to address the assumption that plants are generally highly opportunistic and capable of dynamically sampling sources based on season, stress, and water availability (Bertrand et al., 2012). However, more recent work suggests that there is considerable partitioning in the hydrological cycle and less mixing between compartments than assumed (e.g., Tetzlaff et al., 2014; Soulsby, Birkel & Tetzlaff, 2016; Evaristo et al., 2019; Smith et al., 2019). The term “ecohydrological separation” (ES) has been used to suggest that there are two soil-water pools: one that is available to plants and one that drains to the stream (Brooks, Barnard, Coulombe, & McDonnell, 2009; Goldsmith et al., 2012; McDonnell et al., 2014; Evaristo, Jasechko, & McDonnell, 2015; Bowling, Schulze, & Hall, 2017; Evaristo, Mcdonnell, Scholl, Bruijnzeel, & Chun, 2016; Hervé-Fernández et al., 2016; Berry et al., 2017). This has been referred to as the "two water worlds" (TWW) hypothesis, which states water sampled by vegetation has isotopic characteristics of tightly bound water held at high suctions, as opposed to water that is more mobile and held at lower suctions (McDonnell, 2014). In other words, water that plants take up is not sourced from the same subsurface storage as streamflow. Soils retain a mixture of water that reflects precipitation events over both short- and long-term time scales, and it is uncertain as to why plants do not evenly sample from this soil water isotope distribution although a number of hypotheses exist (Brantley et al., 2017). There are a number of hypotheses and a growing literature on the topic that relate to seasonality, energy limitations, and other ecological factors (Geris et al.,

2017; McCutcheon et al., 2017; Benettin et al., 2018), but a global meta-analysis confirms an absence of data with regards to soil and groundwater in permafrost regions (Evaristo, Jasechko and McDonnell, 2015; Amin et al., 2019).

Understanding whether ecohydrological separation occurs and the water that vegetation uses is critical for rapidly transitioning northern environments. What water is used by plants and what water reaches the stream and recharges deeper aquifers has not been evaluated in permafrost environments, yet is particularly important as permafrost thaw and decreased frozen ground will dramatically change surface-groundwater partitioning and soil moisture (Woo, 1990; Walvoord & Striegl, 2007; Subin et al., 2013; Walvoord and Kurylyk, 2016). Much research suggests that transpired water is derived from older, deeper, and difficult to access sources of water, and direct soil evaporation from younger more surficial water with larger pores (Evaristo et al., 2015). Concurrently, the issue of ecohydrological separation is particularly vexing in environments where one would anticipate that frozen ground is a first-order control on water sources. Investigation into ecohydrological separation has been undertaken in some cold environments with or without snowmelt-driven stream response (Li et al., 2007; Geris et al., 2015; McCutcheon et al., 2017; Knighton et al., 2019; Qiu et al., 2019). However, to our knowledge, there has been no testing of this hypothesis in permafrost regions.

The objective of this paper is to test whether ecohydrological separation occurs in a cold, permafrost-influenced headwater environment dominated by shrub vegetation. Specifically, we will address:

1. What pools of water do plants sample?

2. Is there an influence of frozen ground and snow on plant and soil water?
3. Does shrub size, slope position, or water table position (wetness) influence the plant and soil water sampled?

These three questions will provide important insights into how meteoric water is processed by the catchment, and elucidate interactions between infiltrated water and plant water use.

4.2 METHODS

4.2.1 Site description

All data was collected within the headwaters of Wolf Creek Research Basin (WCRB), a long-term research watershed located approximately 20 km south of Whitehorse in Yukon Territory, Canada. The climate in this area is classified as continental subarctic and the 30-year climate normal (1981-2010) obtained from Whitehorse Airport (706 m) has a mean annual precipitation of 262.3 mm, with approximately 45% falling as snow (Carey et al., 2010). There is a notable orographic influence on precipitation, with records from upper elevations of WCRB showing precipitation exceeding 400 mm in many years (Rasouli et al., 2019).

Much of the detailed vegetation and soil sampling were conducted within two headwater catchments. Granger Creek (GC) spans elevations of 1310 to 2080 m a.s.l. with vegetation ranging from shrub taiga to alpine tundra, dependent primarily on elevation and aspect. Below 1500 m.a.s.l., willow (Salix sp.) and birch (Betula sp.) are common as dwarf shrubs with a gradual increase in height downslope towards the riparian zone. White spruce (Picea glauca) occur sporadically along the south-facing slope. Above 1500 m a.s.l., lichen and bare rock predominate (Quinton et al., 2004; McCartney et al., 2006; Carey et al.,

2013). Buckbrush Creek (BB; 60°31′18.01″ N, 135°12′17.27″ W), another headwater catchment, drains an area of 5.75 km^2 and is located approximately 2 km west of GC catchment (Figure 4-1). BB catchment ranges in elevation from 1324 to 2080 m a.s.l. and has similar physiographic characteristics to GC.

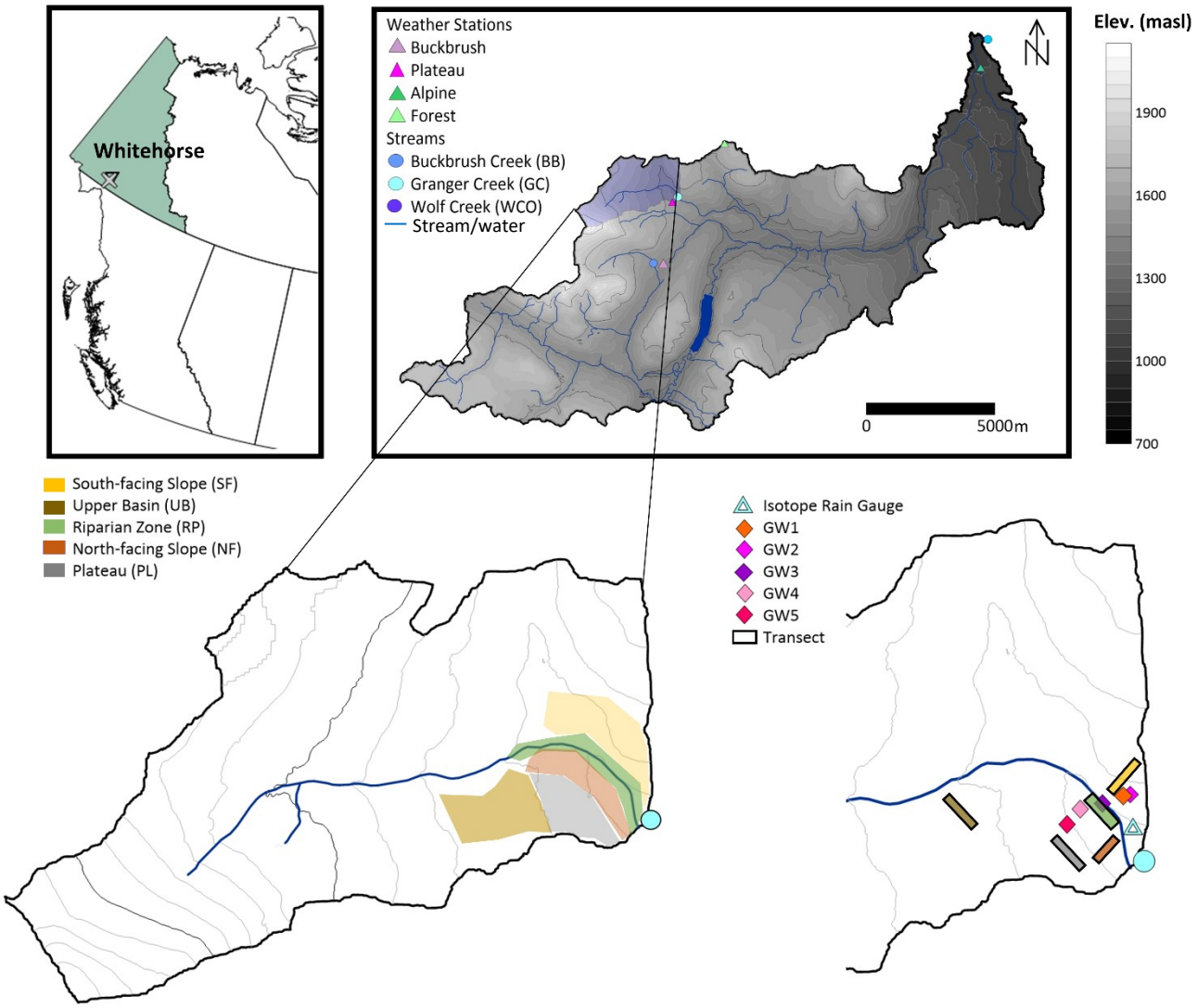

Figure 4-1. (Left) Inset map of Wolf Creek Research Basin (WCRB) located ~20 km south of Whitehorse in Yukon Territory, Canada. (Right) Within WCRB, Buckbrush Creek (BB) outlet is shown next to the nearby Buckbrush Weather Station (WCB) and Granger Creek (GC) catchment is delineated. Additional isotope precipitation gauge locations Alpine and Forest are shown. (Bottom left) GC is shown in greater detail with hydrologic response units (HRUs) shown by color. (Bottom right) Locations of the isotope precipitation gauge, wells and typical transect locations within GC headwater catchment are shown.

The geological setting for GC and BB is defined by sedimentary sandstone, siltstone, limestone, and conglomerate. Atop bedrock, thick stony till and glacial drift cover most of the basin. Below 1650 m a.s.l., soils in the top metre are generally comprised of

silts and sands, while higher elevations (taiga and lower tundra ecozones) have a veneer of surface organic soils with variable thickness (0.1-0.4 m). South-facing slopes have a thin organic layer overlying sandy soils, whereas north-facing slopes have thicker organic layers (10-30 cm) and are underlain with discontinuous permafrost. Between the slopes in the lower portion of Granger Basin, a wide riparian zone (50 to 100 m) exists with a consistently raised water table. Elevation and aspect are the main controls of permafrost distribution and it is assumed that ~50 % of the catchment is underlain by permafrost (Lewkowicz & Ednie, 2004). South-facing slopes are dominated by seasonal frost, while north-facing slopes and higher elevations are historically considered to have permafrost, yet the exact disposition remains uncertain (Carey, 2003).

Vegetation surveys were conducted in 2016 using the point-intercept method along 48 transects located within different hydrologic response units (HRUs) previously identified within Granger Basin (McCartney et al., 2006). Surveyed HRUs in GC applicable to this study were broadly classified as: (1) Riparian zone (RP), (2) south-facing slopes (SF), (3) north-facing slopes (NF) and (4) high-elevation plateau (PL) (Figure 4-1). For all transects, a straight rod was lowered vertically through the canopy at each 1 m increment along the 50 m transect. Any contact with shrubs or other vegetation was considered a single count or "intercept" and the vegetation type and/or species was recorded. A total of 2400 points were sampled within GC basin using the transect approach. Within the RP, transects were laid out on either side of GC at multiple locations down the length of the stream. For each slope, a series of five 50 m transects were laid out perpendicular to the slope direction (and parallel to the stream), from the bottom towards the top of each slope.

Each parallel transect was separated from the other by a minimum of 50 m. This arrangement was repeated several times from the outlet towards the headwater of GC. Surveys were also conducted at PL and BB in 2015 using the point-intercept method along a 150 m transect.

Observations from throughout WCRB showed that willow species tended to predominate in areas with a higher water table, with recorded riparian (RP) willow shrub species reaching heights in excess of 200 cm. Birch shrub species also tended to grow taller in wetter areas but were less frequent in areas with a consistently near-surface water tables. At Granger Creek catchment, willow shrub height tended to decrease with increasing elevation along north- and south-facing slope with mean heights typically greater than mean birch shrub height (Table 4-1). A general trend of decreasing birch shrub height with increasing distance upslope was noted for both north- and south-facing slope. Plateau (PL) vegetation surveys showed the smallest mean shrub heights of ~56 cm and ~58 cm for birch and willow species, respectively. Due to its lower elevation and deeper soils, shrubs in the Buckbrush catchment were notably taller in areas close to the WCB weather station (Table 4-1).

Catchment	Slope aspect	Location	Vegetation height (cm) *Birch* Mean ± SD	*Willow* Mean ± SD
Buckbrush (BB)	N/A	Near tower	86.8 (43.8)	125.4 (36.2)
Granger (GC)	South-facing (SF)	RP	87.9 (28.5)	138.4 (33.9)
		Slope	84.3 (31.8)	105.1 (33.1)
	North-facing (NF)	RP	77.2 (21.6)	141.7 (58.3)
		Slope	83.7 (33.2)	102.4 (33.1)
		PL	55.8 (22.6)	57.8 (17.8)

Table 4-1. Summary of vegetation characteristics for transects reported in different hydrologic response units (HRUs) of Granger Creek catchment and for a transect located adjacent to the Buckbrush weather station.

4.2.2 Meteorological measurements

The longterm Buckbrush weather station (WCB) is located approximately 2 km south of Granger Basin and records all radiation components, air temperature, wind speed, vapour pressure, and total precipitation year-round, with some gaps due to power loss (Rasouli et al., 2019). A snow pillow and a SR50A snow depth sensor are located at the WCB location. The snow depth is reported every 30 minutes while the snow pillow calculated SWE every 3 hours. Rainfall data at 30-minute sampling resolution summed to the daily average reported in this study were obtained from a tipping bucket rain gauge a WCB weather station and verified against an Alter-shielded Pluvio total precipitation gauge at the same location (Figure 4-1).

4.2.3 Hydrometric measurements

The long-term rating curve at Granger Basin outlet (Granger Creek, GC) was updated by frequent measurements in 2015-2016 using a SonTek FlowTracker

(SonTek/Xylem Inc., CA, USA) across a range of flow conditions each year once the channel was ice free. A stilling well containing a pressure transducer (Solinst Levelogger) was compensated with an adjacent, above-water Solinst Barologger to generate water pressure/stage at 15-minute intervals (Solinst Canada Ltd., ON, Canada). Loggers were in place once channels were no longer ice-covered and removed in September or October to prevent freezing. When snow and ice covered the stream, discharge was manually measured with salt-dilution gauging.

4.2.4 Liquid water isotopes and calculation of the local meteoric water line (LMWL)

Surface water isotope samples were collected in 20 ml PETG displacement vials. Rainfall was collected in 20 ml vials if sample volume was sufficient and if not, in 7ml PETG vials. Precipitation that fell as snow was collected in a plastic ziplock bag with as little airspace as possible, allowed to melt gradually and then collected in 20 ml displacement vials. From 1994 to 2006, precipitation samples were collected in GC (1350 m.a.s.l.). For 2015-2016, rain and snow were collected from a range of elevations located in the low-elevation forest area near Wolf Creek outlet (WCO) (750 m.a.s.l.), below the mid-elevation shrub canopy at WCB (1250 m.a.s.l.), beside GC outlet, and at the high-elevation Alpine site (1615 m.a.s.l.) (Figure 4-1).Whenever possible, duplicates were collected for a given rain event and the averaged event values were retained in the record. Snowmelt isotope samples were collected from snowmelt lysimeters in Granger Basin during the 2015 melt period and to a lesser extent in 2016. Precipitation (1994-1998, 2002-2008, 2013-2016) was collected from recent snowfall and following rain events from multiple sites dispersed throughout WCRB. Sites were chosen to accommodate the

elevation differences of ~1300 m between WCO to sites located above treeline. Precipitation samples were collected opportunistically in winter and typically at lower elevations due to site access limitations. Rainfall was collected in rain gauges manufactured according to IAEA standards (IAEA/GNIP V2.02, 2014) with modifications for low magnitude rainfall events (Figure 4-S3).

Figure 4-2. Photo of Alpine Alter-shielded Geonor total precipitation gauge and solar panel with adjacent IAEA-standard precipitation collector (shown by yellow arrow).

Surface water isotope samples were collected from two headwater streams in WCRB: Buckbrush Creek (BB) and Granger Creek (GC), from 2013 to 2016. More intensive sampling occurred during spring through fall. Samples were collected throughout the winter every 2 to 8 weeks depending on site access. Isotope samples were typically collected by hand during site visits, however, a Teledyne Isco autosampler was used to collect sample water while researchers were not stationed near GC (Teledyne ISCO, NE,

USA). Isco autosampler bottles were emptied within 1-7 days of sample collection, with shorter duration spans when the probability of evaporation was higher.

Groundwater isotope samples were collected from shallow wells primarily located in the riparian zone of GC and BB catchments. Whenever possible, samples were collected from wells located upslope of the GC riparian zone (Figure 4-1). Wells were emptied and sampled once water levels returned to their pre-bailed water level. Samples were filtered if well water had considerable dissolved material or particulates.

Stable isotopes of precipitation, snowmelt, stream, and well water (δ^2H and $\delta^{18}O$) were determined using a Los Gatos Research DTL-100 Water Isotope Analyzer at the University of Toronto. δ^2H and $\delta^{18}O$ values are generally expressed in delta notation (δ) as

$$\delta = \left(\frac{R_{sample}}{R_{standard}} - 1\right) x\ 1000 \qquad \text{(Equation 1)}$$

Where δ is the ratio of $^2H/^1H$ and $^{18}O/^{16}O$ ratio relative to Vienna Standard Mean Ocean Water (V-SMOW) expressed in per mil (‰), R is the ratio ($^2H/^1H$ and $^{18}O/^{16}O$) of sample and standard (V-SMOW), respectively. Five standards of known isotope composition, with δ^2H ranging from −154‰ to −4‰, purchased from Los Gatos Research were used for calibration, in addition to periodic checks using the international standards, VSMOW2 and SLAP2. During analytical runs, samples were interweaved with standards at a ratio of 3:1.

The local meteoric water line (LMWL) for southern Yukon was calculated using 198 precipitation samples spanning 1994-2016 collected within WCRB. Historical precipitation samples are presented in Boucher and Carey (2010). Snow and snowmelt samples accounted for 67 of the total samples while rainfall comprised the remaining 131. The composition of the calculated LMWL was dominated by rainfall rather than snow for

recent years, and isotope values were not volume-weighted. The regression model was considered a good fit due to the large correlation coefficient (close to 1), a small standard error relative to the data magnitude, and a p-value less than 0.0001 (Helsel and Hirsch, 1992).

4.2.5 Soil vapour and plant xylem water isotopes

Samples of soil and xylem water were collected in GC in different HRUs (Figure 4-1) at different growth stages from spring to fall. Repeat sampling occurred in the riparian zone (RP), along the north- and south-facing slopes (NF and SF, respectively), plateau (PL) and upper basin (UB) areas. Along the south- and north-facing slopes, vegetation and soil isotope samples were taken at slope positions from high (VS1) to low slope positions (VS4) (Figure 4-3).

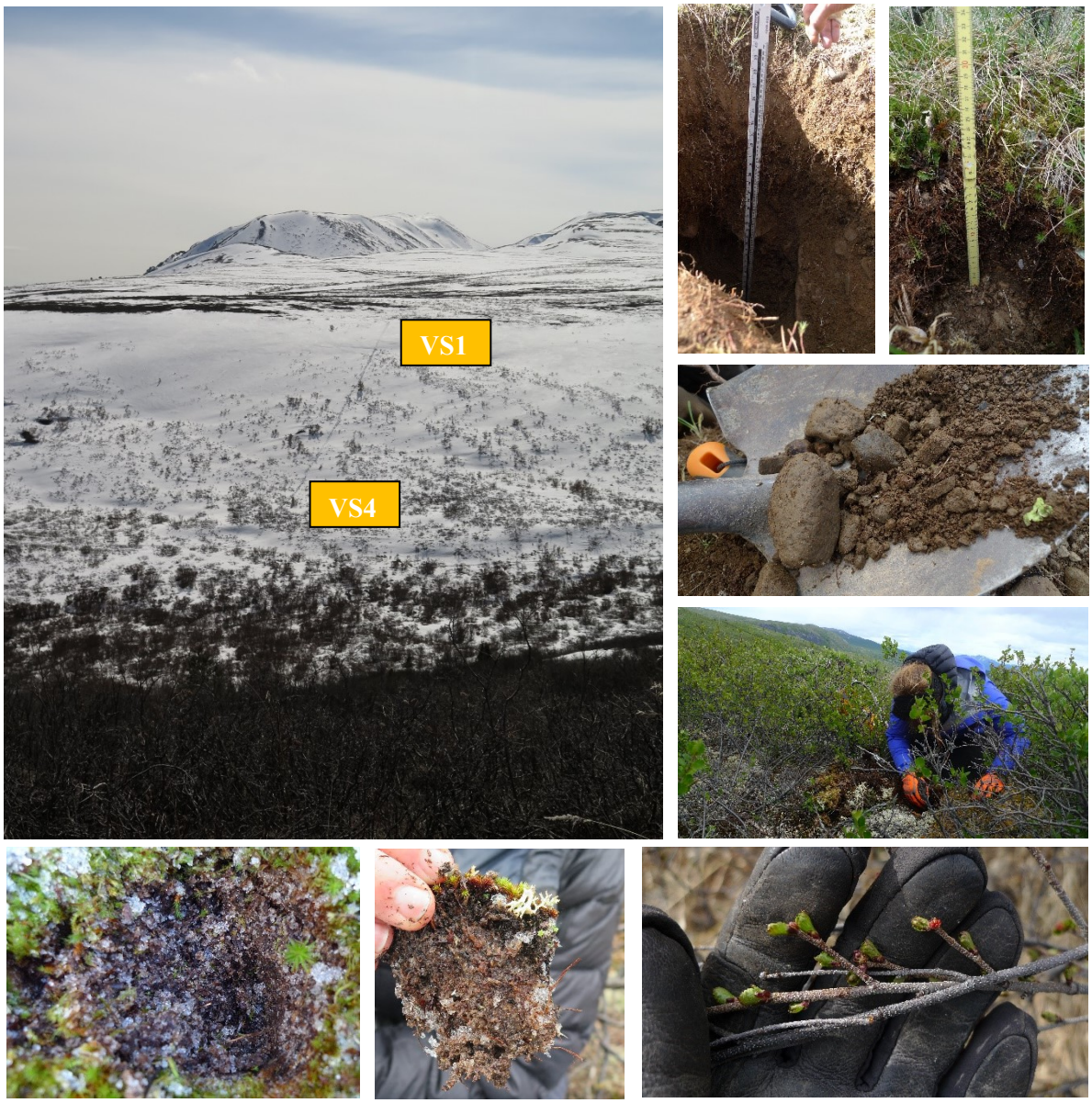

Figure 4-3. (Top left) Composite of photographs showing north-facing (NF) slope transect from VS4 to VS1 and plateau (PL) in winter taken from snow-free south-facing (SF) slope. (Top right) Two soil pits from mid-summer season, shovel showing soil from > 40 cm depth at PL, vegetation sampling. (Bottom left to right) Frozen ground during April, organic soil with ice crystals, birch shrub branches to be destructively sampled for xylem isotope composition.

The stable isotopic composition (δ^2H and $\delta^{18}O$) of soil water was sampled using the direct-equilibration method of Wassenaar et al. (2008), and were analysed at the University

of Saskatchewan with the methodology described by Hendry et al. (2015). The general procedure for the direct- equilibration method was as follows: Disturbed soil samples were stored in sealed bags and dry air was added to the bag in the laboratory. During 2 or 3 days of storage at constant temperature, an isotopic equilibration between the soil water and the headspace developed, and then, the vapour of the saturated headspace was sampled directly via laser spectrometry using a Los Gatos Research instrument (model TWIA-45-EP, Los Gatos Research, CA, USA) (Figure 4-4). Bags with standard waters of known isotopic composition, ranging the expected soil water isotopic composition, were also analysed using the above method and analytical instrumentation. These standard waters were used for calibration to derive the isotopic composition of the liquid soil waters from the vapour measurements, in reference to the Vienna standard mean ocean water as proposed by Wassenaar et al. (2008). The accuracy of the direct-equilibration method was ±0.31‰ for $\delta^{18}O$ and ±1.13‰ for $\delta^{2}H$ (Sprenger, Tetzlaff, & Soulsby, 2017).

Plant water isotopic compositions were sampled using cryogenic extraction at 100°C under vacuum of < 30 millitorr over 60 minutes (McCutcheon et al., 2016). The accuracy of such analyses is given as ±0.15 ‰ for δ18O and ±0.69 ‰ for δ2H (West et al., 2006). To avoid analytical bias arising from alcohol contamination (Martín-Gómez et al., 2015), we also analyzed a subset of extracted waters using a ThermoFisher TC/EA coupled with Thermo Delta V Plus mass spectrometer housed in the Stable Isotope Laboratory at Boise State University. Column and GC temperatures were set at 1250 and 90 °C respectively, the flush rate was 90 ml/min, and sample injection volume was c. 0.2 µl. To avoid magnet jump instabilities, H and O were analyzed separately. Samples were

standardized against reference waters from Los Gatos Research; typical reproducibilities were d18O ~ ±0.3‰ (2s) and dD ~ ±1.7‰ (2s).

Figure 4-4. Photo taken by K. Janzen showing soil sample bags being equilibrated with dry gas before isotope analysis.

4.2.6 lc-excess calculation

The lc-excess of isotopes samples is a commonly used metric for expressing δ^2H evaporative fractionation from the LMWL and was calculated according to Landwehr and Coplen (2006):

$$lc - excess = \delta^2H - a * \delta^{18}O - b \qquad \text{(Equation 2)}$$

Where a and b are the slope and intercept of the LMWL, respectively. Typically, lc-excess quantifies the offset of sampled waters from meteoric waters (i.e., LMWL) with negative values indicating evaporative fractionation under non-equilibrium conditions. In contrast, positive lc-excess values indicate mixing of water sources (Landwehr and Coplen, 2006).

4.2.7 Statistical analyses, data manipulation and visualisation

Linear regressions were performed in R software (R Core Team, 2019). Significant difference was determined using Wilcoxon rank sum test on non-parametric stable isotope data using base R. Data handling and visualization was accomplished in R using ggplot (Wickham, 2016), ggpubr (Kassambara, 2019), tidyr (Wickham & Henry, 2019), dplyr (Wickham et al., 2019), cowplot (Wilke, 2009), magrittr (Milton Bache & Wickham, 2014), lubridate (Grolemund & Wickham, 2011), naniar (Tierney et al., 2020), and Hmisc (Harrell, 2020).

4.3. RESULTS

4.3.1 Weather and streamflow

Mean air temperature at Buckbrush weather station from 1 April to 31 October was 7.0 ℃ and 8.3 ℃ in 2015 and 2016, respectively (Figure 4-5). Total precipitation for the same period was greatest in 2016 (250 mm), followed by 2018 (235 mm) and 2015 (201 mm). Summer and fall months in 2015 and 2016 were characterized by atypical, large magnitudes of rainfall totalling 107 mm (170 mm including fall) and 110 mm (203 mm including fall), respectively (Figure 4-5).

The maximum snowpack in 2015 approached 174 mm SWE by mid-March before melt began on 11 April. Daily average air temperature was generally below 0 ˚C throughout April and an additional 30 mm of snowfall caused accumulated SWE to reach ~144 mm by 3 May. At this point, the snowpack declined rapidly over 9 days coincident with consistently increasing air temperature during the atypically warm May. Snowpack accumulation was much less in 2016 compared to 2015 with the greatest accumulated SWE ranging from 111 to 113 mm recorded between 20-26 March. Snowmelt began on 27 March and progressed over 30 days until late April. Snow-free days were observed at Buckbrush weather station on 12 May 2015 and 27 April 2016. In both years, snowpacks persisted past these dates at GC due to differences in elevation, aspect, and the presence of shaded depressions.

The 2015 and 2016 hydrographs for GC exhibited patterns typical of northern watersheds, with a distinct late season increase attributed to rainfall (Figure 4-5), which is rare in the GC historical record (Carey et al., 2013 a,b; Rasouli et al., 2019; Chapter 2 (Shatilla and Carey, 2019)). Stream discharge first increased on 9 May 2015, while freshet began on 14 May 2015, with an increase in flow from ~0.02 $m^3 s^{-1}$ to daily flows averaging ~0.5 $m^3 s^{-1}$ over a nine-day period. Peak 2015 daily discharge was 0.67 $m^3 s^{-1}$ on 22 May, after which, flows declined to summer levels of ~0.2 $m^3 s^{-1}$. Accumulated rainfall of ~125 mm between 17 August and 11 September led to an increase in flow to ~0.46 $m^3 s^{-1}$ on 14 September before a gradual decline until the transducer was removed on 1 October. Flows in 2016 differed from 2015, with a distinct response to snowmelt, which occurred much earlier in the year in comparison to the 25-year record (Chapter 2 (Shatilla and Carey,

2019)). There was no distinct snowmelt freshet event in 2016; instead, a gradual increase in flows was punctuated with hydrograph rises that corresponded to both snowmelt and summer rainfall events. Flow magnitude was similar to 2015, and large late-season rainfall (~115 mm between 17 August and 10 September) once again resulted in high September flows.

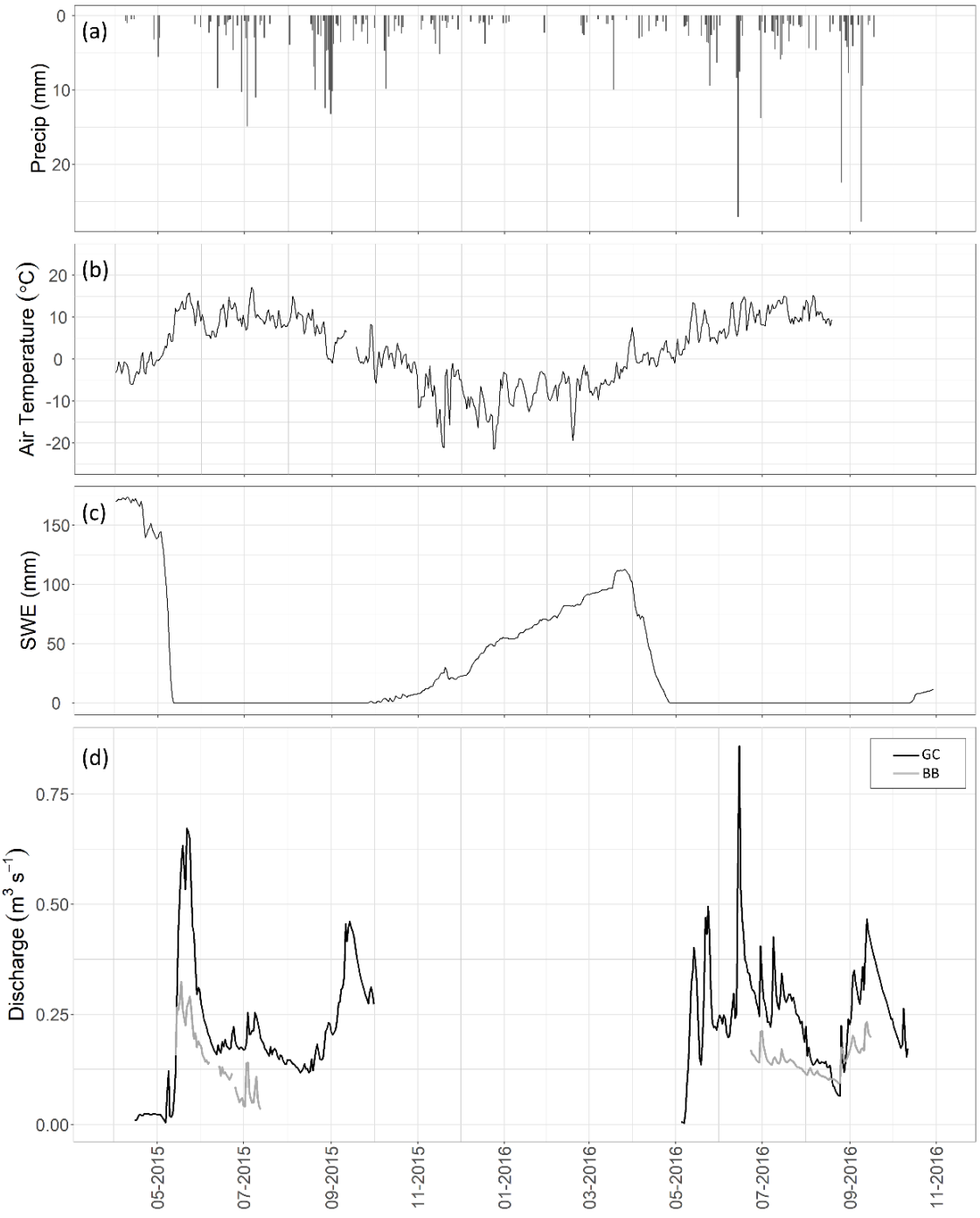

Figure 4-5. (a) Precipitation daily sum from 30-minute tipping bucket rain gauge record, (b) average daily air temperature from 30-minute measurements and (c) snow pillow record from 3-hour measurements at Buckbrush weather station (WCB). (d) Daily average discharge measurements at Buckbrush Creek (BB) and Granger Creek (GC) outlets.

Flows declined again until the transducer was removed on 17 October. Streamflow at BB is described in Chapter 2 (Shatilla and Carey, 2019).

4.3.2 Stable Isotopes

The stable isotope composition of precipitation exhibited a large range, with snow more depleted in heavy isotopes than rain as expected (Figure 4-6, Table 4-2). Rain exhibited a greater overall variability than snow, yet the sample size and seasonal representation was greater. Snowmelt water collected in lysimeters was enriched compared with bulk snow samples, an observation that has been reported elsewhere (Sitchler, Rauert & Martinec, 1981). While all seasons are represented, we do not estimate a volume-weighted isotope precipitation due to the complexities of accumulation, melt, and interception of both snow and rain. Using all rain and snow δ^2H and $\delta^{18}O$ values, the local meteoric water line (LMWL) was computed: $\delta^2H = 6.15*\delta^{18}O-32.26$ ($r^2 = 0.99$, n = 191, $p < 0.0001$). To our knowledge, no other LMWL has been reported for Southern Yukon.

The isotopic composition of GC and BB stream water was clustered along the LMWL, as was groundwater sampled from near-stream riparian wells (Figure 4-6). The streamwater had a bulk isotopic composition lying between rain and snow and the lack of variance suggests streamwater is well mixed (Tetzlaff et al., 2009). Streamwater $\delta^{18}O$ and δ^2H exhibited seasonal variation of -23.50 ‰ to -18.07 ‰ for $\delta^{18}O$ and -181.45 ‰ to -136.80 ‰ for δ^2H. For groundwater, 47 samples showed a limited variation from -22.78 ‰ to -19.45 ‰ for $\delta^{18}O$ and -169.36 ‰ to -151.73 ‰ for δ^2H (Table 4-2). In addition, streamwater largely fell along the LMWL.

Departures of isotope signatures from the LMWL occur as a result of kinetic fractionation induced by evaporation and the differing slope and intercept are referred to as the local evaporation line (LEL) (Kendall & McDonnell, 1990). Bulk soil water isotope values fell along the LMWL while also exhibiting varying degrees of evaporative enrichment (Figure 4-6, Table 4-2). The soil evaporation line (SEL) calculated for bulk soil was $2.70*\delta^{18}O - 106.68$ (adjusted $r^2 = 0.584$, $p < 0.001$). While bulk soil and xylem isotope values did overlap in dual isotope space, the bulk soil water isotope signal had a large range with mean values more enriched in heavy isotopes compared to xylem water from birch and willow species (Table 4-2). In addition, bulk soil and xylem waters exhibited a large range for each discrete sampling period over the two years, and there were some shifts in the variance based on time of year at GC (Figure 4-7) and BB (Figure 4-S1). The xylem water isotope signal had minimal overlap with the LMWL and often appeared almost parallel to the LMWL, with a regression equation of $3.175*\delta^{18}O-111.37$ ($r^2 = 0.53$, $p < 0.01$). Willow species average values exhibited greater depletion in $\delta^{18}O$ and $\delta^{2}H$ compared to birch species averages (Table 4-2).

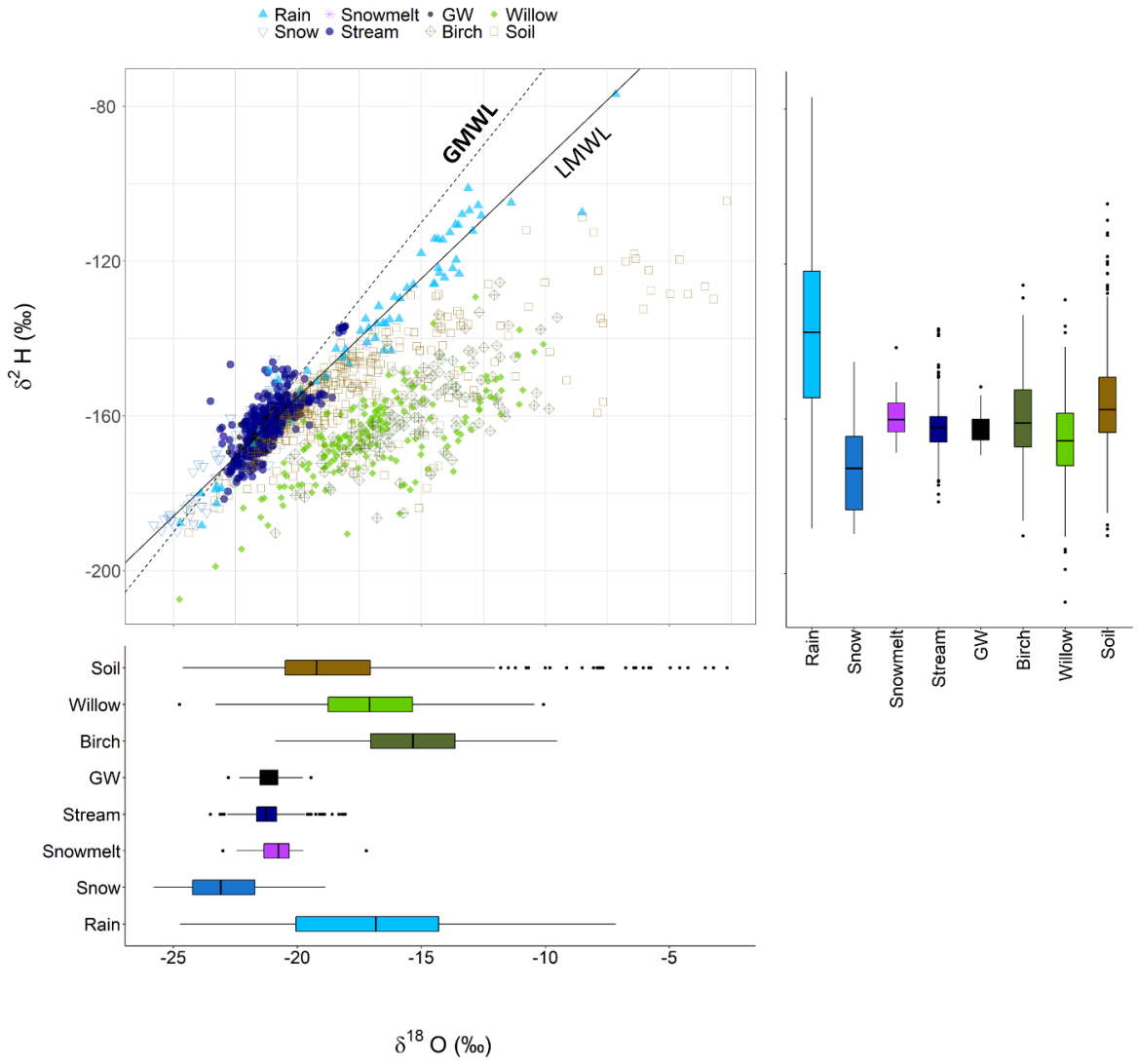

Figure 4-6. Precipitation data and LMWL for Wolf Creek Research Basin from 1994-2016. Granger Basin and Buckbrush Basin isotope data spanning 2015-2016 for bulk soil water, xylem water, groundwater from shallow riparian wells, stream and snowmelt water.

	n	δ2H			δ18O			lc-excess		
		Mean ± SD	Min	Max	Mean ± SD	Min	Max	Mean ± SD	Min	Max
LMWL	*191*	*-150.02±23.83*	*-189.77*	*-76.86*	*-19.17±3.81*	*-25.79*	*-7.16*	*-0.065±5.21*	*-22.79*	*15.33*
Precip	180	-149.50±24.39	-189.77	-76.86	-19.07±3.89	-25.79	-7.16	-0.11±5.26	-22.79	15.33
Rain	127	-139.85±21.48	-188.35	-76.86	-17.42±3.33	-24.52	-7.16	-0.58±4.92	-22.79	13.97
Snow	53	-172.62±12.54	-189.77	-145.30	-23.02±1.61	-25.79	-18.87	1.01±5.91	-10.49	15.33
Snowmelt	11	-158.55±7.63	-168.76	-141.60	-20.63±1.51	-23.00	-17.22	1.04±3.31	-4.43	7.85
GW	47	-162.46±4.01	-169.36	-151.73	-21.13±0.67	-22.78	-19.45	-0.40±2.36	-6.54	7.02
Headwater streams	*693*	*-162.08±5.91*	*-181.45*	*-136.80*	*-21.16±0.79*	*-23.50*	*-18.07*	*0.13±3.83*	*-10.28*	*24.99*
BB	102	-159.95±7.43	-172.58	-136.80	-20.89±0.91	-22.98	-18.07	0.64±3.23	-8.63	8.13
GC	591	-162.45±5.52	-181.45	-146.1	-21.20±0.75	-23.50	-18.59	0.04±3.92	-10.28	24.99
Xylem	*313*	*-162.85±11.86*	*-207.35*	*-125.50*	*-16.19±2.70*	*-24.75*	*-9.52*	*-31.07±11.35*	*-65.33*	*-7.88*
Birch	142	-159.61±11.78	-190.26	-125.50	-15.37±2.44	-20.89	-9.52	-32.96±10.90	-65.33	-7.88
Willow	169	-165.55±11.34	-207.35	-129.25	-16.86±2.74	-24.75	-10.08	-29.55±11.57	-57.88	-7.95
Soil (bulk)	*434*	*-155.68±12.94*	*-190.20*	*-104.50*	*-18.18±3.67*	*-24.63*	*-2.67*	*-11.77±15.15*	*-78.35*	*8.24*

Table 4-2. Summary statistics of δ2H, δ18O and lc-excess for each component of precipitation, groundwater, headwater streams (GC and BB), xylem water (birch and willow species) and bulk soil water.

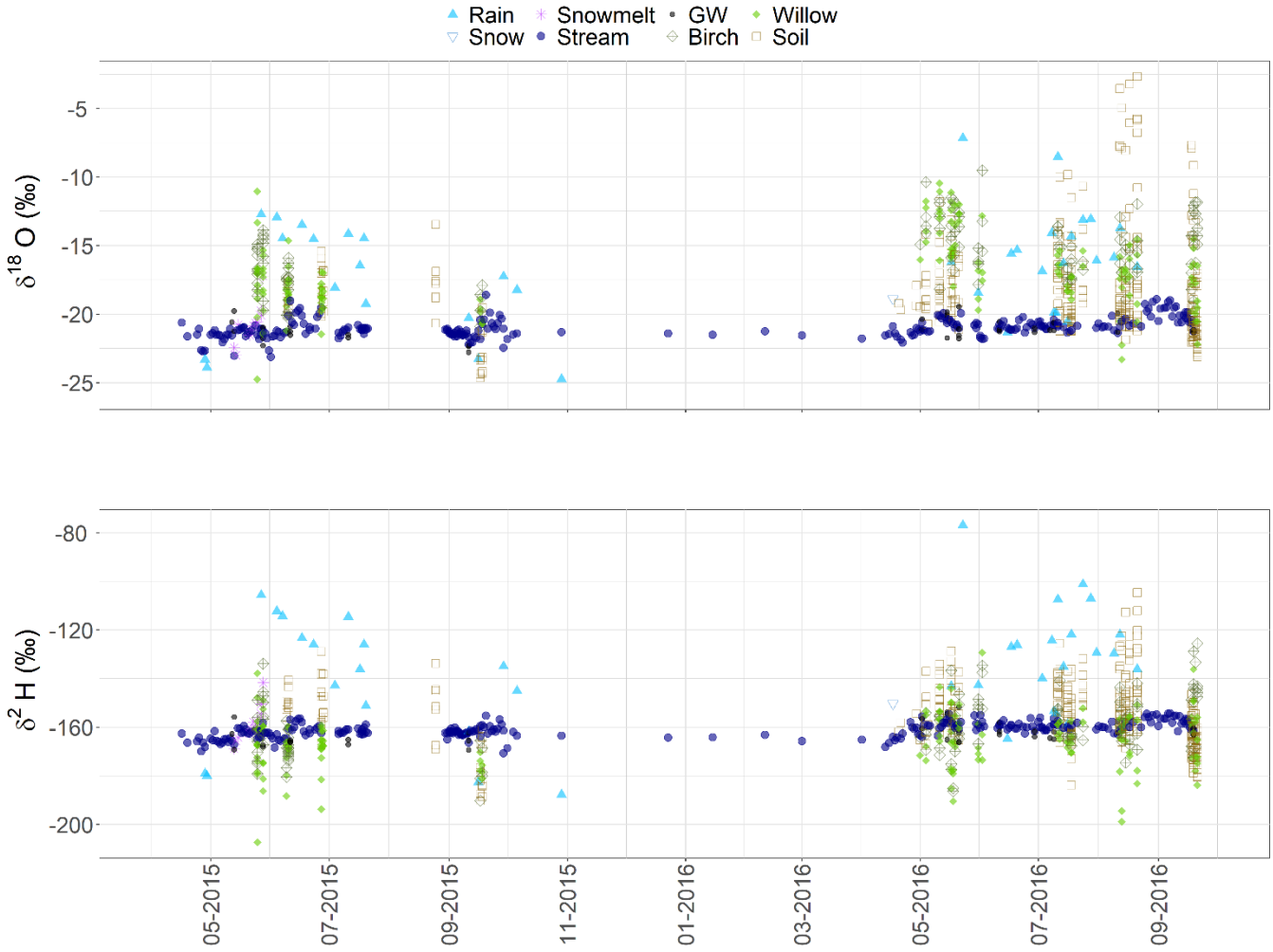

Figure 4-7. Time series of $\delta^{18}O$ and $\delta^{2}H$ for precipitation components, streams, shallow groundwater, xylem and bulk soil water at GC in 2015-2016.

Information derived from dual isotope space is often summarized as the deviation of water samples from the GMWL due to evaporative fractionation using "deuterium excess" (Dansgaard, 1964), and more recently, "line-conditioned excess" (Landwehr and Copen, 2006). Deuterium excess (d-excess) and line-conditioned excess (lc-excess) quantify the deviation of water samples from the GMWL and LMWL, respectively. Stable isotope data from WCRB was transformed to lc-excess values using regression line parameters from the WCRB-specific LMWL and Equation 2 (Section 4.2.6). Values of lc-excess that plot closer to 0 ‰ and more closely resemble the LMWL than values with greater distance from 0 ‰. Snow and rain (2015-2016) plot close to 0 ‰ with some variation. Snowmelt samples from lysimeter water collected within Granger Basin plotted at 0 ‰ or slightly above, indicating greater enrichment in heavy isotopes. Stream water lc-excess values for Buckbrush Creek (BB) and Granger Creek (GC) overlapped almost entirely for the two study years with the bulk of samples falling within a similar range as precipitation despite a more evaporated signal (more positive lc-excess). Groundwater and seep lc-excess values plotted close to 0 ‰ with minimal variation between GC- and BB-derived sample waters (Figure 4-8).

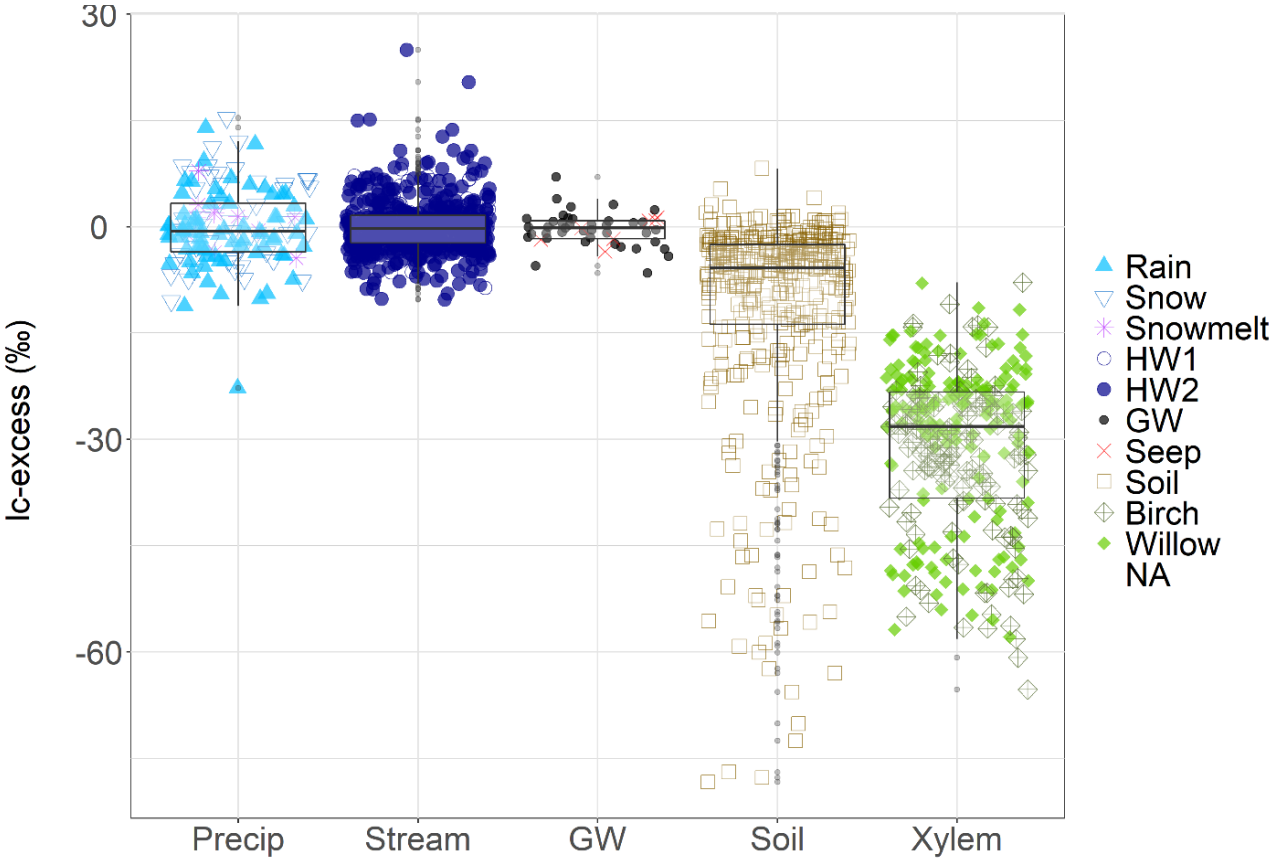

Figure 4-8. Boxplots of lc-excess for each precipitation components (1994-2016), stream, shallow groundwater, flowing (seep), bulk soil and xylem (willow and birch species) at BB (HW1) and GC (HW2) from 2015-2016.

Unlike precipitation, streamflow, and groundwater, which all have lc-excess near 0 ‰, soil and vegetation samples showed considerable spatial and temporal variability in lc-excess values that were strongly negative and an overall isotopic composition that exhibited greater variance in dual isotope space. Soil water was less negative than xylem waters, and on average birch had a more negative lc-excess than willow (Figure 4-8).

To evaluate sources of water for transpiration and ecohydrological separation, soil and vegetation samples were separated into seasons linked with growth stages of vegetation progressing from (i) winter dormancy in early April to mid-May, through (ii) bud burst in

mid-May to end-June, (iii) peak greening at the end of June through July, (iv) lower transpiration in mid-August, followed by (v) senescence in late September (Figure 6). Note that there were small differences in leaf growth and stage between willow and birch based on species differences and environmental factors such as aspect and elevation. The study periods spanned April 2015 to late September 2016 for GC and April 2016 to late September 2016 for BB.

Because of the position of frozen ground, depth of soil sample collection increased throughout the five sampling periods. In early April to mid-May, snow and frozen ground restricted sampling to the upper 10 cm of soil. As thaw progressed, deeper soil samples were obtained. Sampling began in 2015 in GC, with 2016 more fully capturing the seasonal dynamics of soil and xylem waters (Figure 4-7). Beginning in early April to mid-May 2016, bulk soil and xylem water stable isotopes were more enriched in heavy isotopes than recorded in late September 2015 in the near surface at GC (Figure 4-9), suggesting that there was change in composition over winter. Between late September 2015 and early spring period in 2016, vegetation was not transpiring yet there was a shift in xylem isotope composition to more enriched and with an overall greater fractionation. For the mid-May to end-June period, there was sporadic snow early in the period that was completed by mid-June and bud burst of the willow and birch shrubs began. Increasing thaw allowed sampling of deeper soils, yet the majority of these samples fell along the LMWL and there was a slight overlap with xylem water that was notably depleted in $\delta^{18}O$ and had moved closer to the LMWL (Figure 4-9). This was best observed in 2016 at GC due to the number of soil and xylem water samples.

During peak growing season (end-June to end-July), the isotopic composition of near-surface soils moved away from the LMWL indicating isotopic fractionation, whereas deeper soil layers remained superimposed on the LMWL (Figure 4-9) as in other cold environments (Oerter and Bowen, 2017; Amin et al., 2019). Xylem water was positioned closer to the LMWL during the peak growing season, with δ^2H values depleted in heavy isotopes similar to the deeper bulk soil water δ^2H values. $\delta^{18}O$ was enriched in heavy isotopes and plotted proximal to the near-surface soil layers and was compressed in dual-isotope space, suggesting plants are sampling a well-mixed water source. By mid-August, bulk soil isotopes showed their greatest range due to evaporative fractionation in depths down to 25 cm, whereas below 25 cm soil samples remained along the LMWL. Xylem isotopic samples were similar (at GC) to values during the earlier period yet showed increased spread and there was a greater portion of samples with a depleted signature. By late September, colder ground temperatures and advancing seasonal frost developed in soils while shrubs had senesced and become dormant. Near-surface soils were depleted in δ^2H and $\delta^{18}O$ compared to mid-August due to an influx of depleted rainwater (-141.84 to -181.09 δ^2H, -17.49 to -23.73 $\delta^{18}O$) associated with high magnitude rain events in late 2016 (Figure 4-7; Figure 4-S1; Figure 4-S2). Insufficient samples were collected in 2015 at GC, so no similar inference was made. Deep soil samples showed little evaporative effect at any time of year and samples typically remained along LMWL. In late September, when shrubs were dormant, xylem samples closely resembled soil water isotope values (Figure 4-9).

Replotting the dual-isotope data in lc-excess space more clearly shows the differences among the shrub and soil waters for different sampling periods (Figure 4-9).

While most data were collected at GC in 2016, data in 2015 at GC and 2016 at BB support the overall patterns. Near-surface bulk soil lc-excess values were less negative between early April to end-June when ground was frozen and during the initial stages of thaw. As thaw is prolonged and meltwater contributes a large volume of water to soils, soil water isotope composition is similar between the first two sampling periods. By mid-summer, near-surface lc-excess values became more negative (further from zero) while deeper and more well-mixed bulk soil values remained close to zero. Xylem lc-excess values for willow species position slightly closer to 0 ‰ than values from birch shrubs the majority of the time in GC, and most notably later in the study period, but not consistently at BB. Although rooting depths were similar between willow and birch shrubs, willows dominated wetter areas where soil water is assumed to be well-mixed.

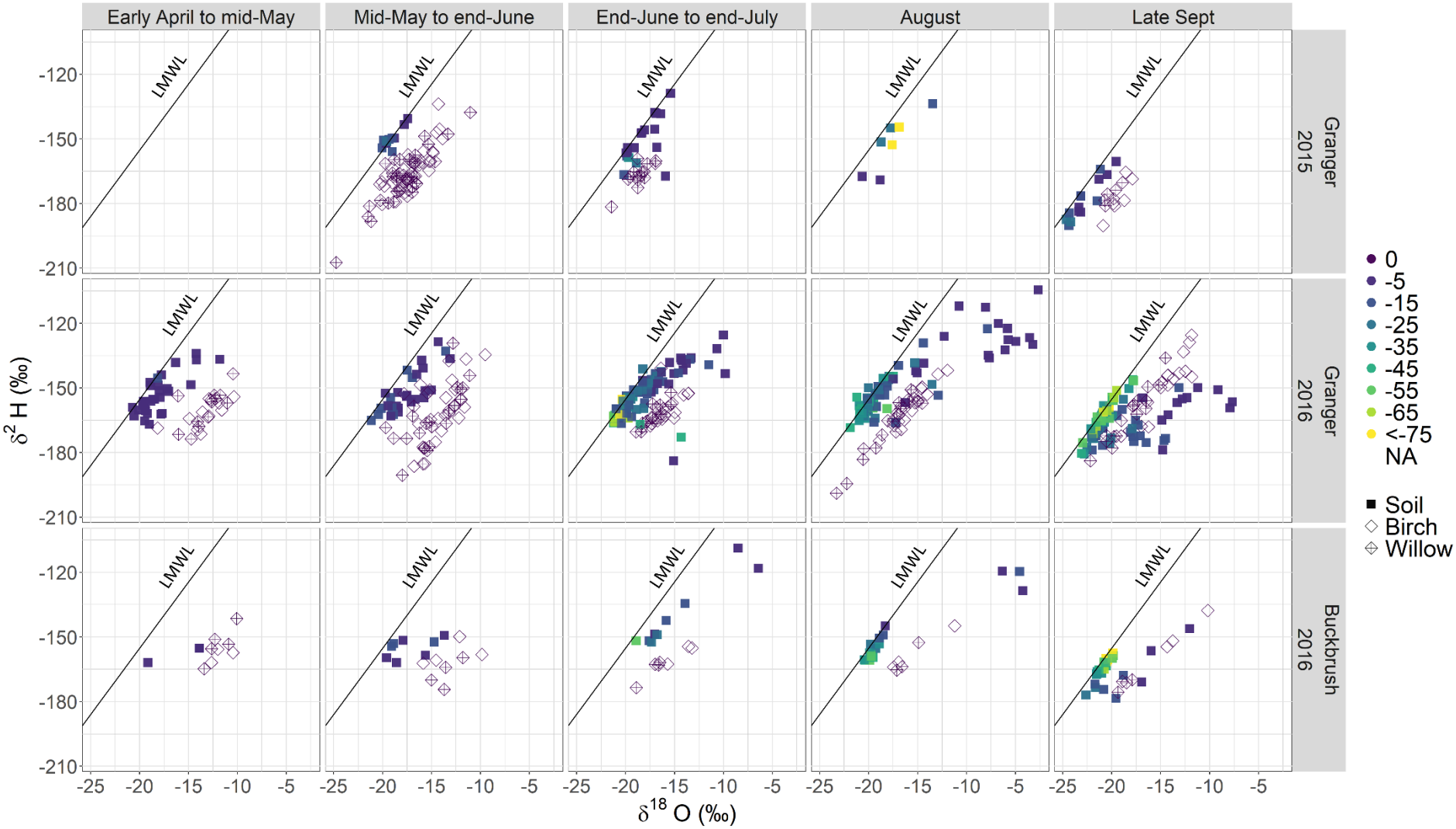

Figure 4-9. Seasonal progression of bulk soil and xylem water isotope signal.

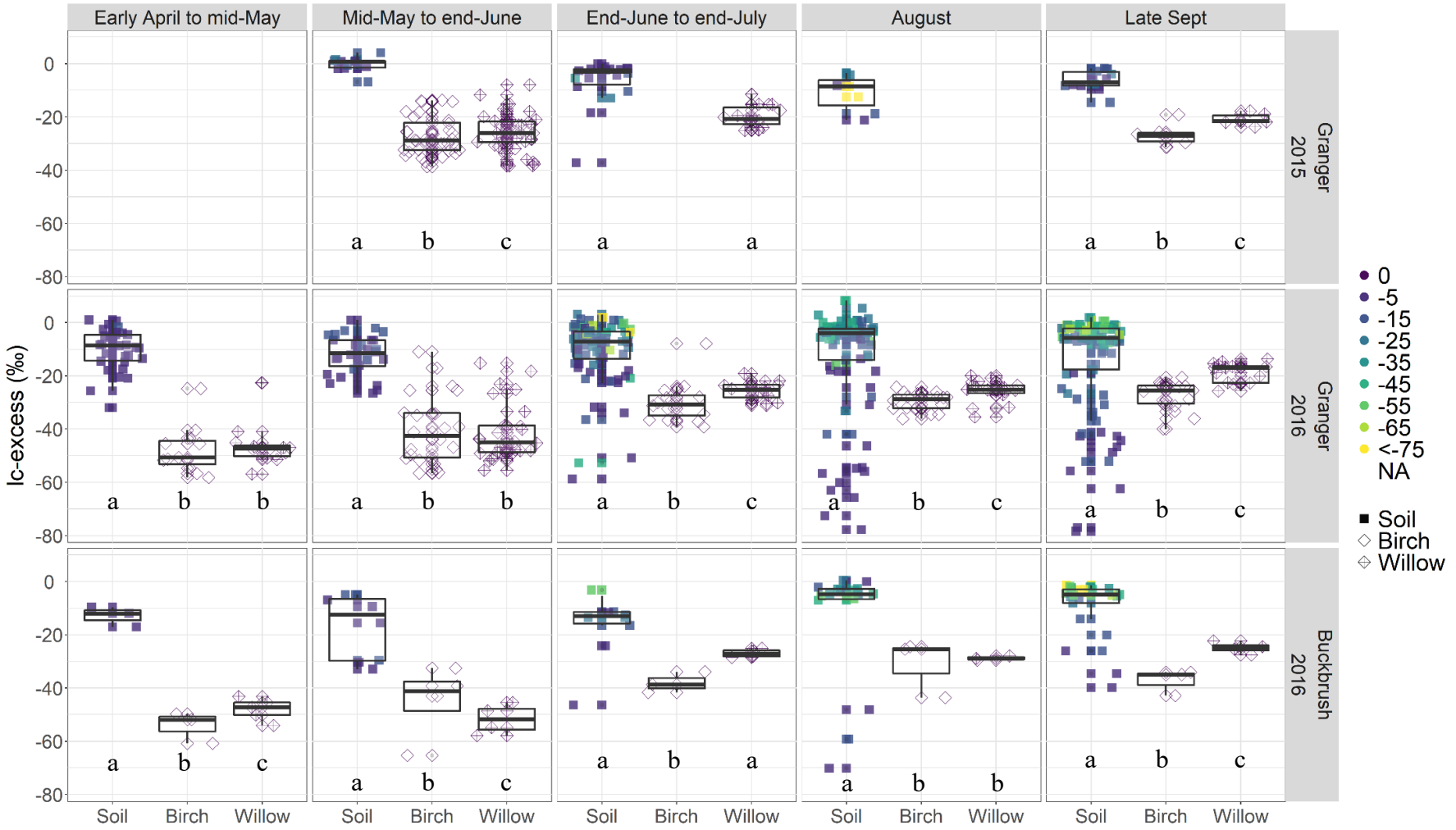

Figure 4-10. Comparisons of bulk soil water and xylem water lc-excess values across years. Results of significant difference tests are indicated with letters. Groups with no significant difference are displayed with the same letter.

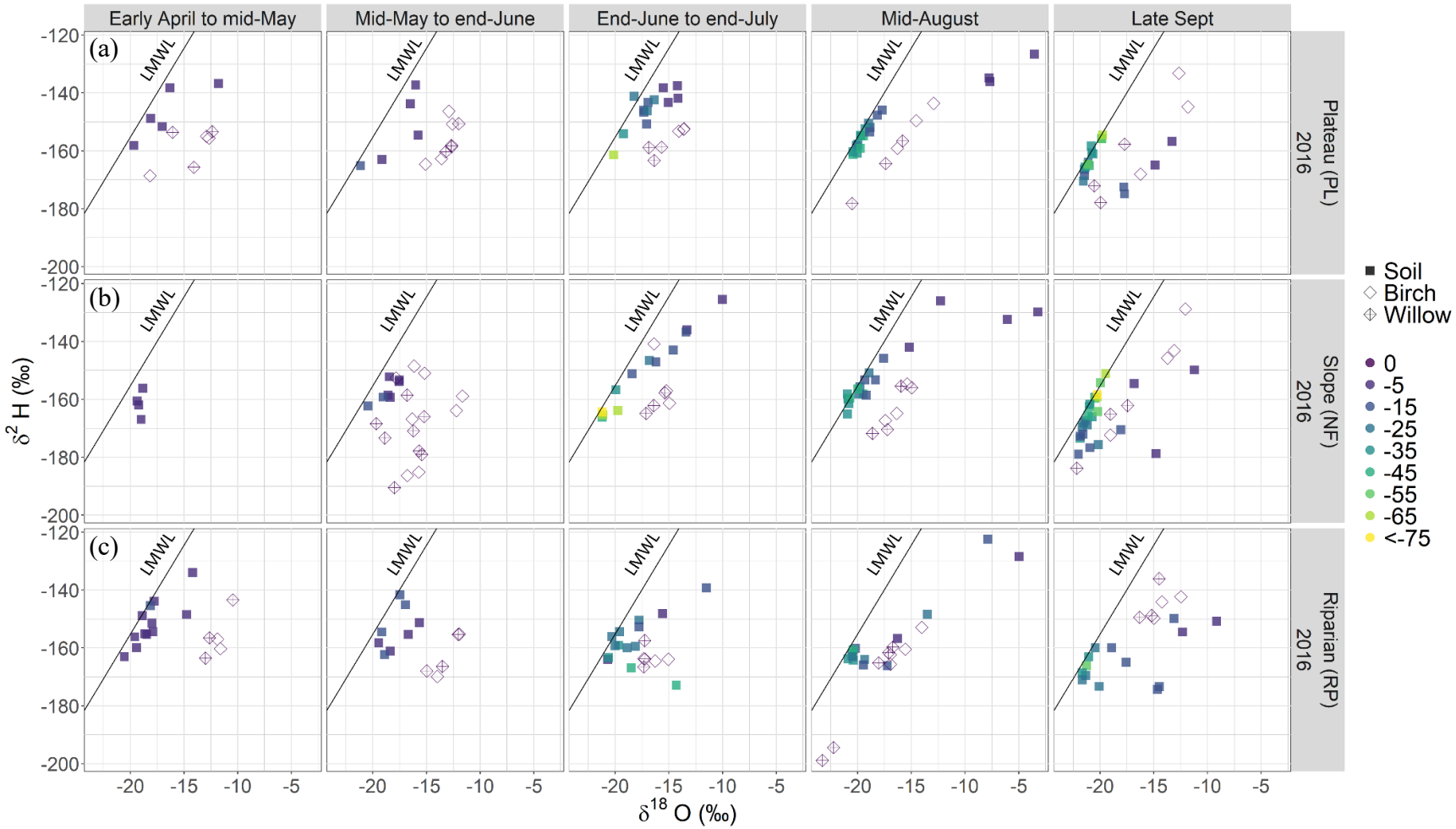

Figure 4-11. Bulk soil and xylem water δ2H and δ18O in dual isotope space for (a) plateau (PL), (b) north-facing slope (NF) and (c) riparian (RP) transects in 2016

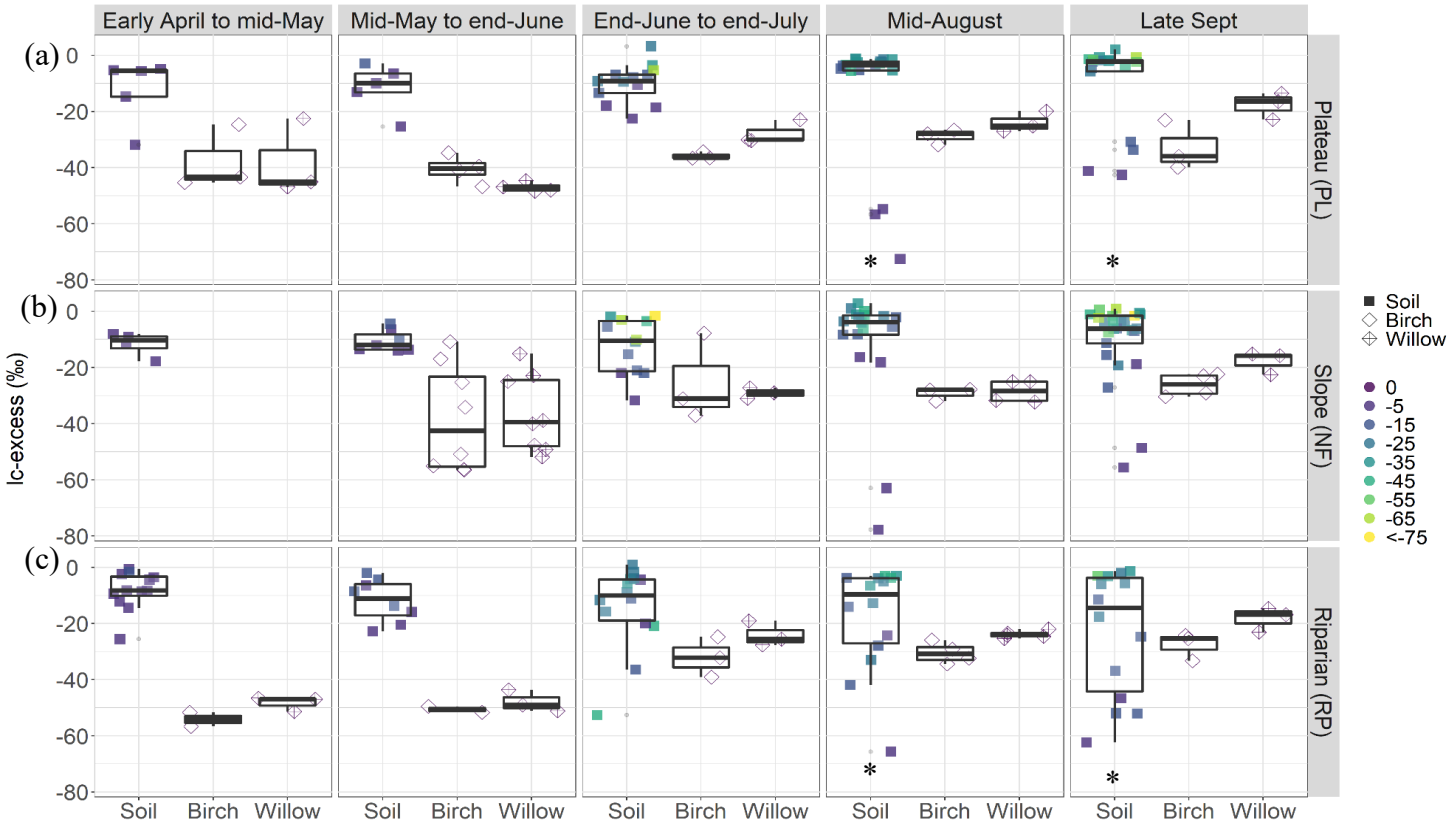

Figure 4-12. Boxplots of bulk soil and xylem water lc-excess for (a) plateau (PL), (b) north-facing slope (NF) and (c) riparian (RP) sites in 2016 at GC. Comparisons of bulk soil water and xylem water lc-excess values across periods of the growing season in 2016. Significant difference is denoted with an asterisk (*). Tests were run between xylem and soil populations in the same period but across HRU types. For all panels, birch and willow lc-excess was significantly different than soil.

4.4. DISCUSSION

4.4.1 General patterns in isotope composition and lc-excess

There is a considerable variability in isotope composition of all waters in space and time (Figure 4-6, Figure 4-7). Meteoric waters sampled over several years provide a robust LMWL for Southern Yukon and reflect expected differences in snow and rain along with temperature effects (Daansgard, 1964). While there is considerable variance in precipitation composition, stream and groundwater isotopes were dampened, suggesting considerable mixing. As previously reported, the lack of a strong depleted signals during snowmelt and overall stability of groundwater and streamflow isotopes suggests that subsurface pathways and mixing predominate (Carey et al., 2013; Piovano et al., 2019). Lc-excess was also similar among precipitation, soil, and groundwater, indicating that water recharging groundwater and streamflow water was not subject to significant evaporative fractionation (Figure 4-8).

Soil and xylem water exhibit large variability compared with streams and groundwater and are subject to evaporative fractionation (Figure 4-6, Table 4-2). Data from GC and BB indicate that soil water generally plots along the LMWL during snowmelt and later in the season at depth where soil moisture is typically high. As the season progresses, soil water samples begin to plot below the LMWL indicating non-equilibrium fractionation processes (Hervé-Fernández et al., 2016). This pattern is expected given that evapotranspiration exceeds rainfall during summer and plants source snowmelt recharge water to satisfy transpiration (Carey and Woo, 2001).

4.4.2 Does ecohydrological separation exist at this site and how does snowmelt influence soil and xylem water patterns?

Determination of TWW/ES presence or absence was based primarily on simultaneous or near-simultaneous sampling of bulk soil and xylem water isotopes in 2016, and to a lesser extent, in 2015. If two separate pools of water did not exist at GC, xylem water lc-excess would be expected to equal or be close to zero with an isotopic composition that plots along the LMWL (Goldsmith et al., 2012). Deviations from the LMWL occur due to non-equilibrium fractionation, whereas movement along the LMWL shows equilibrium fractionation (Kendall & McDonnell, 1998). Xylem water samples were distinct from soil water samples as they plotted separately from soil values in dual-isotope space (Figure 4-9) and had distinct temporal dynamics (Figure 4-7). Xylem and bulk soil water were most similar in the mid-growing season and furthest apart in the late spring (Figure 4-9) and there were distinct species differences between willow and birch shrubs. Throughout the sample period, lc-excess values of xylem water lc-excess for both birch and willow shrub species were much lower than 0 ‰ (Table 4-2) and typically significantly different from bulk soil lc-excess values (Figure 4-10).

A dual isotope approach was used along with lc-excess values to explore ES with additional information provided by the position of bulk soil water along the LMWL. Xylem water stable isotopes showed the greatest enrichment (particularly along the $\delta^{18}O$ axis) and distance from the LMWL prior to snowmelt with the majority of xylem water samples almost parallel to the LMWL. The influx of snowmelt water caused a notable shift in the bulk soil water isotope towards the LMWL (Figure 4-9). The effect of snowmelt water on

soil isotope water composition is an important input and causes a reset of the mobile water content within the soil volume (e.g., Oerter and Bowen, 2017).

From June through September in 2016, bulk soil water values showed evaporative fractionation in the near-surface to 25 cm depth. This result is in line with studies in cold areas with little seasonal difference in precipitation (Geris et al., 2015; Schmid et al., 2016), a snow-dominated, semi-arid environment with relatively little summer rainfall (McCutcheon et al., 2017), global re-analysis of cold regions isotope data (Amin et al., 2019) and other cold environments (Oerter and Bowen, 2017). As soil water became progressively more enriched due to evaporation after the melt period, birch and willow xylem water showed an increasing tendency to overlap with bulk soil water, particularly in the end-June to end-July peak growing period. In August, a period of prolonged drying occurred before sampling and soil waters were enriched along the developing SEL, particularly near-surface soils. However, xylem water results suggest that during this period of water stress, shrub species at GC may be accessing more tightly bound depleted water as there were some willow samples that were below -20 ‰ $\delta^{18}H$ and -180 ‰ $\delta^{2}H$; lower than any bulk water sampled at that time.

Following considerable late August rains, xylem water became more enriched as the bulk soil water became more negative (Figure 4-9), likely due to an influx of highly depleted rainwater. The relatively elastic behaviour observed in xylem water values (relative to bulk soil values) suggests that shrubs are likely opportunistic and use available water sources with no distinct preferences for immobile water, even during periods when soil moisture is limited. Shrubs at GC appear to be accessing sources of water more depleted

than any "blue water" sources or bulk soil water (Figure 4-9). A similar differentiation between the xylem water isotope signal and potential water sources was outlined at only one out of four sites (differing landscape positions) explored in Geris et al. (2017), while temporal dynamics remained similar across all four locations.

From the perspective of lc-excess, there is substantially greater overlap (Figure 4-10), which demonstrates that multiple lines of approach are necessary to fully understand the isotope signal between bulk soil and xylem water from a hydrological perspective (Qiu et al., 2019).

4.4.3 Does shrub size, landscape position or wetness influence bulk soil and xylem water isotope signals?

A distinguishing feature of GC is the difference in soil characteristics and vegetation community and size, based on landscape position (McCartney et al., 2006). To evaluate whether position along a wetness catena influences soil and plant water isotopes, the PL, NF, and RP sites at GC were compared in dual-isotope (Figure 4-11) and lc-excess space (Figure 4-12). The most striking contrasts between shrub size, elevation, and water table position occurs between the RP and PL sites. The NF transect is located at the mid-point between the other two sites, albeit with an increased persistence of snow cover and a shallower frost table due to its aspect (Figure 4-1) The influence of vegetation, elevation, and topography on bulk soil δ^2H and lc-excess at the RP and PL sites was partially detailed in Sprenger et al. (2018).

There were differences in sampling depths based on frozen ground (seasonally) and the RP site had a persistently high water table, which limited sampling at depth. Overall,

riparian soils were slightly more depleted than the NF and PL sites, yet there was considerable scatter in values for all sampling periods. These more depleted values are related to the initial influx of depleted snowmelt water having a stronger influence on bulk soil isotopic composition at RP than precipitation. Bulk soil water δ^2H was negatively correlated to 2-day antecedent precipitation at 5 cm but very weakly correlated with antecedent rainfall for 7-30 days prior to sampling. At soil depths greater than 15 cm, correlations with bulk soil were less than 0.2, suggesting that the RP was typically disconnected from infiltrating rainfall (Sprenger et al., 2018). RP $\delta^{18}O$ and δ^2H were more tightly clustered along the LMWL at depths greater than 15 cm (Figure 4-11), indicating that water was particularly well mixed. At PL, positive correlations were much stronger between antecedent precipitation δ^2H (2-30 day) and bulk soil δ^2H values at 5 cm and 25 cm depth, and relatively strong between 14-30 day antecedent precipitation δ^2H and bulk soil δ^2H (Table 4-S3). This coherence between precipitation δ^2H and bulk soil δ^2H at PL, particularly in contrast to RP, indicates a much greater importance of precipitation on the bulk soil water isotope signal in a more elevated, exposed shrub tundra environment where canopy interception is minimal. The significant differences between RP and PL soil lc-excess provide some evidence that flowpath distribution affects soil water isotope patterns through mixing of water ages while canopy interception may limit the amount of rainfall that infiltrates into the ground.

Sprenger et al. (2018) also demonstrated that 30-day average potential evapotranspiration (PET) and the maximum kinetic fractionation effects were not necessarily synchronized in GC and other high latitude catchments. This delayed kinetic

fractionation was linked to the highly depleted soil values observed in fall (Sprenger et al., 2018) We hypothesise that an influx of depleted rainwater contributed to this effect at GC in 2016. This depletion was observed for soil water in dual isotope space at all three sites in late September, along with an enriched xylem water signal at RP (Figure 4-11). Aggregating samples over entire seasons or years is not uncommon in studies investigating ES (Brooks et al., 2009; Evaristo et al., 2015), yet rainfall can alter soil water isotope values (Sprenger et al., 2016, 2017; Figure 4-S2) and spatiotemporal variability exerts a strong influence on isotope values in some environments (Soulsby, Birkel & Tetzlaff, 2016; Geris et al., 2017; Benettin et al., 2018; Allen et al., 2019). This brings into question the validity of analyzing aggregates of isotope data (in space or time), and to what extent rainfall events or other episodic changes can bias longer-term patterns in contrasting HRUs within the same catchment.

Xylem water isotope values in dual isotope and lc-excess space showed very similar behaviour to what was observed within GC and BB catchments (Figure 4-9 and Figure 4-10) and across HRUs of GC catchment (Figure 4-11 and Figure 4-12), with significant differences between lc-excess of xylem and bulk soil water at all sites (Figure 4-12). For all three sites, the willow xylem water lc-excess was slightly closer to 0 ‰ than birch lc-excess (exception in mid-May to end-June at PL), suggesting a link between more meteoric water in wetter soils typically colonized by willow rather than birch shrubs. The relationship between bulk soil water and xylem water in these three landscape units confirmed that patterns of increasingly positive lc-excess for bulk soil and xylem water throughout the growing season are ubiquitous within this catchment. The drier soils and

dwarf shrubs at PL were directly contrasted with the wetter soils and taller vegetation in the RP, with the only significant differences between soil water lc-excess from August to late September.

4.5 CONCLUSIONS

The application of stable isotopes in hydrological research has become widespread. Whereas traditional application focussed on runoff pathways and storage estimates, more recent work has sought to understand the role of vegetation in cycling water and whether there are separate sources of water for transpiration ("green water") and runoff ("blue water"). In this well-studied headwater catchment, results do not fully support the concept of ecohydrological separation or the "two water worlds" hypothesis. "Blue water" has an isotopic composition that lies compressed along the LMWL and reflects a mixture of precipitation sources that have not experienced considerable evaporation. In contrast, plant xylem and near-surface soil water fall off the LMWL reflecting an evaporative signature with considerably negative lc-excess values. Plant xylem water shifts during the year, in tandem with near-surface soil water that shrubs are presumed to be sampling during the peak of the growing season. While there are some very depleted xylem water values that suggest plants are sampling more tightly-bound, immobile water and ES, most often xylem water shifts towards the composition of near-surface soil water, suggesting there is a relatively rapid response to mobile and available water in the rooting zone.

Overall, there is considerable intra-catchment and within-year variability and variance in soil and xylem water isotopes, suggesting a complex interaction between

antecedent conditions, soil wetness, and plant water use strategies that explain stable isotopes in soils and vegetation. In addition, there appears to be a slight species differentiation in lc-excess, suggesting willows and birches sample slightly different waters. Whether this is simply a function of different rooting architecture or physiological processes is unknown. While vegetation is shifting rapidly in northern environments and shrubs are becoming more widespread, it is unclear as to the effect of this on streamflow and groundwater isotopic signatures, which seem to appear insensitive in GC near-surface processes. As integrated ecohydrological isotopic studies are new, continued research is necessary to evaluate the efficacy of isotopes in tracking sources of water in the critical zone.

References

Allen, S. T., Kirchner, J. W., Braun, S., Siegwolf, R. T., & Goldsmith, G. R. (2019). Seasonal origins of soil water used by trees. *Hydrology and Earth System Sciences*, *23*(2), 1199-1210.

Amin, A., Zuecco, G., Geris, J., Schwendenmann, L., McDonnell, J. J., Borga, M., & Penna, D. (2019). Depth distribution of soil water sourced by plants at the global scale: a new direct inference approach. *Ecohydrology*, e2177.

Benettin, P., Volkmann, T. H., von Freyberg, J., Frentress, J., Penna, D., Dawson, T. E., & Kirchner, J. W. (2018). Effects of climatic seasonality on the isotopic composition of evaporating soil waters. Hydrology and Earth System Sciences 22 (5): 2881-2890.

Berry, Z. C., Evaristo, J., Moore, G., Poca, M., Steppe, K., Verrot, L., Asbjornsen, H., Borma, L. S., Bretfeld, M., Herve-Fernandez, P., Seyfried, M., Schwendenmann, L., Sinacore, K., De Wispelaere, L., & McDonnell, J.J. (2017). The two water worlds hypothesis: Addressing multiple working hypotheses and proposing a way forward, Ecohydrology, e1843, 20. doi:10.1002/eco.1843.

Bertrand G, Masini J, Goldscheider N, Meeks J, Lavastre V, Celle-Jeanton H, Gobat J, Hunkeler D. (2014). Determination of spatiotemporal variability of tree water uptake using stable isotopes (δ18O, δ 2H) in an alluvial system supplied by a high-altitude watershed, Pfynforest, Switzerland. Ecohydrology 7: 319–333. doi:10.1002/eco.1347

Birkel, C., Soulsby, C., & Tetzlaff, D. (2011). Modelling catchment-scale water storage dynamics: Reconciling dynamic storage with tracer-inferred passive storage. Hydrological Processes 25(25): 3924-3936.

Blume-Werry, G., Kreyling, J., Laudon, H., & Milbau, A. (2016). Short-term climate change manipulation effects do not scale up to long-term legacies: Effects of an absent snow cover on boreal forest plants. Journal of Ecology 104 (6): 1638-1648.

Bonfils, C. J. W., Phillips, T. J., Lawrence, D. M., Cameron-Smith, P., Riley, W. J., & Subin, Z. M. (2012). On the influence of shrub height and expansion on northern high latitude climate. Environmental Research Letters 7(1): 015503.

Boucher, J. L., & Carey, S. K. (2010). Exploring runoff processes using chemical, isotopic and hydrometric data in a discontinuous permafrost catchment. Hydrology Research, 41(6), 508-519.

Bowling, D. R., Schulze, E. S., & Hall, S. J. (2017). Revisiting streamside trees that do not use stream water: can the two water worlds hypothesis and snowpack isotopic effects explain a missing water source?. Ecohydrology 10(1): e1771.

Brantley, S. L., Eissenstat, D. M., Marshall, J. A., Godsey, S. E., Balogh-Brunstad, Z., Karwan, D. L., & Chadwick, O. (2017). Reviews and syntheses: on the roles trees play in building and plumbing the critical zone. Biogeosciences (Online), 14(22).

Brooks, J.R., Barnard, H.R., Coulombe, R., & McDonnell, J.J. (2009). Ecohydrologic separation of water between trees and streams in a Mediterranean climate. Nature Geoscience 3: 100–104. doi:10.1038/NGEO722

Brown, J. H., Whitham, T. G., Ernest, S. M., & Gehring, C. A. (2001). Complex species interactions and the dynamics of ecological systems: long-term experiments. Science, 293(5530), 643-650.

Carey, S. K., & Woo, M. K. (2001). Slope runoff processes and flow generation in a subarctic, subalpine catchment. Journal of Hydrology 253 (1-4): 110-129.

Carey, S. K. (2003). Dissolved organic carbon fluxes in a discontinuous permafrost subarctic alpine catchment. Permafrost and Periglacial Processes 14 (2): 161-171.

Carey, S. K., Tetzlaff, D., Seibert, J., Soulsby, C., Buttle, J., Laudon, H., McDonnell, J.J., McGuire, K., Caissie, D., Shanley, J., Kennedy, M., Devito, K., & Pomeroy, J.W. (2010). Inter-comparison of hydro-climatic regimes across northern catchments: Synchronicity, resistance and resilience. Hydrological Processes 24(24): 3591-3602.

Carey, S. K., Boucher, J. L., & Duarte, C. M. (2013). Inferring groundwater contributions and pathways to streamflow during snowmelt over multiple years in a discontinuous permafrost subarctic environment (Yukon, Canada). Hydrogeology Journal, 21(1), 67-77.

Carey, S. K., Tetzlaff, D., Buttle, J., Laudon, H., McDonnell, J., McGuire, K., Seibert, J., Soulsby, C., & Shanley, J. (2013). Use of color maps and wavelet coherence to discern seasonal and interannual climate influences on streamflow variability in northern catchments. Water Resources Research, 49(10), 6194-6207.

Chapin, F.S., Sturm, M., Serreze, M.C., McFadden, J.P., Key, J.R., Lloyd, A.H., McGuire, A.D., Rupp, T.S., Lynch, A.H., Schimel, J.P., & Beringer, J. (2005). Role of land-surface changes in Arctic summer warming. science 310(5748): 657-660.

Dansgaard, W. (1964). Stable isotopes in precipitation. Tellus 16 (4): 436-468.

Domine, F., Barrere, M., Sarrazin, D., Morin, S., & Arnaud, L. (2015). Automatic monitoring of the effective thermal conductivity of snow in a low-Arctic shrub tundra.

Dubbert, M., & Werner, C. (2019). Water fluxes mediated by vegetation: emerging isotopic insights at the soil and atmosphere interfaces. New Phytologist 221(4), 1754-1763.

Evaristo, J., Jasechko, S., & McDonnell, J.J. (2015). Global separation of plant transpiration from groundwater and streamflow. Nature 525:91–94. doi:10.1038/nature14983

Evaristo, J., McDonnell, J. J., Scholl, M. A., Bruijnzeel, L. A., & Chun, K. P. (2016). Insights into plant water uptake from xylem-water isotope measurements in two tropical catchments with contrasting moisture conditions. Hydrological Processes, 30(18), 3210-3227.

Evaristo, J., Kim, M., van Haren, J., Pangle, L. A., Harman, C. J., Troch, P. A., & McDonnell, J. J. (2019). Characterizing the fluxes and age distribution of soil water, plant water, and deep percolation in a model tropical ecosystem. Water Resources Research 55(4): 3307-3327.

Geris, J., Tetzlaff, D., McDonnell, J., Anderson, J., Paton, G., & Soulsby, C. (2015). Ecohydrological separation in wet, low energy northern environments? A preliminary assessment using different soil water extraction techniques. Hydrological Processes 29(25): 5139-5152.

Geris, J., Tetzlaff, D., McDonnell, J. J., & Soulsby, C. (2017). Spatial and temporal patterns of soil water storage and vegetation water use in humid northern catchments. Science of the Total Environment 595: 486-493.

Godsey, S. E., Kirchner, J. W., & Clow, D. W. (2009). Concentration–discharge relationships reflect chemostatic characteristics of US catchments. Hydrological Processes: An International Journal, 23(13), 1844-1864.

Goldsmith, G.R., Muñoz-Villers, L.E., Holwerda, F., McDonnell, J.J., Asbjornsen, H., & Dawson, T.E. (2012). Stable isotopes reveal linkages among ecohydrological processes in a seasonally dry tropical montane cloudforest. Ecohydrology 5: 779–790.

Grolemund, g., & Wickham, H. (2011). Dates and Times Made Easy with lubridate. Journal of Statistical Software, 40(3), 1-25. URL http://www.jstatsoft.org/v40/i03/.

Guo, W., Liu, H., Anenkhonov, O. A., Shangguan, H., Sandanov, D. V., Korolyuk, A. Y., Hu, G., & Wu, X. (2018). Vegetation can strongly regulate permafrost degradation at its southern edge through changing surface freeze-thaw processes. Agricultural and Forest Meteorology 252, 10-17.

Harrell, F.E.(Jr) with contributions from Charles Dupont and many others. (2020).

Hmisc: Harrell Miscellaneous. R package version 4.3-1.https://CRAN.R-project.org/package=Hmisc

Hendry, M. J., Schmeling, E., Wassenaar, L. I., Barbour, S. L., & Pratt, D. (2015). Determining the stable isotope composition of pore water from saturated and unsaturated zone core: improvements to the direct vapour equilibration laser spectrometry method. Hydrology and Earth System Sciences 19 (11): 4427.

Hervé-Fernández, P., Oyarzún, C., Brumbt, C., Huygens, D., Bodé, S., Verhoest, N. E. C., & Boeckx, P. (2016). Assessing the 'two water worlds' hypothesis and water sources for native and exotic evergreen species in south-central Chile. Hydrological Processes 30(23): 4227-4241.

Hirsch, R., & Helsel, D. R. (1992). Statistical methods in water resources. Studies in Environmental Science, Elsevier Science & Technology, New York, NY.

International Atomic Energy Agency & Global Network of Isotopes in Precipitation. (2014). IAEA/GNIP precipitation sampling guide, V2.02. http://www-naweb.iaea.org/napc/ih/IHS_resources_gnip_faq.html (Last accessed: 1 March 2020).

Jorgenson, M. T., V. Romanovsky, J. Harden, Y. Shur, J. O'Donnell, E. A. G. Schuur, M. Kanevskiy, & Marchenko, S. (2010), Resilience and vulnerability of permafrost to climate change. Can. J. For. Res.-Revue, Canadienne De Recherche Forestiere 40 (7): 1219–1236.

Kassambara, A. (2019). ggpubr: 'ggplot2' Based Publication Ready Plots. R package version 0.2.4. https://CRAN.R-project.org/package=ggpubr

Kendall, C., & McDonnell, J.J. (Eds.) (1998). Isotope Tracers in Catchment Hydrology. Elsevier Science B.V., Amsterdam, 839 p.

Knighton, J., Souter-Kline, V., Volkman, T., Troch, P. A., Kim, M., Harman, C., Morris, C., Buchanan, B., & Walter, M. T. (2019). Seasonal and topographic variations in ecohydrological separation within a small, temperate, snow-influenced catchment. Water Resources Research, 55(8), 6417-6435.

Krogh, S. A., Pomeroy, J. W., & Marsh, P. (2017). Diagnosis of the hydrology of a small Arctic basin at the tundra-taiga transition using a physically based hydrological model. Journal of Hydrology 550: 685-703.

Krogh, S. A., & Pomeroy, J. W. (2018). Recent changes to the hydrological cycle of an Arctic basin at the tundra–taiga transition. Hydrology and Earth System Sciences 22 (7): 3993.

Lafleur, P. M., & Humphreys, E. R. (2018). Tundra shrub effects on growing season energy and carbon dioxide exchange. Environmental Research Letters, 13(5), 055001.

Landwehr, J. M., & Coplen, T. B. (2006). Line-conditioned excess: a new method for characterizing stable hydrogen and oxygen isotope ratios in hydrologic systems. In International conference on isotopes in environmental studies (pp. 132-135). Vienna: IAEA.

Lavergne, A., Graven, H., De Kauwe, M. G., Keenan, T. F., Medlyn, B. E., & Prentice, I. C. (2019). Observed and modelled historical trends in the water-use efficiency of plants and ecosystems. Global change biology 25 (7): 2242-2257.

Leuzinger, S., Luo, Y., Beier, C., Dieleman, W., Vicca, S., & Körner, C. (2011). Do global change experiments overestimate impacts on terrestrial ecosystems?. Trends in ecology & evolution, 26(5), 236-241.

Lewkowicz, A. G., & Ednie, M. (2004). Probability mapping of mountain permafrost using the BTS method, Wolf Creek, Yukon Territory, Canada. Permafrost and Periglacial Processes 15(1): 67-80.

Li, S. G., Romero-Saltos, H., Tsujimura, M., Sugimoto, A., Sasaki, L., Davaa, G., & Oyunbaatar, D. (2007). Plant water sources in the cold semiarid ecosystem of the upper Kherlen River catchment in Mongolia: A stable isotope approach. Journal of Hydrology, 333 (1): 109-117.

Loranty, M. M., Abbott, B. W., Blok, D., Douglas, T. A., Epstein, H. E., Forbes, B. C., Jones, B.M., Kholodov, A.L., Kropp, H., Malhotra, A., Mamet, S. D., Myers-Smith, I.H., Natali, S.M., O'Donnell, J.A., Phoenix, G.K., Rocha, A.V., Sonnentag, O., Tape, K.D. & Walker, D. (2018). Reviews and syntheses: Changing ecosystem influences on soil thermal regimes in northern high-latitude permafrost regions. Biogeosciences 15 (17): 5287-5313.

McCartney, S. E., Carey, S. K., & Pomeroy, J. W. (2006). Intra-basin variability of snowmelt water balance calculations in a subarctic catchment. Hydrological Processes: An International Journal 20 (4): 1001-1016.

McCutcheon, R. J., McNamara, J. P., Kohn, M. J., & Evans, S. L. (2017). An evaluation of the ecohydrological separation hypothesis in a semiarid catchment. Hydrological Processes 31 (4): 783-799.

McDonnell, J.J. 2014. The two water worlds hypothesis: ecohydrological separation of water between streams and trees? WIREs Water 1:323–329.

McFadden, J. P., Eugster, W., & Chapin III, F. S. (2003). A regional study of the controls on water vapor and CO2 exchange in arctic tundra. Ecology, 84(10), 2762-2776.

Milton Bache, S., & Wickham, H. (2014). magrittr: A Forward-Pipe Operator for R. R package version 1.5. https://CRAN.R-project.org/package=magrittr

Myers-Smith, I. H., & Hik, D. S. (2013). Shrub canopies influence soil temperatures but not nutrient dynamics: an experimental test of tundra snow–shrub interactions. Ecology and Evolution, 3(11), 3683-3700.

Natali, S. M., Schuur, E. A., Mauritz, M., Schade, J. D., Celis, G., Crummer, K. G., Johnston, C., Krapek, J., Pegoraro, E., Salmon, V.G., & Webb, E. E. (2015). Permafrost thaw and soil moisture driving CO2 and CH4 release from upland tundra. Journal of Geophysical Research: Biogeosciences 120 (3): 525-537.

O'Donnell, J. A., Harden, J. W., McGuire, A. D., & Romanovsky, V. E. (2011). Exploring the sensitivity of soil carbon dynamics to climate change, fire disturbance and permafrost thaw in a black spruce ecosystem. Biogeosciences. 8: 1367-1382, 8, 1367-1382.

Penna, D., Hopp, L., Scandellari, F., Allen, S. T., Benettin, P., Beyer, M., Geris, J., Klaus, J., Marshall, J.D., Schwendenmann, L., Volkmann, T. H. M., Freiin von Freyberg, J., Amin, A., Ceperley, N., Engel, M., Frentress, J., Giambastiani, Y., McDonnell, J.J., Zuecco, G., Llorens, P., Siegwolf, R.T.W., Dawson, T.E., & Kirchner, J.W. (2018). Ideas and perspectives: Tracing terrestrial ecosystem water fluxes using hydrogen and oxygen stable isotopes-challenges and opportunities from an interdisciplinary perspective. Biogeosciences 15 (21): 6399-6415.

Phoenix, G. K., Emmett, B. A., Britton, A. J., Caporn, S. J., Dise, N. B., Helliwell, R., Jones, l., Leake, J.R., Leith, I.D., Sheppard, L.J., Sowerby, A., Pilkington, m.g., Roew, E.C., Ashmore, M.R., & Power, S.A. (2012). Impacts of atmospheric nitrogen deposition: responses of multiple plant and soil parameters across contrasting ecosystems in long-term field experiments. Global Change Biology 18(4): 1197-1215.

Piovano, T. I., Tetzlaff, D., Carey, S. K., Shatilla, N. J., Smith, A., & Soulsby, C. (2019). Spatially distributed tracer-aided runoff modelling and dynamics of storage and water ages in a permafrost-influenced catchment. Hydrology and Earth System Sciences 23: 2507–2523. doi: 10.5194/hess-23-2507-2019

Pomeroy, J. W., Toth, B., Granger, R. J., Hedstrom, N. R., & Essery, R. L. H. (2003). Variation in surface energetics during snowmelt in a subarctic mountain catchment. Journal of Hydrometeorology, 4(4), 702-719.

Pomeroy, J. W., Bewley, D. S., Essery, R. L. H., Hedstrom, N. R., Link, T., Granger, R. J., Sicart, J.E., Ellis, C.R., & Janowicz, J. R. (2006). Shrub tundra snowmelt. Hydrological Processes: An International Journal 20 (4):923-941.

Qiu, X., Zhang, M., Wang, S., Evaristo, J., Argiriou, A. A., Guo, R., Chen, R., Hongfei, M., Cunwei, C., & Qu, D. (2019). The test of the ecohydrological separation hypothesis in a dry zone of the northeastern Tibetan Plateau. Ecohydrology 12 (3): e2077.

Quinton, W. L., Carey, S. K., & Goeller, N. T. (2004). Snowmelt runoff from northern alpine tundra hillslopes: major processes and methods of simulation.

R Core Team (2019). R: A language and environment for statistical computing. R Foundation for Statistical Computing, Vienna, Austria. URL https://www.R-project.org/.

Rasouli, K., Pomeroy, J. W., Janowicz, J. R., Williams, T. J., & Carey, S. K. (2019). A long-term hydrometeorological dataset (1993–2014) of a northern mountain basin: Wolf Creek Research Basin, Yukon Territory, Canada. Earth System Science Data 11(1): 89-100.

Shatilla, N. J., & Carey, S. K. (2019). Assessing inter-annual and seasonal patterns of DOC and DOM quality across a complex alpine watershed underlain by discontinuous permafrost in Yukon, Canada. Hydrology & Earth System Sciences 23 (9).

Smith, A. A., Tetzlaff, D., & Soulsby, C. (2019). Using StorAge Selection functions to quantify ecohydrological controls on the time-variant age of evapotranspiration, soil water, and recharge. Hydrology and Earth System Sciences 23: 3319-3334. doi: 10.5194/hess-23-3319-2019

Soulsby, C., Birkel, C., & Tetzlaff, D. (2016). Modelling storage-driven connectivity between landscapes and riverscapes: towards a simple framework for long-term ecohydrological assessment. Hydrological Processes, 30(14), 2482-2497.

Sprenger, M., Leistert, H., Gimbel, K., & Weiler, M. (2016). Illuminating hydrological processes at the soil-vegetation-atmosphere interface with water stable isotopes. Reviews of Geophysics 54: 674–704, doi:10.1002/ 2015RG000515.

Sprenger, M., Tetzlaff, D., & Soulsby, C. (2017) Soil water stable isotopes reveal evaporation dynamics at the soil-plant-atmosphere interface of the critical zone. Hydrology and Earth System Sciences 21: 3839-3858. doi.org/10.5194/hess-21-3839-2017

Sprenger, M., Tetzlaff, D., Buttle, J., Carey, S. K., McNamara, J. P., Laudon, H., Shatilla, N.J., & Soulsby, C. (2018). Storage, mixing, and fluxes of water in the critical zone across northern environments inferred by stable isotopes of soil water. Hydrological processes 32 (12): 1720-1737.

Stichler, W., Rauert, W., & Martinec, J. (1981). Environmental isotope studies of an alpine snowpack. Hydrology Research 12 (4-5): 297-308.

Subin, Z. M., Koven, C. D., Riley, W. J., Torn, M. S., Lawrence, D. M., & Swenson, S. C. (2013). Effects of soil moisture on the responses of soil temperatures to climate change in cold regions. Journal of Climate 26 (10): 3139-3158.

Tetzlaff, D., Seibert, J., McGuire, K. J., Laudon, H., Burns, D. A., Dunn, S. M., & Soulsby, C. (2009). How does landscape structure influence catchment transit time across different geomorphic provinces?. Hydrological Processes: An International Journal, 23(6), 945-953.

Tetzlaff, D., Birkel, C., Dick, J., Geris, J., & Soulsby, C. (2014). Storage dynamics in hydropedological units control hillslope connectivity, runoff generation, and the evolution of catchment transit time distributions. Water resources research 50(2): 969-985.

Tetzlaff, D., Buttle, J., Carey, S. K., McGuire, K., Laudon, H., & Soulsby, C. (2015). Tracer-based assessment of flow paths, storage and runoff generation in northern catchments: A review. Hydrological Processes 29 (16), 3475–3490. doi: 10.1002/hyp.10412

Teufel, B., Sushama, L., Arora, V. K., & Verseghy, D. (2019). Impact of dynamic vegetation phenology on the simulated pan-Arctic land surface state. Climate dynamics, 52(1-2), 373-388.

Teufel, B., & Sushama, L. (2019). Abrupt changes across the Arctic permafrost region endanger northern development. Nature Climate Change, 9(11), 858-862.

Tierney, N., Cook, D., McBain, M., & Fay, C. (2020). naniar: Data Structures, Summaries, and Visualisations for Missing Data. R package version 0.5.0. https://CRAN.R-project.org/package=naniar

van den Bergh, T., Körner, C., & Hiltbrunner, E. (2018). Alnus shrub expansion increases evapotranspiration in the Swiss Alps. Regional Environmental Change 18(5): 1375-1385.

Vowles, T., & Björk, R. G. (2019). Implications of evergreen shrub expansion in the Arctic. Journal of Ecology, 107(2), 650-655.

Wallace, C. A., & Baltzer, J. L. (2019). Tall Shrubs Mediate Abiotic Conditions and Plant Communities at the Taiga–Tundra Ecotone. Ecosystems, 1-14.

Walvoord, M. A., & Striegl, R. G. (2007). Increased groundwater to stream discharge from permafrost thawing in the Yukon River basin: Potential impacts on lateral export of carbon and nitrogen. Geophysical Research Letters 34(12).

Walvoord, M. A., & Kurylyk, B. L. (2016). Hydrologic impacts of thawing permafrost—A review. Vadose Zone Journal 15 (6).

Wassenaar, L. I., Hendry, M. J., Chostner, V. L., & Lis, G. P. (2008). High resolution pore water δ2H and δ18O measurements by H2O (liquid)− H2O (vapor) equilibration laser spectroscopy. Environmental science & technology 42(24): 9262-9267.

Wickham, H. (2016). ggplot2: Elegant Graphics for Data Analysis. Springer-Verlag New York.

Wickham, H., & Henry, L. (2019). tidyr: Tidy Messy Data. R package version 1.0.0. https://CRAN.R-project.org/package=tidyr

Wickham, H., François, R., Henry, L., & Müller, K. (2019). dplyr: A Grammar of Data Manipulation. R package version 0.8.3. https://CRAN.R-project.org/package=dplyr

Wilke, C.O. (2019). cowplot: Streamlined Plot Theme and Plot Annotations for 'ggplot2'. R package version 1.0.0. https://CRAN.R-project.org/package=cowplot

Wolkovich, E. M., Cook, B. I., Allen, J. M., Crimmins, T. M., Betancourt, J. L., Travers, S. E., Pau, S., Regetz, J., Davies, T.J., Kraft, N.J.B., Ault, T.R., Bolmgren, K., Mazer, S.J., McCabe, G.J., McGill, B.J., Parmesan, C., Salamin, N., Schwartz, M.D., & Cleland, E.E.. (2012). Warming experiments underpredict plant phenological responses to climate change. Nature 485(7399): 494-497.

Woo, M. K. (1990). Consequences of climatic change for hydrology in permafrost zones. Journal of cold regions engineering 4 (1): 15-20.

Wookey, P.A., Aerts, R., Bardgett, R.D., Baptist, F., Bråthen, K.A., Cornelissen, J.H., Gough, L., Hartley, I.P., Hopkins, D.W., Lavorel, S., & Shaver, G.R. (2009). Ecosystem feedbacks and cascade processes: understanding their role in the responses of Arctic and alpine ecosystems to environmental change. Global Change Biology 15(5): 1153-1172.

Yang, Z. P., Ou, Y. H., Xu, X. L., Zhao, L., Song, M. H., & Zhou, C. P. (2010). Effects of permafrost degradation on ecosystems. Acta Ecologica Sinica 30 (1): 33-39.

Zwieback, S., Chang, Q., Marsh, P., & Berg, A. (2019). Shrub tundra ecohydrology: rainfall interception is a major component of the water balance. Environmental Research Letters, 14(5), 055005.

Supplemental Information

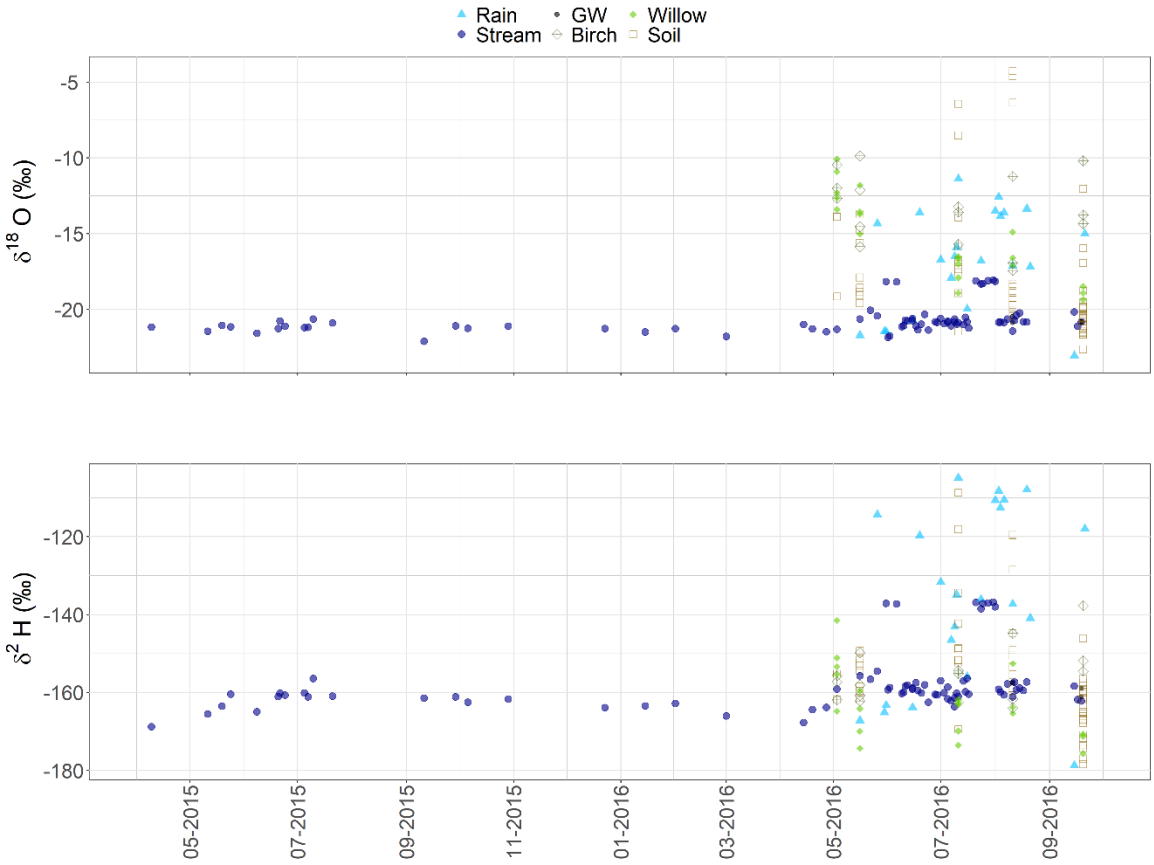

Figure 4-S1. Time series of $\delta^{18}O$ and $\delta^{2}H$ from Buckbrush (BB) Creek spanning 2015 to 2016.

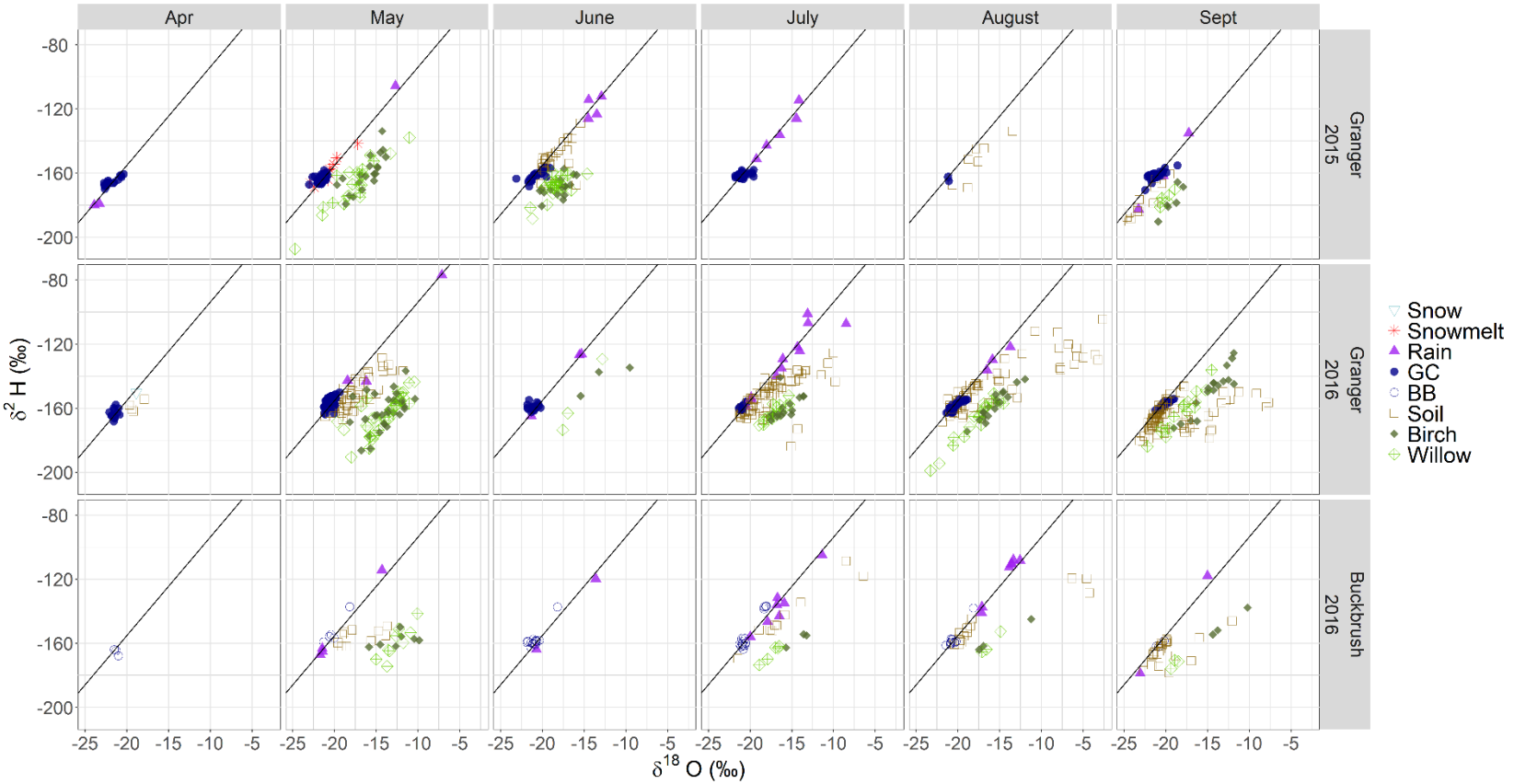

Figure 4-S2. Snow (light blue, empty downward triangle), snowmelt (red, asterisk), rain (purple, triangle), stream water at GC (dark blue, circle), BB (dark blue, empty circle), bulk soil (brown, empty square) birch (dark green, diamond) and willow (green, diamond with inset cross) isotope composition shown in dual isotope space for every month at Granger Basin in 2015-2016 and at Buckbrush basin in 2016.

Figure 4-S3. Close-up of modified IAEA/GNIP-compliant isotope precipitation gauges deployed in Wolf Creek Research Basin (WCRB).

CHAPTER 5

SUMMARY AND CONCLUSIONS

5.1 Research significance

Northern environments are under increasing pressure from the effects of climate change, and have undergone abrupt alterations to their hydroclimatic regime within the last few decades. Enhanced warming and other observed changes have resulted in permafrost thaw, intensification of the freshwater cycle, and altered vegetation community and characteristics along both altitudinal and latitudinal gradients. Feedbacks have increased soil temperature resulting in changes to soil moisture regimes, hydrological flowpath distribution, and hydrochemical sources and transport. Observed and predicted catchment responses to a changing hydroclimatic regime are difficult to measure or support. Other barriers persist including logistical obstacles, increased costs and more extreme working conditions that are inherent to the study of remote northern catchments but limit scientific studies in these challenging environments. Longterm hydroclimate and hydrochemical datasets at scales < 200 km^2 in the discontinuous to continuous permafrost zone are sparse, particularly in North America, with a handful of established research areas in Canada (e.g, DeBeer et al., 2014; Spence and Hedstrom, 2018; Rasouli et al., 2019; Quinton et al., 2019) and the United States (e.g., Kane et al., 2004). Process-based studies are essential to understanding how northern systems will respond to climate warming and change, however, large scale observations can be (mis)used as the basis for mechanistic understanding in the absence of studies at smaller scales. Additionally, while permafrost is

often a first order control on hydrological flowpaths, which determine hydrochemical source areas and export, it is common that results from cold or snow-dominated environments are considered equivalent for permafrost areas.

This thesis utilised natural tracers and novel approaches within the context of a multidecadal dataset to better understand the interplay of ecohydrological processes, catchment function and stream hydrochemistry in a cold montane catchment with discontinuous permafrost. A nested study design permitted an expansion built on current understanding of catchment function at the ~7 km^2 headwater to ~180 km^2. Previous research in this area acted as a foundation from which we questioned conceptual models developed for larger river systems and the ubiquity of cold region observations from non-permafrost regions. Additionally, conceptual models specific to this location have been validated or revised using overlapping hydrometric, tracer, hydrochemical and optical datasets. Samples were collected at varying temporal resolutions across seasons to incorporate catchment conditions distinct from the well-studied snowmelt and summer periods.

5.2 Research summary

The principal conclusions of this thesis are outlined below for each chapter:

A combination of DOC concentrations and optical indices collected at the outlet of different landscape elements within a nested study design were examined in **Chapter 2**. Results showed DOM composition was most variable during freshet with high A254, SUVA254 and low FI and BIX. This means that in-stream fluorescing DOM was more

aromatic and comprised of older, terrestrially-derived material. DOM composition differed across landscape elements but was relatively insensitive to flow variation during summer and fall. The influence of increasing watershed scale and downstream mixing of landscape contributions was an overall dampening of DOC concentrations and optical indices with increasing groundwater contribution with patterns reported at the headwater scale conserved further downstream. Findings support a projected shift from predominantly organic soils (high aromaticity, less fresh) to decomposing vegetation (more fresh and lower aromaticity). DOC concentrations and load at the headwater were compared to results from a decade ago. These changes are likely linked to flow and transport through deeper flow pathways and enhanced groundwater contributions to runoff over time and with increasing catchment size.

Chapter 3 explored how novel technologies (i.e., high-frequency monitoring of chromophoric dissolved organic matter (CDOM)) and analysis approaches (i.e., normalized CQ hysteresis metrics) can be utilized at the event, seasonal and annual scale. High-frequency monitoring provided new insights into previously undiscovered dissolved organic carbon (DOC) dynamics, improved our understanding of dissolved organic matter processes and evaluated export estimates. Increased temporal resolution of monitoring in a headwater catchment demonstrated that there are in-stream dynamics that have not yet been observed in, or explained by, current conceptual models. From the event to the annual scale, patterns between solute concentrations and discharge are complex and different types of CQ analysis provided information about overall system behavior through log slopes (chemostasis, accretion/mobilization, dilution) as well as hysteresis behavior at the event,

seasonal and annual scale. Hysteresis metrics related to loop geometry revealed differences between behavior at the event scale relative to seasonal and annual patterns. Use of the HydRun toolkit at Wolf Creek Research Basin revealed that high diel variability complicated event extracted and few snowmelt-driven CQ event patterns could be appropriately summarized by the conventional hysteresis metrics. Correlations between later season event CQ hysteresis and other variables (e.g., event rainfall, and antecedent rainfall, air temperature and soil moisture) showed that factors interact to lead to varying precursor conditions, which was not accounted for in our analysis. Event response is often non-linear and threshold-mediated (Ali et al., 2015) so complex interactions merit further study and monitoring.

Chapter 4 introduced a robust stable isotope dataset and incorporated historical precipitation isotope data to develop a local meteoric water line for Southern Yukon. Isotopic composition of meteoric waters were matched in space and time with results of newly developed isotope analysis methods for shrub xylem and bulk soil water. The isotopic composition was used to assess whether the ecohydrological separation (ES) operated in this alpine permafrost headwater catchment. Shallow soil water during cold conditions, deeper soil water signatures overlapped in dual isotope space while xylem water isotope composition differed significantly, which satisfies the criteria for ES. However, results from 2016 captured movement of xylem water isotope composition towards the bulk soil water signature during the growing season suggesting that willow and birch shrubs opportunistically and dynamically change water source due to availability. The isotope

composition of the 'missing' water source is more depleted in heavy isotopes than any of the isotope signatures recorded within the headwater site.

5.3 Limitations and suggested directions of future research

The results presented in this dissertation have refined existing conceptual models by investigating catchment behavior and function using solute quantity and quality, and natural tracers ($\delta^{18}O$, $\delta^{2}H$). Insights were gleaned from an expansive dataset that builds on historical data while incorporating novel techniques, approaches and spatiotemporally-diverse solute and environmental information. The diversity in the types of data collected, the analysis methodology and techniques, and the applications shown within this thesis and in peer-reviewed publications provided a meaningful opportunity to evaluate limitations and outline future lines of inquiry.

These limitations will be described before discussing potential future research directions made possible by this dataset and by building on lessons learned throughout this process. Relatively new types of data collected for this dissertation include optical and fluorescence data, high-frequency optical measurements, and stables isotopes of bulk soil and xylem water.

Optical characteristics and fluorescence behavior of dissolved organic matter is collected and investigated in hydrological studies, however, this information can often result in an oversimplified interpretation (Rosario-Ortiz and Korak, 2017). Although it was not discussed extensively in Chapter 2, each sample analysed resulted in an excitation-emission matrix (EEM). EEMs can be assessed qualitatively by comparing fluorescence

intensity within specific wavelength ranges typically representative of humic, protein-like and tyrosine substances (i.e., pick peaking). From a quantitative perspective, EEMs can be assembled in an additive linear model and then decomposed into a specific number of independent fluorophores using parallel factor analysis (PARAFAC). A common misconception is that this type of data can be used to characterize distinct chemical constituents of the DOM pool with high certainty using either qualitative or quantitative methods. In reality, only a subset of DOM molecules is capable of absorbing light in the UV−visible range to be characterized as chromophoric DOM (CDOM) and an even smaller portion will exhibit fluorescence (i.e., FDOM) once excited by a light source. In natural environments, an added complication is that the optical and fluorescence behavior of molecules catalogued within EEMs are not necessarily due to the presence of individual chemical constituents but can result from superposition or interaction between different components. In addition, classifications that are applied (e.g., marine-like, protein-like) in this research and elsewhere rely on early investigations that employed cross-validation with laboratory analyses and assume consistency across environments. The optical fluorescence community has outlined and addressed several of these limitations in Rosario-Ortiz and Korak (2017) including a careful consideration of the environmental context, cross-validation of sample results with other chemical methods and an understanding of the representativeness of FDOM and CDOM within the larger DOM reservoir.

CDOM at high frequency represents the same subset of DOM as discrete samples but has been shown to be highly correlated with DOC. The analysis undertaken to assess event hysteresis and characteristics using 15-minute measurements of CDOM, SpC and

discharge was weakened by high diel variability. The diel amplitude in all three signals often masked event response or led to more complex C-Q hysteresis that could not be summarized by the normalized metrics. Initial exploration into drivers of 24-hour variation in streamflow, SpC and CDOM was undertaken in 2018 and precluded water temperature and viscosity as main causes for observed variability. This diel signal is ubiquitous in streams and rivers but the potential processes and mechanisms that cause this behavior are often hypothesized (Nimick et al., 2011) yet rarely confirmed. Diel behavior was observed early during snowmelt and throughout the open-water period at Granger Creek and Wolf Creek. Gleaning insights into underlying drivers will guide the development of a processing step prior to C-Q analysis to separate underlying variability from event response.

In addition to ongoing methodological development to determine the isotope composition of bulk soil and xylem water, there have been many calls for greater knowledge transfer across disciplines to better understand vegetation physiological and hydraulic processes (Brantley et al., 2017) that may cause fractionation. Studies over the last decade introduced soil water in a catchment compartmentalized into immobile and mobile components (Brooks et al., 2009, McDonnell, 2014, Evaristo et al., 2015). The "two water worlds" or ecohydrological separation (TWW/ES) hypothesis suggested that the immobile fraction of soil water was separate from mobile water and preferentially uptaken by plants despite the implied energetic inefficiency (McDonnell, 2014). A central assumption of TWW/ES is that isotopic fractionation during water uptake and transpiration processes is negligible (Dawson & Ehleringer, 1991; Roden & Ehleringer 1999) as this immobile water is taken up by root systems (McDonnell, 2014). Additional focus on this

topic has demonstrated that plants can discriminate against isotopes of oxygen and hydrogen as a function of soil water loss and soil type (Vargas et al., 2017) although more research is needed to determine to what extent this applies across vegetation species, environmental conditions and characteristics. Hypotheses that relate plant physiological mechanisms (Brantley et al., 2017) and isotopic fractionation during eco/hydrological processes could be answered by greater integration between research domains. An investigation into isotopic fractionation at the root-soil interface by Ellsworth and Williams (2007) occurred prior to the formulation of TWW/ES and recorded potential fractionation in line with Vargas et al. (2017). These studies provide nuance and lessen the binary introduced by early TWW/ES research by negating the assumption of negligible fractionation between soil and plant xylem water in all environments regardless of vegetation type, soil type and characteristics, and myriad other factors.

Further research into plant water use using stable isotopes should aim to take advantage of new methodological and analytical insights into plant xylem water (Millar et al., 2019) and soil water isotopic composition measurements (Oerter et al., 2014; Orlowski et al., 2018). Improved assessments of the limits of analytical techniques as well as improved certainty (Orlowski, Breuer, and McDonnell, 2016; Orlowski, Pratt and McDonnell, 2016; Newberry et al., 2017) have emerged in recent years as investigations of TWW/ES have occurred in catchments globally. The utility of stable isotope tracers depends on increased scrutiny across soil types, analytical methods and analytical setups at different laboratories (e.g., Orlowski et al., 2018 for cryogenic distillation of soil water) to ensure standardized results for individual catchments. Although this standardization is

important for reconciling local results with regional or global studies, standardization of results within individual studies can still provide important insights into water use and ecohydrological interactions between different compartments of catchment systems. Synchronous measurements of evapotranspiration, soil moisture and xylem isotopic composition at greater temporal resolution could provide greater insights into plant water use at key stages of the growing season in the three ecozones of Wolf Creek Research Basin. Decoupling of evaporation and transpiration in this environment would mean that water cycle compartments and isotope composition could be tracked and linked to fluxes more explicitly. Other key applications using stable isotopes include determining the distribution of water ages associated within catchment compartments (including storage) and further tests of catchment flowpaths using tracer-aided modelling. From the standpoint of stream water stable isotopes, greater effort should be expended to increase the temporal resolution of sampling due to observations from 24 hour sampling campaigns in CDOM, SpC and stables isotopes (expressed as lc-excess in Figure 5-1).

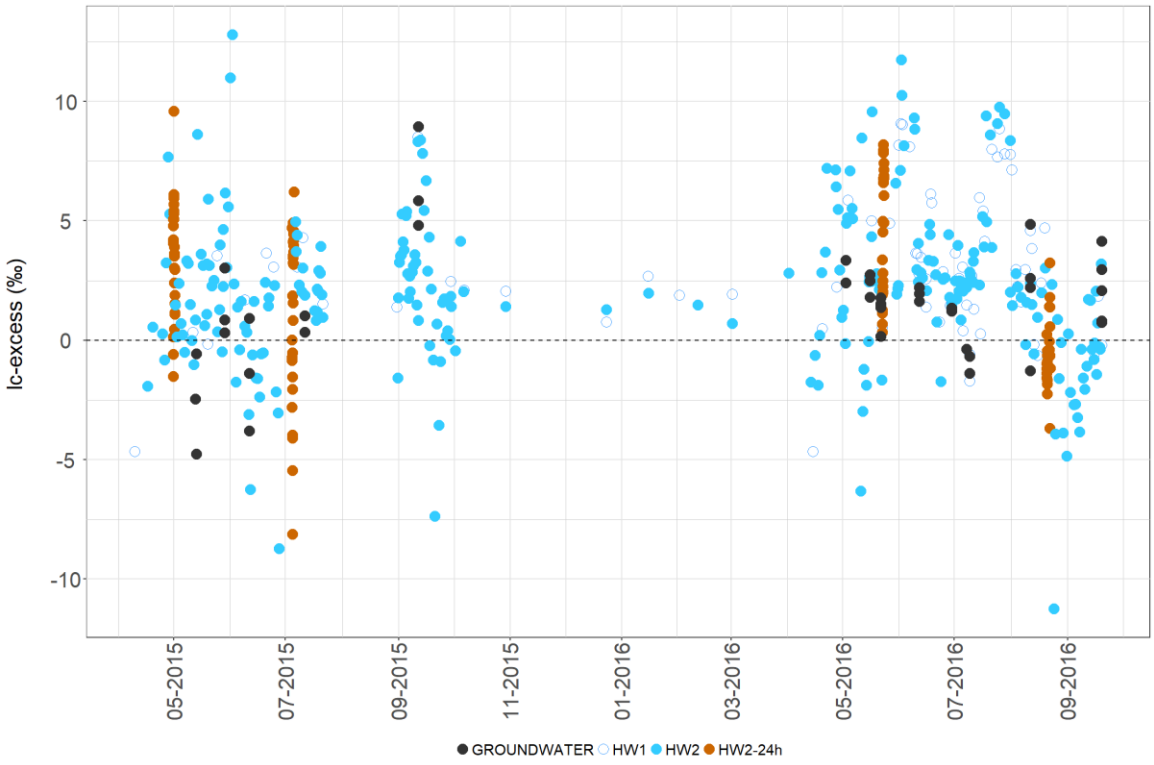

Figure 5-1. Time series of lc-excess values for 24-hour sampling campaigns (orange) at Granger Creek, samples taken at daily or sub-weekly resolution at Granger Creek (blue, filled circle), Buckbrush Creek (blue circles, empty) and from riparian groundwater well (black, filled circles).

References

Brantley, S. L., Eissenstat, D. M., Marshall, J. A., Godsey, S. E., Balogh-Brunstad, Z., Karwan, D. L., Papuga, S. A., Roering, J., Dawson, T. E., Evaristo, J., Chadwick, O., McDonnell, J.J. and K. Weathers, 2017. Reviews and syntheses: on the roles trees play in building and plumbing the critical zone. Biogeosciences, 14:5115-5142. doi: 10.5194/bg-14-5115-2017.

Brooks, J. R., Barnard, H. R., Coulombe, R., & McDonnell, J. J. (2009). Ecohydrologic separation of water between trees and streams in a Mediterranean climate. Nature Geoscience, 3(2), 100-104.

Dawson, T. E., & Ehleringer, J. R. (1991). Streamside trees that do not use stream water. Nature,350(6316), 335–337

DeBeer, C. M., Wheater, H. S., Quinton, W. L., Carey, S. K., Stewart, R. E., MacKay, M. D., & Marsh, P. (2015). The changing cold regions network: Observation, diagnosis and prediction of environmental change in the Saskatchewan and Mackenzie River basins, Canada. Science China Earth Sciences, 58(1), 46-60.

Ellsworth, P. Z., & Williams, D. G. (2007). Hydrogen isotope fractionation during water uptake by woody xerophytes. Plant and Soil, 291(1-2), 93-107.

Evaristo, J., Jasechko, S., & McDonnell, J.J. (2015). Global separation of plant transpiration from groundwater and streamflow. Nature 525, 91–94. doi:10.1038/nature14983

Kane, D.L., Gieck, R.E., Kitover, D.C., Hinzman, L.D., McNamara, J.P., & Yang, D. (2004). Hydrological cycle on the north slope of Alaska. In Kane, D. & Yang, D. (Eds.), Northern Research Basins Water Balance, pp. 224-236. International Association of Hydrological Sciences Press.

McDonnell, J. J. (2014). The two water worlds hypothesis: Ecohydrological separation of water between streams and trees?. Wiley Interdisciplinary Reviews: Water, 1(4), 323-329.
Millar, C., Pratt, D., Schneider, D. J., Koehler, G., & McDonnell, J. J. (2019). Further experiments comparing direct vapor equilibration and cryogenic vacuum distillation for plant water stable isotope analysis. Rapid communications in mass spectrometry: RCM, 33(23), 1850-1854.

Newberry, S. L., Nelson, D. B., & Kahmen, A. (2017). Cryogenic vacuum artifacts do not affect plant water-uptake studies using stable isotope analysis. Ecohydrology, 10(8), e1892.

Nimick, D. A., Gammons, C. H., & Parker, S. R. (2011). Diel biogeochemical processes and their effect on the aqueous chemistry of streams: A review. Chemical Geology, 283(1-2), 3-17.

Oerter, E., Finstad, K., Schaefer, J., Goldsmith, G. R., Dawson, T., & Amundson, R. (2014). Oxygen isotope fractionation effects in soil water via interaction with cations (Mg, Ca, K, Na) adsorbed to phyllosilicate clay minerals. Journal of Hydrology, 515, 1-9.

Orlowski, N., Pratt, D. L., & McDonnell, J. J. (2016). Intercomparison of soil pore water extraction methods for stable isotope analysis. Hydrological Processes, 30(19), 3434-3449.

Orlowski, N., Breuer, L., & McDonnell, J. J. (2016). Critical issues with cryogenic extraction of soil water for stable isotope analysis. Ecohydrology, 9(1), 1-5.
Orlowski, N., Breuer, L., Angeli, N., Boeckx, P., Brumbt, C., Cook, C.S., Dubbert, M., Dyckmans, J., Gallagher, B., Gralher, B., Herbstritt, B., Hervé-Fernández, P., Hissler, C., Koeniger, P., Legout, A., MacDonald, C.J., Oyarzún, C., Redelstein, R., Seidler, C., Siegwolf, R., Stumpp, C., Thomsen, S., Weiler, M., Werner, C., and McDonnell, J.J. (2018). Inter-laboratory comparison of cryogenic water extraction systems for stable isotope analysis of soil water. Hydrology and Earth System Sciences, European Geosciences Union, 2018, 22 (7), 3619-3637. doi: 10.5194/hess-22-3619-2018.

Quinton, W., Berg, A., Braverman, M., Carpino, O., Chasmer, L., Connon, R., Craig, J., Devoie, É., Hayashi, M., Haynes, K. and Olefeldt, D., 2019. A synthesis of three decades of hydrological research at Scotty Creek, NWT, Canada. Hydrology & Earth System Sciences, 23(4).

Rasouli, K., Pomeroy, J. W., Janowicz, J. R., Williams, T. J., & Carey, S. K. (2019). A long-term hydrometeorological dataset (1993–2014) of a northern mountain basin: Wolf Creek Research Basin, Yukon Territory, Canada. Earth System Science Data 11(1): 89-100.

Roden, J. S., & Ehleringer, J. R. (1999). Hydrogen and oxygen isotoperatios of tree-ring cellulose for riparian trees grown long-term under hydroponically controlled environments. Oecologia,121(4), 467–477.

Rosario-Ortiz, F. L., & Korak, J. A. (2017). Oversimplification of dissolved organic matter fluorescence analysis: potential pitfalls of current methods. Environmental Science and Technology 51, 2, 759-761. doi: 10.1021/acs.est.6b06133

Spence, C., & Hedstrom, N. (2018). Hydrometeorological data from baker creek research watershed, Northwest Territories, Canada. Earth System Science Data, 10(4), 1753-1767.

Vargas, A. I., Schaffer, B., Yuhong, L., & Sternberg, L. D. S. L. (2017). Testing plant use of mobile vs immobile soil water sources using stable isotope experiments. New Phytologist, 215(2), 582-594.